KONINKLIJK BELGISCH INSTITUUT VOOR NATUURWETENSCHAPPEN
OD NATUUR – BEHEERSEENHEID VAN HET MATEMATISCH MODEL

# MOnitoring en MOdellering van het cohesieve sedimenttransport en evaluatie van de effecten op het mariene ecosysteem ten gevolge van bagger- en stortoperatie (MOMO)

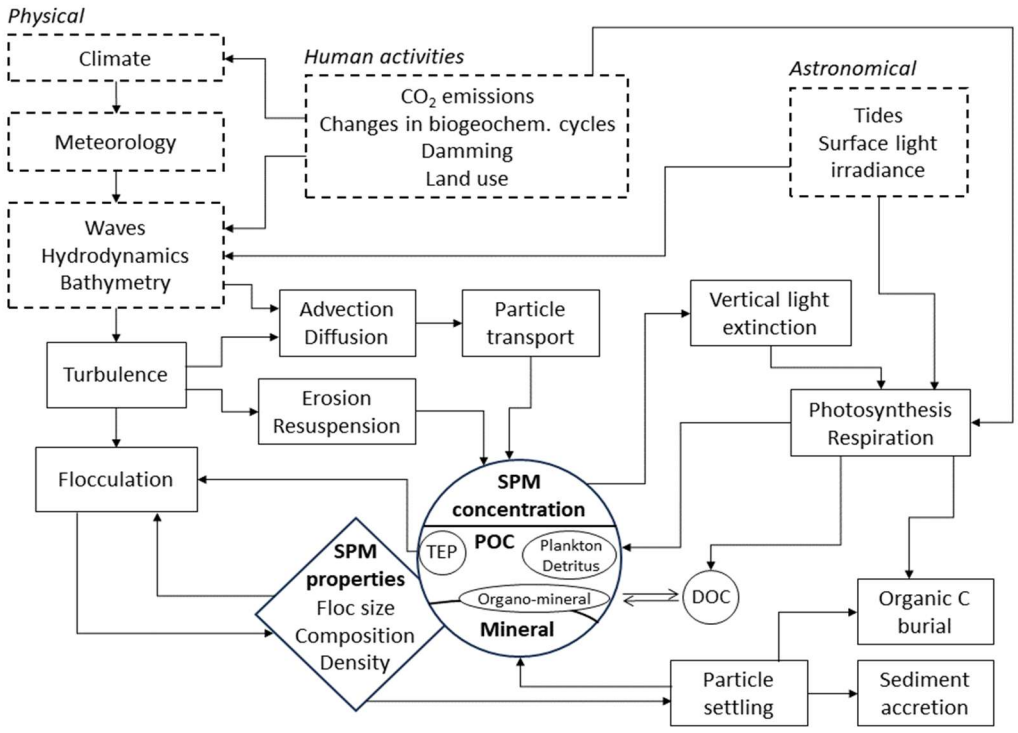


## Activiteitsrapport (1 juli - 31 december 2025)

Michael Fettweis, Matthias Baeye, Jean-Philippe Belliard, Xavier Desmit, Saumya Silori, Duc Tran, Benjamin van Roozendael

MOMO/10/MF/202603/NL/AR/8

KBIN-OD Natuur - BMM
Vautierstraat 29
B–1000 Brussel
België

# Inhoudstafel

# 1. Inleiding

## 1.1. Voorwerp van deze opdracht

Het MOMO-project (monitoring en modellering van het cohesieve sedimenttransport en de evaluatie van de effecten op het mariene ecosysteem ten gevolge van bagger- en stortoperatie) maakt deel uit van de algemene en permanente verplichtingen van monitoring en evaluatie van de effecten van alle menselijke activiteiten op het mariene ecosysteem waaraan België gebonden is overeenkomstig het verdrag inzake de bescherming van het mariene milieu van de noordoostelijke Atlantische Oceaan (1992, OSPAR-Verdrag). De OSPAR Commissie heeft de objectieven van haar Joint Assessment and Monitoring Programme (JAMP) gedefinieerd tot 2021 met de publicatie van een holistisch "quality status report" van de Noordzee en waarvoor de federale overheid en de gewesten technische en wetenschappelijke bijdragen moeten afleveren ten laste van hun eigen middelen.

De menselijke activiteit die hier in het bijzonder wordt beoogd, is het storten in zee van baggerspecie waarvoor OSPAR een uitzondering heeft gemaakt op de algemene regel "alle stortingen in zee zijn verboden" (zie OSPAR-Verdrag, Bijlage II over de voorkoming en uitschakeling van verontreiniging door storting of verbranding). Het algemene doel van de opdracht is het bestuderen van de cohesieve sedimenten op het Belgisch Continentaal Plat (BCP) en dit met behulp van zowel numerieke modellen als het uitvoeren van metingen. De combinatie van monitoring en modellering zal gegevens kunnen aanleveren over de transportprocessen van deze fijne fractie en is daarom fundamenteel bij het beantwoorden van vragen over de samenstelling, de oorsprong en het verblijf ervan op het BCP, de veranderingen in de karakteristieken van dit sediment ten gevolge van de bagger- en stortoperaties, de effecten van de natuurlijke variabiliteit, de impact op het mariene ecosysteem in het bijzonder door de wijziging van habitats, de schatting van de netto input van gevaarlijke stoffen op het mariene milieu en de mogelijkheden om deze laatste twee te beperken.

Voor een synthese van de resultaten uit de vergunningsperioden 2017-2021 en 2022-2026 zie de Vooruitgangsrapporten (Lauwaert et al., 2019; Fettweis et al., 2024) en het Syntheserapport (Lauwaert et al., 2021)? Deze werden gepubliceerd conform art. 10 van het K.B. van 12 maart 2000 ter definiëring van de procedure voor machtiging van het storten in de Noordzee van bepaalde stoffen en materialen.

## 1.2. Algemene doelstellingen

Het onderzoek uitgevoerd in het MOMO project kadert in de algemene doelstellingen om de baggerwerken op het BCP en in de kusthavens te verminderen, om de effecten van het storten van baggerspecie te kwantificeren en om een gedetailleerd inzicht te verwerven van de fysische processen die plaatsvinden in het mariene kader waarbinnen deze baggerwerken worden uitgevoerd. Dit impliceert enerzijds beleidsondersteunend onderzoek naar de vermindering van de sedimentatie op de baggerplaatsen en het evalueren van alternatieve stortmethoden. Anderzijds is vernieuwend onderzoek noodzakelijk om beter de effecten van het storten van baggerspecie in te schatten. Dit onderzoek is specifiek gericht op het dynamische gedrag van slib in de waterkolom en op de bodem en de interacties tussen fysische en biologische processen en zal uitgevoerd worden met behulp van modellen, in situ metingen en remote sensing data.

De specifieke acties die binnen dit onderzoek uitgevoerd worden om de algemene doelstellingen in te vullen zijn:

**1. Streven naar een efficiënter stortbeleid** door een optimalisatie van de stortlocaties.

**2. Continue monitoring van het fysisch en biogeochemisch milieu** waarbinnen de baggerwerken worden uitgevoerd (Taak 1) en aanpassing van de monitoring aan de nog op te stellen targets voor het bereiken van de goede milieutoestand (GES), zoals gedefinieerd zal worden binnen MSFD;

**3. Uitbouw en optimalisatie van het numerieke modelinstrumentarium**, ter ondersteuning van het onderzoek (Taak 2.1).

## 1.3. Algemeen Onderzoek 2012-2026

Het onderzoek heeft als doel om de effecten van baggerspeciestortingen op het mariene ecosysteem (fysische en biogeochemische aspecten) te onderzoeken. Hiervoor worden in situ metingen verzameld, gebruik gemaakt van remote sensing data en worden numerieke modellen ingezet. Voor de vergunningsperiode 2022-2026 worden volgende taken voorzien:

1) In situ en remote sensing metingen en data-analyse

De monitoring van effecten van baggerspeciestortingen gebeurd met behulp van een vast meetstation in de nabijheid van MOW1, en met meetcampagnes met de RV Belgica (een 10-tal meetcampagnes voor het verzamelen van traject informatie, profielen en de calibratie van sensoren; en een 10-tal campagnes voor het onderhoud van het meetstation te MOW1). De geplande monitoring is gericht op het begrijpen van processen, zodoende dat de waargenomen variabiliteit en de effecten van baggerspeciestortingen in een correct kader geplaatst kunnen worden. Een belangrijk deel is daarom gericht op zowel het uitvoeren van de in situ metingen, het garanderen van kwalitatief hoogwaardige data en het archiveren, rapporteren en interpreteren ervan. Remote sensing data afkomstig van onder andere satellieten worden gebruikt om een ruimtelijk beeld te bekomen.

2) Uitbouw en optimalisatie van het modelinstrumentarium

Het tijdens de voorbije jaren verbeterde en aangepaste slibtransportmodel zal verder worden ontwikkeld. Dit zal parallel gebeuren met de nieuwe inzichten die voorvloeien uit de metingen en de procesgerichte interpretatie van de metingen.

3) Ondersteunend wetenschappelijke onderzoek

Monitoring gebaseerd op wetenschappelijke kennis is essentieel om de effecten van menselijke activiteiten (hier het storten van baggerspecie) te kunnen inschatten en beheren. Om te kunnen voldoen aan de door OSPAR opgelegde verplichtingen van monitoring en evaluatie van de effecten van menselijke activiteiten is het ontwikkelen van nieuwe monitorings- en modelleractiviteiten nodig. Dit houdt in dat onderzoek dat de actuele stand van de wetenschappelijke kennis weerspiegelt wordt uitgevoerd en dat de hieruit voortvloeiende nieuwe ontwikkelingen geïntegreerd zullen worden in zowel de verbetering van het modelinstrumentarium als voor het beter begrijpen van het kustnabije ecosysteem.

## 1.4. Onderzoek Januari 2022 – December 2024

Voor de periode 2019-2021 werd rekening gehouden werd met de aanbevelingen voor de minister ter ondersteuning van de ontwikkeling van een versterkt milieubeleid zoals geformuleerd in het “Syntheserapport over de effecten op het mariene milieu van baggerspeciestortingen (2021)” dat uitgevoerd werd conform art. 10 van het K.B. van 12 maart 2000 ter definiëring van de procedure voor machtiging van het storten in de Noordzee van bepaalde stoffen en materialen.

## Taak 1: In situ en remote sensing metingen en data-analyse

### Taak 1.1 Langdurige metingen te MOW1 en W05

Sinds eind 2009 worden er continue metingen uitgevoerd te MOW1 met behulp van een meetframe (tripode). Met dit frame worden stromingen, slibconcentratie, korrelgrootte-verdeling van het suspensiemateriaal, saliniteit, temperatuur, waterdiepte en zeebodem altimetrie gemeten. Om een continue tijdreeks te hebben, wordt gebruik gemaakt van 2 tripodes. Na ongeveer 1 maand wordt de verankerde tripode voor onderhoud aan wal gebracht en wordt de tweede op de meetlocatie verankerd. Op de meetdata wordt een kwaliteitsanalyse uitgevoerd, zodat de goede data onderscheiden kunnen worden van slechte of niet betrouwbare data.

Veranderingen in kustnabije ecosystemen zijn dikwijls gecorreleerd met veranderingen van de helderheid van het water of de concentratie aan particulair suspensiemateriaal (SPM) en dus ook met het gehalte aan particulair organisch materiaal. De zone waar de invloed van het minerale en kustnabij suspensiemateriaal overgaat in een zone met dominantie van organisch suspensiemateriaal van mariene origine is van bijzonder belang. De monitoring wordt uitgebreid met de verankering van een meetboei in locatie W05 (51°N 24.96', 2°E 48.7'). W05 is één van de drie monitoringspunten waar waterstalen en sensormetingen maandelijks worden uitgevoerd.

### Taak 1.2 Calibratie van sensoren tijdens in situ metingen

Tijdens meetcampagnes met de R/V Belgica zullen een voldoende aantal 13-uursmetingen uitgevoerd worden met als hoofddoel het kalibreren van optische of akoestische sensoren en het verzamelen van verticale profielen. De metingen zullen plaatsvinden in het kustgebied van het BCP (MOW1, W05). De optische metingen (Optical Backscatter Sensor) zullen gekalibreerd worden met de opgemeten hoeveelheid materie in suspensie (gravimetrische bepalingen na filtratie) om te komen tot massa concentraties

### Taak 1.3 Bio-geo-chemische monitoring van het SPM (BGCMonit)

SPM bestaat uit minerale deeltjes van fysicochemische (b.v. kleimineralen, kwarts, veldspaat) en biogene oorsprong (b.v. calciet, aragoniet, opaal), levend (bacteriën, fyto- en zoöplankton) en niet-levend organisch materiaal (b.v. fecale pellets, detritus, exopolymeren), en partikels van menselijke oorsprong (microplastiek). Het SPM kan door hydrofobe organische polluenten of metalen gecontamineerd zijn. De samenstelling en concentratie van het SPM inclusief de hydrofobe polluenten verandert in functie van de tijd en de locatie. Deze variaties worden beïnvloed door de interacties tussen de fysische processen (getij, meteo, klimaat), biologische cycli (algenbloei), chemische processen (koolstofcyclus) en menselijke activiteiten (aanvoer van nutriënten, bagger- en stortactiviteiten, offshore constructies). De samenstelling van het particulair en opgelost suspensiemateriaal zal bepaald worden tijdens meetcampagnes met de RV Belgica tijdens een 10-tal campagnes per jaar. Naast de totale hoeveelheid aan SPM worden ook de concentraties aan verschillende organische bestanddelen (POC, PON, TEP, chlorofyl en phaeofytine) bepaald. De opgeloste stoffen zijn inorganische nutriënten, DOC, DIC en alkaliniteit. Stalen van suspensiemateriaal zullen genomen worden met de centrifuge om de samenstelling ervan te bepalen.

### Taak 1.4: Archivering en verwerking van de data

De meetdata worden gearchiveerd en er wordt een kwaliteitsanalyse uitgevoerd, zodat de goede data onderscheiden kunnen worden van slechte of niet betrouwbare data. Slechte data kunnen bv optreden doordat het instrument slecht heeft gewerkt en verkeerd werd ingesteld. Niet betrouwbare data zijn typisch geassocieerd met bv biofouling. De data en metadata worden gearchiveerd. De metingen worden verwerkt en geïnterpreteerd. En

zullen dienen als basis voor het verder gebruik bij wetenschappelijke vraagstellingen.

## Taak 2: Uitbouw en optimalisatie van het modelinstrumentarium

### Taak 2.1: Opstellen van een slibtransportmodel voor het BCP met Coherens V2

Een slibtransportmodel zal worden geïmplementeerd met de software Coherens V2. De software laat toe om rekening te houden met gemengde sedimenten en dus met de interactie tussen zand en slib en laat morfologische berekeningen toe door een verbeterde implementatie van het schema voor het massabehoud en gebruik van lagen met gemengde sedimenten. Verdere aanpassingen en verbeteringen aan het model zullen worden uitgevoerd, meer bepaald:

- Kritische bodemschuifspanning voor erosie van gemengde sedimenten,
- Formulering voor de bodemschuifspanning,
- Koppeling van het model met het TILES voxel model voor een betere voorstelling van de bodemkarakteristieken.

### Taak 2.2: Validatie van het slibtransportmodel voor het jaar 2013 (stortproef)

Een eerste toepassing van het model kan het jaar 2013 zijn, waarin de terreinproef voor alternatieve stortplaats alsook een intensieve monitoring plaatsvond. Deze laatste zal gebruikt worden voor de validatie van het model. Verder zal het model vergeleken worden met andere modellen van het BCP.

### Taak 2.3: Optimalisatie baggerwerken

Een operationeel stortmodel zal worden opgezet in overleg met aMT. Dit model zal geïntegreerd worden in de binnen BMM-OD Natuur beschikbare operationele modellen. Het model zal gebruikt worden om in functie van de voorspelde fysische (wind, stroming, golven, sedimenttransport, recirculatie), economische (afstand, grootte baggerschip) en ecologische aspecten op korte termijn een keuze te kunnen maken tussen de beschikbare stortlocaties. Een eerste test hiervoor werd uitgevoerd in Van den Eynde en Fettweis (2011) waarin werd aangetoond dat door een optimale positie te kiezen voor het storten van baggerspecie in functie van de meteorologische omstandigheden, een vermindering van de aanslibbing van de vaargeulen en haven van Zeebrugge kan worden verwacht.

Het model zal worden gebruikt voor de optimalisatie van de baggerwerken. Verschillende simulaties kunnen worden uitgeoefend waarbij de invloed van de verschillende mogelijke stortplaatsen kunnen worden geëvalueerd.

### Taak 2.4: Flocculatiemodel

De inzichten die voortvloeien uit de in situ data (Taken 1.4, 3.1 en 3.2) zullen worden geïntegreerd in een numeriek model dat het verband tussen SPM, TEP en flocculatie langsheen temporele (getij, seizoenen) en geografische (waterkolom, onshore-offshore) schalen combineert. Het model zal worden opgezet als 1D verticaal en zal gekoppeld worden met het 2 klassen populatie model van Lee et al. (2011). Hierdoor zal de verticale verdeling van de minerale en de organische fractie van het SPM en hun interactie kunnen worden voorspeld.

## Taak 3: Ondersteunend wetenschappelijk onderzoek

Monitoring gebaseerd op wetenschappelijke kennis is essentieel om de effecten van menselijke activiteiten (hier het storten van baggerspecie) te kunnen inschatten en beheren. Om te kunnen voldoen aan de door OSPAR opgelegde verplichtingen van monitoring en evaluatie van de effecten van menselijke activiteiten is een verdere implementatie van huidige en het ontwikkelen van nieuwe monitoringsactiviteiten nodig. Meer specifiek gericht op de activiteit ‘storten van baggerspecie’ worden hier – wat het fysische milieu betreft - turbiditeit, samenstelling van de zeebodem, bathymetrie en

hydrografische condities beoogt. Deze taak speelt hierop in door de ontwikkeling en de implementatie van nieuwe tools die de actuele stand van de wetenschappelijke kennis weerspiegelen teneinde de mathematische modellen te optimaliseren en verfijnen.

### Taak 3.1: SPM samenstelling - minerale fractie

Door de aanwezigheid van gemengde sedimenten in de zeebodem (zand en slib) zal tijdens sterke stroming en of hoge golven ook een gemengde minerale fractie in suspensie komen. Dit heeft twee consequenties voor monitoring. Ten eerste reageren akoestische en optische sensoren verschillend op zand en slib, zodat de verzamelde tijdreeksen een grotere onnauwkeurigheid hebben tijdens zo'n momenten (Fugate & Friedrichs, 2002; Baschek et al., 2017; Schwarz et al, 2017; Fettweis et al., 2019). Ten tweede bevatten zandkorrels geen mineraal-gebonden organisch materiaal en stalen genomen tijdens dit soort momenten kunnen dus de onzekerheid van het SPM-POM model vergroten. Indien er geen rekening gehouden wordt hiermee zal de SPM concentratie onder- of overschat worden alsook de afgeleid organische fracties. Doel is om de zand en slibfractie te identificeren door gebruik te maken van innovatieve meettechnieken (Pearsons et al., 2021) die optische en akoestische sensoren combineren. Het ultieme doel is om te komen tot tijdreeksen van zand- en slibconcentratie te MOW1.

Uit visuele inspecties van de bodemsamenstelling te MOW1 tijdens de laatste jaren blijkt dat het sediment zandiger is geworden. De hypothese is, dat dit verband houdt met erosie van de vooroever na de strandopspuitingen die de voorbije jaren werden uitgevoerd. Aan de hand van de boven aangehaalde methode zal nagegaan worden of er een trend naar zandaanrijking kan vastgesteld worden in de omgeving van MOW1.

### Taak 3.2: SPM samenstelling - organische fractie

Het semi-empirisch POM-SPM model (Fettweis et al., 2022) zal verfijnd worden met de nieuwe data verzameld in taak 1.3. Hierdoor zal de inschatting van de minerale en de vers en mineraal-gebonden organische fractie nauwkeuriger kunnen worden gedaan.

Op basis van dit POM-SPM model kan de samenstelling van het suspensiemateriaal (minerale fractie, vers en mineraal gebonden POC, PON en TEP) worden berekend voor de tijdreeksen te MOW (vanaf 2005) en voor de satellietdata (vanaf 1997). Dit zal toelaten om de geografische en temporele variabiliteit van de transitiezone tussen het kustgebonden turbiditeitsmaximum en de offshore wateren te kwantificeren. De dynamica van het suspensiemateriaal in beide gebieden is verschillend, wat consequenties heeft naar de modellering ervan. Verder kan uit de lange tijdsreeksen gekeken worden of het gebruik van de stortplaatsen, meer bepaald S1, geleid heeft tot een zeewaartse uitbreiding van het turbiditeitsmaximum.

### Taak 3.3: Trends in SPM concentratie

Om significante statistische trends te kunnen documenteren in SPM concentratie over de laatste decades, zijn metingen nodig die een lange tijdspanne omvatten en een groot gebied omvatten. Deze data zijn helaas niet beschikbaar. Wat er wel beschikbaar is zijn de tripode metingen te MOW1 (vanaf 2005) en op andere locaties, de puntmetingen verzameld met onderzoeksschepen in het Belgisch Deel van de Noordzee sinds ongeveer 1970 (cf. Belspo 4DEMON project) en satellietbeelden (vanaf 1997). De tripode data geven de temporele variabiliteit weer, maar zijn heel beperkt wat ruimtelijke spreiding betreft. De 4DEMON en satellietbeelden zijn beschikbaar over een lange periode en over een groot gebied, maar kunnen de temporele schaal niet oplossen. Om deze heterogene datasets samen te kunnen gebruiken, zal gekeken worden naar de statistische verschillen tussen de datasets en naar een manier om deze te combineren. Doel is om mogelijke trends in de SPM concentratie te identificeren en deze te linken aan natuurlijke veranderingen of aan menselijke activiteiten.

De trendanalyse van de historische data zal de basis vormen om de verandering van de SPM concentratie in de nabijheid van de nieuwe stortplaats ZBW te kwantificeren.

### Taak 4: Rapportage en outreach

Om de zes maanden zal er een activiteitenrapport worden opgesteld dat de onderzoeksresultaten beschrijft. Jaarlijks wordt er een 'factual data' rapport opgesteld van de verzamelde meetgegevens. De resultaten uit het onderzoek zullen tevens worden voorgesteld op workshops, conferenties en in de wetenschappelijke literatuur.

## 1.5. Aanpassing onderzoeksplan naar aanleiding van de niet beschikbaarheid van de RV Belgica

Het onderzoek uitgevoerd door het KBIN heeft als doel om de effecten van baggerspeciestortingen op het mariene ecosysteem (fysische en biogeochemische aspecten) te onderzoeken. Hiervoor worden in situ metingen verzameld, gebruik gemaakt van remote sensing data en worden numerieke modellen ingezet. Door het wegvallen van de RV Belgica sinds juni 2024 tot vermoedelijk 2026 kan het verzamelen van in situ data (monitoring) enkel deels worden uitgevoerd. Ter verantwoording van het begrootte budget voor 2024 en 2025 wordt er een overzicht over de geplande activiteiten met betrekking tot de in situ monitoring gegeven als ook extra taken beschreven die verantwoorden waarvoor het voorziene budget zal gebruikt worden.

### Taak 1: In situ en remote sensing metingen en data-analyse

Taak 1.1 Langdurige metingen te MOW1 en W05

De Zeetijger zal ingezet worden voor het voortzetten van de langdurige meting met behulp van een meetframe (tripode) te MOW1. Het uitbreiden van de langdurige monitoring met een meetboei te W05 zal worden uitgevoerd.

Taak 1.5 Analysemethode TEP

De analysemethode voor de TEP (transparant exoplymeric particle) werd recent verbeterd (zie activiteitsrapport MOMO/10/MF/202410/AR/5). TEP-concentratie wordt bepaald met behulp van de kationische kleurstof Alciaan Blauw. In de literatuur wordt vermeld dat dit soort kleurstoffen zich kunnen hechten aan kleimineralen, waardoor de TEP-concentratie mogelijks verkeerd wordt bepaald. Er zal daarom onderzocht worden of de aanwezigheid van kleimineralen (zie hieronder) in het SPM een invloed kan hebben op de TEP-concentratie.

### Taak 3: Ondersteunend wetenschappelijk onderzoek

Taak 3.4 SPM-samenstelling – mineralogie en interactie met organisch materiaal

Deze taak zal worden aangevuld met een mineralogische analyse van het suspensiemateriaal. We zullen hiervoor materiaal gebruiken dat in 2023 werd verzameld met een centrifuge (RV Belgica). Een mineralogische karakterisatie (bulk en kleimineralogie) van het suspensiemateriaal werd in 2004-2007 uitgevoerd en diende als basis voor een herkomstonderzoek van het slib op het BCP. Met deze nieuwe analyse willen we nagaan of er zich veranderingen hebben voorgedaan en indien ja, waarom.

Mineralen en organisch materiaal vertonen beide cohesieve eigenschappen en interacties kunnen leiden tot organo-minerale associaties. In natuurlijke systemen komen mineralen en organisch materiaal altijd samen voor en zijn organo-minerale associaties op moleculaire tot mm-schaal alomtegenwoordig. Deze interacties vinden op verschillende manieren plaats, variërend van de sorptie van kleine en grotere organische moleculen aan oppervlakken door bijvoorbeeld waterstofbruggen of van der Waals-krachten, tot intercalatie in expandeerbare kleimineralen, de occlusie in kleine kleimineraalaggregaten

(flocculi), het incorporeren van grote organische deeltjes (bijvoorbeeld fytoplankton, bacteriën) in vlokken en de vorming van biofilms. In mariene sedimenten en in het suspensiemateriaal wordt het gehalte aan organische materiaal voornamelijk bepaald door de mineralen en de beschikbaarheid van organisch materiaal. Met behulp van de mineralogische karakteristieken zal een betere beschrijving van de stabiliteit van de organische fractie kunnen worden bepaald.

Taak 3.5: Trends in SPM concentratie en stortoperaties

Doel van dit onderzoek is om mogelijke trends in de SPM concentratie te identificeren en deze te linken aan natuurlijke veranderingen of aan menselijke activiteiten. Deze bestaande taak zal worden aangevuld met een onderzoek op het effect van stortplaats ZBW. Onderzoeksvragen zijn 1) of de herlocatie van de stortplaats ZBW tot een vermindering van de aanslibbing (SPM concentratie) in de haven van Zeebugge heeft geleid en 2) wat de veranderingen in SPM concentratie ter hoogte van ZBW is. Hiervoor zullen tripode en remote sensing data worden gebruikt.

## 1.6. Gerapporteerde en uitgevoerde taken

Periode Januari 2022 - Juni 2022

Taak 1.1: De meetreeks te MOW1 werd verdergezet.
Taak 1.2: Calibratie van OBS sensoren werd uitgevoerd tijdens RV Begica campagnes 2022/01, 2022/03, 2022/06, 2022/09 en 2022/14.
Taak 3.1: De akoestische en optische sensoren werden gebruikt om veranderingen in sedimentsamenstelling te zien te MOW1. Eerste resultaten worden getoond in hoofdstuk 2.
Taak 3.2: Intensieve bio-geochemische monitoring werd uitgevoerd te MOW1, W05 en W08 tijdens RV Belgica campagnes 2022/01, 2022/03, 2022/07, 2022/11, 2022/14). Eerste resultaten worden besproken in hoofdstuk 3.
Taak 4: zie hoofdstuk 1.7

Periode Juli 2022 - December 2022

Taak 1.1: De meetreeks te MOW1 werd verdergezet.
Taak 1.2: Calibratie van OBS sensoren werd uitgevoerd tijdens RV Begica campagnes 2022/17, 2022/19, 2022/21, 2022/24, 2022/28 en 2022/32.
Taak 2.4: De interactie van phytoplankton en SPM resulteert in de vorming van grotere vlokken met hogerer valsnelheden. In een labo experiment werd de flocculatie bestudeerd tussen klei en phytoplankton deeltjes. Een twee-klassen flocculatiemodel werd opgesteld om de experimentele data kwantitatief te analyseren, zie paper in appendix 1.
Taak 3.2: Intensieve bio-geochemische monitoring werd uitgevoerd te MOW1, W05 en W08 tijdens RV Belgica campagnes 2022/17, 2022/19, 2022/21, 2022/24, 2022/28 en 2022/32). Eerste resultaten worden besproken in hoofdstuk 3.
Taak 3.3: Het informatieverlies van niet continue tijdreeksen werd bepaald. Dit zal de basis vormen voor de trendanalyse in SPM concentratie over een langere periode, zie hoofdstuk 2.
Taak 4: zie hoofdstuk 1.7

Periode Januari 2023 - Juni 2023

Taak 1.1: De meetreeks te MOW1 werd verdergezet.
Taak 1.2: Calibratie van OBS sensoren werd uitgevoerd tijdens RV Begica campagnes 2023/01, 2023/04, 2023/06, 2023/08 en 2023/10.
Taak 2.4: Een 2D horizontaal flocculatiemodel werd gevalideerd voor het BCP (zie appendix 3). De resultaten tonen het nut van een flocculatiemodel voor grootschalig SPM transport modellering. Tegelijkertijd onderstrepen ze tekortkomingen die het gevolg zijn van de transitie tussen kust en offshore en die zich uiten in verschillende SPM dynamica (zie ook hoofdstuk 2). Dit dient

opgenomen te worden in toekomstige modelleringen.

Taak 3: De resultaten beschreven in hoofdstuk 2 hebben mogelijks consequenties voor het storten van baggerspecie. Zij tonen immers aan dat er een duidelijk verschil tussen een kustnabije zone die gedomineerd wordt door minerale deeltjes en een offshore zone die vooral uit organische deeltjes bestaat. Er is geen (of weinig) uitwisseling tussen deze twee zones, zie hoofdstuk 3.

Taak 3.1: Analysen werden uitgevoerd gebaseerd op akoestische en optische sensoren van de tripode te MOW1 om de slib en zand fractie van het SPM te bepalen.

Taak 3.2: De biogeochemische monitoring werd verdergezet te MOW1, W05 en W08 tijdens RV Belgica campagnes 2023/01, 2023/04, 2023/06, 2023/08 en 2023/10.

<u>Periode Juli 2023 – December 2023</u>

Taak 1.1: De meetreeks te MOW1 werd verdergezet.

Taak 1.2: Calibratie van OBS sensoren werd uitgevoerd tijdens RV Belgica campagnes 2023/17 en 2023/25.

Taak 1.3: De biogeochemische monitoring werd verdergezet te MOW1, W05 en W08 tijdens RV Belgica campagnes 2023/17 en 2023/25.

Taak 2.4: De interactie tussen phytoplankton en minerale partikels werd verdergezet, resultaten werden voorgesteld op de INTERCOH conferentie (zie Appendix 1).

Taak 3.1: De analysen gebaseerd op akoestische en optische sensoren van de tripode te MOW1 om de slib en zand fractie van het SPM te bepalen, werden verdergezet. Eerste resultaten werden op de INTERCOH conferentie voorgesteld (zie Appendix 1)

Taak 3.2: De verandering in samenstelling van het SPM werd bestudeerd over de waterkolom, conclusies met betrekking tot de gehele waterkolom in turbide gebieden worden besproken in hoofdstuk 2 (en Appendices 2-12) en werden voorgesteld op de INTERCOH conferentie (zie Appendix 1).

Taak 4: zie hoofdstuk 1.7

<u>Periode Januari 2024 – Juni 2024</u>

Taak 1.1: De meetreeks te MOW1 werd verdergezet.

Taak 1.2: Calibratie van OBS sensoren werd uitgevoerd tijdens RV Belgica campagnes 2024/01 en 2024/03.

Taak 1.3: De biogeochemische monitoring werd verdergezet te MOW1, W05 en W08 tijdens RV Belgica campagnes 2024/01 en 2024/03.

Taak 3.1: De analysen gebaseerd op akoestische en optische sensoren van de tripode te MOW1 om de slib en zand fractie van het SPM te bepalen worden besproken in hoofdstuk 2 voor de langdurige meetreeks te MOW1.
De mineralogische samenstelling van het SPM werd bepaald in 4 locaties (MOW1, W03, W05 en W08).

Taak 3.2: Er werd gewerkt aan een klimatologie van de biogeochemische parameters (particulair en opgelost) langsheen de kust-offshore gradiënt.

Taak 4: zie hoofdstuk 1.7

<u>Periode Juli 2024 – December 2024</u>

Taak 1.1: De meetreeks te MOW1 werd enkel verdergezet tot september 2024, wegens het niet beschikbaar zijn van de Belgica.

Taak 1.2: idem voor de calibratie van de OBS sensoren.

Taak 1.3: idem voor de biogeochemisch monitoring te MOW1, W05 en W08.

Taak 2.4: De interactie van biologische en minerale bestanddelen werd gemodelleerd in een 0D flocculatiemodel. Het model simuleert de fytoplankton groei en de productie van organisch material, inclusief de ‘transparent exopolymer particles’ (TEP) en is gekoppeld aan het ‘two-class population balance equation’ flocculatie model zie Appendix 1;

Taak 3.1: Akoestische en optische sensoren van de tripode te MOW1 om de slib en zand fractie van het SPM te bepalen. Resultaten werden voorgesteld op de PECS concferentie, zie Appendices 2 en 3.

Taak 3.2: De studie van de biogeochemische karakterisatie van particulaire en opgeloste parameters op het BCP werd afgewerkt. Een uitgebreid verslag ervan zal in het komende rapport worden opgenomen, een samenvatting van de resultaten is te vinden in hoofdstuk 3.
Er werd meegewerkt aan een review paper over SPM dynamica, zie Appendix 4.

Taak 3.4: SPM-samenstelling – mineralogie en interactie met organisch materiaal, zie hoofdstuk 2.

Taak 3.5 Er werd verder gewerkt aan de analyse van trends en langdurige veranderingen in SPM concentratie en stortoperaties.

Taak 4: zie hoofdstuk 1.7

<u>Periode Januari 2025 – Juni 2025</u>

Taak 1.1: De meetreeks te MOW1 werd hervat vanaf April tot Juni.

Taak 1.2: Calibratie van de OBS sensoren kon niet worden uitgevoerd wegens het niet beschikbaar zijn van de Belgica of een alternatief onderzoeksschip

Taak 1.3: idem voor de biogeochemisch monitoring te MOW1, W05 en W08

Taak 1.5 Er werd begonnen met de valorisatie van de analysemethode TEP.

Taak 3.2: De studie van de biogeochemische karakterisatie van particulaire en opgeloste parameters op het BCP werd afgewerkt, zie hoofdstuk 2.

Taak 3.5 Er werd verder gewerkt aan de analyse van trends en langdurige veranderingen in SPM concentratie en stortoperaties.

Taak 4: zie hoofdstuk 1.7

<u>Periode Juli 2025 – December 2025</u>

Taak 1.1: De meetreeks te MOW1 kon niet verdergezet worden wegens het niet beschikbaar zijn van de Belgica of een ander schip.

Taak 1.2: Calibratie van de OBS sensoren kon niet worden uitgevoerd wegens het niet beschikbaar zijn van de Belgica of een alternatief onderzoeksschip

Taak 1.3: idem voor de biogeochemisch monitoring te MOW1, W05 en W08. In de plaats hiervan werden data geanalyseerd die tijdens het storten van baggerspecie te S1 werden verzameld met behulp van optische en akoestische sensoren, zie hoofdstuk 3.

Taak 1.5 Valorisatie van de analysemethode TEP werd beëindigd, zie appendix 2.

Taak 3: Een state of the art review werd opgesteld, zie hoofdstuk 2.

Taak 3.5 Er werd verder gewerkt aan de analyse van trends en langdurige veranderingen in SPM concentratie en stortoperaties.

Taak 4: zie hoofdstuk 1.7 en appendices 1, 3 en 4.

## 1.7. Publicaties (2022-2026)

Hieronder wordt een overzicht gegeven van publicaties met directe betrokkenheid van het KBIN waar resultaten en data uit het MOMO project in werden gebruikt.

<u>Activiteits-, Meet- en Syntheserapporten</u>

Fettweis M, Baeye M, Belliard JP, Desmit X, Silori, S, Tran D, van Roozendael B. 2026. MOMO activiteitsrapport (1 juli - 31 december 2025). BMM-rapport MOMO/10/MF/202602/NL/AR/8, 70pp + app.

Hindryckx K. 2025. Rapport van de RV Belgica Meetcampagnes en Verankering van Meetsystemen 2021. BMM-rapport OD Natuur-MDO/2025-11/MOMO/2021, 108pp.

Hindryckx K. 2025. Rapport van de RV Belgica Meetcampagnes en Verankering van Meetsystemen 2020. BMM-rapport OD Natuur-MDO/2025-09/MOMO/2020, 155pp.

Fettweis M, Desmit X, Silori, S. 2025. MOMO activiteitsrapport (1 januari - 30 juni 2025). BMM-rapport MOMO/10/MF/202509/NL/AR/7, 41pp + app.

Hindryckx K. 2025. Rapport van de RV Belgica Meetcampagnes en Verankering van Meetsystemen 2019. BMM-rapport OD Natuur-MDO/2025-06/MOMO/2019, 241pp.

Fettweis M, Silori S, Tran D, Desmit X. 2025. MOMO activiteitsrapport (1 juli - 31 december 2024). BMM-rapport MOMO/10/MF/202502/NL/AR/6, 34pp + app.

Fettweis M, De Witte B, Van Hoey, Seghers S, Vanermaete, Timmermanx S, Hermans L. 2024. Vooruitgangsrapport juni 2024 over de effecten op het mariene milieu van baggerspeciestortingen. MF/2024/10, 34pp.

Fettweis M, Tran D, Knockaert M, Desmit X. 2024. MOMO activiteitsrapport (1 januari - 30 juni 2024). BMM-rapport MOMO/10/MF/202410/NL/AR/5, 27pp.

Fettweis M, Silori S, Desmit X. 2024. MOMO activiteitsrapport (1 juli - 31 december 2023). BMM-rapport MOMO/10/MF/202403/NL/AR/4, 29pp + app.

Fettweis M, Desmit X. 2023 MOMO activiteitsrapport (1 januari - 30 juni 2023). BMM-rapport MOMO/10/MF/202310/NL/AR/3, 28pp + app.

Fettweis M, Desmit X. 2023 MOMO activiteitsrapport (1 juli – 31 december 2022). BMM-rapport MOMO/10/MF/202303/NL/AR/2, 27pp + app.

Fettweis M, Baeye M, Desmit X. 2022 MOMO activiteitsrapport (1 januari – 30 juni 2022). BMM-rapport MOMO/10/MF/202210/NL/AR/1, 21pp + app.

Thesis

Brysse F. 2024. Optimalisatie en validatie van de 'Multiskan Skyhigh spectrofotometer' voor analyse van transparante exopolymeerpartikels (TEP) in zeewater. VIVES Hogeschool Campus Roeselare, Bachelor thesis in de agro- en biotechnologie, 55pp + app.

Conferenties/Workshops

Fettweis M, Silori S, Desmit X**.** 2025. SPM concentration and composition along nearshore to offshore transects. Workshop on Particle Dynamics in Coastal Marine Environments, GTK Headquarters, 28 October, Espoo (Finland).

Delhaye L, Taymans C, van Kan P, Fettweis M. 2025. Intra-annual variability of marine floc morphology in southern North Sea coastal waters using in-situ high-resolution underwater imaging and the SANDI Python package. Particles in Europe, 17-19 September, Ostend (Belgium).

Fettweis M. 2025. Concentration and composition of suspended particulate matter along nearshore to offshore transects. Particles in Europe, 17-19 September, Ostend (Belgium).

Silori S, Desmit X, Schartau M, Terseleer N, Riethmüller R, Fettweis M. 2025. Vertical dynamics of suspended particulate matter and chlorophyll-a in a well-mixed coastal turbid system. Particles in Europe, 17-19 September, Ostend (Belgium).

Van Roozendael B, Baeye M, Tran D, Verney R, Fettweis M. 2025. Multi-sensor observations of suspended particulate matter in a tidal coastal environment. Particles in Europe, 17-19 September, Ostend (Belgium).

Fettweis M, Belliard J-P, Desmit X, Silori S, Tran D, Meysman F. 2025. Environmental conditions for alkalinity enhancement in the Belgian part of the North Sea. 56$^{th}$ Int. Liège Coll. on Ocean Dynamics, 26-30 May, Liège (Belgium).

Fettweis M, Silori S, Desmit M. 2025. Composition of SPM along nearshore to offshore transects. Workshop on flocculation, 21 May, Delft (NL).

Silori S, Desmit X, Schartau M, Terseleer N, Riethmüller R, Fettweis M. 2025. Vertical dynamics of suspended particulate matter and chlorophyll-a in a well-mixed coastal turbid system. Workshop on flocculation, 21 May, Delft (NL).

Desmit X, Silori S, Delhaye L, Van der Zande N, Terseleer N, **Fettweis M**, Dujardin J, De Rijcke M, Brun A, Amadei Martinez L, Vyverman W, Sabbe K, Schartau M, Riethmüller R. 2025. Organic and inorganic particle interactions and their dynamics on the North Sea shelf. VLIZ, 15 May, Ostend.

Delhaye LJ, Taymans C, Fettweis M. 2025. Intra-annual variability in the morphology of marine flocs in the southern North Sea using in-situ high-resolution underwater imaging. EGU General Assembly, 27 April 2 May, Vienna (Austria) .

Desmit X, Riethmüller R, Silori S, Schartau M, Fettweis M. 2025. Budgeting the particulate organic matter from the suspended particulate matter in shelf seas. EGU General Assembly, 27 April - 2 May, Vienna (Austria).

Fettweis M, Belliard J-P, Maris T, Amadei Martinez L, Silori S, Desmit X. 2025. The organic matter dynamics along the salinity gradient of the Scheldt estuary. Ems-Scheldt workshop, 13-14 February, Delmenhorst (Germany).

Tran D, Verney R, Fettweis M. 2024. New insights into near-bed SPM concentration and sand/mud fraction. AGU Meeting, 9-13 December, Washington DC (USA).

Baeye M, Fettweis M, Verney R. 2024. On the effects of SPM composition on the inherent acoustic and optical particle properties of the SPM. Physics of Estuaries and Coastal Seas, 23-27 September, Bordeaux (France).

Tran D, Verney R, Fettweis M. 2024. New insights into near-bed SPM concentration and sand/mud fraction in the use of Sediment Composition Index. Physics of Estuaries and Coastal Seas, 23-27 September, Bordeaux (France).

Terseleer N, Kerimoglu O, Lee BJ, Fettweis M, Desmit X. 2024. A coupled biogeochemical-flocculation model to unravel suspended particulate matter dynamics on the Belgian shelf. Symposium on Advances in Marine Ecosystem Modelling Research, 8-11 July, Plymouth (UK).

Fettweis M. 2024. A universe of particles in a sip of water: Composition, concentration and size along the land-ocean transition. Geo-Colloquium University Kiel, 18 June, Kiel (Germany).

Fettweis M. 2024. Jerico Research Infrastructure @ RBINS. Conference on EU Research Infrastructures – Belgian Presidency EU2024. 4-5 June, Brussels (Belgium).

Desmit X, Terseleer Lillo N, Fettweis M, Kallend A, Sabbe K, Dujardin J, De Rijcke M. 2024 Impact of plankton-mineral interactions on the carbon cycle in the Southern North Sea. Particles in Belgium workshop, 3 May, VLIZ, Ostend.

Silori S, Fettweis M, Desmit X, Terseleer N, Riethmüller R, Schartau M. 2024. Vertical profiles of Chlorophyll and SPM at seasonal and tidal scales in a turbid, well-mixed coastal zone. Particles in Belgium workshop, 3 May, VLIZ, Ostend.

Tran D, Fettweis M. 2024 Characterizing the composition of sand and mud suspension in coastal and estuarine environments using combined optical and acoustic measurements. Particles in Belgium workshop, 3 May, VLIZ, Ostend.

Fettweis M, Delhaye L, Lee BJ, Riethmüller R, Schartau M, Silori S, Desmit X. 2023. Vertical variations of suspended particle composition reflect particle dynamics. INTERCOH, 18-22 September, Inha University, Incheon (Korea).

Ho QN, Fettweis M, Hur J, Lee SD, Lee BJ. 2023. The role of microalgae in cohesive sediment flocculation: Insights from stochastic modeling and laboratory experiments. INTERCOH, 18-22 September, Inha University, Incheon (Korea).

Huynh TT, Fettweis M, Lee BJ. 2023. Application of an 1-DV TCPBE model with Bayesian calibration to diagnose the flocculation potential in the laboratory experiments and field measurement. INTERCOH, 18-22 September, Inha University, Incheon (Korea).

Pham TTTP, Ho QN, Lee SD, Fettweis M, Lee BJ. 2023. Isolation and characterization of the molecular composition of algal dissolved organic matter. INTERCOH, 18-22 September, Inha University, Incheon (Korea).

Tran D, Desmit X, Verney R, Fettweis M. 2023. Application of sediment composition index to predict suspended particulate matter concentration in the North Sea. INTERCOH, 18-22 September, Inha University, Incheon (Korea).

Kallend A, Dujardin J, De Rijcke M, Fettweis M, Sabbe K, Vyverman W, Desmit X. 2023. Interactions between phytoplankton, marine gels and suspended particulate matter in a dynamic, shallow coastal system before and during the phytoplankton spring bloom. ASLO Aquatic Sciences Meeting, 4–9 June, Palma de Mallorca (Spain).

Schartau M, Fettweis M, Desmit X, Terseleer N, Riethmüller R. 2023. From brown to blue water: Unraveling spatio-temporal variations in organic matter composition of suspended particulate matter. ASLO Aquatic Sciences Meeting, 4–9 June, Palma de Mallorca (Spain).

Baeye M, Delhaye L, Fettweis M. 2022. Acoustic and optical turbidity response to altering particle size distribution during extreme events. EuroSea/OceanPredict workshop, 29 June – 1 July, Exeter (UK).

Fettweis M, Desmit X, Terseleer N, Parmentier K, Van der Zande D, Schartau M, Lee BJ, Riethmüller R. 2022. The characteristics of the organic matter in biomineral flocs. Ocean Science Meeting, 24 February – 4 March, Honolulu (USA).

<u>Peer reviewed artikels</u>

Silori S, Desmit X, Fettweis M. 2025. Spatio-temporal variation in particulate and dissolved organic matter dynamics in the southern North Sea. Biogeochemistry 168.

https://doi.org/10.1007/s10533-025-01288-7
Silori S, Desmit X, Schartau M, Terseleer N, Riethmüller R, Fettweis M. 2025. Vertical dynamics of suspended particulate matter and chlorophyll-a in a well-mixed coastal turbid system. Estuarine, Coastal and Shelf Science. https://doi.org/10.1016/j/ecss.2025.109545
Fettweis M, Silori S, Adriaens R, Desmit X. 2025. Clay minerals and the stability of organic carbon in suspension along nearshore to offshore transects. Geochimica et Cosmochimica Acta. 395, 229-237.
Huynh TT, Kim J, Lee SD, Fettweis M, Bi Q, Kim SS, Lee SY, Choi YY, Lee BJ. 2024. Spatiotemporal dynamics of suspended particulate matter in the water environment: A review. Water 16, 3613.
Desmit X, Schartau M, Terseleer N, Van der Zande D, Riethmüller R, Fettweis M. 2024. The transition between coastal and offshore areas in the North Sea unraveled by the suspended particle composition. Science of the Total Environment 915, 169966.
Escobar S, Bi Q, Fettweis M, Monbaliu J, Wongsoredjo S, Toorman E. 2023. A 2DH flocculation model for coastal domains. Ocean Dynamics 73, 333-358.
Fettweis M, Riethmüller R, Van der Zande D, Desmit X. Water quality monitoring in coastal seas: How significant is the information loss of patchy time series? Science of the Total Environment 873, 162273.
Fettweis M, Schartau M, Desmit X, Lee BJ, Terseleer N, Van der Zande D, Parmentier K, Riethmüller R. 2022. Organic matter composition of biomineral flocs and its influence on suspended particulate matter dynamics along a nearshore to offshore transect. Journal of Geophysical Research Biogeosciences, 126, e2021JG006332.
Ho NQ, Fettweis M, Hur J, Desmit X, Kim JI, Jung DW, Lee SD, Lee S, Choi YY, Lee BJ. 2022. Flocculation kinetics and mechanisms of microalgae- and clay-containing suspension in different microalgae growth phases. Water Research 226, 119300.
Ho QN, Fettweis M, Spencer KL, Lee BJ. 2022. Flocculation with heterogeneous composition in water environments: A review. Water Research. 118147.

# 2. Suspended particulate matter along the land-ocean continuum: State of the art[1]

Suspended particulate matter (SPM) is present in all natural waters and plays a key role in biogeochemical, biological, and geological processes. SPM is involved in the transport, settling, deposition and resuspension of mineral and biogenic material, in the remineralization of organic matter (OM) and in the partitioning of $CO_2$ between ocean and atmosphere (Baumas & Bizic, 2024). It has an important impact on aquatic ecosystems, as it influences light and nutrient availability and thus primary production, serves as a food source for suspension feeding organisms and impacts water quality. SPM in aquatic environments is a mixture of mineral grains, microorganisms (such as bacteria and phytoplankton), detritus, adsorbed organic substances and xenobiotic particles (Ho et al., 2022). Interactions between them are driven by physical, chemical and biological processes that vary along the land-ocean transition, leading to large spatial and temporal variability in the size, shape, composition, concentration, and transport pathways of the SPM (Eisma, 1986; Maerz et al., 2016; Blattmann et al., 2019; Moulton et al., 2023; Desmit et al., 2024; Silori et al., 2025). OM in sediments is primarily associated with the mineral phase (Hedges & Keil, 1995). In contrast, the particulate OM (POM) in suspension have a large range of lability and reactivity depending on environmental conditions, such as the dissolved oxygen concentration, mineral protection, priming effects or microbial activity (Ittekkot, 1988; Mayer, 1994; Etcheber et al., 2007; Arndt et al., 2013; Hemingway et al., 2019; Liu et al., 2024).

SPM occurs as flocs, i.e. loose heterogeneous structures composed of minerals and OM, with size ranges from micrometre to millimetre. They can be considered as individual ecosystems with autonomous and interactive chemical, physical, and biological processes occurring within their structure (Ho et al., 2022). A characteristic and universal feature of SPM is that the composition becomes more organic and the floc sizes larger with decreasing SPM concentration (SPMC) (Figure 2.1). Consequently, along the land-ocean continuum, flocs largely consist of minerals in estuarine and nearshore turbidity maximum zones, while they contain gradually more organic matter when turbidity decreases. In oligotrophic environments, such as open oceans, SPM consists mostly of large, OM rich, fluffy aggregates (Alldredge & Silver, 1988). The shape and variability of the relationships between SPMC, its particulate organic carbon (POC) content, and floc size, are caused by spatio-temporal variations in biological, physical, and chemical processes. The decrease of POC content with SPMC and its seasonality has been described by a semi-empirical model that divides the POC into a labile and refractory fraction (Schartau et al., 2019; Fettweis et al., 2022). Figure 2.1 shows that these relationships hold regardless of latitude, climate, geomorphic setting and marine to freshwater systems. In this review, we explain the processes underlying these relationships, and discuss the current understanding of the characteristics, dynamics and interactions of POM and minerals along the land-ocean continuum by combining physical and biological knowledge and processes. The role of SPM in biogeochemical cycles and contaminant transport as well as the effects of climate change and human activities on SPM characteristics are discussed.

[1] This chapter has been written by M Fettweis, JP Belliard, S Silori, N Terseleer, D Tran, L Amadei Martinez, A Brun, K Sabbe, M De Rijcke, BJ Lee, R Riethmüller, X Shen, R Verney and X Desmit X. It has been submitted to Nature Reviews Earth and Environment in August 2025.

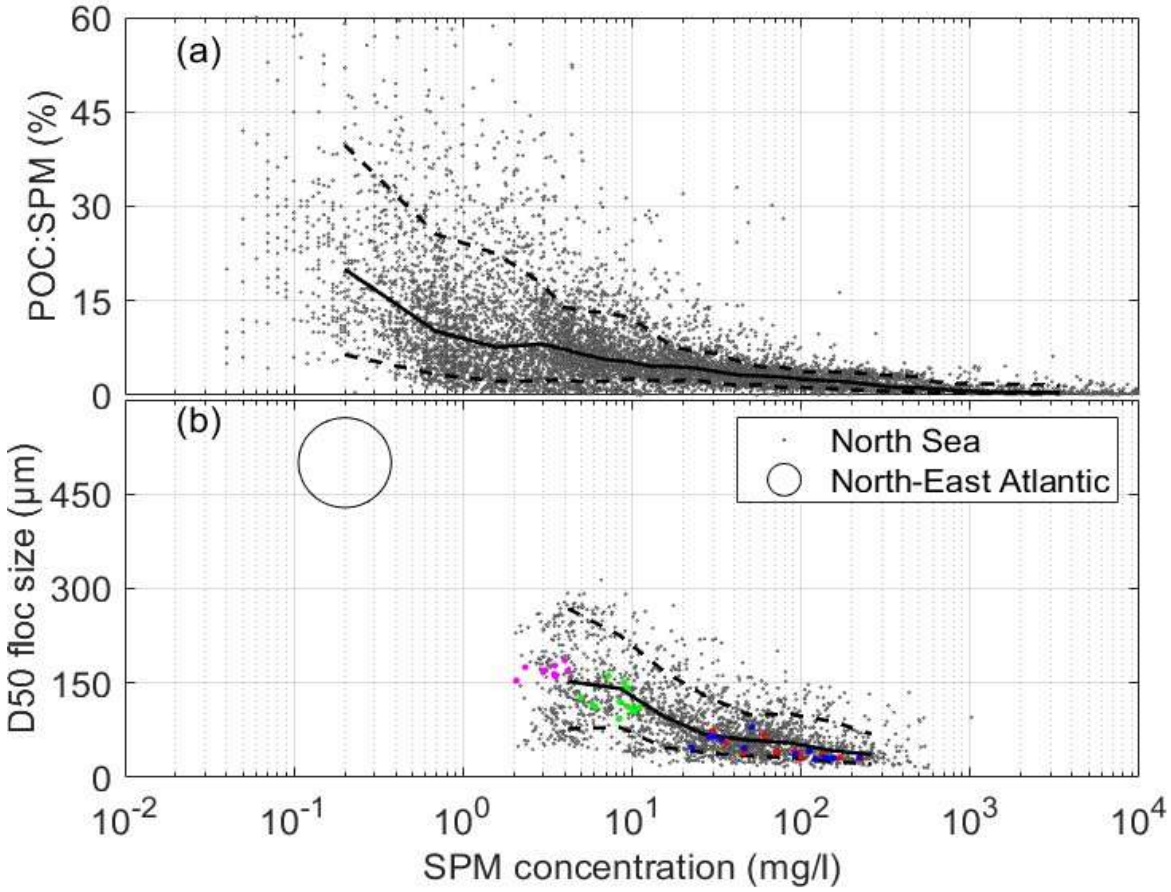


*Figure 2.1: (a) Particulate Organic Carbon (POC) content of the SPM as a function of SPMC among several aquatic ecosystems, i.e. from rivers, estuaries, shelf seas and oceans, and spanning a large latitudinal gradient (10362 water sample data). (b) In situ median floc size of the SPM measured with a LISST 100X (Agrawal & Pottsmith, 2000) as a function of SPMC in the North Sea and the English Channel (2420 data points). The data from the North Sea are from Fettweis et al. (2022, 2025) and Neukermans et al. (2012), and from the North-East Atlantic from McCave et al. (2001). The coloured dots highlight data that were sampled consecutively during single tidal cycles, each colour is a different tidal cycle. The lines in both figures are the median (solid) and 10 and 90 percentile (dashed) of the POC content or floc size over 25 log-scaled SPMC classes. SPM and POC data are from Alexandrova & Shevchenko (1997), Belliard et al. (2022), Belyaev et al. (2010a, 2010b, 2010c), Bezborodov & Eremeev (1993a, 1993b), Bouchez et al. (2014), Bouillon et al. (2003, 2009, 2014), Dellwig et al. (2007), Dellwig & Brumsack (2008), Doxaran et al. (2012), Fettweis et al. (2022, 2025), Goberville et al. (2010), Gordeev et al. (2007), Kaiser et al. (2019), Ke et al. (2022), Lee et al. (2023), Lein et al. (2012), Lizotte et al. (2021), Lukashin et al. (2003), Massicotte et al. (2023), McClelland et al. (2023), Moreira-Turcq et al. (2003), Neukermans et al. (2012), Nemirovskaya & Sivkov (2012), OMEX Project Members & Bizarro (2004a-e), Romankevich et al. (1994), Romankevich & Vetrov (2001), Schulz et al. (2022a), Seyler & Bonaventura (2001), Suzumura et al. (2004), Tamooh et al. (2012), Waniek et al. (2019; 2021; 2022), Zhang et al. (1992).*

## 2.1. Composition of SPM

SPM can be described according to structural and compositional (mineral and organic) characteristics (Figure 2.2). The former are size (from dissolved to particulate) and organization (primary particles, flocculi, microflocs, macroflocs, marine snow), see Wentworth (1922) and Lee et al. (2012). The distinction between dissolved, colloidal, and particulate is based on filterability and settleability. This distinction has biogeochemical implications and determines the transport pathways.

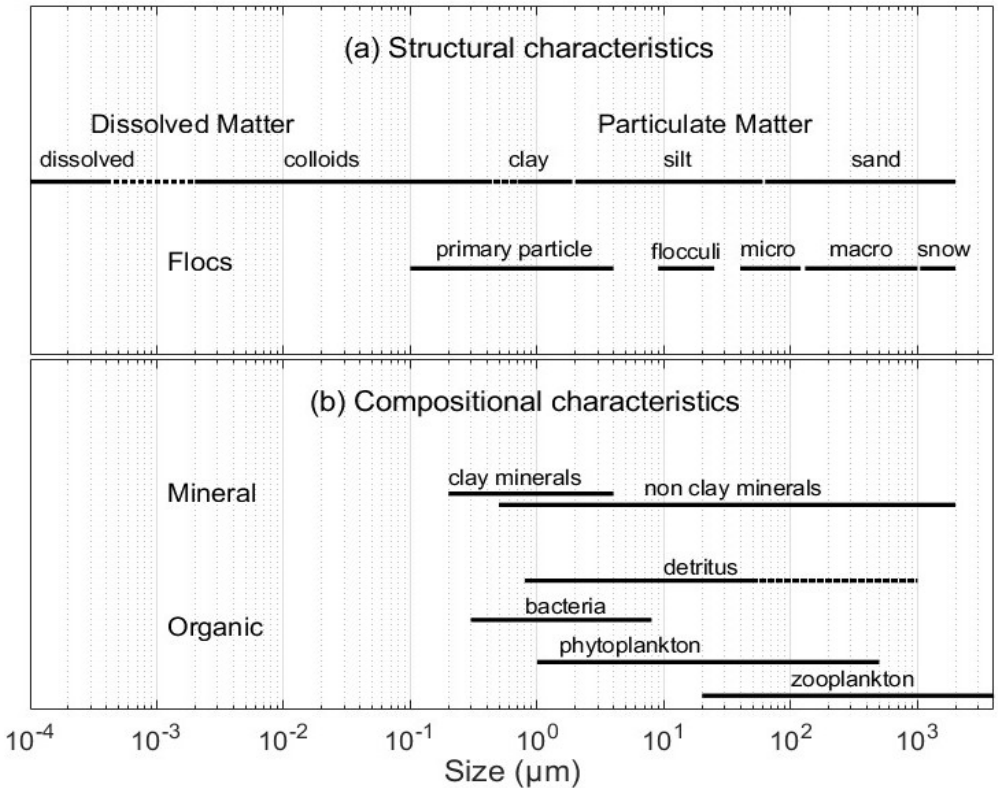


*Figure 2.2: Structural and compositional characteristics of the SPM as a function of size.*

### *2.1.1. Minerals*

The inorganic fraction of SPM consists of detrital (from erosion and weathering of parental rocks), biogenic (synthesized by organisms) and authigenic (formed through geochemical processes) minerals. Their sizes are generally below 10 µm and can reach up to mm scale for biogenic minerals (Eisma & Kalf, 1987; Schmidt et al., 2006; Zhang et al., 2017). The detrital minerals can be grouped into non-clay and clay minerals (kaolinite, chlorite, illite, smectite, vermiculite). The former are typically silicates (such as quartz, feldspars, amphibole, mica), (hydr)oxides and other minerals (gypsum). The most common biogenic minerals (carbonates and opal) are formed by plankton (diatoms, foraminifera, radiolaria, coccolithophores), bacteria and larger organisms (molluscs, sponges, corals).

The spatial distribution of suspended minerals is influenced by sediment sources on land, the transport paths from land to ocean by rivers, estuaries, glaciers and atmospheric inputs, coastal and seafloor erosion by currents and waves, and particle size. Biogenic minerals, in addition, are linked to a specific ecosystem during formation (James & Jones 2015). Authigenic minerals derive mainly from hydrothermal activities and volcanism in deep oceans (Chamley, 1989). Spatial variation in sediment composition in the oceans reflects, in addition to the above-mentioned pathways, also the biological productivity, particle sinking, carbonate dissolution at great depth, hydrothermal activity, and material transport along submarine canyons (Hayes, 2021). This distribution is to a certain extent a proxy of the suspended mineral composition, except in the deep basin, where most biogenic minerals are not preserved. Clay minerals are formed through chemical weathering, and this depends on latitude (Griffin et al., 1968; Rateev et al., 1969; Fagel, 2007). Kaolinite and smectite are today more prominent in the tropic-humid zone, while chlorite and illite are more common at moderate and high latitudes. This latitudinal signal in the distribution of clay minerals is, however, blurred by the erosion of geological layers or the presence of authigenic clays.

### *2.1.2. Organic Matter*

The OM fraction of SPM is a mix of living planktonic organisms (phytoplankton, bacteria, viruses, fungi, heterotrophic protists), detritus, exudates, and molecules originating from autochthonous and allochthonous sources (Arndt et al., 2013; Baumas & Bizic, 2024). The POM fraction of SPM is about 2.5 times higher than the POC content shown in Figure 2.1 (Leipe et al., 2011). At the molecular level, the major components of OM include carbohydrates, proteins, amino acids, lipids, and humic and nucleic acids (Kharbush et al., 2022). The stability of the OM varies between two extremes, from fast degradation within hours to days to preservation at geological time scales (Middelburg et al, 1993; Mayer, 1995; Baltar et al., 2021).

Phytoplankton are autotrophic organisms that include diatoms, dinoflagellates, radiolaria, ciliata and cyanobacteria. Many species are mixotrophic, meaning that they can take up organic carbon (OC) from their environment (Flynn et al., 2019; Koppelle et al., 2022; Kumar et al., 2024; Martens et al., 2024). Phytoplankton occurs as single cells, aggregates or flocs (Kiørboe et al., 1990). Bacterioplankton contains the archaeal and bacterial components of the plankton. They recycle high molecular weight compounds (proteins, polysaccharides, lipids) from the dissolved organic matter (DOM) pool, which are not accessible to most other organisms (Azam et al., 1983). The virioplankton interferes with the transfer of microbial POM to higher trophic levels (Wilhelm & Suttle, 1999). Viral lysis releases cell debris and newly produced viruses into the environment (Middelboe & Lyck, 2002; Middelboe & Jørgensen, 2006; Chen et al., 2021). Phytoplankton cell sizes range from less than 1 to 200 µm, bacterial cells are between 0.5 and 1 µm and giant viruses are in the range of 0.2 to 1.6 µm (Cole et al., 1988; Ducklow, 2001; Finkel et al., 2010; Hingamp et al., 2013). After their death, these microorganisms contribute to the POM pool as detritus.

Bacteria and phytoplankton produce exopolymeric substances (EPS), which are the main precursor of marine gels like transparent exopolymer particles (TEP). EPS production varies between species, growth phase, and environmental conditions (Passow, 2002; Bhaskar et al., 2005). EPS can be released by active exudation or passive leakage, viral or bacterial lysis, or sloppy feeding by zooplankton (Møller, 2007; Thornton, 2014). Marine gels like TEP play an important role in SPM dynamics as they have high stickiness and can enhance flocculation. TEP are also a rich substrate for microbes and subject to remineralization (Engel et al. 2020). Heterotrophic bacteria break down DOM and TEP into smaller molecules, which enhances the adsorption of DOM to mineral surfaces and contributes to the formation of refractory DOM (Jiao et al., 2010; Kleber et al., 2021).

## 2.2. Organo-mineral interactions

The interaction between minerals and OM is controlled by their cohesive and adhesive properties (Figure 2.3). These are caused by weak intermolecular forces such as hydrophobic and steric stabilization, polymeric bridging, hydrogen bonds, electric double layer (EDL) and van der Waals forces. The size, mineral composition, and the biophysical properties of the OM determine the types of interaction involved (Premuzic et al., 1982; Mayer, 1994). Clay minerals, due to their large specific surface area (SSA), small size and high cation exchange capabilities, have the highest cohesive properties of mineral particles (Whittaker et al., 2019; Cai et al., 2023). TEP and its precursor EPS form a large part of the aquatic OM, their stickiness is related to their hydrophobic characteristics and due to the presence of ionizable functional groups, such as sulfate half-ester and carboxyl groups, which form hydrogen bonds and metal ion bridges with alkaline earth ions like calcium (Mopper et al., 1995; Zhou et al., 1998; Chen et al., 2021; Walch et al., 2022).

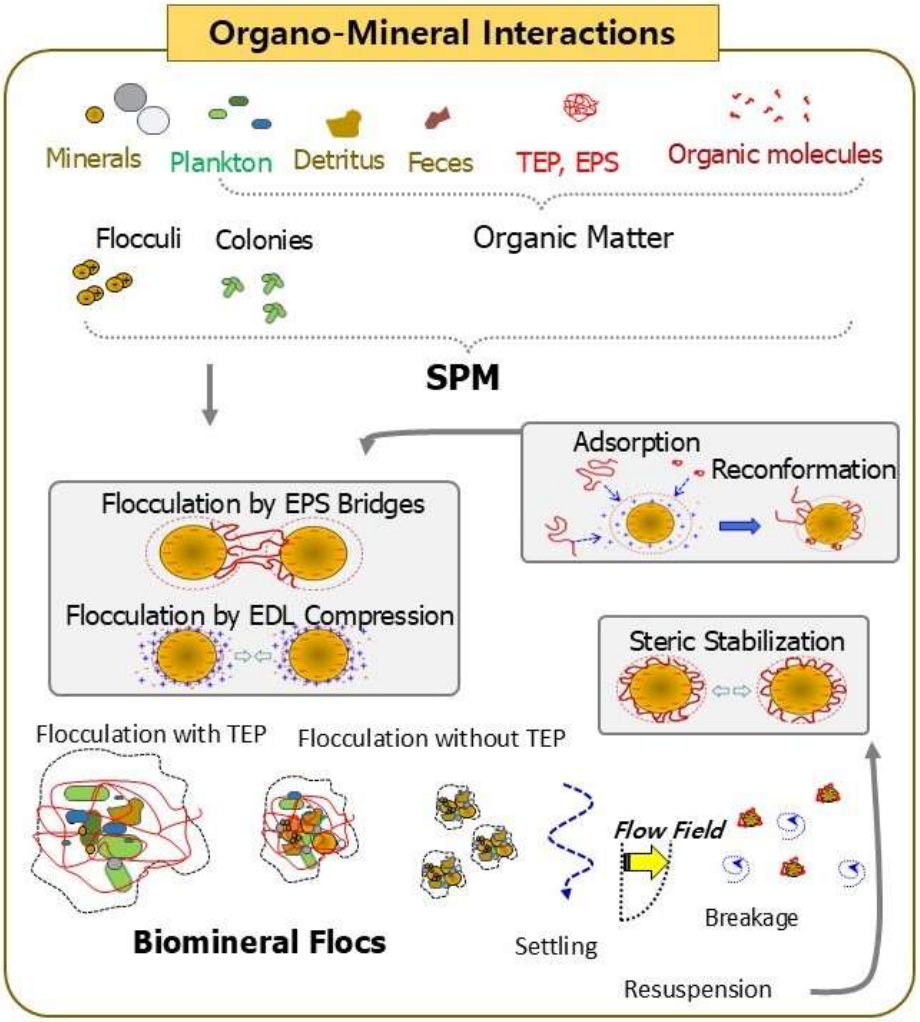


*Figure 2.3: The organo-mineral interactions comprise processes acting on molecular to nano scales (adsorption and reconformation, flocculation by EPS bridges and electric double layer compression) and micro to mm scales (collision, floc growth and break up by turbulence).*

### *2.2.1. Adsorption of organic matter to mineral surfaces*

The primary interaction between minerals and OM occurs on molecular to nano scales (Keil & Mayer; 2014; Deng et al., 2022). Organic molecules can be adsorbed onto mineral surfaces and become intercalated into the inner layers of swelling clay minerals, forming an organo-mineral particle (Dubbin et al., 2014). A strong positive correlation between the mineral SSA and the OC exists (Mayer, 1994; Keil & Mayer, 2014). Clay minerals have the largest SSA (smectite: 500-800 $m^2/g$; illite: 60-120 $m^2/g$; kaolinite: 10-20$m^2/g$) (Zhao et al., 2023); non clay minerals of clay size have a SSA of about 1 $m^2/g$. The mineral adsorbed OC in the SPM depends thus largely on the clay mineral composition, which varies along latitudes (see §2.1.1) and by local sources. For example, in the turbid nearshore of the North Sea (SPMC >30 mg/l) about 30% of the POC is adsorbed to mineral surfaces. This amount decreases towards the offshore in parallel with a decreasing clay mineral content (Fettweis et al., 2025).

Herman & Heip demonstrated systematic variation in POC:DOC ratios as a function of SPMC, suggesting important exchanges between particulate and dissolved pools through adsorption and desorption. Desorption of OM can lead to their further transformation and replacement by other organic molecules. Below 50 mg/l SPMC the POC:DOC ratios is well below 1, indicating a dominance of the dissolved fraction in the OM pool (Osterholz et al.,

2021), whereas ratios above 1 are found in higher turbid waters (Abril et al., 2002; Zhao & Gao, 2019), see Figure 2.4. In addition to adsorption and desorption, this SPMC dependency was also found to be due to photosynthesis and respiration, advection and diffusion, and resuspension and deposition (Fettweis et al., 2025).

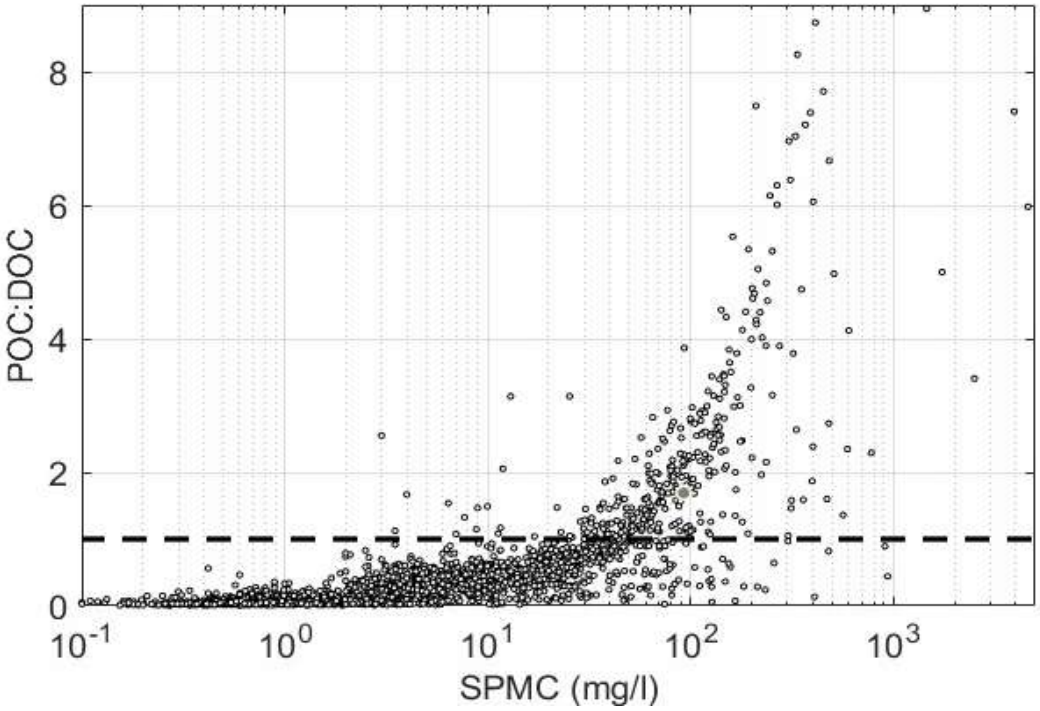


*Figure 2.4: POC:DOC ratio as a function of SPM concentration from rivers, estuaries, shelf seas and oceans (2821 data points). The dashed line indicates a ratio of 1. Data are from Belyaev et al. (2010a, 2010b, 2010c), Bouillon et al. (2009), Dellwig & Brumsack (2008), Fettweis et al. (2022, 2025), Kaiser et al. (2019), Malcolm & Durum (1976), Massicotte et al. (2023), Moreira-Turcq et al. (2003), Romankevich & Vetrov (2010b, 2010c), Seyler & Bonaventura (2001), Tammoh et al. (2012), Waniek et al. (2019, 2021, 2022), Zhang et al. (1992).*

### *2.2.2. Biomineral flocs*

The organo-mineral and organic particles (detritus, cells, TEP), both occurring in the clay to sand size range, are the building blocks (primary particles) of biomineral flocs (Figure 2.2). Clay minerals possess permanently net negative layer charges, resulting in repulsive forces between particles. These repulsive forces are overcome by the van der Waals attractive forces in the presence of cations or exopolymers (Partheniades 2009; Jiang et al., 2022; Abolfazli & Strom, 2023), resulting in the formation of relatively strong flocculi (Figures 2.2 & 2.3). A key parameter governing these interactions is the zeta potential, which reflects both the magnitude and sign of electrostatic surface charge. Particles with low zeta potential experience weaker repulsive forces, making them more prone to aggregation[119] (Mietta et al., 2009). Thus, the specific mineral composition and electrochemical behavior of particles are critical factors shaping the efficiency and stability of floc formation.

Flocculi are the smallest clay mineral-based aggregates of 10–20 µm in size that are hardly broken down to the primary particles (Lee et al., 2012; Tan et al., 2017). Micro- and macroflocs are composed of inorganic and organic particle assemblages that are held together by edge-to-face or edge-to-edge electrochemical bonds and by organic gels such as TEP. TEP gives flocs their strength and plastic nature (Droppo, 2001; Passow, 2002; Ye et al., 2023). Organic particles, like phytoplankton or bacterioplankton, can form colonies that

combine multiple cells into codependent aggregates. They can also be integrated into flocs (floc-attached) or occur as single cells (Jackson, 1990; Riebesell, 1991; Silori et al., 2025). In colonies, exudates are more concentrated and exchanges between mutualistic organisms are increased (Lürling, 2020). At the same time, colonies and flocs can act as protection against predators, pathogens and environmental stressors like UV, toxicants, or desiccation (Morris et al., 1995; Passow & Alldredge, 1999; Prieto et al., 2001; Vincent et al., 2021). In addition, due to the lower density of TEP compared to water (Azetsu-Scott & Passow, 2004) and depending on the presence of mineral particles, floc-attached phytoplankton can have a positive or negative buoyancy.

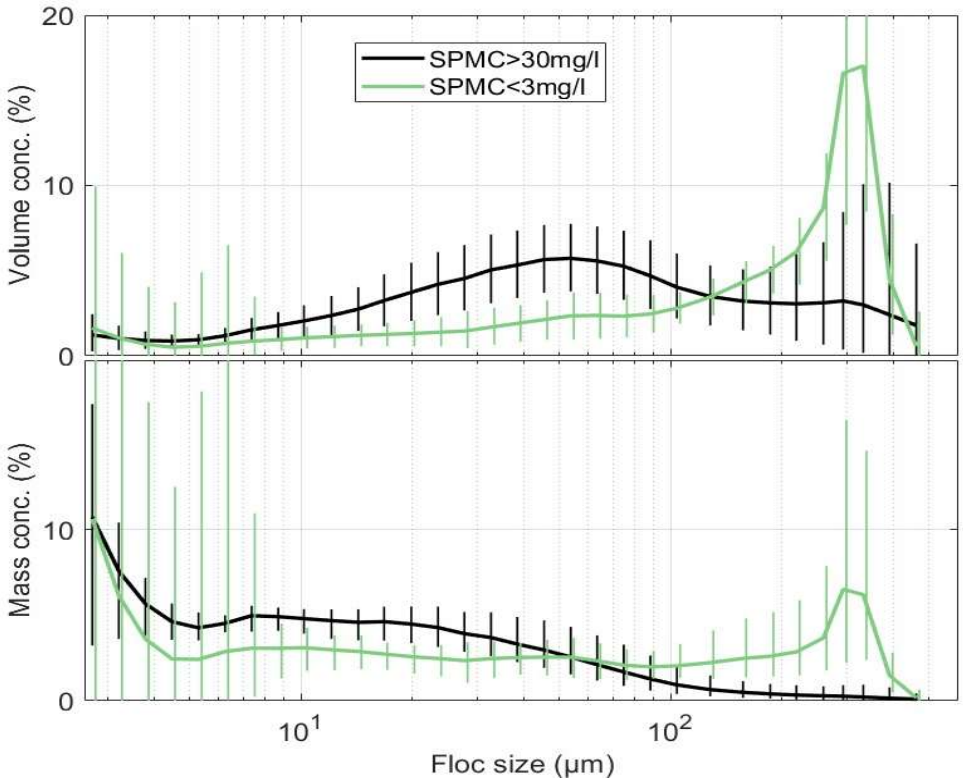


*Figure 2.5: Ensemble averaged size distribution by volume (above) and by mass (below) for two SPMC ranges (data are from Figure 2.1b). The volume/mass concentrations are normalized by dividing all values by the total volume/mass. The vertical lines are the geometric standard deviations.*

Flocculation is a dynamic balance between simultaneous collision of particles and flocs and breakup of flocs, which occurs across the µm to mm scale (Krone 1962; Fugate & Friedrichs, 2003; Winterwerp & van Kesteren 2004). Collision is caused by Brownian motion, which is relevant for the thermal diffusion of µm particles at low turbulence; turbulent motion, which is important at larger scales and differential settling, while floc breakup occurs at high turbulent shear (Eisma, 1986, Winterwerp, 1998). As a result, micro- and macroflocs can change size, density and shape due to variations in SPMC, shear stress and composition (Lee et al., 2012). The size of the flocs is also correlated to their composition (Figure 2.1) and to the lability of the OM. The latter explains seasonal variations in the size of biomineral flocs (Fettweis et al., 2022). The heterogeneity in composition and the variability on tidal to seasonal time scales results in floc size distributions (FSD) that are multimodal. Because larger flocs are fluffier, the FSDs differ for volume and mass. The distributions shown in Figure 2.5 are calculated from the data of Figure 2.1b; the conversion of volume to mass was done following the method of Fall et al. (2021). At low SPMC, the

FSD by volume is dominated by large particles comprising about 60% of the total volume but representing only about 25% of the mass. At high SPMC, the FSD by volume has a multimodal distribution with peaks around flocculi, microflocs and macroflocs, and only about 3% of the mass falls in the macrofloc size range. The largest part of the mass occurs in the microfloc, flocculi and primary particle size range, where the OM content is lower.

The relationship between shear stress and floc size in natural systems and the increasing proportion of organic matter at decreasing SPMC is shown in Figure 2.6. It is an adaptation of Dyer's model, which was based on lab experiments with turbulence and SPMC as variables. Dyer's results are only in agreement with those from natural systems, above about 10 mg/l, below which the OM content of the SPM increases significantly with SPMC (Figure 2.1). Flocculation has immediate effects on the physical properties of flocs like settling and transport (§2.3) and impacts biogeochemical processes (§2.5).

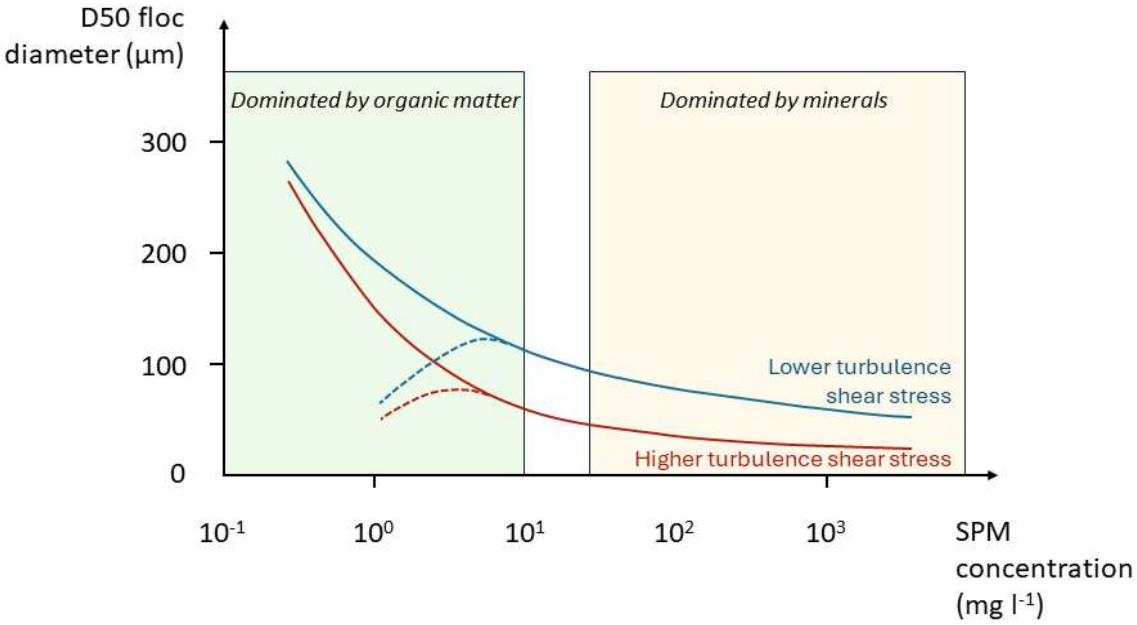


*Figure 2.6: Conceptual relationship between the median floc diameter and the SPMC under two different turbulent shear stress conditions, with dashed lines illustrating Dyers' results from experimental setup (adapted from* Dyer, 1989*), and solid lines illustrating results from field sampling (Figure 2.1).*

## 2.3. Influence of transport, settling and biology

In this chapter we describe how physical and biological processes affect the interaction between mineral and organic particles on various spatial and temporal scales (Figure 2.7).

### *2.3.1. Horizontal and vertical transport*

Transport processes have an impact on SPM concentration by moving particles. Advective particle transport occurs with the horizontal and vertical movement of water masses. The former is caused by large-scale wind-induced currents, tidal flows and river discharge. The latter exists in upwelling or downwelling areas, in estuaries where mixing of fresh- and seawater creates vertical circulation patterns and in wind induced vertical mixing[137] (Burchard et al. 2018). Turbulent and molecular diffusion is another transport mechanism of SPM. The latter acts at the nanometer scale and is driven, among others, by Brownian motion, whereas turbulent diffusion acts on the scales of turbulent eddies (from mm to hundreds of km) and can disperse particles over larger horizontal distances, making this the dominant mechanism for horizontal diffusion in most aquatic systems[138] (Thorpe, 2005).

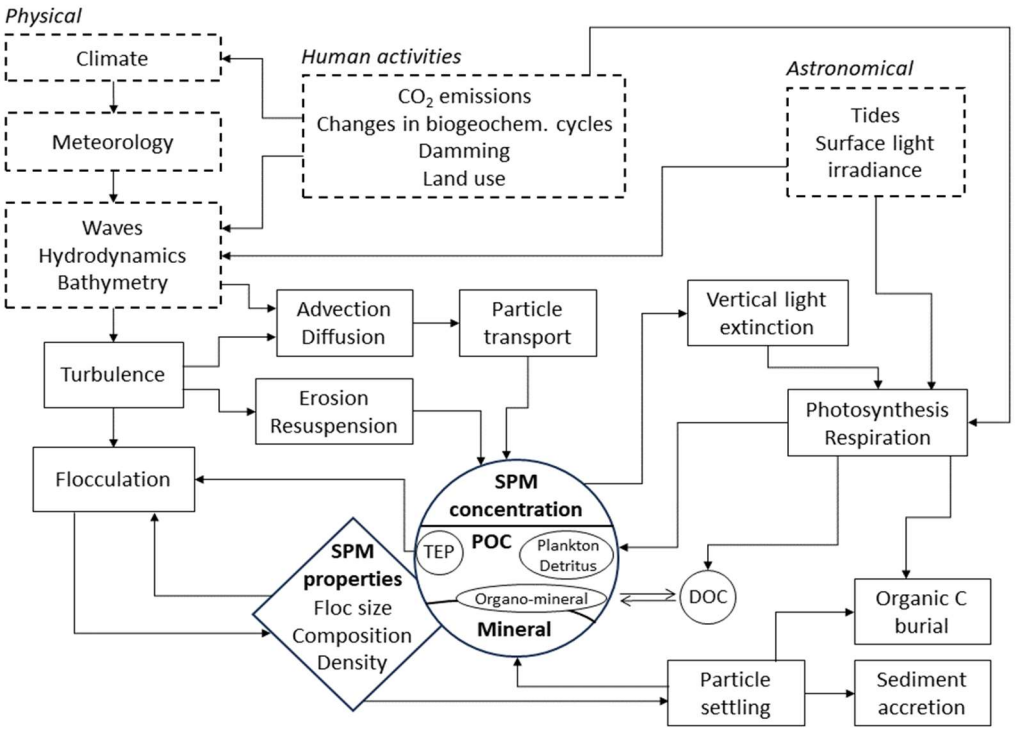


*Figure 2.7: Processes affecting the dynamics and biogeochemistry of SPM. Arrows mean 'has an influence on'; external drivers are framed with dashed lines, processes are framed with rectangles, and concentrations with rounded shapes.*

Turbulence is a major factor controlling the vertical movements of fine-grained particles. While moderate levels of turbulence permit flocculation in turbid areas, where the collision probability is significant, high levels of turbulence will result in floc breakup. The equilibrium floc size is proportional to the size of the smallest turbulent eddies, the so-called Kolmogorov microscale of turbulence (Eisma; 1986, Scully & Friederichs, 2007; Verney et al., 2009). As bathymetry controls the propagation of turbulent kinetic energy between the surface and bottom boundaries of the water column, it is a controlling factor of settling, resuspension and whether particles reach the surface. In shallow waters, there is typically an increased shear stress on the bed that enhances resuspension and thus increases SPMC. This effect decreases with increasing water depth, up to the point where the resuspended particles only remain in the lower layers (Maerz et al., 2016; Desmit et al., 2024). This has a profound effect on SPM composition (Figure 2.1). The enrichment of POC with decreasing SPMC occurs not only along the horizontal axis, but also in the water column (Silori et al., 2025). SPM at the water surface is thus enriched in POC, as the SPMC generally increases towards the bed. The reason for this behaviour is the occurrence of differential settling. During high turbulence, flocs are broken up, and the organic matter enriched particles, due to density differences, settle slower than the mineral enriched ones. This process explains also that light-limited turbid environments, such as coastal zones and estuaries, can have high primary production, because phytoplankton is enriched in the photic layer (Silori et al., 2025).

### *2.3.2. Settling and resuspension*

Vertical settling of SPM is influenced by its density, shape and size and can be described by Stokes' law in reasonable approximation, where the settling velocity of a single spherical and solid particle in a fluid is related to the viscosity of the fluid, the density of the particle and the particle size. This widely used relationship provides a fundamental understanding

of the settling behaviour of small particles (Lynch et al. 2014). Stokes' law is, however, not applicable to flocs. If we treat flocs as self-similar fractal structures (Kranenburg, 1994), which means that they have the same internal structure across different size scales, the settling velocity of the flocs can be calculated by relating the primary particle density and size to the floc properties using a dimensionless parameter called fractal dimension (Winterwerp, 1998). In this sense the fractal dimension is a measure of how primary particles fill the floc's volume; this approach provides a straightforward way to take into account floc properties in settling velocity. The fractal dimension ranges between 1.4 for very fragile flocs to about 2.4 for strong flocs (Dyer & Manning, 1999). Figure 2.8 shows that the density and the settling velocity of flocs increase with increasing SPMC. The figure does not show the occurrence of hindered settling above a concentration of a few g/l, which decreases the settling velocity (Dankers & Winterwerp, 2007). At low concentrations (< a few mg/l), large flocs (marine snow) have generally settling velocities below 1 mm/s (Asper, 1987; Alldredge et al. 1990; Berelson, 2001). However, TEP, due to its positive buoyancy and irregular shapes, can reduce the settling velocities of larger flocs (McDonnell & Buesseler, 2010; Chajwa et al., 2024).

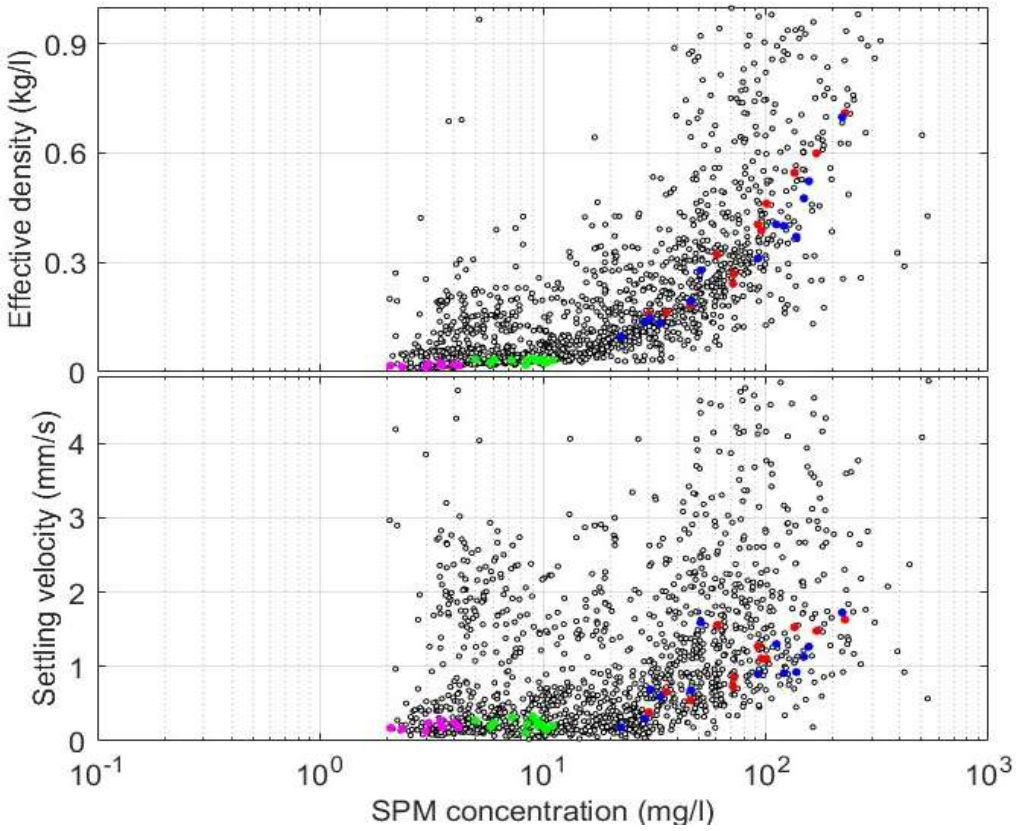


*Figure 2.8: Effective density and settling velocity* following Winterwerp (1998) *calculated for the data in Figure 2.1b assuming a fractal dimension between 2.2 (SPMC >30 mg/) and 1.9 (SPMC <3 mg/l). The coloured dots highlight data during single tidal cycles in high (red and blue) and low turbid areas (magenta and green dots).*

Particle settling and processes such as tides and waves, contribute to the formation of high SPMC layers just above the seafloor (nepheloid layer) in oceans, continental margins or shelf seas (McCave, 1986). Bed shear stress can keep particles in this layer for extended periods of time, allowing for long-distance transport depending on current velocity (Thorpe, 2005). In tidal environments, resuspension and deposition follow the ebb-flood and spring-neap tidal cycle. After settling, the flocs can remain on the bed during certain periods (0.25-

12 days), before being resuspended. This depends also on the presence of benthic fauna and flora that contribute to bed stabilisation or destabilisation (Stone et al., 2011). Flocs can change size while on the bed, but when resuspended they quickly revert to sizes that are in equilibrium with the local turbulence (Tran & Strom 2019). Based on the positive relationship linking settling velocity with particle size and density, denser particles will settle faster and will be transported over smaller horizontal distances than less dense particles of the same size, influencing the residual SPM transport. The latter depends further on the time a floc remains deposited, gravitational circulation induced by density gradients, ebb-flood asymmetry and tidal straining (Scully & Friederichs, 2007; Burchard et al., 2008; Geyer & MacCready, 2014).

### *2.3.3. Biological processes*

Microorganisms attached to flocs affect the settling velocity. Phytoplankton have developed adaptations to reduce their settling velocities. This includes cell surface protuberances that increase surface-to-volume ratios, ionic regulation of the cells' density, colony- or chain-formation, active swimming, the presence of inflatable gas vacuoles, and the excretion of mucilage (Walsby & Reynolds, 1980; Boyd & Gradmann, 2002; Laurenceau-Cornec et al., 2015; Gemmell et al., 2016; Arrieta et al., 2020). Mucilage with cross-linked polysaccharides immobilizes water, forming a gel of 98% water around the cell, which decreases the density of the particle, increases its size, and increases the viscosity at the cell-water interphase, all of which decrease the settling velocity. Mucilage can, however, only reduce the settling velocity, while the varying size of the gas vacuole can provide lift.

Biological processes can change floc size and composition. Filter feeders and zooplankton consume flocs and produce fecal pellets. Fecal pellets from zooplankton are compact, rapidly sinking excreta of different sizes that serve as important carriers of detritus, minerals, and microbial cells (Wilson et al., 2008; Kiørboe, 2011; Iversen et al., 2017; Burd, 2024). Zooplankton also exhibit sloppy feeding, where partially digested or unconsumed particles are released (Møller, 2005; 2007). Microbial degradation affects the OM content and thus the composition of particles and flocs. This process is affected by complex, yet poorly understood micro-scale ecological interactions within the particle community (Enke et al., 2018; Nguyen et al., 2022). In addition, the degree of microbial colonization alters the fine-scale morphology of aggregates, increasing drag and affecting settling velocities (Zhang et al., 2025).

## 2.4. Natural variability and system complexity

As this review summarizes and explains the processes shaping the relationship between POC content and SPMC in natural systems (Figure 2.1a), it is relevant to address the variability observed in the data. For low SPMC values, the range of POC content vary by two orders of magnitude, while it varies between <1 and 5% at high SPMCs. Similar variabilities are observed with plotting density, settling velocity and POC:DOC ratios as a function of SPMC. These variabilities can be assigned to regular (seasons, tides) and irregular (turbulence, spatial patchiness, meteorology) natural processes that give rise to additional complexity in the system, and to measurement errors.

SPM dynamics follow the trajectories of nonlinear chaotic systems (Sugihara & May, 1990). The observed variability is linked to the complexity of physical and biological processes and to our inability to fully capture the complexity of particles and flocs at appropriate temporal and spatial scales. Therefore, each measurement of SPM properties, and the derived parameters, can be seen as a random event selecting one outcome in a wide range of values (apparent stochasticity). Correlatively, measurements miss spatial and temporal representativeness. Only through the law of large numbers can statistically

meaningful relationships be obtained, such as the one in Figures 2.1, 2.4, 2.5 and 2.8. Beside that inherent complexity of the SPM dynamics, any error in the measurements will result in additional variabilities. The data in these figures have been collected through water sampling and by using sensors (LISST 100X). Uncertainties related to sampling and analytical procedures, i.e. the POC, DOC and SPM concentrations obtained from filtration and subsequent analysis, have been estimated. Uncertainties and limitations of sensor measurements, such as the floc size (Figure 2.1b) derived from laser diffraction technology (Agrawal & Pottsmith, 2000), are linked to the complexity of particle shapes and the occurrence of out-of-range particle sizes (Andrews et al., 2010; Graham et al., 2012). Thus, uncertainties linked to sampling, analysis and sensor measurements can reach high values, such as about 10% for excess density or 100% for settling velocity (Fettweis 2008).

To discriminate between analytical errors and natural variability, the measurement uncertainty can be compared to the observed total variance in the data. Fettweis et al. (2022) reported an uncertainty of SPMC measurements from about 10% (SPMC <5 mg/l) to about 3% (>100 mg/l). The POC measurements have an additional analytical uncertainty of 12%, resulting in an uncertainty of the POC:SPM ratio of about 24% at low and 15% at high SPMC. The observed variance in the POC:SPM ratio in Figure 2.1a (estimated as the difference of the P10 and P90 values and noted in % POC content of the SPM) is 20 (between 5 and 25 in % POC content of the SPM) at low and 5 (between 0 and 5 in % POC content of the SPM) at high SPMC (Table 2.1). The measuring uncertainty is thus lower by a factor of 4 to 5 than the observed variability across the range of SPMC. This means that other sources of variability, such as natural processes (seasonal variations, tides, biogeochemical cycles and the incomplete knowledge of microscale features of the particles and flocs themselves) and the complexity of the system (apparent stochasticity), are responsible for the largest part of the variability. Figures 2.1 and 2.8 show that during a tidal cycle the system tends to move along the expected curve following the increase and decrease of SPMC, while not reproducing the variability observed in the data. The variance due to seasonality in the POC content of the SPM has been modelled by Fettweis et al. (2022). They have shown that the seasonal variability in POC:SPM values between winter and spring is about 10 at low and 1 at high SPMC (both in % POC content of the SPM). This corresponds to 50% and 20% of the total variance, respectively. The remaining variability in POC:SPM ratio is then caused by the complexity of SPM dynamics and amounts to 5.2 at low and 3.25 at high SPMC (in % POC content of the SPM) or 26% and 65% of the total variance respectively. A comparable analysis can be found in Schartau et al. (2019).

*Table 2.1: Sources of variability in the POC:SPM ratio in Figure 2.1a (estimates expressed in % POC content of the SPM and in % of the total variability) for low (about 1 mg/l) and high (about 100 mg/l) SPMC.*

| | Low SPMC | High SPMC |
|---|---|---|
| Total variability | 20 | 5 |
| Measuring uncertainty | 4.8 (=24%) | 0.75 (=15%) |
| Seasonality | 10 (=50%) | 1 (=20%) |
| Complexity of the system | 5.2 (26%) | 3.25 (=65%) |

## 2.5. Implications for biogeochemical cycles

Particle-reactive chemical species, including nutrients, trace metals, and organic pollutants, can associate with mineral and organic particles. Their transport and fate are therefore intricately linked to SPM dynamics, which in turn contributes to determining biogeochemical cycles and ecosystem functioning.

### *2.5.1. Carbon*

Particle dynamics and the carbon cycle are complex and influence each other. A typical feedback loop is illustrated by marine gels influencing the vertical fluxes of particles, while the vertical and horizontal transport of particles determines the fate of the associated POC. Shelf seas play an important role in pumping atmospheric $CO_2$ (Laruelle et al., 2018), part of which is stored and exported in its dissolved form to the ocean (Thomas et al., 2004), or as OC associated with mineral surfaces in the sediments (Burdige, 2005; Keil & Mayer, 2014). Continental shelf and deltaic deposits are responsible for storing about 90% of preserved OC in the ocean (Hedges & Keil, 1995), corresponding to a burial of ~0.35 Pg C $yr^{-1}$ (organic and inorganic carbon; Regnier et al., 2013), although such estimates bear large uncertainty (Bauer et al., 2013), and patterns of preservation vary with the lateral source and receiving basin characteristics (Blair & Aller, 2012). Preserved OC is mostly associated with mineral surfaces (Keil et al., 1994) and contributes to the atmospheric balance between $O_2$ and $CO_2$ that controls the climate on geological time scales (Hemingway et al., 2019). In marine sediments, OC degradation varies not only with the nature of OC compounds but also with the physical and biogeochemical characteristics of the environment (La Rowe et al., 2020; Kleber et al., 2021). Rivers export approximately 0.15 to 0.24 Pg POC and 0.24 Pg DOC per year to the oceans (Hedges et al., 1997; Li et al. 2017). Yet, terrestrial OC is swiftly degraded in the marine system (Hedges et al., 1997; Bauer et al., 2013). Blattmann et al. (2019) have shown that phyllosilicate mineralogy determines the fate of this terrestrial OC. OC associated with smectite will quickly be desorbed into the DOC pool and replaced by its marine counterpart; whereas the OC associated with phyllosilicates from plutonic rocks is preserved in the ocean. The resuspension of settled POC in shelf seas can, in turn, foster the exchange of OC between the adsorbed and the dissolved fractions, thereby enriching the refractory pool of DOC in the water column (Liu et al., 2024). These processes highlight the link between OC and SPM dynamics, and the complexity of quantifying the pathways of OC preservation in marginal seas.

### *2.5.2. Other biogeochemical cycles*

Phosphorus, a key component of life and driver of photosynthesis (Westheimer, 1987), enters the aquatic system through volcanism, on the long term, and through soil erosion and direct inputs, on the short term, the latter becoming the dominant source under human pressure (Filipelli, 2008). Along the land-estuarine gradient, more than 90% of phosphorus is bound to SPM (Föllmi, 1996), making its transport and availability largely governed by SPM dynamics. Although it can be associated with mineral particles and with OM, its pathway is particularly linked to its adsorption to Fe (hydr)oxides (Froelich, 1988; van Raaphorst & Kloosterhuis, 1998; Compton et al., 2000). Changes in the physicochemical conditions along the estuarine–coastal gradient introduce complexities to the adsorption–desorption dynamics of phosphorus (Deborde et al., 2007; Némery & Garnier, 2007; Shen et al., 2008). Increasing salinity induces desorption of phosphates from Fe and Al (hydr)oxides, thereby increasing dissolved phosphorus concentrations (Wang & Li, 2010; Li et al., 2013). Anoxic bottom waters and sediments can accelerate the release of particle bound phosphates through the dissolution of Fe hydroxides, with reoxygenation reversing this effect (Middelburg & Levin, 2009; Mort et al., 2010; Hall et al., 2017). Under oxic

conditions, the co-precipitation of Fe hydroxides and phosphates can increase phosphorus retention in the sediment layer of estuaries, preventing their downstream transport (Wollast, 1982). At concentrations close to those found in coastal waters (1-5 µM), phosphate can also desorb from phosphorus-enriched sediment particles and return to the dissolved pool of the water column (Soetaert et al., 2006). These seasonal interactions between particles and phosphorus govern its transport along the estuarine gradient and its availability in coastal waters.

In contrast to phosphate, nitrate and nitrite exhibit limited affinity for SPM due to electrostatic repulsion from negatively charged mineral surfaces and organic functional groups. However, ammonium and organic nitrogen can associate with SPM through ionic bonding and more complex interaction mechanisms (Hedges & Keil, 1999; Tappin et al., 2010). Consequently, particulate organic nitrogen constitutes over 50% of the total annual nitrogen flux transported by rivers globally (Tappin, 2002). Like phosphorus, studies report increased desorption of nitrogen cations from sediments in saline waters, due to increased competition from metal cations for particle exchange sites (Morin & Morse, 1999; Fitzsimons et al., 2006). Flocs play a critical role in nitrogen cycling as their surface and inner core may offer adjacent oxic and anoxic niches for microbial communities (Liu et al., 2013; Xia et al., 2017; Sanders & Laanbroek, 2018; Zhu et al., 2018). This coexistence of aerobic and anaerobic microenvironments on the same floc facilitates the coupling of nitrification (aerobic process) with denitrification (anaerobic). Evidence suggests that higher SPMC can enhance denitrification or coupled nitrification-denitrification rates (Xia et al., 2017, Zeng et al., 2018), leading to both $N_2$ loss and the production of nitrous oxide ($N_2O$), a potent greenhouse gas and stratospheric ozone-depleting substance (Schulz et al., 2022b; Wan et al., 2023).

### *2.5.3. Contaminant transport*

Persistent organic pollutants (POPs), such as organochlorine pesticides, polyaromatic hydrocarbons are highly stable organic compounds. With minimal dissolution in water, POPs tend to accumulate on solid surfaces, primarily associated with OM (Zhou et al., 2000; Tolosa et al., 2004). Hence, their binding affinity is strongly influenced by the characteristics of the OM, such as aromaticity and polarity (Sobek et al., 2004; Ahmed et al., 2015). POP sorption generally increases with salinity due to salting-out (Turner, 2003). In recent decades, growing concern has emerged over a diverse group of pollutants collectively termed emerging contaminants**,** which include novel entities, such as pharmaceutical residues, halogenated flame retardants, and micro- and nanoplastics (Steffen et al., 2015). Studies indicate a wide range of interactions and preservation mechanisms for these contaminants in sediments, making it difficult to establish a generalized pattern of their associations with particles (Cantwell et al., 2016; Thiebault et al., 2017). While some pollutants exhibit a strong affinity for OM and minerals (Guo et al., 2018; Berbel et al., 2021), others display higher water solubility, reducing their sequestration potential in estuaries (Cantwell et al., 2016; Celis-Hernandez et al., 2020). Furthermore, microplastics are increasingly recognized as a component of SPM (Ho et al., 2022). Their fluxes remain, however, uncertain as riverine inputs far exceed observed oceanic accumulation (Lopez et al., 2021; Weiss et al., 2021). This discrepancy has prompted investigations into the role of flocculation and settling processes in estuarine and coastal waters. Studies indicate that buoyant microplastics can aggregate with other SPM constituents, leading to settling and deposition (Laursen et al., 2022; Wu et al., 2024). Although trace metals, such as Cu, Fe, Mn and Zn, have low concentrations, they serve as essential micronutrients for phytoplankton, while others, including Cd, Hg, and Pb, can be toxic (Morel & Price, 2003; Twining & Baines, 2013). Trace metals bind reversibly with a wide range of compounds, such as carbonates,

clays, Fe and Mn (hydr)oxides, POC and colloidal OC, and can be uptaken by phytoplankton (Bianchi, 2007; Petit et al., 2009). In aquatic systems, metal complexation with DOM is a dominant process controlling trace metal concentrations, distribution, and fate (Tang et al., 2002; Whitby et al., 2024). While DOM complexation maintains trace metals in solution by altering their speciation, DOM adsorption onto particles enhances metal association with SPM. Functional groups such as -COOH, -OH, $-SR_2$, and $-NR_2$ (R = $-CH_2$ or -H) are primarily responsible for complexation with trace metals (Hering & Morel, 1989). Environmental factors such as salinity, pH, and redox conditions influence the association of trace metals with dissolved and particulate phases (Wen et al., 1999,). Although trace metal partitioning decreases with increasing SPMC, the intrinsic particle properties are the major controlling factor (Benoit et al., 1994; Tang et al., 2002; Cindrić et al., 2015).

## 2.6. Human activities and climate change

Human activities including climate change have clearly modified the SPM fluxes towards the oceans by changing the residence time, concentration, and composition of SPM along the land-ocean continuum, resulting in often contradictory changes of the SPMC and thus also of the POC concentration (Figure 2.1).

### *2.6.1. Human activities affecting SPM characteristics*

Important anthropogenic impacts on SPM fluxes are due to dam constructions and land use change. On the global scale, over 60,000 large dams have trapped an estimated 3,200 Pg of sediments since 1950 (Syvitski et al., 2019), which has led to a 49% reduction in SPM delivery to the coastal ocean (Dethier et al., 2022). This also has consequences for the POC fluxes and composition towards the oceans. For instance, Lu et al. (2023) report that dam construction in the Yellow river has intercepted the old petrogenic POC from the Loess Plateau and enhanced the downstream younger biospheric POC fluxes towards the coast. On the other hand, Regnier et al. (2013)pinpointed how human activities have increased the export of OC from land to sea by 0.1 Pg per year since pre-industrial times. The resulting net land-ocean perturbation in carbon flux is relatively small due to offsetting processes like outgassing and burial within the river system. Given the estimates of POC and DOC export from rivers to the oceans (Li et al., 2017; see §2.5.1), this human induced increase represents about 20% of the total OC flux from land to ocean.

Despite these globally decreasing SPM fluxes, opposite trends are observed regionally. For example, in tropical regions, especially within 20°S-20°N, SPM fluxes are rising due to much lower dam infrastructure development concomitant with urban development, agricultural expansion, riverbank erosion and widespread land use changes (Dethier et al., 2022). Notable examples include rivers in the Amazon basin, where deforestation have amplified sediment loads (Latrubesse et al., 2009), as well as various other south American and southeast Asian rivers which have been affected by cropland expansion (Restrepo & Syvitski, 2006; Dislich et al., 2017). Sediment mining represents another anthropogenic driver of SPM and POC fluxes. It can increase SPMC by destabilizing riverbanks and channel morphology or by the release of particles into the water column during dredging operations (Spearman, 2015; Hackney et al., 2020). These activities remobilize previously stored sediment and OC with consequences on marine and coastal ecosystems that remain little-known.

In estuarine and marine environments, SPM characteristics are impacted by additional activities such as deepening of navigation channels, dredging, and dumping, trawling, offshore wind farms, artificial islands, land reclamation, and aquaculture. For example, the North Sea is today more turbid than 100 years ago due to these activities (Capuzzo et al., 2015). In estuaries, channel deepening/straightening and reclamation of intertidal areas

have led to an increase in tidal asymmetry and in landward SPM transport due to tidal pumping (van Maren et al., 2015; Cox et al., 2019). Land reclamation can lead to loss of sediment sinks and thus increasing SPMC (Flemming & Nyandwi, 1994; van Maren et al., 2016). In contrast, on shelf seas, effects of these activities remain local and modest beyond the impacted area (Spearman, 2015). However, if the scale of the activity is large (such as offshore wind farms in the North Sea, trawling) it can lead to changes on basin scales (Capuzzo et al., 2015; Daewel et al., 2022).

### *2.6.2. Impact of changing climate on SPM characteristics*

Climate change due to anthropogenic greenhouse gas emissions alters hydrological regimes, intensifies extreme weather, and accelerates glacial retreat all of which affect SPM fluxes. Sea level rise (SLR), which has accelerated from 0.3 mm/yr over the past 4,000 years to approximately 3.7 mm/yr today (Nerem et al., 2018; Fox-Kemper et al., 2021), exacerbates coastal erosion and inundation. This rapid change, when compounded by human impacts, can compromise the sediment budget necessary for maintaining elevation in deltas, estuaries, and their intrinsic ecosystems. For example, recent research demonstrates that sediment availability is already limited in the Wadden Sea (Colina Alonso et al., 2024). In North America, SLR has already outpaced sediment accumulation in subsiding low-lying coastal zones such as the Mississippi delta (Jankowski et al., 2017; Rodriguez et al. 2020; Törnqvist et al., 2020). A quarter of all sandy shorelines worldwide are currently eroding, driven by insufficient sediment availability, increased storm frequencies and coastal constructions, a trend which is likely to accelerate in the future (Vousdoukas et al., 2020). At interannual timescales, climate fluctuations such as the El Niño–Southern Oscillation exert strong control over riverine SPM fluxes, as evidenced in rivers in east and southeast Asia and South America[256, 257, 258] (Wang et al., 2011; Restrepo et al., 2015; Schuerch et al., 2016). Rising temperatures are expected to impact SPM fluxes toward the sea (Syvitski et al. 2022). Permafrost and riverbed thaws begin to mobilize previously locked-in sediments, enhancing SPM transport and reducing phytoplankton blooms due to decreasing light availability (Kokelj et al., 2013; Farquharson et al., 2019; Szeligowska et al., 2024). For example, SPM delivery from Greenland towards the ocean is today about 56% higher than during the period 1961-1990 (Overeem et al., 2017).

### *2.6.3. Geographic and latitudinal variability*

Geographic and latitudinal variation plays a significant role in determining the net outcome of anthropogenic activities and climate change on SPM and POC fluxes. In high latitude regions, warming-driven glacial retreat and permafrost thaw dominate. The Arctic's changing cryosphere leads to increased sediment delivery and carbon burial to the coast, giving rise to SPM "hotspots" (Syvitski et al., 2022). In mid-latitude regions, SPM dynamics often reflect a complex balance between reduced riverine input due to dams and increased sediment delivery from intensifying land use and urban runoff (Dethier et al., 2022). Large river systems are heavily dammed, reducing their SPM export, yet their deltas and nearby shoreline areas continue to receive sediments from tributaries, legacy deposits, and land use activities (Nienhuis et al., 2020; Rodriguez et al., 2020). Low-latitude tropical river basins exhibit high SPMC due to intense rainfall, steep topography, and widespread land use change (Dethier et al., 2022). These rivers contribute disproportionately to global SPM loads. POC fluxes mirror these changes, where (sub)tropical rivers contribute disproportionately to global POC flux due to high productivity and erosion rates (Cai, 2011). In sum, SPM and POC dynamics in the anthropocene reflect a profound reorganization of Earth's sediment cycle.

## 2.7. Future needs and perspectives

We have shown that SPM concentration and composition can be used as an indicator for the balance between physical (turbulence) and biogeochemical processes (production, remineralization). High SPM concentration coincides with the dominance of mineral particles and the occurrence of biomineral flocs. These high turbidity zones, generally located nearshore or in estuaries, are characterized by strong tidal currents, intensive resuspension and settling, flocculation in phase with the tides and high primary productions. With decreasing SPM concentration organic matter becomes more dominant and biological flocs are getting more prominent. Physical processes are less important, and flocculation occurs on seasonal time scales. The seasonal variation in primary production influences the balance between the physical and biogeochemical processes as the composition and thus also the lability of organic matter changes. The latter depends not only on the composition but also on the environmental conditions. It may range from high, for example living cells, to low, for example organo-mineral association (Ittekkot, 1988; Mayer, 1994; Etcheber et al., 2007; Arndt et al., 2013; Singh et al., 2016; Hemingway et al., 2019). The more labile the OM is, the larger the biomineral flocs may become in high turbidity areas (Fettweis et al., 2022).

To date, our understanding of the physical influence of turbulent shear, concentration, collision rate, salinity to the floc size, density and settling velocity is relatively robust (Winterwerp, 1998; McAnally & Mehta, 2000; Verney et al., 2011, Ho et al., 2022). Also, the understanding of biological processes that affect suspended particles is relatively robust. There is, however, a need to better understand and model the impact of biological activities such as growth, metabolism and decay of microorganisms on flocculation processes and vice versa to predict the SPM flux, more specifically the fate and flux of minerals, carbon, pollutants and microplastics.

### *2.7.1. Monitoring*

The objective of monitoring the concentration and composition of particles is to understand the biogeochemical processes in aquatic systems and to evaluate the ecological status of an area. The data are further needed to quantify variations at different time scales, understanding the element cycles and their underlying processes and validating model predictions related to major trends such as global warming or the discharge of nutrients into the sea. Improving the in situ measurements by enlarging the number of parameters, as well as measuring frequency and duration, and increasing the accuracy should be a continuous goal (Sugihara & May, 1990; Fettweis et al. 2023). This has always led to an increased understanding of the processes and has served as a means for calibration and validation of more complex numerical models.

Figures 2.1, 2.3, 2.6 and 2.7 show that measuring only SPM concentration is sufficient for a first characterization of SPM composition, density and settling velocity, as well as the DOC concentration. Measurements of SPM concentration are well established and are done by water sampling and filtration or with acoustic and optic sensor measurements (e.g. Fettweis et al., 2019). Lower uncertainty in the composition is obtained when measuring the mineral and organic fractions separately. Traditionally this relies on water sampling (POC, PON, DOC, pigments, microscopy) and on optical (fluorimeter, flow cytometry or particle cameras) and acoustic sensors or instruments (e.g., Erickson et al., 2011; Haynes et al., 2016; van der Hout et al., 2017; Tran et al., 2024). The amount of OM associated with minerals can be determined straightforwardly by bulk and clay mineralogical analysis (e.g. Środoń et al., 2001; Zeelmaekers et al., 2015) and the measurement of the specific surface area (Macht et al., 2011; Zhu et al., 2015), however such data are rare and do not sufficiently resolve temporal and spatial scales of aquatic systems. The lability of the OM (fresh -

refractory) is difficult to measure and requires extended analytical methods (Hellings et al., 1999; Zander et al. 2020).

New insights into the dynamics of particles will require a quantification of the temporal and spatial variation of the organic and mineral substances in the SPM. Better characterisation of the composition is further needed in the benthic boundary layer, where solid grains (silt and sand sized) may become part of the SPM and where physical processes (turbulence suppression) are affected by the very high SPM concentrations (Toorman, 2011). SPM concentration in shallow areas is largely controlled by resuspension and deposition and asks for a method to distinguish between sand and flocs, especially in the benthic boundary layer, where solid grains (silt and sand sized) may become part of the SPM. The use of acoustic and optical sensors in parallel provides perspectives, see Pearson et al. (2020) and Tran et al. (2024). Characterisation and quantification of the OM is needed for the labile fraction, such as the plankton species succession and biomass and the timing and quantity of marine gel and DOM production as well as of the refractory fraction. The latter incorporates the characterisation of organic detritus and organo-mineral adsorptions. The lability of the OM is a key parameter in biological numerical models or in carbon cycle studies (see below) and can be measured based on the specification of POM and DOM with respect to molecular weight (Kellerman et al., 2015; Canuel & Hardison 2016; Lee et al., 2019).

Transport of SPM is controlled by several factors, including settling velocity (amongst others), which varies according to SPM concentration and composition. Settling velocity can be directly or indirectly (see Figure 2.8) be measured (Puls & Kühl, 1995; Manning et al. 2002; van Rijn et al., 2024). However, large quantities of data of the settling velocities of individual particles/flocs in the SPM is needed to better quantify vertical transport through differential settling and to distinguish between settleable and non settleable fractions.

### *2.7.2. Modelling*

Numerical models can be useful tools to study the complex interactions and dynamics related to organo-mineral flocs, if both physical and biological factors are integrated. Particle aggregation processes in aquatic systems were first mathematically formalized by Smoluchowski in the early 20th century for colloidal systems (Smoluchowski, 1916). In oceanography, while the mathematical frameworks primarily originate from this physical aggregation theory, they have been adapted to address two major domains: the dynamics of marine organic aggregates (such as marine snow) and the behavior of mineral particles (controlling sediment transport and water clarity in coastal systems). Though these domains share common fundamental principles in describing particle interactions and size evolution, they have historically developed different modeling approaches due to their distinct focus and applications. Traditional floc models primarily focus on mineral particles, neglecting the critical role of biological matter, such as EPS and TEP, and active microorganisms (Ye et al., 2023; Deng et al., 2023; Parrella et al., 2024). Conversely, planktonic models usually emphasize nutrient-related phytoplankton activities and aggregation processes, seldom considering their interactions with inorganic particles (e.g., Kriest et al., 1999; Jackson et al., 2005; Kerimoglu et al., 2022). This conventional bias within mineral-based and biological aggregation models has limited the insights of how the organo-mineral flocs form and transport in natural waters.

In the biological domain, the interest in including aggregation processes was mainly focused on its effect on phytoplankton bloom dynamics (including their termination) or the distribution and characteristics of sinking particles like marine snow. Early modeling works incorporated coagulation (aggregation) processes and/or organic aggregates into plankton dynamics models without detailed or mechanistic description of the aggregation processes

(e.g., Jackson, 1990; Kriest and Evans, 1999). Then, since their description in the 1990's (Alldredge et al., 1993), TEP, which increase particle adhesion through their sticky nature, have emerged as key mediators in the aggregation processes and were progressively included into biogeochemical models. Schartau et al. (2007) developed a low-complexity numerical model specifically addressing carbon overconsumption and TEP formation, describing two distinct modes of carbon overconsumption - DOC exudation during phytoplankton growth and POC production under nutrient limitation - while introducing explicit TEP formation through coagulation of dissolved organic matter. Oguz (2017) integrated particle aggregation dynamics with pelagic ecosystem structure, considering two TEP size classes and their interactions with the food web. More recently, Kerimoglu et al. (2022) presented an intermediate-complexity model incorporating TEP formation through coalescence of dissolved organic matter in different size classes, their aggregation with phytoplankton and bacterial cells, and subsequent formation of larger aggregates, particularly emphasizing the interactions between nutrient stress, TEP production, and aggregation processes having an effect on the diatom bloom termination in a mesocosm study.

In parallel, mineral particle aggregation modeling has developed along different lines, addressing both in situ-related scientific questions and practical applications like wastewater treatment. In this field, which has a particular focus on resolving observed size spectra, computational cost of the models is an important constraint to the realism and potential applications of the various approaches. Various methodologies have emerged, each with distinct trade-offs. Simplified Lagrangian models (Winterwerp, 1998; Maggi, 2009; Kuprenas et al., 2018; Safar et al., 2023; Cui et al., 2023; Jalón-Rojas et al., 2024) track a single size class and are computationally efficient, making them suitable for large-scale simulations (Escobar et al., 2023; Nghiem et al., 2024), but they fail to simulate the multipeak nature of floc size distributions. The Lattice Boltzmann Model offers more detailed insights by explicitly simulating fluid-particle interactions and capturing detailed flocculation dynamics including particle collisions and breakage behavior, but its high computational demands typically limit applications to small-scale simulations (Ladd, 1994; Kim and Stolzenbach, 2004; Zhang et al., 2013; Yu et al., 2024). Population balance models (PBM) have emerged as a comprehensive approach to representing floc size distributions (Smoluchowski, 1917; Ramkrishna & Singh, 2014; Nguyen et al., 2016; Jeldres et al., 2018; Penaloza-Giraldo et al., 2023; Shettigar et al., 2024), solving integro-partial differential equations that couple aggregation and breakage processes by discretization or class methods (Kumar & Ramkrishna, 1996; Lee et al., 2011; Shen et al., 2018), moment methods (Marchisio et al., 2003; Prat & Ducoste, 2006; Su et al., 2007; Shen et al., 2019), or Monte Carlo methods (Khelifa & Hill, 2006; Zhu et al., 2022; Sewerin, 2024), at an acceptable computational cost. Pursuing the same goal of minimizing computational cost while representing elaborate size distribution dynamics, distribution-based models have also emerged next to size class-based models (Maerz & Wirtz, 2009; Maerz et al., 2011).

Despite these parallel developments in both biological and mineral aggregation modeling, and although the heterogeneous composition of flocs is well acknowledged (Ho et al., 2022), existing models do not effectively integrate EPS-TEP dynamics with biological-mineral aggregation processes. While recent attempts have introduced biological variables into traditional floc models (Maggi, 2009; Zhu et al., 2022; Bai et al., 2024), a truly integrated approach combining both organic and mineral fully resolved dynamics remains to be achieved. This separation between approaches remains a significant limitation given the intrinsically heterogeneous nature of marine aggregates, suggesting an important direction for future model developments. Indeed, current modeling work evidenced interesting

feedback loops with biologically driven changes in aggregation properties of mineral particles affecting their transport dynamics which, in return, affect the biological growth through the effect on the water clarity in highly turbid coastal waters. Moreover, while mechanistic flocculation models perform well for short-term simulations or within areas of similar turbidity, they require adjustments of parameters like flocculation efficiency to account for seasonal variations and changing SPM concentrations. The integration of biological and mineral approaches is therefore particularly crucial for long-term and large-scale modeling across nearshore-offshore gradients, where biological influences on flocculation vary significantly both spatially and temporally. These interactions between biological and mineral processes can significantly impact our estimation of carbon fluxes, particularly in coastal waters where they affect both the transport of organic matter and the light availability for primary production.

The development of integrated biological-mineral models necessitates comprehensive datasets that simultaneously capture multiple aspects of flocculation processes. While floc size distributions remain fundamental measurements, they need to be complemented by systematic quantification of biological components, particularly EPS and TEP concentrations, along with their chemical characterization. Traditional measurements like chlorophyll-a would benefit from enhanced spatial and temporal resolution, with particular attention to their vertical distribution and their partitioning between water column and floc-attached forms (see Silori et al., 2025). This is crucial for understanding the dynamic coupling between suspended particles and biological processes. The growing evidence for EPS/TEP's significant influence on suspended particulate matter dynamics (Fettweis et al., 2022) highlights several key data requirements. First, the physiological regulation of EPS/TEP production needs more detailed investigation across different phytoplankton species and under varying environmental conditions. Second, the role of different plankton functional groups in EPS/TEP dynamics requires systematic study - from bacterial degradation to zooplankton modification of these substances. These data are essential for developing and validating biogeochemical models that can accurately represent these processes. Advanced analytical techniques can significantly contribute to building these integrated datasets. Flow cytometry can provide high-frequency data on particle characteristics and biological community composition. Similarly, automated scanning imagery techniques offer detailed information about particle morphology and associated biological components. When combined with traditional measurements, these approaches can provide the multi-parameter datasets needed to constrain and evaluate next-generation coupled biological-mineral models. Additionally, controlled laboratory experiments focusing on specific process interactions (e.g., mineral-EPS binding kinetics, biological modification of floc properties) remain crucial for parameterizing these complex interactions.

## 2.8. Summary

This review provides a transdisciplinary approach to particle dynamics bridging physical and biological processes in aquatic environments. From a physical point of view, interest in the past has mainly focused on cohesive sediment dynamics in estuaries and coastal areas. From a biological point of view, interest has mainly focused on phytoplankton bloom dynamics and on the characteristics of sinking organic particles such as marine snow. Currently, both perspectives are merging as is reflected in Figure 2.1. The decrease in floc size and POC content with increasing SPMC follows a general relationship common to aquatic ecosystems around the globe; it is not influenced by human activities or climate change. The latter, instead, shifts SPM characteristics along the curve, without changing the general curve. Figure 2.1 shows that SPMC can be used as an indicator for their

characteristics (composition, size, density,…), which fundamentally depend on the relative importance of physical (turbulence) and biogeochemical processes (production, remineralization). Knowing the SPMC is thus sufficient for a reasonable estimate of the SPM composition, density and settling velocity, as well as the DOC concentrations. However, future work must recognize that natural processes and the complexity of the system are responsible for the largest part of the observed variability in the measured parameters.

New insights into particle dynamics will require a quantification of the temporal and spatial variation in the organic and mineral substances in the SPM. Given the heterogeneous composition of flocs, only integrated approaches will increase the understanding of flocculation processes involving both organic and mineral particles[165, 266, 267] (Enke et al., 2018; Zhu et al., 2022; Bai et al., 2024). This necessitates comprehensive datasets that simultaneously capture multiple aspects of organo-mineral interactions at various temporal and spatial scales. While SPMC, POC concentration and floc size distributions remain fundamental measurements, they need to be complemented by systematic quantification of organic and mineralogical components along with their chemical characterization. Traditional measurements like chlorophyll-a would benefit from enhanced spatial and temporal resolution, with particular attention to their vertical distribution and their partitioning between water column and floc-attached forms. The growing evidence for TEP's influence on SPM dynamics highlights several key data requirements. First, the physiological regulation of TEP production needs more detailed investigation across different phytoplankton species and under varying environmental conditions. Second, the role of different plankton functional groups in TEP dynamics requires systematic study - from bacterial degradation to zooplankton modification of these substances. Advanced analytical techniques can contribute to building these integrated datasets. Flow cytometry can provide high-frequency data on particle characteristics and biological community composition. Similarly, automated scanning imagery techniques offer detailed information about particle morphology and associated biological components. When combined with traditional measurements, these approaches can provide the multi-parameter datasets needed to constrain and evaluate next-generation coupled biological-mineral models. Additionally, controlled laboratory experiments focusing on specific process interactions (mineral-EPS binding kinetics, biological modification of floc properties) remain crucial for parameterizing these complex interactions. Better characterisation of the composition is further needed in the benthic boundary layer, where solid grains (silt and sand sized) can become part of the SPM and where physical processes (turbulence suppression) are affected by the very high SPM concentrations.

# 3. Evaluating sediment plume characteristics from dredging and dumping operations

In recent decades, dredging activities have significantly increased in the southern North Sea and the English Channel (ICES 2019; Wilson & Heath, 2019) a region within the NW European marine continental shelf already facing substantial human pressures such as fishing, shipping, offshore wind farms, aquaculture and undersea cables. The removal of sediments inevitably is of major concern as it disrupts the benthic environments and releases particles into the water column (Boyd et al., 2003; Robinson et al., 2005; Cooper et al., 2007; Cooper et al., 2011; Wyns et al., 2021; Kint et al., 2023). The latter is manifested by two types of plumes: a surface one due to overflow of mainly fine sediments from the dredging vessel or a benthic one due to dumping operation itself and the disturbance of the seabed by the drag head (Duclos et al., 2013; Decrop et al., 2015; Spearman, 2015). Dredging overflow occurs at the dredging site during operations, primarily to enhance the dredger's capacity by permitting excess water, along with suspended fine sediments, to overflow, thereby retaining coarser material in the hopper. In contrast, the disposal of dredged material takes place following the dredging process, once the collected material has been transported to a designated disposal site, it is intentionally released. This release of material can have several environmental impacts. For example, an increase of the SPM concentration (SPMC), may modulate primary production, affect trophic interactions and food webs, alter the composition of surface sediments and influences the benthic-pelagic coupling, the biogeochemical cycles and the transport of contaminants (Boyd et al., 2003; Cloern & Jassby, 2012; Cutroneo et al., 2012; Duclos et al., 2013; Jones et al., 2016; Caballero et al., 2018). Further, higher SPMC due to dumping of dredged material may increase the accumulation of sediments in ports and navigation channels and thus of the dredging volumes, with economic and environmental drawbacks (Cox et al., 2019; Fettweis et al., 2016). The impacts of dredging and disposal are highly site-specific, requiring a detailed understanding of local conditions to accurately assess their environmental consequences (Van Lancker et al., 2010).

The European Union's Water Framework Directive (2000/60/EC) and Marine Strategy Framework Directive (2008/56/EC) recognize changes in SPMC caused by human activities as a significant environmental issue (Borja, 2006). To comply with international guidelines set at the Earth Summits in Rio de Janeiro (1992) and Johannesburg (2002) within the Integrated Coastal Zone Management framework, it's essential to better grasp the physical impacts of dredging on the seafloor and marine ecosystems (Duclos et al., 2013; Vander Velpen et al., 2022). The international framework for dumping at sea of dredged material is the (regional) OSPAR Convention (1992) and the (worldwide) London Convention (1972) and Protocol (1996). These conventions and their associated guidelines consider the presence of any contaminants within the sediment and whether some alternative beneficial use is possible. In implementing these guidelines, e.g. action levels (sediment quality criteria) must be defined, dumping sites must be chosen and a permanent monitoring and research program must be carried out. Recently, the Marine Strategy Framework Directive (EC-MSFD 2008), has been implemented (Buhl-Mortensen et al., 2017). The Directive is based on an ecosystem approach to managing the impact of human activities on the marine environment through the establishment of targets and associated indicators.

The main goal of this study is to evaluate dispersion of dredged material through overflow and dumping operations using water samples, optical and acoustic sensors in the direct vicinity of the dredging vessels. Acoustic Doppler Current Profilers (ADCP's), Optical Backscatter Sensors (OBS) and Laser In-Situ Scattering and Transmissometers (LISST) have

been widely used as an indicator for both natural SPMC and sediment plumes generated by dredging operations (Kim & Voulgaris, 2003; Gartner, 2004; Downing 2006; Gray & Gartner, 2009; Duclos et al., 2013; Cutroneo et al., 2012; Baeye & Fettweis, 2015; Park & Lee, 2016; Caballero et al., 2018; Manik et al., 2020). The use of acoustic and optical sensors in parallel provides means to characterize the SPM composition in addition to the concentration, because of their different sensitivity to particle size and density (Fettweis et al., 2019; Tran et al., 2024). The aim of the study is to evaluate the employability of such sensors in the monitoring of sediment plumes with various compositions. As such, field measurements achieved in the framework of this study included acoustic and optic sensors along with water samples to characterize the dredging plume composition and concentration in the most comprehensive way possible.

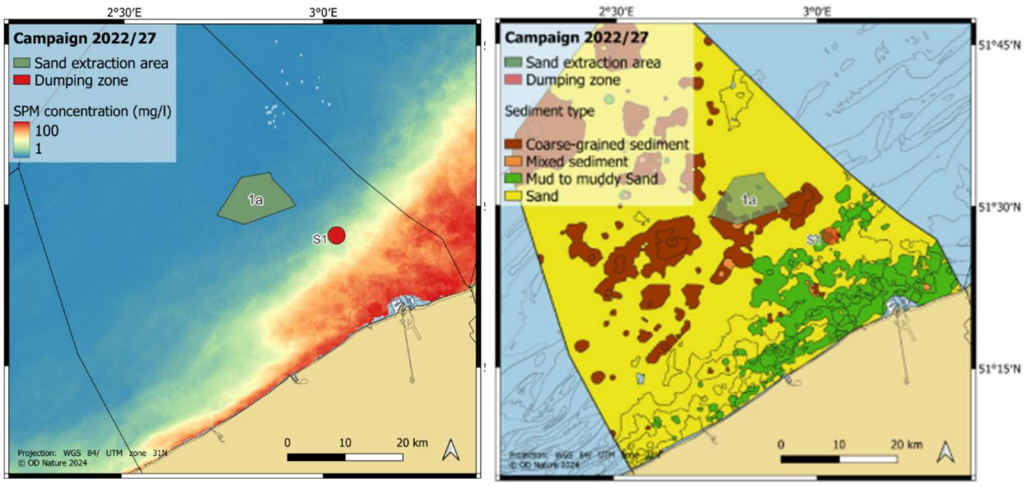


*Figure 3.1. Map of the BPNS displaying the locations of experiments conducted. The background on the map features the average surface SPMC for the winter period of 2019, derived using the algorithm by (Nechad et al., 2010) to the standard Sentinel-3/OLCI remote sensing reflectance product (RRS) provided by EUMETSAT water processor.*

## 3.1. Materials and method

### *3.1.1. Study area*

A dedicated research campaign was conducted aboard the RV Belgica, aiming to monitor and characterize sediment plumes resulting from dredging activities, including marine aggregate extraction and port maintenance operations. During campaign 2022/27 (from November 2 to November 5, 2022) three distinct experiments were performed, each following different trailing suction hopper dredgers. The first experiment focused on sediment plumes generated during marine aggregate extraction within and around sand extraction area 1a, located on the Thornton Bank. The second and third experiments were dedicated to monitor the disposal of dredged material from the Port of Zeebrugge, conducted in and around dumping site S1, known as Sierra Ventana.

In Figure 3.1, the locations of extraction area 1a and dumping zone S1 are depicted as well as the SPM concentration and the seafloor composition. The background (left map Figure 3.1.) illustrates the average Suspended Particulate Matter (SPM) concentrations during the winter months of 2019. The figure shows that the average SPM concentration at dumping site S1 ranges between 20 to 40 mg/l and is situated in the transition zone between the turbid nearshore and the turbid offshore. The sand extraction area is located further offshore and exhibits SPM concentrations between 5 to 10 mg/l. Nearshore, SPM concentrations can increase significantly, reaching values between 100 and several g/l near the seabed, while offshore, the differences between surface and near-bed concentrations

are less pronounced. (Fettweis et al., 2010). The sand extraction area 1A is characterized by a sandy to coarse grained sediments while the seafloor at dumping zone S1 is composed of mud to muddy sand fractions.

Tides in the region are semi-diurnal, with an average tidal range at Zeebrugge of 4.3 meters during spring tides and 2.8 meters during neap tides. Nearshore, tidal current ellipses are elongated, transitioning to a more circular shape further offshore. Current velocities near Zeebrugge vary between 0.2 and 1.5 m/s during spring tides and 0.2 to 0.6 m/s during neap tides. Offshore, current velocities are lower, ranging from 0.2 to 0.6 m/s during spring tides and 0.1 to 0.3 m/s during neap tides. Flood currents flow north-eastward, while ebb currents are directed south-westward. Winds predominantly come from the southwest, but the highest waves are generated during north-westerly winds, with significant wave heights exceeding 1.5 meters in the nearshore zone 10% of the time. The combination of strong tidal currents and low freshwater discharge from the Westerschelde estuary results in a well-mixed water column with minimal stratification in both salinity and temperature (Fettweis et al., 2010). During the period 2019-2023, $3.7\times10^6$ tons of dry matter (tdm) of muddy and sandy sediments were disposed yearly on dumping site S1 from maintenance operations in the port of Zeebrugge and the navigation channels. During the same period, an average of $2.0\times10^6$ m³ coarse sands were yearly extracted on the Thorntonbank extraction zone 1a.

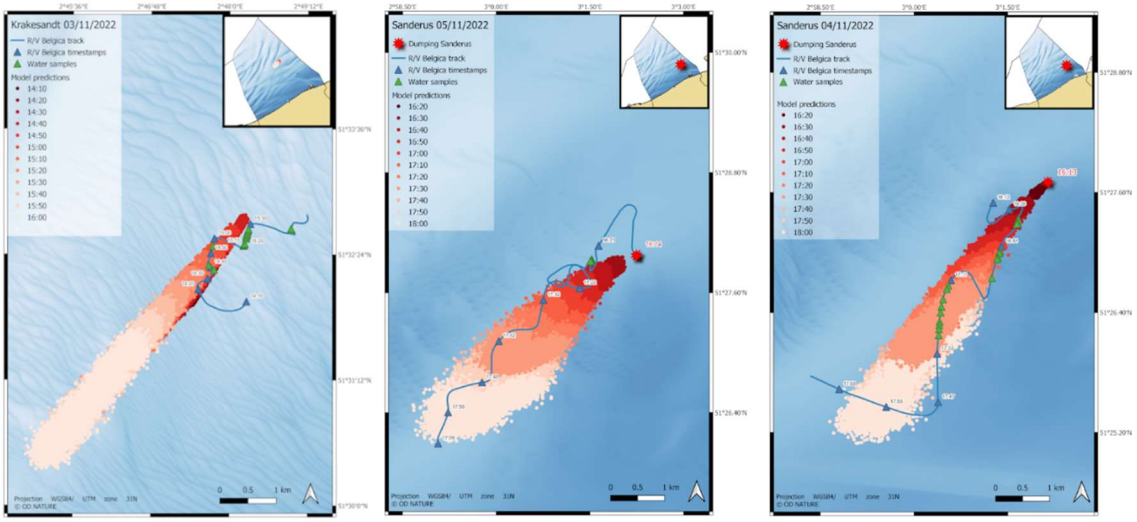


*Figure 3.2. In blue the track of the RV Belgica during the 3 experiments with the blue rectangles showing timestamps of the position of the R/V Belgica. The red dots represent the position of the modelled sediment plume at different timestamps. The green rectangles the moments of water sampling*

### *3.1.2. Vessels and experimental design*

Three experiments were conducted between 3 and 5 November 2022, to monitor and characterize sediment plumes resulting from marine aggregate extraction and dumping of dredged material. During these experiments two trailing suction hopper dredgers (TSHD) were followed; water samples were taken and the water column was measured using different types of sensors. The *Krakesandt* vessel (first experiment), measuring 105 meters in length, 15.85 meters in width, and having a capacity of 3000 m³ (classified as a small TSHD), engaged in sand extraction activities in extraction area 1a. The *Sanderus* vessel (experiments 2 and 3), with a length of 112 meters, a width of 24.6 meters, and a capacity of 6000 m³ (classified as a medium TSHD), conducted maintenance dredging operations in the harbor of Zeebrugge, with the dredged material subsequently disposed of at dumping

site S1. Various experimental designs were evaluated to monitor sediment plumes generated by dredging operations following TSHD vessels. A Lagrangian Particle Tracking model (MFRC, 2022) was used to predict the location and depth of the plumes, guiding the positioning of the RV Belgica for plume monitoring (Figure 3.2). During the Sanderus experiments the RV Belgica waited next to the TSHD that the dumping operations were accomplished and then sailed through the predicted sediment

### *3.1.3. Sensors and sampling*

A comprehensive array of acoustic and optical sensors was deployed to quantify sediment plumes induced by dredging activities. These sensors were installed either on the hull of the vessel or mounted on a rosette sampler. Both configurations included a Sea-Bird Seacat Conductivity, Temperature, and Depth (CTD) profiler to continuously monitor water column characteristics. The rosette sampler was deployed multiple times taking vertical profiles of oceanographic parameters with the attached sensors (CTD, optical sensors).

#### *3.1.3.1. Acoustic Doppler Current Profiler (ADCP)*

An RDI Workhorse Mariner 600 kHz Acoustic Doppler Current Profiler (ADCP) was positioned on the vessel's hull, with its four beams angled at 20° towards the seabed. This configuration allowed for high-resolution measurements of current velocities and echo intensity, the latter serving as a proxy for SPM concentration. ADCP backscatter data are widely used as an indicator for assessing both natural SPM concentration (Gartner 2004; Gray & Gartner, 2009; Park & Lee, 2016) and sediment plumes generated by dredging operations (Cutruneo et al., 2012; Duclos et al., 2013; Caballero et al., 2018) . The echo intensity data is divided in bins of 0.25m and is corrected for the vessel's motion by the acquisition software (RDI, VmDas), this corrected echo intensity is converted into volume backscatter (Sv) using the following equation (Mullison, 2017):

$$S_v = C + \log\left((T_x + 273.16)R^2\right) - L_{DBM} - P_{DBW} + 2\alpha R + \log\left(10^{Kc(E-E_r/10} - 1\right) \quad (3.1)$$

Equation (1) incorporates various parameters, including the backscattering strength ($S_v$), measured in decibels (dB); the received signal strength indicator (RSSI) scale factor ($K_c$), expressed in dB per count; the echo strength (E), measured in counts at each depth cell; the ADCP RSSI reference layer under no signal conditions ($E_r$), also in counts; the slant range (R), representing the distance along the beam to the insonified volume, measured in meters (m); the absorption coefficient (α), expressed in decibels per meter (dB $m^{-1}$); the transmit pulse length ($L_{DBM}$), measured in meters (m); the transmit power ($P_{DBW}$) in Watts; and a constant (C), measured in decibels (dB). The constant C accounts for a combination of terms, including receiver noise factor, noise bandwidth, and transducer efficiency Park & Lee, 2016). Generally, a calibration process is required to determine the RSSI scale factor ($K_c$) to convert signal strength to SPM concentration, where all the fixed terms in equation (3.1) are replaced with the net volume scattering ($S_v'$) which is defined as:

$$S_v' = 10.\log_{10}(SPM/SPM_t) - \log_{10}(R^2) - 2(\alpha_w + \alpha_s)R \quad (3.2)$$

where $SPM_t$ is the reference concentration (g/l), the absorption coefficient α is divided into two components; $\alpha_w$ which is the acoustic attenuation due to seawater and $\alpha_s$ which is the acoustic attenuation due to scatterers in suspension. Acoustic attenuation due to seawater depends mainly on the acoustic frequency and partially on temperature, salinity, pressure, pH and sound speed (Francois & Garrison, 1982.). By combining the instrument-specific terms of Kc, Er, $L_{DBM}$, $P_{DBW}$ and C into a new constant C' and with equation (3.2), equation

(3.1) can be simplified to:

$$S_v' = K_c E + C' \tag{3.3}$$

A widely used approach to determine the coefficient $K_c$ and *C'* involves performing a linear regression of echo intensities (E) against SPM concentrations, which are measured within the same sensing range. These SPM concentrations are typically obtained either from in-situ water samples or derived using optical sensors. The slope of the regression line represents $K_c$, while the intercept corresponds to C'. Once $K_c$ and C' are determined through acoustic calibration, the SPM concentration measured by an ADCP ($SPM_{ADCP}$) can be calculated using the following equation (Park & Lee, 2016):

$$SPM_{ADCP} = 10^{\frac{\{K_c E\ 20\ log_{10} R + 2(\alpha_w + \alpha_s)R + C'}{10}} \tag{3.4}$$

#### *3.1.3.2. Optical sensors*

Two optical sensors were employed during the experiments, both mounted horizontally on the rosette sampler: an optical backscatter sensor (OBS) and a Laser In-Situ Scattering and Transmissometer (LISST-200X) particle sizer (Agrawal & Pottsmith, 2000). The OBS (Sea-Bird Wetlabs ECO-NTU) measures optical scattering at a wavelength of 700 nm to quantify turbidity. This wavelength minimizes interference from coloured dissolved organic matter (CDOM), ensuring more accurate turbidity measurements. Turbidity values are reported in Nephelometric Turbidity Units (NTU), with a sensitivity range of 0–125 NTU. OBS systems are widely used to monitor SPM in natural environments and in plumes generated by dredging activities (Downing, 2006; Cutroneo et al., 2012; Baeye et al., 2015; Fettweis et al., 2019). The LISST-200X is a submersible laser-diffraction based particle size analyser (Agrawal & Mikkelsen, 2009) The low-angle light scattering is used to determine particle sizes in the sample volume, regardless of particle composition. The LISST-200X records scattering intensity across a range of near-forward angles. The captured multi-angle scattering data is transformed into a size distribution using a mathematical inversion process. This inversion finds a size distribution that would generate angular scattering patterns consistent with the observed data. Besides particle size distribution the LISST-200X also calculates water depth, beam attenuation and estimates of particle concentration (volume concentration in µL/l) and mean diameter (Sauter mean diameter in µm)

### *3.1.4. Samples*

Besides sensor data also samples were taken in two different forms, water samples and centrifuge samples. The water samples were taken using a set of Niskin bottles of 10l that were closed at precise moments and depths when the rosette sampler was expected to be positioned inside the sediment plume. Before extraction/dumping activities, profiles and samples of the water column were taken to have background information. From this water samples three replicas were taken, and sample SPM concentration was obtained through filtration and gravimetric measurements in the laboratory. The centrifuge samples were collected using the on-board centrifuge of the RV Belgica. Seawater was pumped from the ship's hull and processed through the centrifuge, after which the samples were retrieved. These samples were subsequently analysed in the laboratory to determine particle size distribution using a Malvern Mastersizer 3000. Samples were pre-treated to remove all organic matter, isolating the inorganic fraction of the SPM.

## 3.2. Results

### *3.2.1. Samples*

The gravimetric measurements of the filtered water samples are shown in Figure 3.2. These values represent the average of three replicate samples collected from each water sample at various time points during the experiments, corresponding to active phases of the TSHD. The results reveal that the range of SPM concentrations is broader during dumping activities compared to sand extraction activities. There is substantial increase in SPM concentrations during dumping, which cannot be attributed to natural variability. In contrast, SPM concentrations during sand extraction do not exhibit a similarly distinct pattern.

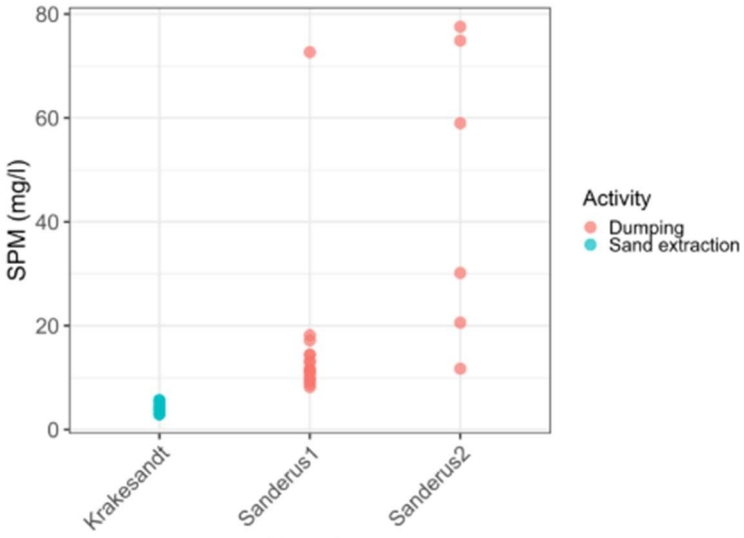


*Figure 3.2: Results from the gravimetric measurements of the water samples. In red the results from the dumping events and in blue from sand extraction activities.*

The mud and sand fractions were calculated from the centrifuge samples and are presented in Figure 3.3. No clear distinction in composition can be observed between the sand extraction event and the first dumping event. In contrast, the second dumping experiment exhibited a notable difference, with a significant increase in the sand fraction compared to the previous two experiments.

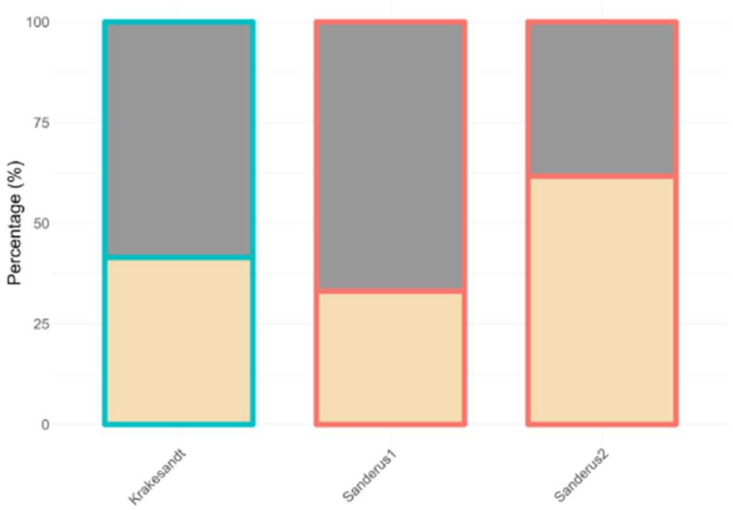


*Figure 3.3: Centrifuge sample results showing the percentage of sand (beige) and mud (grey) in the samples. The blue contour indicates sand extraction activities, while the red contour represents dumping activities.*

Besides measuring the sand/mud fraction we also obtained a complete PSD curve for the centrifuge samples that are represented in Figure 3.4. The sand extraction event (Krakesandt) displays a distinct peak around 300 µm. The first Sanderus experiment exhibits a bimodal distribution, with one peak near 300 µm and a broader peak at smaller particle sizes, whereas the second Sanderus experiment again shows a pronounced peak at approximately 300 µm.

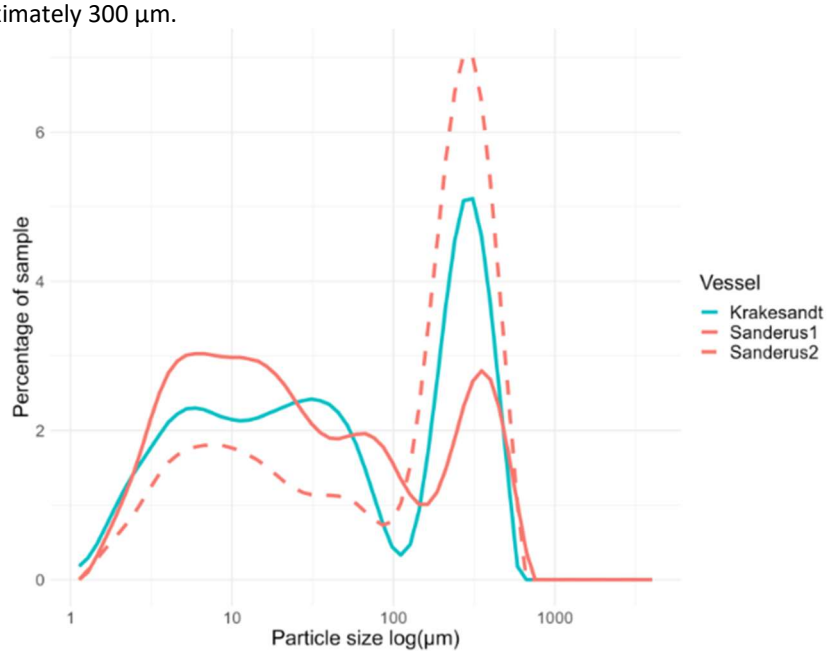


*Figure 3.4: Particle Size Distribution (PSD) of the centrifuge samples obtained during the different experiments. The blue line represents the sand extraction event (Krakesandt), the full red line represents the first dumping event (Sanderus 1) and the dashed red line represent the second dumping event (Sanderus 2).*

### *3.2.2. Optical sensors*

The results of the OBS and LISST-200X profiles are displayed in Figure 3.5. The OBS sensor gives a turbidity value in NTU while the LISST sensors gives a total volume concentration (TVC) which can be interpreted as an estimate of the number of particles measured in the sampled volume of the sensor.

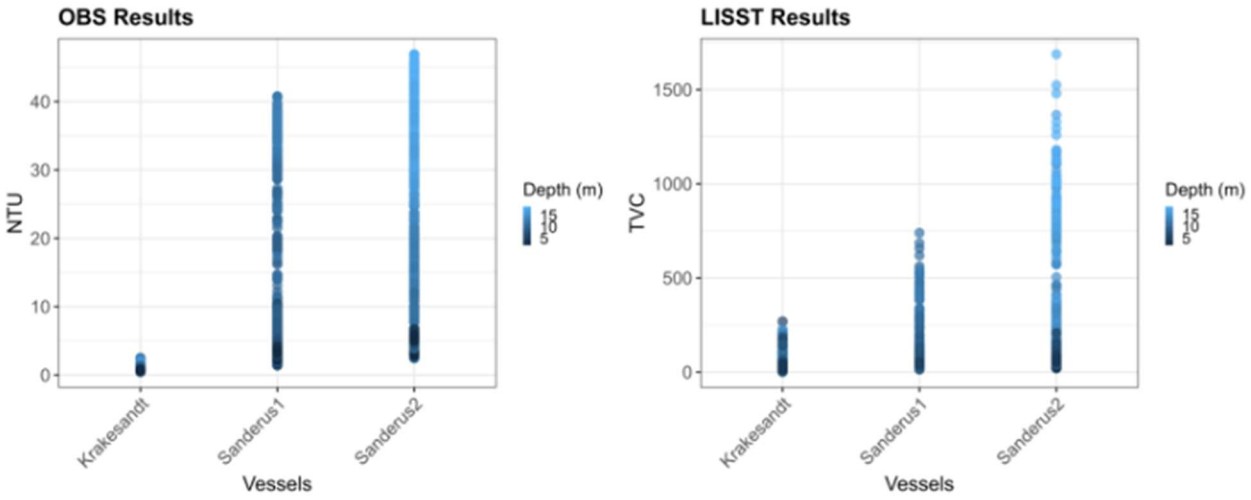


*Figure 3.5: The left graph shows the OBS profiles and the left graph the LISST-200X profiles. The colour scale indicates the depth of the sensor in meters.*

A distinct difference in turbidity levels is observed between the dumping events and sand extraction activities as we observed in the water samples. Depth does seem to play a significant role during the dumping events especially during the second experiment, where turbidity and TVC increases significantly towards the bottom. The LISST-200X sensor registers a slight rise in TVC during the Krakesandt experiment, a change not captured by the OBS measurements. Between the two dumping experiments, a noticeable difference is evident, with the OBS sensor showing only minor variations, while the LISST sensor reveals a more pronounced difference in TVC range. This could potentially be explained by the centrifuge sample results (Figure 3.3, 3.4), where a clear difference was observed between the two samples from the dumping events. The second sample (Sanderus 2) had a significantly higher sand fraction. Similar findings have been reported in previous studies (Downing 2006; Fettweis et al. 2019), indicating that OBS sensors are less sensitive to the sand fraction.

In addition to measuring TVC, the LISST-200X instrument also determines the PSD of the sampled volume. Unlike the centrifuge samples, which are collected at a fixed depth (the hull of the vessel), the LISST-200X conducted measurements throughout the water column using the rosette sampler. Figure 3.7 presents the average PSD curves for all measurements taken at various depths during each experiment. The PSD curves obtained from the optical LISST-200X sensors reveal subtle differences in particle size distribution between the sand extraction event (Krakesandt) and the two dumping events. The primary peak during the sand extraction event is centred around 300 µm, whereas the dumping events show a main peak concentrated in the 100–200 µm range. Additionally, the first dumping event exhibits a slightly higher presence of particles near 50 µm compared to the second. For the sand extraction event, there is also a minor increase in particles around 10 µm.

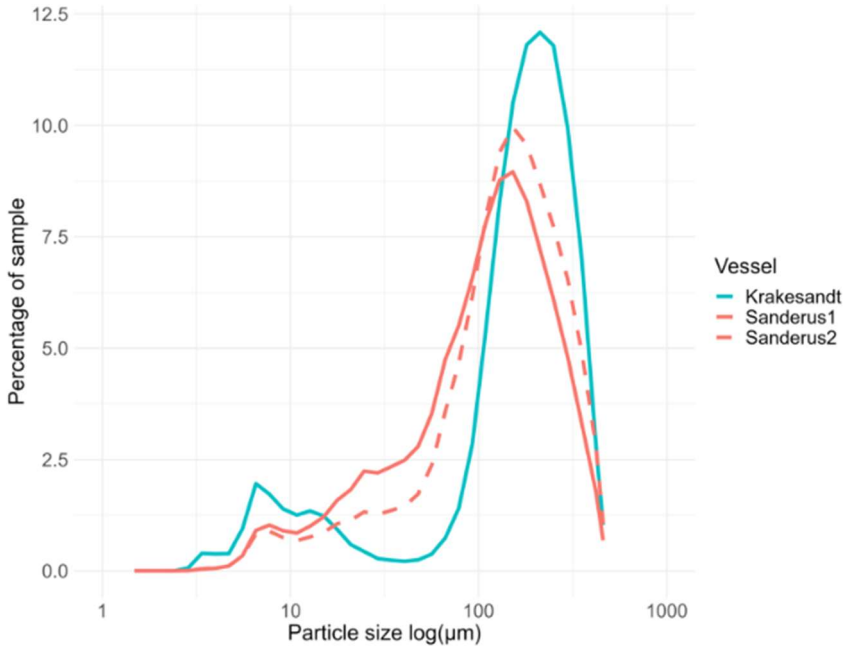


*Figure 3.7: PSD curves of the LISST-200X measurements. The blue line represents the sand extraction event (Krakesandt), the full red line represents the first dumping event (Sanderus 1) and the dashed red line represent the second dumping event (Sanderus 2).*

### *3.2.3. Acoustic Doppler Current Profiler (ADCP)*

The ADCP operated continuously during all the experiments, generating a complete dataset of the entire water column for each experiment (Figure 3.8). Only 90% of the water column is plotted as the last 10% is influenced by the bottom reflection and gives erroneous

interpretation.

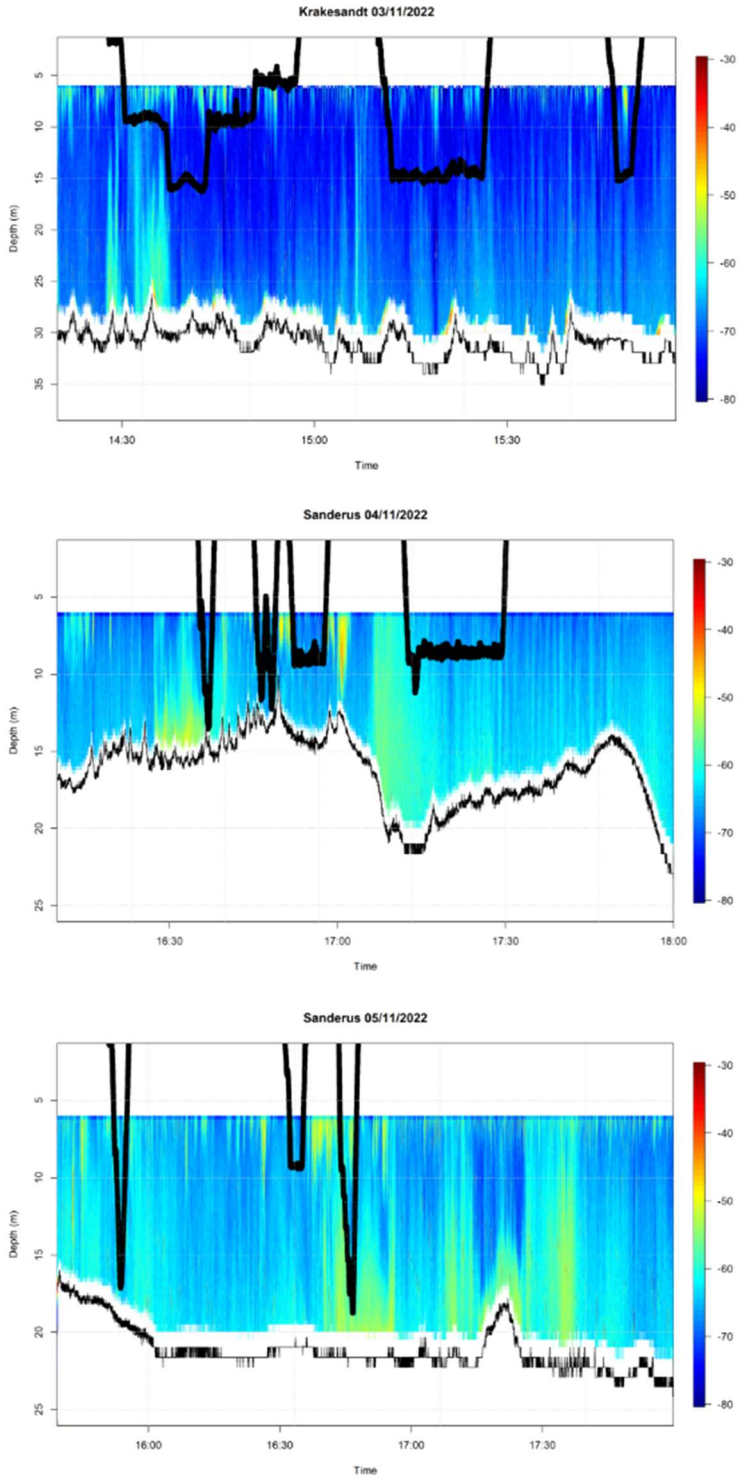


Figure 3.8: *ADCP echograms of the 3 different experiments. The color bar represents the volume backscatter (Sv) in dB. The black lines are the different casts of the rosette sampler.*

Periods of elevated acoustic backscatter within the water column are clearly observed, suggesting the presence of an acoustic reflector. Based on the context, we attribute this reflector to sediment plumes, originating from either sand extraction activities (Krakesandt) or the disposal of dredged material (Sanderus 1 & 2). Additionally, numerous smaller peaks in acoustic backscatter are detected near the vessel's hull, where the ADCP is positioned.

These signals differ from the more pronounced acoustic reflections observed closer to the seabed. To focus our analysis on the sediment plumes, we identified time intervals where the acoustic signal confidently represents such an event. We then compared Sv values between periods inside and outside the plume events using a box plot graph (Figure 3.9).

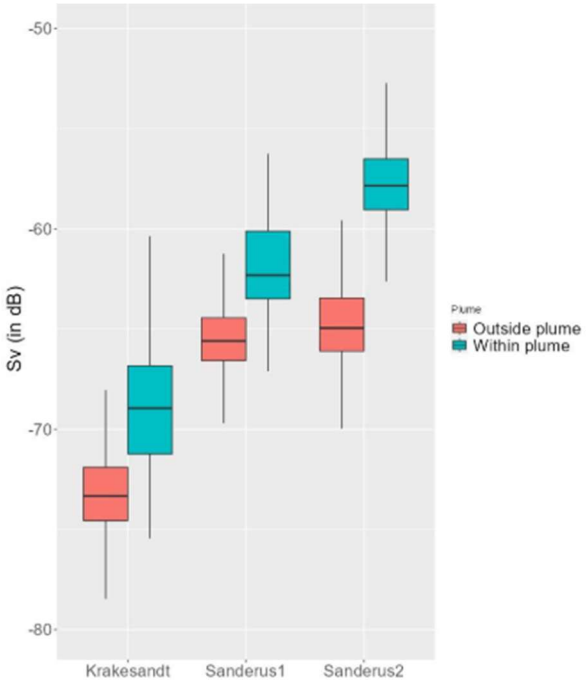


*Figure 3.9: Boxplot of volume backscatter with in red the measurements outside the sediment plume and in blue the measurements within the sediment plume for the 3 different experiments.*

The boxplots reveal a clear distinction in backscatter intensity between periods within and outside the sediment plume for each experiment, confirming the ADCP's effectiveness in detecting these plumes. Additionally, the data show that the background backscatter intensity is significantly higher during the dumping events. This observation can be attributed to the location of the sand extraction event near the Thornton Bank (Figure 3.1), which is situated further offshore. In this area, the background SPM concentration is lower compared to the nearshore region where the dumping zone (S1) is located.

## 3.3. Discussion

### *3.3.1. OBS-SPM relationship*

We took a closer look at the relationship between SPM concentration and the corresponding OBS measurements. For this, we applied a robust linear regression model to estimate SPM values (in mg/l) based on the OBS output.

The results shown in Figure 3.10 highlight a distinct difference in the relationship between the OBS output and the sample SPM concentration derived from the water samples. According to the literature, the sensitivity of OBS varies depending on the type of particles (Downing, 2006; Fettweis et al., 2019; Pearson et al., 2021), which could explain the observed discrepancy between the sample SPM concentrations and OBS measurements between sand extraction and dumping events.

To confirm that the difference in the relationship between the OBS output and the sample SPM is due to different types of particles we looked at the results from the LISST-200X data. We used the same time intervals as for the ADCP (see chapter 3.2.3) to look at how the LISST-200X PSD curves compare within and outside the sediment plume.

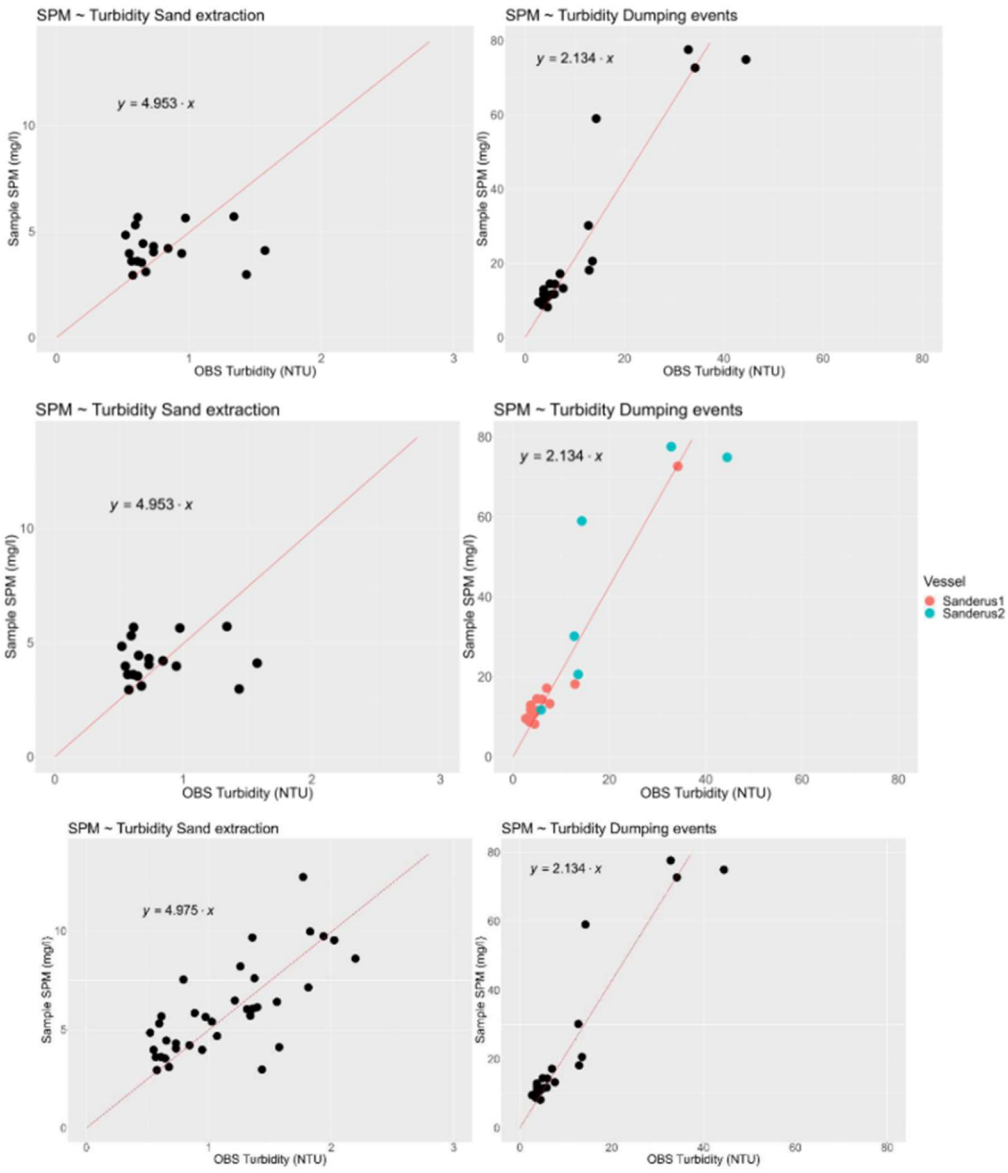


*Figure 3.10: Comparison of relationship SPM ~ Turbidity using a robust linear regression model. The graph on the left shows this for the sand extraction experiments and on the right for the dumping events.*

Figure 3.11 illustrates that there are no notable differences between measurements taken inside and outside plume conditions during the sand extraction experiment, for PSD and TVC ranges. A distinct peak is observed in the coarser fractions (100–300 µm), consistent with observations from the centrifuge samples (see Figure 3.4).

For the dumping events, a clear shift towards finer fractions (10–100 µm) is observed under plume conditions during the first experiment (Sanderus 1). Additionally, an increase in TVC indicates a higher concentration of suspended material in the water column. Conversely, during the second dumping experiment (Sanderus 2), an opposite trend is evident, with a shift towards coarser fractions under plume conditions. This is accompanied by a significant increase in TVC, suggesting an even greater amount of suspended material. The more pronounced presence of the coarser fraction for the second experiment and the smaller particles for the first dumping experiment was also observed in the centrifuge samples (Figure 3.4).

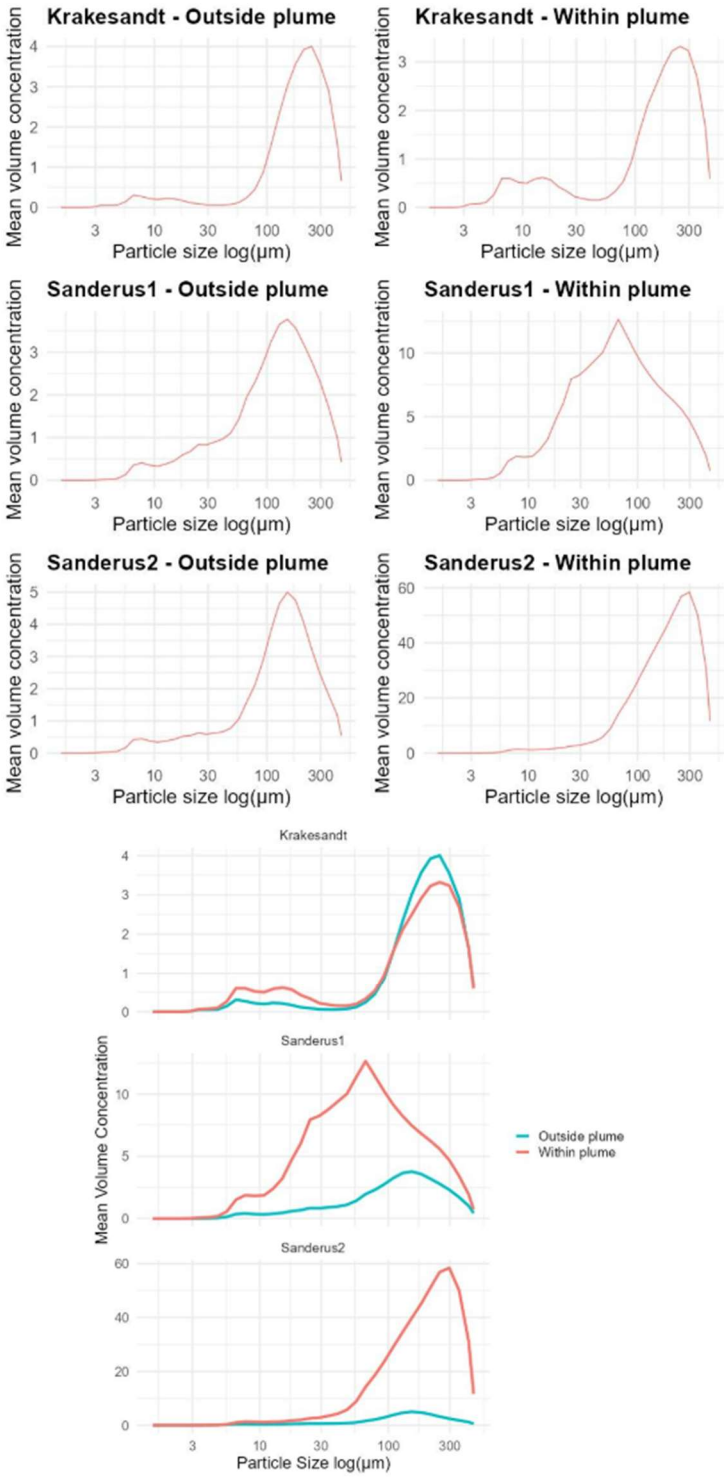


*Figure 3.11: Comparison of PSD curves obtained from the LISST-200X between moments inside and outside the sediment plume conditions.*

These findings suggests that during the first experiment, the sediment plume may not have been captured by both optical sensors, give n the absence of shifts in NTU, PSD or TVC ranges. The second experiment (Sanderus 2), however, clearly recorded a sediment plume, characterized by an increase in NTU and TVC and a shift toward finer fractions, aligning with expectations for dredged material disposal from Zeebrugge harbour. In contrast, the third experiment (Sanderus 2) showed a substantial increase in NTU and TVC, suggesting a high particle load in suspension, yet with a shift toward coarser fractions, which is unexpected

for dredged material disposal.

Both dumped material in these experiments were dredged in the outer harbour of Zeebrugge (see Figure 3.12). The material dredged in this area consist of mainly mud, although along the eastern side of the harbour (Sanderus 2) sand may also be present. This raises questions about the properties of the sediment plumes themselves. Initial observations suggest that while sand extraction events may not generate readily identifiable sediment plumes from the optical instruments, the plumes from dredged material disposal were successfully captured. The remaining question is why similar sources and conditions yielded such contrasting PSD compositions and TVC ranges between the experiments.

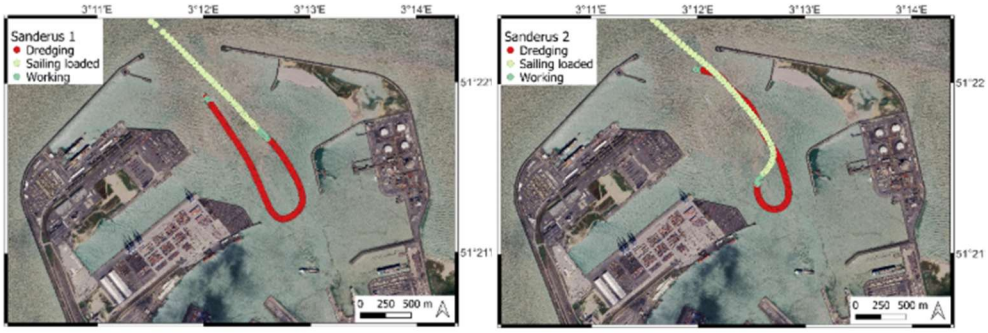


*Figure 3.12: Location of dredging during both experiments (Sanderus 1 on the left, Sanderus 2 on the right), prior to dumping at S1.*

Looking at the acoustic response of the ADCP to the sediment plumes we noticed a clear distinction in backscatter intensity between periods inside and outside the sediment plume for each experiment (see Figure 3.10). This raises the question why the acoustic sensor is able to capture the sediment plume from sand extraction that is not captured by the optical sensor, likely due to variations in SPM composition. According to the literature, backscatter intensity is influenced by the composition of SPM (Deines, 1999; Gartner, 2004; Guerrero et al., 2011; Kim & Voulgaris, 2014; Manik et al., 2021; Vergne et al., 2021).

To enable comparison across sensors, we generated boxplots (Figure 3.13) aligned to the same timestamps for measurements inside and outside the plume, as defined for the ADCP, to the two optical sensors. This setup allows for a direct examination of results from both optical and acoustic sensors operating within the same time window providing a more integrated view of plume conditions.

Figure 3.13 demonstrates that for sand extraction activities, there is no statistically significant difference in optical sensor readings (OBS and LISST) between conditions inside and outside the sediment plume. However, during the dumping of dredged material, both sensors show a clear and significant difference in optical response between plume and non-plume conditions. Additionally, both sensors indicate a notable difference between the first (Sanderus 1) and second (Sanderus 2) dumping events. As previously mentioned, LISST data revealed differences in particle size distribution (PSD) between these events, with coarser fractions more prominent in the second dumping event.

In the first dumping experiment (Sanderus 1), an increase in particle number (TVC) is observed, with particles primarily in the finer fraction range (10-100 µm). The second dumping experiment (Sanderus 2) shows an even greater rise in particle number (TVC), dominated by coarser particles (100-300 µm), though fine particles remain present. According to the filtration results, SPM concentrations are similar between the two dumping events. This may indicate that coarser sand particles significantly impact the acoustic signal but do not influence turbidity as measured by the OBS. This observation

could explain why, during sand extraction events, backscatter intensity increases for plume measurements, yet the OBS does not register a corresponding rise in turbidity. The presence of even a small amount of sand particles can enhance backscatter intensity, as these particles function as strong reflectors of acoustic signals, whereas OBS readings remain unaffected.

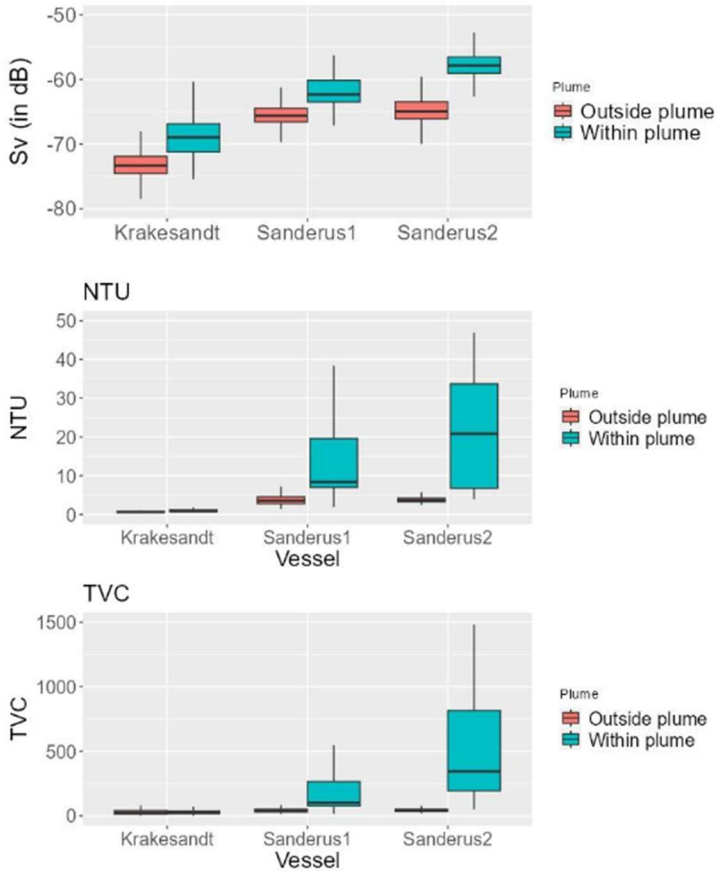


*Figure 3.13: Boxplots of different acoustic (1) and optical measurements (2,3) matching the same time-intervals and depths for inside and outside plume conditions.*

To verify the observed differences in acoustic response to varying sediment characteristics, we examined the relationship between SPM concentration (SPMv) and the signal-to-noise ratio (E-Er) across the different experiments. The analysis revealed that the slope of this relationship was similar for Krakesandt and Sanderus 2, while Sanderus 1 exhibited a much steeper gradient. This pattern supports the hypothesis that the presence of sand particles in suspension, as seen in Krakesandt and Sanderus 2, significantly alters the acoustic response, differing sharply from that observed with finer suspended sediments.

## 3.4. Conclusion

The monitoring of sediment plumes in the Belgian part of the North Sea, specifically from marine aggregate extraction and the dumping of dredged material, has underscored notable differences in plume behaviour and sediment composition. Optical sensors (OBS and LISST) and acoustic sensors (ADCP) revealed that sediment plumes from dumping events are more distinct in turbidity and particle size distribution (PSD) compared to those from sand extraction activities. For dumping events, a significant increase in SPM concentration was observed, with a bimodal PSD, particularly showing a shift toward finer particle fractions during Sanderus 1 and coarser fractions during Sanderus 2. This bimodal

trend suggests variable plume compositions potentially related to the dredging source and specific operational conditions.

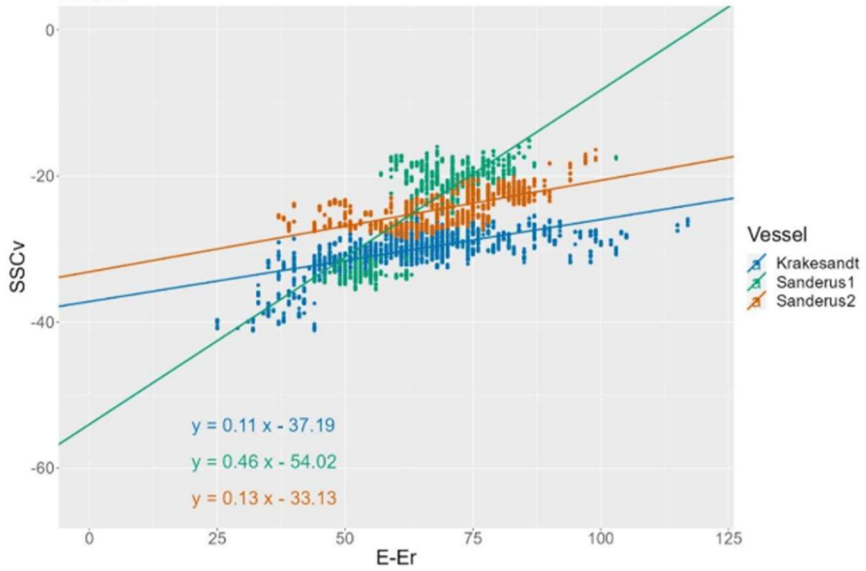


*Figure 3.14: Relationship between the SPM concentration (SSCv) and the signal to noise ratio (E-Er) for the different experiments*

The results further demonstrate that acoustic sensors, sensitive to coarser particles, captured increased backscatter intensity even in sand extraction events where optical sensors did not register high turbidity. This indicates that sand particles, acting as strong reflectors, contribute significantly to acoustic backscatter without affecting optical turbidity measurements. Therefore, integrating acoustic and optical sensor data proves crucial in accurately characterizing plume properties and dynamics, especially in environments where particle composition varies significantly.

In summary, this study highlights the distinct characteristics of sediment plumes from different dredging activities and underscores the importance of multi-sensor approaches for comprehensive sediment plume monitoring. These insights can enhance future environmental impact assessments and improve predictive models for sediment dispersion in marine environments, supporting sustainable marine resource management.

# 4. Referenties


Abolfazli E, Strom K. 2023. Salinity impacts on floc size and growth rate with and without natural organic matter. Journal of Geophysical Research 128, e2022JC019255.

Abril G, Nogueira M, Etcheber H, Cabeçadas G, Lemaire E, Brogueira MJ. 2002. Behaviour of organic carbon in nine contrasting European estuaries. Estuarine, Coastal and Shelf science 54, 241-262.

Agrawal Y, Pottsmith H. 2000. Instruments for particle size and settling velocity observations in sediment transport. Marine Geology 168, 89–114.

Agrawal YC, Mikkelsen OA. 2009. Instruments for particle size and settling velocity observations in sediment transport. Optic Express *17*, 23066–23077

Ahmed AA, Thiele-Bruhn S, Aziz SG, Hilal RH, Elroby SA, Al-Youbi AO, Leinweber P, Kühn O. 2015. Interaction of polar and nonpolar organic pollutants with soil organic matter: Sorption experiments and molecular dynamics simulation. Science of the Total Environment 508, 276-287.

Alexandrova OA, Shevchenko VP. 1997. Concentrations of particulate organic carbon in the Kara Sea and in the Obskaya Guba (Ob River estuary) in September 1993. PANGAEA.

Alldredge AL, Silver MW. 1988. Characteristics, dynamics and significance of marine snow. Progress in Oceanography 20, 41-82.

Alldredge AL, Granata TC, Gotschalk CC, Dickey TD. 1990. The physical strength of marine snow and its implications for particle disaggregation in the ocean. Limnology & Oceanography 35, 1415–1428.

Andrews S, Nover D, Schladow S. 2010. Using laser diffraction data to obtain accurate particle size distributions: The role of particle composition, Limnology & Oceanography Methods 8, 507–526.

Arndt S, Jørgensen BB, LaRowe DE, Middelburg JJ, Pancost RD, Regnier P. 2013. Quantifying the degradation of organic matter in marine sediments: A review and synthesis. Earth Science Review 123, 53-86.

Arrieta J, Jeanneret R, Roig P, Tuval I. 2020. On the fate of sinking diatoms: the transport of active buoyancy-regulating cells in the ocean. Philosophical Transaction of the Royal Society A 378, 20190529.

Asper VL. 1987. Measuring the flux and sinking speed of marine snow aggregates. Deep Sea Research 34, 1–17.

Azam F, Fenchel T, Field JG, Gray JS, Meyer-Reil LA, Thingstad F. 1983. The ecological role of water-column microbes in the sea. Marine Ecology-Progress Series, 10, 257-263.

Azetsu-Scott K, Passow U. 2004. Ascending marine particles: Significance of transparent exopolymer particles (TEP) in the upper ocean. Limnology & Oceanography 49, 741–748.

Baeye M, Fettweis M. 2015. In Situ Observations of Suspended Particulate Matter Plumes at an Offshore Wind Farm, Southern North Sea. Geo-Marine Letters 35, 247–255

Bai X, Hazi F, Takacs I, Wadhawan T, Parker WJ. 2024. A comprehensive floc model for simulating simultaneous nitrification, denitrification, and phosphorus removal. Science of the Total Environment 927, 172013.

Baltar F, Alvarez-Salgado XA, Arístegui J, Benner R, Hansell DA, Herndl GJ, Lønborg C. 2021. What is refractory organic matter in the ocean? Frontiers in. Marine Science 8, 642637.

Bauer JE, Cai WJ, Raymond P, Bianchi TS, Hopkinson CS, Regnier PAG. 2013. The changing carbon cycle of the coastal ocean. Nature 504, 61–70.

Baumas C, Bizic M. 2024. A focus on different types of organic matter particles and their significance in the open ocean carbon cycle. Progress in Oceanography 224, 103233.

Belliard J-P, Hernandez S, Temmerman S, Suello RH, Dominguez-Granda LE, Rosado-Moncayo AM, Ramos-Veliz JA, Parra-Narera RN, Pollete-Ramirez K, Govers G, Borges AV, Bouillon S. 2024. Carbon dynamics and CO2 and CH4 exchange in the mangrove

dominated Guayas river delta, Ecuador. Estuarine, Coastal and Shelf Science 267,107766.

Belyaev NA, Peresypkin VI, Ponyaev MS. 2010a. (Table 1) Concentrations of dissolved and particulate organic carbon in waters of the Kara Sea along the section to the east northeast of the Yamal Peninsula. PANGAEA.

Belyaev NA, Peresypkin VI, Ponyaev MS. 2010b. (Table 2) Concentrations of dissolved and particulate organic carbon in waters of the Kara Sea along the St. Anna Trough section. PANGAEA.

Belyaev NA, Peresypkin VI, Ponyaev MS. 2010c. (Table 3) Concentrations of dissolved and particulate organic matter in waters along the section from the Obskaya Guba to the Kara Sea. PANGAEA.

Benoit G. Oktay-Marshall SD, Cantu II A, Hood EM, Coleman CH, Corapcioglu MO, Santchi PH. 1994. Partitioning of Cu, Pb, Ag, Zn, Fe, Al and Mn between filter-retained particles, colloids, and solution in six Texas estuaries. Marine Chemistry. 45, 307-336.

Berbel GBB, Hortellani MA, de Souza Sarkis JE, Chiozzini VG, Teixeira Fávaro TE, Sutti BO, Sakazaki NO, de Santis Bragaet E. 2021. Emerging contaminants (Rh, Pd, and Pt) in surface sediments from a Brazilian subtropical estuary influenced by anthropogenic activities. Marine Pollution Bulletin, 163, 111929.

Berelson WM. 2001. Particle settling rates increase with depth in the ocean. Deep Sea Research II 49, 237–251.

Bezborodov AA, Eremeev VN. 1993a. (Table 48) Concentrations of suspended matter and its composition in Black Sea waters at Station BE-93-4271 in summer 1984. PANGAEA.

Bezborodov AA, Eremeev VN. 1993b. (Table 50) Concentrations of suspended matter and its composition in Black Sea waters at Station BE-93-3377 in spring 1988. PANGAEA.

Bhaskar PV, Grossart HP, Bhosle NB, Simon M. 2005. Production of macroaggregates from dissolved exopolymeric substances (EPS) of bacterial and diatom origin. FEMS Microbiological Ecology 53, 255-264.

Bianchi TS. 2007. Biogeochemistry of Estuaries. Oxford University Press.

Blair NE, Aller RC. 2012. The fate of terrestrial organic carbon in the marine environment. Annual Review of Marine Science 4, 401–423.

Blattmann TM, Liu Z, Zhang Y, Zhao Y, Haghipour N, Montluçon DB, Eglinton TI. 2019. Mineralogical control on the fate of continentally derived organic matter in the ocean. Science 66, 742-745.

Boyd SE, Limpenny DS, Rees HL, Cooper KM, Campbell S. 2003. Preliminary observations of the effects of dredging intensity on the re-colonisation of dredged sediments off the southeast coast of England (Area 222). Estuarine, Coastal and Shelf Science *57*, 209–223.

Bouchez J, Galy V, Hilton RG, Gaillardet J, Moreira-Turcq P, Andrea Pérez M, France-Lanord C, Mauriceet L.2014. Source, transport and fluxes of Amazon River particulate organic carbon: Insights from river sediment depth-profiles. Geochimica et Cosmochimica Acta 133, 280–298.

Bouillon S, Frankignoulle M, Dehairs F, Velimirov B, Eiler A, Abril G, Etcheber H, Borges AV. 2003. Inorganic and organic carbon biogeochemistry in the Gautami Godavari estuary (Andhra Pradesh, India) during pre-monsoon: The local impact of extensive mangrove forests. Global Biogeochemical. Cycles 17, 1114.

Bouillon S, Abril G, Borges AV, Dehairs F, Govers G, Hughes HJ, Merckx R, Meysman FJR, Nyunja J, Osburn C, MiddelburgJJ. 2009. Distribution, origin and cycling of carbon in the Tana River (Kenya): a dry season basin-scale survey from headwaters to the delta, Biogeosciences 6, 2475–2493.

Bouillon S, Yambélé A, Gillikin DP, Teodoru C, Darchambeau F, Lambert T, Borges AV. 2014. Contrasting biogeochemical characteristics of the Oubangui River and tributaries (Congo

River basin). Scientific Reports 4, 5402.
Boyd C, Gradmann D. 2002. Impact of osmolytes on buoyancy of marine phytoplankton. Marine Biology 141, 605–618.
Burchard H, Flöser G, Staneva JV, Riethmüller R, Badewien T. 2008. Impact of density gradients on net sediment transport into the Wadden Sea. Journal of Physical Oceanography 38, 566–587.
Burchard H, Schuttelaars HM, Ralston DK. 2018 Sediment trapping in estuaries. Annual Review of Marine Science 10, 371–395.
Burd AB. 2016. Modeling the vertical flux of organic carbon in the global ocean Annual Review of Marine Science 16, 135–161.
Burdige DJ. 2005. Burial of terrestrial organic matter in marine sediments: A re-assessment. Global Biogeochemical Cycles 19.
Caballero I, Navarro G, Ruiz J. 2018. Multi-Platform Assessment of Turbidity Plumes during Dredging Operations in a Major Estuarine System. International Journal of Applied Earth Observation and Geoinformation 68, 31–41
Cai W-J. 2011. Estuarine and coastal ocean carbon paradox: CO2 sinks or sites of terrestrial carbon incineration? Annual Review of Marine Science 3, 123–145.
Cai C, Cai j, Liu H, Wang X, Zeng X, Wang Y. 2023. Occurrence of organic matter in argillaceous sediments and rocks and its geological significance: A review. Chemical Geology 639, 121737.
Cantwell MG, Katz DR, Sullivan JC, Ho K, Burgess RM, Cashman M. 2016. Selected pharmaceuticals entering an estuary: Concentrations, temporal trends, partitioning, and fluxes. Environment Chemistry 35, 2665-2673.
Capuzzo E, Stephens D, Silva T, Barry J, Forster RM. 2015. Decrease in water clarity of the southern and central North Sea during the 20th century. Global Change Biology 21, 2206–2214.
Celis-Hernandez O, Cundy AB, Croudace IW, Ward RD, Busquets R, Wilkinson JL. 2021. Assessing the role of the “estuarine filter” for emerging contaminants: pharmaceuticals, perfluoroalkyl compounds and plasticisers in sediment cores from two contrasting systems in the southern UK. Water Research 189, 116610.
Chajwa R, Flaum E, Bidle KD, Van Mooy B, Manu Prakash A. 2024. Hidden comet tails of marine snow impede ocean-based carbon sequestration. Science 386, eadl5767.
Chamley H. 1989. Clay sedimentology. Springer Verlag, 623pp.
Chen CS, Shiu RF, Hsieh YY, Xu C, Vazquez CI, Cui Y, Hsu IC, Quigg A, Santschi PH, Chin WC. 2021. Stickiness of extracellular polymeric substances on different surfaces via magnetic tweezers. Science of the Total Environment 757. 143766.
Cindrić AM, Garnier C, Oursel B, Pižeta I, Omanović D. 2015. Evidencing the natural and anthropogenic processes controlling trace metals dynamic in a highly stratified estuary: The Krka River estuary (Adriatic, Croatia). Marine Pollution Bulletin 94, 199-216.
Cloern JE, Jassby AD. 2012. Drivers of change in estuarine-coastal ecosystems: Discoveries from four decades of study in San Francisco Bay. Review in Geophysics 50, RG4001.
Cole JJ, Findlay S, Pace ML. 1988. Bacterial production in fresh and saltwater ecosystems: A cross-system overview. Marine Ecology Progress Series 43, 1-10.
Colina Alonso A, van Maren DS, Oost AP, Esselink P, Lepper R, Köster F, Bartholdy J, Bijleveld AI, Wang ZB. 2024. A mud budget of the Wadden Sea and its implications for sediment management. Communication Earth & Environment 5, 153.
Compton JS, Mallinson DJ, Glenn CR, Filippelli GM, Föllmi KB, Shields GA, Zanin YN. 2000. Variations in the global phosphorus cycle. Special Publication Society of Sedimentary Geology 66, 21–33.

Cooper K, Boyd S, Aldridge J, Rees H. 2007. Cumulative impacts of aggregate extraction on seabed macro-invertebrate communities in an area off the east coast of the United Kingdom. Journal of Sea Research 57, 288-302.

Cooper K, Ware S, Vanstaen K, Barry J. 2011. Gravel seeding – a suitable technique for restoring the seabed following marine aggregate dredging? Estuarine, Coastal and Shelf Science 91, 121-132.

Cox TJS, Maris T, Van Engeland T, Soetaert K, Meire P. 2019. Critical transitions in suspended sediment dynamics in a temperate meso-tidal estuary. Scientific Report 9, 12745.

Cui Z, Huang L, Fang H, Han D, Bombardelli F. 2023. Exploring cohesive sediment flocculation with surface heterogeneity: A theoretical Lagrangian-type flocculation model. Water Resources Research 59, e2022WR034374.

Cutroneo L, Castellano M, Pieracci A, Povero P, Tucci S, Capello M. 2012. The Use of a Combined Monitoring System for Following a Turbid Plume Generated by Dredging Activities in a Port. Journal of Soils and Sediments 12, 797–809.

Daewel U, Akhtar N, Christiansen N, Schrum C. 2022. Offshore wind farms are projected to impact primary production and bottom water deoxygenation in the North Sea. Communication Earth & Environment 3, 292.

Dankers PJT, Winterwerp JC. 2007Hindered settling of mud flocs: Theory and validation. Continental Shelf Research 27, 1893-1907.

Deborde, J. et al. The dynamics of phosphorus in turbid estuarine systems: Example of the Gironde estuary (France). Limnology & Oceanography 52, 862-872. (2007)

Decrop B, De Mulder T, Toorman E, Sas M. 2015. Numerical Simulation of Near-Field Dredging Plumes: Efficiency of an Environmental Valve. Journal of Environmental Engineering 141, 04015042.

Deines KL. 1999. Backscatter estimation using broadband Acoustic Doppler Current Profilers. In: Proceedings of the IEEE Sixth Working Conference on Current Measurement; San Diego.

Dellwig O, Bosselmann K, Kölsch S, Hentscher M, Hinrichs J, Böttcher ME, Reuter R, Brumsack H-J. 2007.. Geochemical analysis of surface water samples of a tidal basin of the German Wadden Sea. PANGAEA.

Dellwig O, Brumsack H-J. 2008. Geochemical analysis of surface water samples of BrumsackHJ_CRA_030722_TP3. PANGAEA.

Deng Z, Huang D, He Q, Chassagne C. 2022. Review of the action of organic matter on mineral sediment flocculation. Frontiers in Earth Science 10, 965919.

Desmit X, Schartau M, Riethmüller R, Terseleer N, Van der Zande D, Fettweis M. 2024. The transition between coastal and offshore areas in the North Sea unraveled by suspended particle composition. Science of the Total Environment 915, 169966.

Dethier EN, Renshaw CE, Magilligan FG. 2022. Rapid Changes to Global River Suspended Sediment Flux by Humans. Science 376, 1447–1452.

Dislich C, Keyel AC, Salecker J, Kisel Y, Meyer KM, Auliya M, Barnes AD, Corre MD, Darras K, Faust H, Hess B, Klasen S, Knohl A, Kreft H, Meijide A, Nurdiansyah F, Otten F, Pe'er G, Steinebach S, Tarigan S, Tölle MH, Tscharntke T, Wiegand K. 2017. A review of the ecosystem functions in oil palm plantations, using forests as a reference system. Biological Reviews 92, 1539-1569.

Downing J. Twenty-Five Years with OBS Sensors: The Good, the Bad, and the Ugly. Continental Shelf Research 26, 2299–2318

Doxaran D, Ehn J, Bélanger S, Matsuoka A, Hooker S, Babin M. 2012. Optical characterisation of suspended particles in the Mackenzie River plume (Canadian Arctic Ocean) and implications for ocean colour remote sensing. Biogeosciences 9, 3213–3229.

Droppo IG. 2001. Rethinking what constitutes suspended sediment. Hydrological Processes

15, 1551–1564.

Dubbin WE, Vetterlein JP, Jonsson JL. 2014. Fatty acids promote fulvic acid intercalation by montmorillonite. Applied Clay Science, 97–98, 53-61.

Ducklow HW. 2001. Bacterioplankton. In: Encyclopedia of Ocean Sciences, Ed. Steele JH, Academic Press, 217-224.

Duclos PA, Lafite R, Le Bot S, Rivoalen E, Cuvilliez A.2013. Dynamics of Turbid Plumes Generated by Marine Aggregate Dredging: An Example of a Macrotidal Environment (the Bay of Seine, France). Journal of Coastal Research 29, 25–37

Dyer KR. 1989. Sediment processes in estuaries: Future research requirements. Journal of Geophysical Research 94, 14327–14339.

Dyer KR, Manning AJ. 1999. Observation of the size, settling velocity and effective density of flocs, and their fractal dimensions. Journal of Sea Research 41, 87-95.

Eisma D. 1986. Flocculation and de-flocculation of suspended matter in estuaries. Netherlands Journal of Sea Research 20, 183-199.

Eisma D, Kalf J. 1979. Distribution and particle size of suspended matter in the Southern Bight of the North Sea and the Eastern Channel. Netherlands Journal of Sea Research 13, 298-324.

Engel A, Endres S, Galgani L, Schartau M. 2020. Marvelous marine microgels: on the distribution and impact of gel-like particles in the oceanic water-column. Frontiers in Marine Science 7, 865 405.

Enke TN, Leventhal GE, Metzger M, Saavedra JT, Cordeo OX. 2018. Microscale ecology regulates particulate organic matter turnover in model marine microbial communities. Nature Communications 9, 2743.

Escobar S, Bi Q, Fettweis M, Monbaliu J, Wongsoredjo S, Toorman E. 2023. A 2DH flocculation model for coastal domains. Ocean Dynamics 73, 333-358.

Etcheber H, Taillez A, Abril G, Garnier J, Servais P, Moatar F, Commarieu M-V. 2007. Particulate organic carbon in the estuarine turbidity maxima of the Gironde, Loire and Seine estuaries: origin and lability. Hydrobiology 588, 245–259.

Fagel N. 2007. Clay minerals, deep circulation and climate. In: Developments in Marine Geology (Eds. Hillaire–Marcel C, De Vernal A.), Elsevier 1, 139-184.

Fall KA, Friedrichs CT, Massey GM, Bowers DG, Smith JS. 2021. The importance of organic content to fractal floc properties in estuarine surface waters: Insights from video, LISST, and pump sampling. Journal of Geophysical Research 126, e2020JC016787.

Farquharson LM, Romanovsky VE, Cable WL, Walker DA, Kokelj SV, Nicolsky D. 2019. Climate change drives widespread and rapid thermokarst development in very cold permafrost in the Canadian high Arctic. Geophysical Research Letters 46, 6681–6689.

Fettweis M. 2008. Uncertainty of excess density and settling velocity of mud flocs derived from in situ measurements. Estuarine Coastal and Shelf Science 78, 428-436.

Fettweis M, Francken F, Van den Eynde D, Verwaest T, Janssens J, Van Lancker V. 2010. Storm influence on SPM concentrations in a coastal turbidity maximum area (southern North Sea) with high anthropogenic impact. Continental Shelf Research 30, 1417-1427.

Fettweis M, Baeye M. 2015. Seasonal variation in concentration, size, and settling velocity of muddy marine flocs in the benthic boundary layer. Journal of Geophysical Research: Oceans 120, 5648-5667.

Fettweis M, Riethmüller R, Verney R, Becker M, Backers J, Baeye M, Chapalain M, Claeys S, Claus J, Cox T, Deloffre J, Depreiter D, Druine F, Flöser G, Grünler S, Jourdin F, Lafite R, Nauw J, Nechad B, Röttgers R, Sotollichio A, Vanhaverbeke W, Vereecken H. 2019. Uncertainties associated with in situ long-term observations of suspended particulate matter concentration using optical and acoustic sensors. Progress in Oceanography, 178, 102162.

Fettweis M, Schartau M, Desmit X, Lee BJ, Terseleer N, Van der Zande D, Parmentier K, Riethmüller R. 2022. Organic matter composition of biomineral flocs and its influence

on suspended particulate matter dynamics along a nearshore to offshore transect. Journal of Geophysical Research: Biogeosciences 127, e2021JG006332.

Fettweis M, Riethmüller R, Van der Zande D, Desmit X. 2023. Water quality monitoring in coastal seas: How significant is the information loss of patchy time series? Science of the Total Environment 873, 162273.

Fettweis M, De Witte B, Van Hoey, Seghers S, Vanermaete, Timmermanx S, Hermans L. 2024. Vooruitgangsrapport juni 2024 over de effecten op het mariene milieu van baggerspeciestortingen. MF/2024/10, 34pp.

Fettweis M, Silori S, Adriaens R, Desmit X. 2025. Clay minerals and the stability of organic carbon in suspension along coastal to offshore transects. Geochimica et Cosmochimica Acta 395, 229-237.

Filippelli GM. 2008. The global phosphorus cycle: Past, present, and future. Elements 4, 89–95.

Finkel ZV, Beardall J, Flynn KJ; Quigg A, Rees TAV, Raven JA. 2010. Phytoplankton in a changing world: cell size and elemental stoichiometry. Journal of Plankton Research 32, 119–137.

Fitzsimons MF, Millward GE, Revitt DM, Dawit MD. 2006. Desorption kinetics of ammonium and methylamines from estuarine sediments: consequences for the cycling of nitrogen. Marine Chemistry 101, 12-26.

Flemming BW, Nyandwi N. 1994. Land reclamation as a cause of fine-grained sediment depletion in backbarrier tidal flats (Southern North Sea). Netherlands Journal of Aquatic Ecology 28, 299–307.

Flynn KJ. 2019.Mixotrophic protists and a new paradigm for marine ecology: where does plankton research go now? Journal of Plankton Research 41, 375–391.

Francois RE, Garrison GR. 1982. Sound absorption based on ocean measurements. Part II: Boric acid contribution and equation for total absorption. Journal of the Acoustic Society of America 72, 1879–1890.

Froelich PN. 1988. Kinetic control of dissolved phosphate in natural rivers and estuaries: A primer on the phosphate buffer mechanism. Limnology & Oceanography 33, 649–668.

Fox-Kemper B, Hewitt HT, Xiao C, Aðalgeirsdóttir G, Drijfhout SS, Edwards TL, Golledge NR, Hemer M, Kopp RE, Krinner G, Mix A, Notz D, Nowicki S, Nurhati IS, Ruiz L, Sallée J-B, Slangen ABA, Yu Y, 2021: Ocean, Cryosphere and Sea Level Change. In Climate Change 2021: The Physical Science Basis. Contribution of Working Group I to the Sixth Assessment Report of the Intergovernmental Panel on Climate Change. Cambridge University Press, Cambridge, United Kingdom and New York, NY, USA, 1211–1362.

Fugate DC, Friedrichs CT. 2003. Controls on suspended aggregate size in partially mixed estuaries. Estuarine, Coastal and Shelf Science 58, 389–404.

Gall MP, Strzepek R, Maldonado M, Boyd PW. 200). Phytoplankton processes. Part 2: Rates of primary production and factors controlling algal growth during the Southern Ocean Iron RElease Experiment (SOIREE). Deep Sea Research Part II 48, 2571–2590.

Gartner JW. 2004. Estimating Suspended Solids Concentrations from Backscatter Intensity Measured by Acoustic Doppler Current Profiler in San Francisco Bay, California. Marine Geology 211, 169–187.

Gemmell BJ, Oh G, Buskey EJ, Villareal TA. 2016. Dynamic sinking behaviour in marine phytoplankton: Rapid changes in buoyancy may aid in nutrient uptake. Proc. R. Soc. B. 283, 20161126.

Geyer WR, MacCready P. 2014. The estuarine circulation. Annual Review of Fluid Mechanics 46, 175-197.

Goberville E, Beaugrand G, Sautour B, Tréguer P, SOMLIT Team. 2010. Climate-driven changes in coastal marine systems of western Europe. Marine Ecology Progress Series 408, 129–147.

Gordeev VV, Beeskow B, Rachold V. 2007. Geochemistry of the Ob and Yenisey Estuaries: A Comparative Study. Reports on Polar and Marine Research 565, Alfred Wegener Institut für Polar- und Meeresforschung, Bremerhaven.

Graham GW, Davies EJ, Nimmo-Smith WAM, Bowers DG, Braithwaite K.M. 2012. Interpreting LISST-100X measurements of particles with complex shape using digital in-line holography. Journal of Geophysical Research 117, C05034.

Gray JR, Gartner JW. 2009. Technological Advances in Suspended-Sediment Surrogate Monitoring. Water Resources Research 45, 10–29.

Griffin JJ, Windom H, Goldberg ED. 1968. The distribution of clay minerals in the World Ocean. Deep Sea Research 15, 433–459.

Grillo M, Schiaparelli S, Durazzano T, Guglielmo L, Granata A, Huettmann F. 2024. Machine learning applied to species occurrence and interactions: the missing link in biodiversity assessment and modelling of Antarctic plankton distribution. Ecological Processes 13, 56.

Guo XP, Liu X, Niu ZS, Lu DP, Zhao S, Sun XL, Wu JY, Chen YR, Tou FY, Hou L, Liu M, Yang Y. 2018. Seasonal and spatial distribution of antibiotic resistance genes in the sediments along the Yangtze Estuary, China. Environmental Pollution 242, 576-584.

Hackney CR, Darby SE, Parsons DR, Leyland J, Best JL, Aalto R, Nichols AP, Houseago RC. 2020. River bank instability from unsustainable sand mining in the lower Mekong River. Nature Sustainability 3, 217–225.

Hall POJ, Rosell EA, Stefano B, Dale AW, Hylén A, Kononets M, Nilsson M, Sommer S, van de Velde S, Viktorsson L. 2017. Influence of natural oxygenation of Baltic proper deep water on benthic recycling and removal of phosphorus, nitrogen, silicon and carbon. Frontiers in Marine Science 4, 27.

Hayes CT. 2021. Global ocean sediment composition and burial flux in the deep sea. Global Biogeochemical Cycles 35, e2020GB006769.

Hedges JI, Keil RG. 1995. Sedimentary organic matter preservation: an assessment and speculative synthesis. Marine Chemistry 49, 81-115.

Hedges JI, Kei RG, Benner R. 1997. What happens to terrestrial organic matter in the ocean? Organic Geochemistry 27, 195-212.

Hedges JI, Keil RG. 1999. Organic geochemical perspectives on estuarine processes: sorption reactions and consequences. Marine Chemistry 1,55-65.

Hemingway JD, Rothman DH, Grant KE, Rosengard SZ, Eglinton TI, Derry LA, Galy VV. 2019. Mineral protection regulates long-term global preservation of natural organic carbon. Nature 570(7760), 228-231.

Herman PM, Heip CH. 1999. Biogeochemistry of the MAximum TURbidity Zone of Estuaries (MATURE): some conclusions. Journal of Marine Systems 22, 89-104.

Hering JG, Morel FM. 1989. Kinetics of trace metal complexation: ligand-exchange reactions. Environmental Science and Technology 24, 242-252.

Hingamp P Grimsley N, Acinas SG, Clerissi C, Subirana L, Poulain J, Ferrera I, Sarmento H, Villar E, Lima-Mendez G, Faust K, Sunagawa S, Claverie J-M, Moreau H, Desdevises Y, Bork P, Raes J, de Vagas C, Karsenti E, Kandels-Lewis S, Jaillon O, Not F, Pesant S, Wincker P, Ogata H. 2013. Exploring nucleo-cytoplasmic large DNA viruses in Tara Oceans microbial metagenomes. The ISME Journal 7, 1678–1695.

Ho QN, Fettweis M, Spencer KL, Lee BJ. 2022. Flocculation with heterogeneous composition in water environments: A review. Water Research 213, 118147.

ICES. 2019. Working group on the effects of extraction of marine sediments on the marine ecosystem (WGEXT). ICES Cooperative Research Report 1, 87.

Ittekkot V. 1988. Global trends in organic matter in river suspensions. Nature 332, 436–438.

Iversen MH, Pakhomov EA, Hunt BPV, van der Jagt H, Wolf-Gladrow D, Klaas C. 2017. Sinkers

or floaters? Contribution from salp pellets to the export flux during a large bloom event in the Southern Ocean. Deep-Sea Research II 138, 116–25 (2017).

Jackson GA. 1990. A model of the formation of marine algal flocs by physical coagulation processes. Deep-Sea Research 37, 1197-1211.

Jalón-Rojas I, Sous D, Marieu V. 2024. A wave-resolving 2DV Lagrangian approach to model microplastic transport in the nearshore. Geoscientific Model Development Discussions, 1-26.

James NP, Jones BG. 015. Origin of carbonate rocks. John Wiley & Sons, 464pp.

Jankowski KL, Törnqvist TE, Fernandes AM. 2017. Vulnerability of Louisiana's coastal wetlands to present-day rates of relative sea-level rise. Nature Communications 8, 14792.

Jeldres RI, Fawell PD, Florio B . 2018. Population balance modelling to describe the particle aggregation process: A review. Powder Technology 326, 190–207.

Jiang T, Wu Y, Liu C, Whittle AJ, Guo D, Zhang G. 022. Kinetics of flocculated illite suspensions affected by ionic strength, pH, and hydrodynamic shearing. Applied Clay Science 221, 106462.

Jiao N, Herndl GJ, Hansell DA, Benner DA, Benner R, Kattner G, Wilhelm SW, Kirchman DL, Weinbauer MG, Luo T, Chen F, Azam F. 2010 Microbial production of recalcitrant dissolved organic matter: Long-term carbon storage in the global ocean. Nature Reviews Microbiology 8, 593–599.

Jones, R, Bessell-Browne P, Fisher R, Klonowski W, Slivkoff M. 2016. Assessing the Impacts of Sediments from Dredging on Corals. Marine Pollution Bulletin 102, 9–29.

Kaiser D, Konovalov SK, Arz HW, Voss M, Krüger S, Pollehne F, Jeschek J, Waniek JJ. 2019. Black Sea water column dissolved nutrients and dissolved and particulate organic matter from winter 2013, Maria S. Merian cruise MSM33. PANGAEA.

Ke Y, Calmels D, Bouchez J, Quantin C. 2022. MOdern River archivEs of Particulate Organic Carbon: MOREPOC. Earth System Science Data 14, 4743–4755.

Keil RG, Mayer LM. 2014. Mineral Matrices and Organic Matter. In: Turekian HDHK (Ed.) Treatise on Geochemistry, 2nd Edn., Elsevier, 337–359.

Keil RG, Montluçon DB, Prahl FG, Hedges JI. 1994. Sorptive preservation of labile organic matter in marine sediments. Nature 370, 549-552.

Kerimoglu O, Hintz NH, Lücken L, Blasius B, Böttcher L, Bunse C, Dittmar T, Heyerhoff B, Mori C, Striebel M, Simon M. 2022. Growth, organic matter release, aggregation and recycling during a diatom bloom: A model-based analysis of a mesocosm experiment. Microbiology (preprint).

Kharbusch JJ, Close, HG, Van Mooy BAS, Arnosti C, Smittenberg RH, Le Moigne FAC, Mollenhauer G, Scholz-Böttcher B, Obreht I, Joch BP, Becker KW, Iversen MH, Mohr W. Particulate organic carbon deconstructed: Molecular and chemical composition of particulate organic carbon in the ocean. Frontiers in Marine Science 7, 518.

Khelifa A, Hill PS. 2006. Models for effective density and settling velocity of flocs. Journal of Hydraulic Research 44, 390–401.

Kim AS, Stolzenbach KD. 2004. Aggregate formation and collision efficiency in differential settling. Journal of Colloid and Interface Science 271, 110–119.

Kim YH, Voulgaris G. 2003. Estimation of suspended sediment concentration in estuarine environments using acoustic backscatter from an ADCP. Proceedings of Coastal Sediments.

Kint L, Barette F, Degrendele K, Roche M, Van Lancker V. 2023. Sediment variability in intermittently extracted sandbanks in the Belgian part of the North Sea. Frontiers in Earth Science 11.

Kiørboe T, Andersen KP, Dam H. 1990. Coagulation efficiency and aggregate formation in marine phytoplankton. Marine Biology 107. 235-245.

Kiørboe T. 2011. How zooplankton feed: Mechanisms, traits and trade-offs. Biological Reviews 86, 311-339.

Kleber M, Bourg IC, Coward EK, Hansel CM, Myneni SC, Nunan N. 2021. Dynamic interactions at the mineral–organic matter interface. Nature Reviews Earth & Environment 2, 402-421.

Kokelj SV, Lacelle D, Lantz TC, Tunnicliffe J, Malone L, Clark ID, Chin KS. 2013. Thawing of massive ground ice in mega slumps drives increases in stream sediment and solute flux across a range of watershed scales. Journal of Geophysical Research 118, 681–692.

Koppelle S, López-Escardó D, Brussaard CPD, Huisman J, Philippart CJM, Massana R, Wilken S. 2022. Mixotrophy in the bloom-forming genus Phaeocystis and other haptophytes. Harmful Algae, 117, 102292.

Kranenburg C. 1994. On the fractal structure of cohesive sediment aggregates. Estuarine, Coastal & Shelf Science 39, 451e460.

Kriest I, Evans GT. 1999. Representing phytoplankton aggregates in biogeochemical models. Deep Sea Research Part I 46, 1841–1859.

Krone RB. 1962. Flume studies of the transport of sediment in estuarial shoaling processes. Final Report, Hydraulic Engineering Laboratory and Sanitary Engineering Research Laboratory, University of California, Berkeley.

Kumar M, Tibocha-Bonilla JD, Füssy Z, Lienig C, Schwenk SM, Levesque AV, Al-Bassam MM, Passi A, Neal M, Zuniga C, Kayom F, Espinoza JL, Lim H, Polson SW, Zeigler Allen L, Zengler K. 2024. Mixotrophic growth of a ubiquitous marine diatom. Science Advances 10, eado2623.

Kumar S, Ramkrishna D. 1996. On the solution of population balance equations by discretization—I. A fixed pivot technique. Chemical Engineering Science 51, 1311–1332.

Kuprenas R, Tran D, Strom K. 2018. A Shear-Limited Flocculation Model for Dynamically Predicting Average Floc Size. Journal of Geophysical Research: Oceans, 123(9), 6736–6752.

Ladd AJC. 1994. Numerical simulations of particulate suspensions via a discretized Boltzmann equation. Part 2. Numerical results. Journal of Fluid Mechanics, 271, 311–339.

LaRowe DE, Arndt S, Bradley JA, Estes ER, Haarfrost A, Lang SQ, Lloyd KG, Mahmoudi N, Orsi WD, Shah Walter SR, Steen AD, Zhao R. 2020. The fate of organic carbon in marine sediments - New insights from recent data and analysis. Earth-Science Reviews 204, 103146.

Latrubesse EM, Amsler ML, de Morais RP, Aquino S. 2009. The geomorphologic response of a large pristine alluvial river to tremendous deforestation in the South American tropics: The case of the Araguaia River. Geomorphology 113, 239–252.

Laurenceau-Cornec EC, Trull TW, Davies DM, De La Rocha CL, Blain S. 2015. Phytoplankton morphology controls on marine snow sinking velocity. Marine Ecology Progress Series 520, 35–56.

Laursen SN, Fruergaard M, Andersen TJ. 2022. Rapid flocculation and settling of positively buoyant microplastic and fine-grained sediment in natural seawater. Marine Pollution Bulletin 178, 113619.

Lauwaert B, Fettweis M, De Witte B, Van Hoei G, Timmermans S, Hermans L. 2019. Vooruitgangsrapport (juni 2019) over de effecten op het mariene milieu van baggerspeciestortingen (Vergunningsperiode 01/01/2017 – 31/12/2021). RBINS-ILVO-AMT-CD rapport. BL/2019/01, 28pp.

Lauwaert B, De Witte B, Festjens F, Fettweis M, Hermans L, Lesuisse A, Le H-M, Seghers S, Timmermans S, Vanavermaete D, Van Hoey G. 2021. Synthesis report on the effects of dredged material dumping on the marine environment (licensing period 2017-2021). RBINS-ILVO-AMT-AMCS-FHR report BL/2021/10, 67pp.

Lee BJ, Toorman E, Molz FJ, Wang J. 2011. A two-class population balance equation yielding bimodal flocculation of marine or estuarine sediments. Water Research 45, 2131–2145.

Lee BJ, Fettweis M, Toorman E, Molz F. 2012. Multimodality of a particle size distribution of cohesive suspended particulate matters in a coastal zone. Journal of Geophysical Research Ocean 117, C03014.

Lee J, Liu JT, Lin Y-S, Chen C-TA, Wang B-S. 2023. The contrast in suspended particle dynamics at surface and near bottom on the river-dominated northern South China Sea shelf in summer: Implication on physics and biogeochemistry coupling. Frontiers in Marine Science 10.

Lein AY, Kravchishina MD, Politova NV, Savvichev AS, Veslopolova EF, Mitskevich IN, Ul'yanova NV, Shevshenko VP, Ivanov MV. 2012. (Table 3-1) Concentrations of suspended matter, particulate organic carbon, carbonate carbon, total carbon and $\delta^{13}$C-Corg values in suspended matter from waters of the White Sea in July 2010. PANGAEA.

Leipe T, Tauber F, Vallius H, Virtasalo J, Uścinowicz, Kowalski N, Hille S, Lindgren S, Myllyvirta T. 2011. Particulate organic carbon (POC) in surface sediments of the Baltic Sea. Geo-Marine Letters 31, 175–188.

Li M, Whelan MJ, Wang GQ, White SM. 2013. Phosphorus sorption and buffering mechanisms in suspended sediments from the Yangtze Estuary and Hangzhou Bay, China. Biogeosciences 10, 3341-3348.

Li M, Peng C, Wang M, Xue W, Zhang K, Wang K, Shi G, Zhu Q. 2017. The carbon flux of global rivers: A re-evaluation of amount and spatial patterns. Ecological Indicators 80, 40–51.

Liu T, Xia X, Liu S, Mou X, Qiu Y. 2013. Acceleration of denitrification in turbid rivers due to denitrification occurring on suspended sediment in oxic waters. Environmental Science and Technology 47, 4053-4061.

Liu, X. et al. Sediment resuspension as a driving force for organic carbon transference and rebalance in marginal seas. Water Res. 257, 121672 (2024).

Lizotte, M. et al. Suspended particulate matter (SPM), Total particulate carbon (TPC) and Total particulate nitrogen (TPN) concentrations in the surface water of the Mackenzie Delta Region during 4 expeditions from spring to fall in 2019. PANGAEA (2021).

López AG, Najjar RG, Friedrichs MA, Hickner MA, Wardrop DH. 2021. Estuaries as filters for riverine microplastics: simulations in a large, coastal-plain estuary. Frontiers in Marine Science 26, 715924.

Lu T, Wang H, Hu L, Wu X, Bi N, Dang Y, Assavapanuvat P, Bianchi TS. 2023. Dynamic transport of particulate organic carbon in the Yellow River during dam-orientated water-sediment regulation. Marine Geology 460, 107054.

Lukashin VN, Kosobokova KN, Shevchenko VP, Shapiro GI, Pantiulin AN, Pertzova NM, Deev MG, Klyuvitkin AA, Novigatsky AN, Soloviev KA, Prego R, Latche L. 2003. (Table 4) ConcentraBitions of suspended matter and particulate chemical elements near the Gorlo Strait of the White Sea. PANGAEA.

Lürling, M. Grazing resistance in phytoplankton. Hydrobiologia 48, 237-249 (2021).

Lynch DR, Greenberg DA, Bilgili A, McGillicuddy DJ, Manning JP, Aretxabaleta AL. 2014. Particles in the coastal ocean: Theory and applications. Cambridge University Press.

Macht F, Eusterhues K, Pronk GJ, Totsche KU. 2011. Specific surface area of clay minerals: Comparison between atomic force microscopy measurements and bulk-gas (N2) and -liquid (EGME) adsorption methods. Applied Clay Science 53, 20-26.

Maerz J, Hofmeister R, van der Lee EM, Gräwe U, Riethmüller R, Wirtz KW. 2016. Maximum sinking velocities of suspended particulate matter in a coastal transition zone. Biogeosciences 13, 4863-4876.

Maggi F. 2009. Biological flocculation of suspended particles in nutrient-rich aqueous ecosystems. Journal of Hydrology 376, 116-125.

Malcolm RL, Durum WH. 1976. Organic carbon and nitrogen concentrations and annual

organic carbon load of six selected rivers of the United States. USGS Water-Supply Paper 1817-F.

Manik HM, Gultom DA.; Firdaus; Elson, L. Evaluation of ADCP Backscatter Computation for Quantifying Suspended Sediment Concentration. In Proceedings of the IOP Conference Series: Earth and Environmental Science; Institute of Physics Publishing, February 7 2020; Vol. 429.

Marchisio DL, Vigil RD, Fox RO. 2003. Quadrature method of moments for aggregation–breakage processes. Journal of Colloid and Interface Science 258, 322–334.

Martens N, Ehlert E, Putri W, Sibbertsen M, Schaum CE. 2024. Organic compounds drive growth in phytoplankton taxa from different functional groups. Proc. R. Soc. B. 291, 20232713.

Massicotte P, Babin M, Fell F, Fournier-Sicre V, Doxaran D. 2023. The coastal surveillance through observation of ocean color (COAST`OOC) dataset. Earth System Science Data 15, 3529–3545.

Mayer LM. 1994. Surface area control of organic carbon accumulation in continental shelf sediments. Geochimica et Cosmochimica Acta 58, 1271-1284.

Mayer LM. 1995. Sedimentary organic matter preservation: an assessment and speculative synthesis - A comment. Marine Chemistry 49, 127-136.

McCave IN. 1986. Local and global aspects of the bottom nepheloid layers in the world ocean. Journal of Sea Research 20, 167-181.

McCave IN, Hall IR, Antia AN, Chou L, Dehairs F, Lampitt RS, Thomsen L, van Weering TCE, Wollast R. 2001. Distribution, composition and flux of particulate material over the European margin at 47°-50°N. Deep-Sea Research II 48, 3107-3139.

McClelland, J.W. et al. Arctic Great Rivers Observatory. Water Quality Dataset. (2023).

McDonnell AMP, Buesseler KO. 2010. Variability in the average sinking velocity of marine particles, Limnology & Oceanography 55, 20852096.

Middelboe, M. & Lyck, P.G. Regeneration of dissolved organic matter by viral lysis in marine microbial communities. Aquat Microb Ecol 27, 187–194 (2002).

Middelboe, M. & Jørgensen, N.O.G. Viral lysis of bacteria: An important source of dissolved amino acids and cell wall compounds. J Marine Biol. Ass. UK 86, 605-612 (2006).

Middelburg JJ, Vlug T, Vandernat F. 1993. Organic-matter mineralization in marine systems. Global Planetary Change 8, 47-58.

Middelburg JJ, Levin LA 2009. Coastal hypoxia and sediment biogeochemistry. Biogeosciences 6, 1273-1293.

Middelburg JJ. 2019. Marine Carbon Biogeochemistry: A Primer for Earth System Scientists. Springer, 118pp.

Mietta, F. Chassagne, C. & Winterwerp, J.C. Shear-induced flocculation of a suspension of kaolinite as function of pH and salt concentration. J. Coll Interface Sci 336, 134-141 (2009).

Mitra, A. et al. 2014. The role of mixotrophic protists in the biological carbon pump. Biogeosciences 11, 995–1005.

Møller EF. 2005. Sloppy feeding in marine copepods: prey-size-dependent production of dissolved organic carbon. Journal of Plankton Research 27, 27-25.

Møller EF. 2007. Production of dissolved organic carbon by sloppy feeding in the copepods Acartia tonsa, Centropages typicus, and Temora longicornis. Limnology & Oceanography 52, 79-84.

Mopper, K. et al. The role of surface-active carbohydrates in the flocculation of a diatom bloom in a mesocosm. Deep Sea Res. 42, 47-73 (1995).

Morel, F.M. & Price, N.M. The biogeochemical cycles of trace metals in the oceans. Science 300, 944-947 (2003).

Moreira-Turcq, P., Seyler, P., Guyot, J.L. & Etcheber, H. Exportation of organic carbon from the Amazonas river and its main tributaries. Hydrol. Process. 17, 1329-1344 (2003).

Morin, J. & Morse, J.W. Ammonium release from resuspended sediments in the Laguna Madre estuary. Mar. Chem. 65(1-2), 97-110 (1999).

Morris, D.P. et al. The attenuation of solar UV radiation in lakes and the role of dissolved organic carbon. Limnology & Oceanography 40, 1381-1391 (1995).

Mort HP, Slomp CP, Gustafsson BG, Andersen TJ. 2010. Phosphorus recycling and burial in Baltic Sea sediments with contrasting redox conditions. Geochimica et Cosmochimica Acta 74, 1350-1362.

Moulton M, Suanda SH, Garwood JC, Kumar N, Fewings MR, Pringle JM. 2023. Exchange of plankton, pollutants and particles across the nearshore region. ? Annual Review of Marine Science 15, 167-202.

Mullison J. 2017. Backscatter Estimation Using Broadband Acoustic Doppler Current Profilers - Updated. In Proceedings of the ASCE Hydraulic Measurements & Experimental Methods Conference; Durham, 2017.

Nechad B, Ruddick KG, Park Y. 2010. Calibration and validation of a generic multisensor algorithm for mapping of total suspended matter in turbid waters. Remote Sensing of Environment 114, 854-866.

Némery J, Garnier J. 2007. Typical features of particulate phosphorus in the Seine estuary (France). Hydrobiology 588, 271-290.

Nemirovskaya IA, Sivkov VP. 2012. (Table 1) Suspended matter and particulate organic compounds in waters of the southeastern Baltic Sea. PANGAEA.

Nerem RS, B. D. Beckley BD, Fasullo JT, Hamlington BD , Masters D, Mitchum GT. 2018. Climate-change–driven accelerated sea-level rise detected in the altimeter era. PNAS 115, 2022–2025.

Neukermans G, Ruddick K, Loisel H, Roose P. 2012. Optimization and quality control of suspended particulate matter concentration measurement using turbidity measurements. Limnology & Oceanography Methods 10, 1011-1023.

Nghiem, J. A., Li, G. K., Harringmeyer, J. P., Salter, G., Fichot, C. G., Cortese, L., & Lamb, M. P. (2024). Validating floc settling velocity models in rivers and freshwater wetlands. EGUsphere, 2024, 1–55.

Nguyen, T. T., Laurent, F., Fox, R. O., & Massot, M. (2016). Solution of population balance equations in applications with fine particles: Mathematical modeling and numerical schemes. Journal of Computational Physics, 325, 129–156.

Nguyen, T.T.H., et al. Microbes contribute to setting the ocean carbon flux by altering the fate of sinking particulates. Nat Commun 13, 1657 (2022).

Nienhuis, J.H. et al. Global-scale human impact on delta morphology has led to net land area gain. Nature 577, 514–518 (2020).

OMEX Project Members & Bizarro, A.R. 2004a. Organic matter measured in surface water during AURIGA cruise PLUTUR2. PANGAEA (2004a).

OMEX Project Members & Bizarro, A.R. 2004b. Organic matter measured in surface water during AURIGA cruise PLUTUR3. PANGAEA (2004b).

OMEX Project Members & Bizarro, A.R. 2004c. Organic matter measured in surface water during AURIGA cruise PLUTUR4. PANGAEA (2004c).

OMEX Project Members & Bizarro, A.R. 2004d. Organic matter measured in surface water during AURIGA cruise PLUTUR5. PANGAEA (2004d).

OMEX Project Members & Bizarro, A.R. 2004e. Organic matter measured in surface water during AURIGA cruise PLUTUR6. PANGAEA (2004e).

Osterholz H, Kilgour DPA, Storey DS, Lavik G, Ferdelman TG, Niggemann J, Dittmar T. 2021.

Accumulation of DOC in the South Pacific Subtropical Gyre from a molecular perspective. Marine Chemistry 231, 103955.

Overeem, I. et al. Substantial export of suspended sediment to the global oceans from glacial erosion in Greenland. Nature Geosci 10, 859–863 (2017).

Park HB, Lee G-h. 2016. Evaluation of ADCP Backscatter Inversion to Suspended Sediment Concentration in Estuarine Environments. Ocean Science Journal 51, 109–125.

Parrella, F., Brizzolara, S., Holzner, M., & Mitrano, D. M. (2024). Impact of heteroaggregation between microplastics and algae on particle vertical transport. Nature Water, 1-12.

Partheniades, E. Cohesive Sediments in Open Channels, Butterworth-Heinemann, 384pp (2009).

Passow U, Alldredge AL. 1995. A dye-binding assay for the spectrophotometric measurement of transparent exopolymer particles (TEP). Limnology and Oceanography 40, 1326-1335.

Passow U. 2002. Transparent exopolymer particles (TEP) in aquatic environments. Progress in Oceanography 55, 287-333.

Penaloza-Giraldo, J. A., Hsu, T.-J., Manning, A. J., Ye, L., Vowinckel, B., & Meiburg, E. (2023). On the importance of temporal floc size statistics and yield strength for population balance equation flocculation model. Water Research, 233, 119780.

Petit, J.C.J., Bouezmarni, M., Roevros, N., & Chou, L. The use of acidimetric titration as a novel approach to study particulate trace metal speciation and mobility: Application to sediments of the Scheldt estuary. App. Geochem. 24, 1875-1888 (2009).

Prat, O. P., & Ducoste, J. J. (2006). Modeling spatial distribution of floc size in turbulent processes using the quadrature method of moment and computational fluid dynamics. Chemical Engineering Science, 61(1), 75–86.

Premuzic, E.T., Benkovitz, C.M., Gaffney, J.S. & Walsh, J.J. The nature and distribution of organic matter in the surface sediments of world oceans and seas. Organic Geochem. 4, 63–77 (1982).

Prieto L, Sommer F, Stibor H, Koeve W. 2001. Effects of Planktonic Copepods on Transparent Exopolymeric Particles (TEP) Abundance and Size Spectra. Journal of Plankton Research 23, 515–525.

Ramkrishna D, Singh MR. 2014. Population Balance Modeling: Current Status and Future Prospects. Annual Review of Chemical and Biomolecular Engineering, 5(1), 123–146.

Rateev, M.A., Gorbunova, Z.N., Lisitzyn, A.P., & Nosov, G.L. The distribution of clay minerals in the oceans. Sedimentology, 13, 21–43 (1969).

Regnier, P. et al. Anthropogenic perturbation of the carbon fluxes from land to ocean. Nature Geosci. 6, 597–607 (2013).

Restrepo, J.D. & Syvitski, J.P.M. Assessing the effect of natural controls and land use change on sediment yield in a major Andean river: the Magdalena drainage basin, Colombia. Ambio 35, 65–74 (2006).

Restrepo, J.D., Kettner, A.J. & Syvitski, J.P. Recent deforestation causes rapid increase in river sediment load in the Colombian Andes. Anthropoc. 10, 13–28 (2015).

Riebesell, U. Particle aggregation during a diatom bloom. I. Physical aspects. Marine Ecology Progress Series 69, 273-280 (1991).

Robinson JE, Newell RC, Seiderer LJ, Simpson NM. 2005. Impacts of aggregate dredging on sediment composition and associated benthic fauna at an offshore dredge site in the southern North Sea. Marine Environmental Research 60, 51-68.

Rodriguez, A.B., McKee, B.A., Miller, C.B., Bost, M.C. & Atencio, A.N. Coastal sedimentation across North America doubled in the 20th century despite river dams. Nat. Comm. 11, 3249 (2020).

Romankevich, E.A., Vetrov, A.A. (Table 3.6.1) Concentrations of suspended matter and

particulate organic carbon in waters along the section Ob River estuary - Kara Sea in September 1993. PANGAEA (2001a).

Romankevich, E.A., Vetrov, A.A. (Table 3.6.2) Concentrations of suspended matter and particulate organic carbon in surface waters along the section Enisey River estuary - Kara Sea in September 1993. PANGAEA (2001b).

Romankevich, E.A., Vetrov, A.A. (Table 3.9) Concentrations of suspended matter and particulate and dissolved organic carbon in waters of the Lena River and adjacent parts of the Laptev Sea in September 1989. PANGAEA (2001c)

Romankevich, E.A., Vetrov, A.A. (Table 3.10) Concentrations of suspended matter and particulate and dissolved organic carbon in waters of the Lena River and adjacent parts of the Laptev Sea in September 1991. PANGAEA (2001d).

Röttgers, R., Heymann, K. & Krasemann, H. Suspended matter concentrations in coastal waters: methodological improvements to quantify individual measurement uncertainty. Estuar. Coast. Shelf Sci. 151, 148–155 (2014).

Safar, Z., Deng, Z., & Chassagne, C. (2023). Applying a logistic growth equation to model flocculation of sediment in the presence of living and dead organic matter. Frontiers in Marine Science, 10.

Sanders, T. & Laanbroek, H.J. The distribution of sediment and water column nitrification potential in the hyper-turbid Ems estuary. Aquat. Sci. 80, 1-13. (2018)

Schartau M, Riethmüller R, Flöser G, van Beusekom JEE, Krasemann H, Hofmeister R, Wirtz K. 2019. On the separation between inorganic and organic fractions of suspended matter in a marine coastal environment. Progress in Oceanography 171, 231-250.

Schmidt, D.N., Lazarus, D., Young, J.R. & Kucera, M. Biogeography and evolution of body size in marine plankton. Earth-Sci. Rev. 78, 239-266 (2006).

Schulz, G., Voynova, Y.G., Metzke, M. & Schmidt, L. Nitrogen turnover in the Ems estuary 2020. PANGAEA (2022a).

Schulz, G. et al. 2022b Suspended particulate matter drives the spatial segregation of nitrogen turnover along the hyper-turbid Ems estuary. Biogeosciences 19, 2007–2024.

Schuerch, M. et al. The effect of long-term and decadal climate and hydrology variations on estuarine marsh dynamics: An identifying case study from the Río de La Plata. Geomorphol. 269, 122–132 (2016).

Scully ME, Friedrichs CT. 2007. Sediment pumping by tidal asymmetry in a partially mixed estuary. Journal of Geophysical Research 112, C07028.

Sewerin, F. (2024). A eulerian monte carlo method for the numerical solution of the multivariate population balance equation. Journal of Computational Physics, 509, 113024.

Seyler, P. & Boaventura, G. Trace elements in the mainstream Amazon River. In: McClain, M.E., Victoria, R.L., Richey, J.E. (Eds.) The Biogeochemistry of the Amazon Basin. Oxford University Press, 307-327 (2001).

Shen, X., Lee, B. J., Fettweis, M., & Toorman, E. A. (2018). A tri-modal flocculation model coupled with TELEMAC for estuarine muds both in the laboratory and in the field. Water Research, 145, 473–486.

Shen X, Toorman EA, Lee BJ, Fettweis M. 2018. Biophysical flocculation of suspended particulate matters in Belgian coastal zones. Journal of Hydrology 567, 238-252,

Shen, X., Toorman, E. A., Lee, B. J., & Fettweis, M. (2019). An Approach to Modeling Biofilm Growth During the Flocculation of Suspended Cohesive Sediments. Journal of Geophysical Research: Oceans, 124(6), 4098–4116.

Shen, Z., Zhou, S., & Pei, S.. Transfer and transport of phosphorus and silica in the turbidity maximum zone of the Changjiang estuary. Estuar. Coast. Shelf Sci. 78(3), 481-492. (2008)

Shettigar, N. A., Bi, Q., & Toorman, E. (2024). Assimilating size diversity: Population balance equations applied to the modeling of microplastic transport. Environmental Science &

Technology, 58(36), 16112.
Singh M, Sarkar B, Biswas B, Churchman J, Bolan NS. 2016. Adsorption-desorption behavior of dissolved organic carbon by soil clay fractions of varying mineralogy. Geoderma 280, 47-56.
Silori, S. et al. Vertical dynamics of suspended particulate matter and chlorophyll-a in a well-mixed coastal turbid system. Estuar. Coast. Shelf Sci. (2025).
Smoluchowski, M. v. (1917). Versuch einer mathematischen Theorie der Koagulationskinetik kolloider Lösungen. Zeitschrift Für Physikalische Chemie, 92U(1), 129–168.
Sobek, A., Gustafsson, Ö., Hajdu, S. & Larsson, U. Particle− water partitioning of PCBs in the photic zone: a 25-month study in the open Baltic Sea. Environm. Sci. & Techn. 38, 1375-1382 (2004).
Soetaert K, Middelburg JJ, Heip C, Meire P, Van Damme S, Maris T. 2006. Long-term change in dissolved inorganic nutrients in the heterotrophic Scheldt estuary (Belgium, The Netherlands). Limnology & Oceanography 51, 409-423.
Spearman J. 2015. A review of the physical impacts of sediment dispersion from aggregate dredging. Marine Pollution Bulletin 94, 260–277.
Środoń J, Drits VA, McCarty DK, Hsieh JCC, Eberl DD. 2001. Quantitative XRD analysis of clay-rich rocks from random preparations. Clays and Clay Minerals 49, 514–528.
Steffen, W. et al. Planetary boundaries: Guiding human development on a changing planet. Science 347, 736 (2015).
Stone M, Emelko MB, Droppo IG, Silins U. Biostabilization and erodibility of cohesive sediment deposits in wildfire-affected streams. Water Res. 45, 521-534, (2011).
Su J, Gu Z, Li Y, Feng S, Xu XY. 2007. Solution of population balance equation using quadrature method of moments with an adjustable factor. Chemical Engineering Science 62, 5897–5911.
Sugihara G, May R. 1990. Nonlinear forecasting as a way of distinguishing chaos from measurement error in time series. Nature 344, 734-741.
Suzumura M, Kokubun H, Arata N. 2004. Distribution and characteristics of suspended particulate matter in a heavily eutrophic estuary, Tokyo Bay, Japan. Marine Pollution Bulletin 49, 496-503.
Syvitski JP, Zalasiewicz J, Summerhayes C. 2019. Changes to Holocene/Anthropocene patterns of sedimentation from terrestrial to marine. In: The Anthropocene as a geological time unit: A Guide to the scientific evidence and current debate (eds. Zalasiewicz J, Waters C, Williams M, Summerhayes C) Cambridge Univ. Press, 90-108.
Syvitski JP, Ãngel J, Saito Y, Overeem I, Vörösmarty CJ, Wang H, Olago D. 2022. Earth's sediment cycle during the Anthropocene. Nature Review Earth & Environment 3, 179–96.
Szeligowska M, Benkort D, Przyborska A, Moskalik M, Moreno B, Trudnowska E, Blachowiak-Samolyk K. 2024. Estimates of carbon sequestration potential in an expanding Arctic fjord (Hornsund, Svalbard) affected by dark plumes of glacial meltwater. Biogeosciences 121, 3617-3639.
Tamooh F, Van den Meersche K, Meysman F, Marwick TR, Borges AV, Merckx R, Dehairs F, Schmidt S, Nyunja J, Bouillon S. 2012. Distribution and origin of suspended matter and organic carbon pools in the Tana River Basin, Kenya. Biogeosciences 9, 2905–2920.
Tan X, Liu F, Hu L, Reed AH, Furukawa Y, Zhang G. 2017. Evaluation of the particle sizes of four clay minerals. Applied Clay Science 135, 313-324.
Tang D, Warnken KW, Santschi PH. 2002. Distribution and partitioning of trace metals (Cd, Cu, Ni, Pb, Zn) in Galveston bay waters. Marine Chemistry 78, 29-45.
Tappin AD. 2002. An examination of the fluxes of nitrogen and phosphorus in temperate

and tropical estuaries: Current estimates and uncertainties. Estuarine, Coastal and Shelf Science 55, 885-901.

Tappin AD, Millward GE, Fitzsimons MF. 2010. Particle–water interactions of organic nitrogen in turbid estuaries. Marine Chemistry 122, 28-38.

Thiebault T, Chassiot L, Fougère L, Destandau E, Simonneau A, Van Beek P, Souhaut M, Chapron E. 2017. Record of pharmaceutical products in river sediments: A powerful tool to assess the environmental impact of urban management? Anthropocene 18, 47-56.

Thornton DC. 2014 Dissolved organic matter (DOM) release by phytoplankton in the contemporary and future ocean. European Journal of Phycology 49, 20-46.

Thorpe SA. 2005. The turbulent ocean. Cambridge University Press, 484pp.

Tolosa I, de Mora S, Sheikholeslami MR, Villeneuve J-P, Bartocci J, Cattini C. 2004. Aliphatic and aromatic hydrocarbons in coastal Caspian Sea sediments. Marine Pollution Bulletin 48, 44-60.

Törnqvist TE, Jankowski KL, Li YX, González JL. 2020.Tipping points of Mississippi Delta marshes due to accelerated sea-level rise. Science Advances 6, eaaz5512.

Tran D, Strom K. 2019. Floc sizes and resuspension rates from fresh deposits: Influences of suspended sediment concentration, turbulence, and deposition time. Estuaries Coastal and Shelf Science 229, 106397.

Tran D, Jacquet M, Pearson S, Van Prooijen B, Verney R. 2024. Estimation of Mud and Sand Fractions and Total Concentration From Coupled Optical-Acoustic Sensors. Earth and Space Science 11, e2024EA003694.

Turner, A., Salting out of chemicals in estuaries: implications for contaminant partitioning and modelling. Sci. Tot. Environ. 314, 599-612 (2003).

Twining BS, Baines SB. 2013. The trace metal composition of marine phytoplankton Annual Review of Marine Science 5, 191-215.

Van Lancker V, Bonne W, Garel E, Degrendele K, Roche M, Van den Eynde D, Bellec V, Brière C, Collins M, Velegrakis A. 2010. Recommendations for the Sustainable Exploitation of Tidal Sandbanks. Coastal Education & Research Foundation SI, 151–164.

van Maren DS, van Kessel T, Cronin K, Sittoni L. 2015. The impact of channel deepening and dredging on estuarine sediment concentration. Continental Shelf Research 95, 1-14.

van Maren DS, Oost AP, Wang ZB, Vos PC. 2016. The effect of land reclamations and sediment extraction on the suspended sediment concentration in the Ems Estuary. Marine Geology 376, 147-157.

Van Raaphorst W, Kloosterhuis HT, Berghuis EM, Gieles AJM, Malschaert JFP, Van Noort GJ. 1992. Nitrogen cycling in two types of sediments of the southern North Sea (Frisian Front, Broad Fourteens): field data and mesocosm results. Netherlands Journal of Sea Research 28, 293-316.

Vergne A, Berni C, Le Coz J, Tencé F, Lyon-Villeurbanne I. 2021.Acoustic backscatter and attenuation due to river fine sediments: Experimental evaluation of models and inversion methods. Water Resources Research 57, e2021WR029589.

Verney R, Lafite R, Brun-Cottan J-C. 2009. Flocculation potential of estuarine particles: The importance of environmental factors and of the spatial and seasonal variability of suspended particulate matter. Estuaries and Coasts 32, 678–693.

Vincent F, Porat Z, Schatz D, Vardi A. 2021. Visualizing active viral infection reveals diverse cell fates in synchronized algal bloom demise. PNAS 118, e2021586118.

Vousdoukas M, Ranasinghe R, Mentaschi L, Plomariis TA, Athanasiou P, Luijendijk A, Feyen L. 2020. Sandy coastlines under threat of erosion. Nature Climate Change 10, 260-263.

Walch H, von der Kammer F, Hofmann T. 2022. Freshwater suspended particulate matter—key components and processes in floc formation and dynamics. Water Research 220,

118655.
Walsby AE, Reynolds CS. 1980.Sinking and floating. In: The physiological ecology of phytoplankton. Blackwell, Oxford, 371–412.
Wan XS, Sheng H-X, Liu L, Shen H, Tang W, Zou W, Xu MN, Zheng Z, Tan E, Chen M, Zhang Y, Ward BB, Kao S-J. 2023. Particle-associated denitrification is the primary source of N2O in oxic coastal waters. Nature Communications 14, 8280.
Wang Q, Li Y. 2010. Phosphorus adsorption and desorption behavior on sediments of different origins. Journal of Soils and Sediments 10, 1159-1173.
Wang H, Saito Y, Zhang Y, Bi N, Sun X, Yang Z. 2011. Recent changes of sediment flux to the Western Pacific Ocean from major rivers in east and southeast Asia. Earth-Science Reviews 108, 80–100.
Waniek JJ, Krüger S, Jeschek J, Kreuzer L, Kaiser D. 2019. South China Sea water column dissolved nutrients and particulate organic matter from March 2015. Leibniz Institute for Baltic Sea Research, Warnemünde, PANGAEA.
Waniek JJ, Kuss J, Frazão HC, Schulz-Bull DE, Jeschek J, Sadkowiak B, Kreuzer L, Dierken M. 2021. Hydrochemistry measured on water bottle samples during the cruise Hai Yang Di Zhi Shi Hao in South China Sea in September 2018. PANGAEA
Waniek JJ, Schulz-Bull D, Frazão HC, Sadkowiak B, Kreuzer L, Jeschek J, Dierken M. 2022. Biological and chemical water properties measured in water bottle samples during the cruise SO269 in South China Sea in August/September 2019. PANGAEA
Wen L-S, Santschi P, Gill G, Paternostro C. 1992. Estuarine trace metal distributions in Galveston Bay: Importance of colloidal forms in the speciation of the dissolved phase. Marine Chemistry 63,: 185-212.
Wentworth CK. 1922. A Scale of grade and class terms for clastic sediments. The Journal of Geology 30, 377-392.
Weiss L. 2021. The missing ocean plastic sink: Gone with the rivers. Science 373,107-111.
Westheimer FH. 1987. Why nature chose phosphates. Science 235, 1173–1178.
Whitby H, Park J, Shaked Y, Boiteau RM, Buck KN, Bundy RM. 2024. New insights into the organic complexation of bioactive trace metals in the global ocean from the GEOTRACES era. Oceanography 37, 142-155.
Whittaker ML, Lammers LN, Carrero S, Gilbert B, Banfield JF. 2019. Ion exchange selectivity in clay is controlled by nanoscale chemical–mechanical coupling. PNAS 116, 22052–22057.
Wilhelm SW, Suttle CA. 1999. Viruses and nutrient cycles in the sea: Viruses play critical roles in the structure and function of aquatic food webs. BioScience 49, 781-788.
Wilson SE, Steinberg DK, Buesseler KO. 2008. Changes in fecal pellet characteristics with depth as indicators of zooplankton repackaging of particles in the mesopelagic zone of the subtropical and subarctic North Pacific Ocean. Deep Sea Research 55, 1636-1647.
Wilson RJ, Heath MR. 2019. Increasing turbidity in the North Sea during the 20th century due to changing wave climate. Ocean Science, 15, 1615–1625
Winterwerp JC. 1998. A simple model for turbulence induced flocculation of cohesive sediment. Journal of Hydraulic Research 36, 309–326.
Winterwerp JC, Van Kesteren WG. 2004. Introduction to the physics of cohesive sediment dynamics in the marine environment. Developments in Sedimentology 56. Elsevier, 576pp.
Wollast R. 1982. Behaviour of organic carbon, nitrogen and phosphorus in the Scheldt estuary. Thalassia Jugoslavica 18, 11-34.
Wu N, Grieve SWD, Manning AJ, Spencer KL. 2014. Flocs as vectors for microplastics in the aquatic environment. Nature Water 2, 1082–1090.

Wyns L, Roche M, Barette F, Van Lancker VRL, Degrendele K, Hostens K, De Backer A. 2021. Near-field changes in the seabed and associated macrobenthic communities due to marine aggregate extraction on tidal sandbanks: a spatially explicit bio-physical approach considering geological context and extraction regimes. Continental Shelf Research 229, 104546

Xia X, Liu T, Yang Z, Michalski G, Liu S, Jia Z, Zhang S. 2017. Enhanced nitrogen loss from rivers through coupled nitrification-denitrification caused by suspended sediment. Science of the Total Environment 579, 47-59.

Ye L, Wu J, Huang M, Yan J. 2023. The role of suspended extracellular polymeric substance (EPS) on equilibrium flocculation of clay minerals in high salinity water. Water Research 244, 120451.

Yu X, Balachandar S, Smith J, Manning AJ. 2024. Flocculation Dynamics of Cohesive Sediment in Turbulent Flows Using CFD-DEM Approach. IntechOpen.

Zeng J, Chen M, Zheng M, Qiu Y, He W, Liu X. 2018. Effects of particles on potential denitrification in the coastal waters of the Beibu Gulf in China. Science of the Total Environment 624, 1274-1286.

Zeelmaekers E, Honty M, Derkowski A, Środoń J, De Craen M, Vandenberghe N, Adriaens R, Ufer K, Wouters L. 2015. Qualitative and quantitative mineralogical composition of the Rupelian Boom clay in Belgium. Clay Minerals 50, 249–272.

Zhang S, Gan W-B, Ittekkot V. 1992. Organic matter in large turbid rivers: The Huanghe and its estuary. Marine Chemistry 38, 53-68.

Zhang J-F, Zhang Q-H, Maa JP-Y, Qiao G-Q. 2013. Lattice Boltzmann simulation of turbulence-induced flocculation of cohesive sediment. Ocean Dynamics 63, 1123–1135.

Zhang X, Stavn RH, Falster AU, Rick JJ, Gray D, Gould RW. 2017. Size distributions of coastal ocean suspended particulate inorganic matter: Amorphous silica and clay minerals and their dynamics. Estuarine, Coastal and Shelf Science 189, 243-251.

Zhang N, Li H, Xu F, Thompson CEL, Townend IH, He Q. 2025. Drag acting on suspended sediment increased by microbial colonization. Nature Geoscience 18, 396–401.

Zhao L, Gao L. 2019. Dynamics of dissolved and particulate organic matter in the Changjiang (Yangtze River) Estuary and the adjacent East China Sea shelf. Journal of Marine Systems 198, 103188.

Zhao T, Xu S, Hao F. 2023. Differential adsorption of clay minerals: Implications for organic matter enrichment. Earth Science Reviews 246, 104598.

Zhou J, Mopper K, Passow U. 1998. The role of surface-active carbohydrates in the formation of transparent exopolymer particles by bubble adsorption of seawater. Limnology & Oceanography 43, 1860-1871.

Zhou JL, Hong H, Zhang Z, Maskaoui K, Chen WJWR. 2000. Multi-phase distribution of organic micropollutants in Xiamen Harbour, China. Water Research 34, 2132-2150.

Zhu W, Wang C, Hill J, He Y, Tao B, Mao Z, Wu W. 2018. A missing link in the estuarine nitrogen cycle?: Coupled nitrification-denitrification mediated by suspended particulate matter. Scientific Reports 8, 2282.

Zhu Y, Lin M, Shen X, Fettweis M, Zhang Y, Zhang J, Bi Q, Wu Z. 2022. Biomineral flocculation of kaolinite and microalgae: Laboratory experiments and stochastic modeling. Journal of Geophysical Research Oceans 127, e2022JC018591.

COLOPHON

Dit rapport werd voorbereid door de BMM in maart 2026
Zijn referentiecode is MOMO/10/MF/202603/NL/AR/8

De scheepstijd met de RV Belgica werd voorzien door BELSPO en KBIN-OD Natuur

Indien u vragen hebt of bijkomende copies van dit document wenst te verkrijgen, gelieve een e-mail te zenden naar mfettweis@naturalsciences.be, met vermelding van de referentie, of te schrijven naar:

Koninklijk Belgisch Instituut voor Natuurwetenschappen
OD Natuur – BMM
t.a.v. Michael Fettweis
Vautierstraat 29
B–1000 Brussel
België
Tel: +32 2 627 41 83

BEHEERSEENHEID VAN HET
MATHEMATISCH MODEL VAN DE NOORDZEE

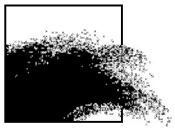

# APPENDIX 1

Bijdragen voor

**Particles in Europe workshop, 17-19 September 2025, Ostend (Belgium)**

# Intra-annual variability of marine floc morphology in southern North Sea coastal waters using *in-situ* high-resolution underwater imaging and the SANDI Python package

Louise Delhaye[a], Céline Taymans[a], Paul van Kan[b] and Michael Fettweis[a]

[a] Royal Belgian Institute of Natural Sciences, OD Nature, Rue Vautier 29, 1000 Brussels (Belgium)

[b] HAN University of Applied Sciences, P.O. Box 2217, NL-6802 CE, Arnhem (the Netherlands)

Corresponding author: Louise Delhaye, ldelhaye@naturalsciences.be

## Introduction

Marine suspended particulate matter (SPM), composed of mineral and organic particles that aggregate into flocs, plays a fundamental role in coastal and oceanographic processes such as sediment transport, carbon cycling, and water clarity (e.g. Fettweis et al., 2006, 2012; Giering et al., 2020b). Before the availability of an instrument capable of measuring the particle size distribution *in-situ* at high frequency and over long time periods (Agrawal & Pottsmith, 2000), the study of SPM mainly relied on optical devices such as back- or side scatter sensors or transmissometers, providing data on turbidity and after calibration, SPM concentration. Instruments like the LISST-100/200x (Laser In-situ Scattering and Transmissometry), have greatly changed our science, however, they provide 'blind' measurements of particle size distributions (PSDs), and are based on the assumption that particles are spherical. While size distribution is an essential metrics, it does not fully capture the complexity of natural particles, which vary in shape, density and composition, parameters that strongly influence settling velocity and transport dynamics (Markussen, 2020; Many et al., 2019; Giering et al., 2020a).

Shape characterization is especially important for understanding particle behavior, yet many studies and instruments still assume spherical geometry (Shen and Maa, 2016). Such assumption leads to errors in estimating dynamics, especially for flocs larger than 60 µm (Vahedi, 2010; Ye et al., 2024). Furthermore, LISST instruments are limited by a narrow size detection range (with a maximum size detection of 250 or 500 µm) and reduced accuracy at the minimum and maximum bins (Andrews et al., 2010).

Floc morphology remains understudied primarily due to the challenges of analyzing fragile, heterogeneous aggregates. Extreme fragility of such flocs requires *in-situ* study as sampling would likely break them down. Laboratory approaches (e.g. gel capture, microscopy, lab-based laser diffraction) are time-intensive, often disruptive, and can lead to unrepresentative sampling (e.g. Jarvis et al., 2005; Ye et al., 2024).

In the past decades, high-resolution *in-situ* underwater imaging has emerged as a non-invasive solution to overcome many of these challenges (e.g. Giering et al., 2020a,b; Many et al., 2019). This approach remains non-destructive while enabling almost continuous measurement. However, underwater imaging still faces several challenges: including inconsistency in metrics terminology ( Russ, 2011; Zhu et al., 2023), variability in sensor systems (Osborn et al., 2021), and lack of standardized image processing protocols. These factors firstly make datasets

comparison difficult between different imaging systems and secondly make comparisons with other techniques (e.g. laser diffraction, sedigraphy, camera sieving) challenging.

To address the first limitations, we developed an open-source, user-friendly software that is intended at creating more standardized underwater particle analysis workflows and results regarding both particle size and morphology. In this study, we present the structure of the software and use it on a dataset of images collected using a particle camera (PCam3). The goal was to verify if the results of the PCam3 using the software could be used as an effective tool to investigate intra-annual variability in floc morphology in the Belgian Part of the North Sea (BPNS).

## Methods

### *Study area*

The study area is located ~4 km offshore from Nieuwpoort in the BPNS, near the Westdiep aquaculture site. It is within a very dynamic environment, influenced by tidal currents and strong seasonal variations, but characterized by low SPM concentrations.

### *Data collection*

As part of the Westdiep aquaculture environmental monitoring, images were collected using a particle camera (PCam3, developed by Herbst Environmental Science) during six oceanographic campaigns on board the *RV Belgica* between April 2023 and March 2024. The camera was attached to the rosette which was profiling the water column every hour for several hours. Before processing, images were manually sorted in order to only retain sharp and high-quality images and excluding those where particles were visibly distorted by water movement or containing semi-transparent particles (likely phytoplankton).

### *Data processing*

In this presentation, we will present SANDI (Sediment ANalysis and Delineation through Images), an open-source Python package developed for automated image-based analysis of flocs, available on GitHub and PyPI. Based on the workflow developed by Markussen (2016), SANDI integrates additional image enhancement options, that can be adapted in a user-friendly interface and generates several shape and size metrics for detected particles. The software supports both single image and batch processing, enabling users to optimize the parameters on a test image before applying it to the entire dataset.

In the present study, the image processing workflow consisted of (1) denoising, (2) histogram stretching, (3) morphological reconstruction, (4) background illumination correction and (5) image resampling at a resolution of 1 µm. Preliminary to the processing of the *in-situ* data, the effect of each of these steps and of their parameters' values was tested on lab samples in order to find the optimal workflow. Particles were then extracted using Otsu's method for thresholding and the ones smaller than 7 adjacent pixels or touching the border of the image were discarded. For each extracted particle, size metrics (e.g. area, perimeter, equivalent spherical diameter, volume) and shape indicators (e.g. roundness, sphericity, aspect ratio, solidity, extent, form factor) were automatically computed.

*Statistical analyses*

Particles were then classified into flocculi (10-50 µm), microflocs (50-200 µm) and macroflocs (> 200 µm), following standard classifications (Lee et al, 2012). To identify natural groups of flocs, automatic clustering methods were used on micro- and macroflocs based on their size and shape metrics.

**Results & discussion**

In the preliminary results, the automatic clustering method grouped flocs into four distinct clusters, ranging from highly irregular and elongated to nearly spherical shapes. The seasonal distribution of these clusters showed clear trends in the morphology of marine suspended flocs: irregular, elongated flocs dominate in early spring probably pointing to the presence of phytoplankton, especially in March, while more regular, rounder ones became increasingly prevalent in autumn and winter, probably indicating the occurrence of mineral-dominated flocs. This suggests that seasonal variables (phytoplankton, marine gel production and flocculation, organic matter content) influence floc morphology.

**Conclusion**

These preliminary results tend to confirm that underwater high-resolution images processed through the SANDI python software can successfully give insights into the morphological variations of suspended particles, enabling to have a better understanding of SPM dynamics in the Belgian part of the North Sea. However, our preliminary results must still be investigated further before any statistically significant conclusion can be drawn.

**References**

Andrews, S., Nover, D., & Schladow, S. Using laser diffraction data to obtain accurate particle size distributions: The role of particle composition, Limnol. Oceanogr. Meth. 8, 507–526 (2010).

Fettweis M., Francken F., Pison V. and Van den Eynde D., 2006. “Suspended particulate matter dynamics and aggregate sizes in a high turbidity area”. Marine Geology 235, 63-74. https://doi.org/10.1016/j.margeo.2006.10.005

Fettweis M., Baeye M., Lee B.J., Chen P. and Yu J.C.S., 2012. “Hydro-meteorological influences and multimodal suspended particle size distributions in the Belgian nearshore area”, Geo-Marine Letters. https://doi.org/10.1007/s00367-011-0266-7

Giering S.L.C., Hosking B., Briggs N. and Iversen M.H, 2020a. “The Interpretation of Particle Size, Shape, and Carbon Flux of Marine Particle Images Is Strongly Affected by the Choice of Particle Detection Algorithm”. Frontiers in Marine Science 7:564. https://doi.org/10.3389/fmars.2020.00564

Giering S.L.C., Cavan E.L., Basedow S.L., Briggs N., Burd A.B., Darroch L.J., Guidi L., Irisson J-O., Iversen M.H., Kiko R., Lindsay D., Marcolin C.R., McDonnell A.M.P., Möller H.O., Passow U., Thomalla S., Trull T.W. and Waite A.M., 2020b. “Sinking Organic Particles in the Ocean-Flux Estimates Fom in-situ Optical Devices”, Frontiers in Marine Science 6:834. https://doi.org/10.3389/fmars.2019.00834

Graham, G.W., Davies, E.J., Nimmo-Smith, W.A.M., Bowers, D.G. & Braithwaite, K.M. Interpreting LISST-100X measurements of particles with complex shape using digital in-line holography. J. Geophys. Res. 117, C05034 (2012).

Jarvis P., Jefferson B. and Parsons S.A., 2005. “Measuring floc structural characteristics”, School of Water Sciences, Cranfield University, Cranfield, 45p.

Lee, B. J., M. Fettweis, E. Toorman, and F. J. Molz (2012), Multimodality of a particle size distribution of cohesive suspended particulate matters in a coastal zone, J. Geophys. Res., 117, C03014, doi:10.1029/2011JC007552.

Many G., Durieu De Madron X., Verney R., Bourrin F., Renosh P., Jourdin F. and Gangloff A., 2019. “Geometry, fractal dimension and settling velocity of locs during flooding conditions in the Rhône ROFI”, Estuarine, Coastal and Shelf Science 219, 1-13. https://doi.org/10.1016/j.ecss.2019.01.017

Markussen T.N., 2016. “Parchar - Characterization of Suspended Particles Through Image Processing in Matlab”, Journal of Open Research Software 4: e26. http://dx.doi.org/10.5334/jors.114.

Markussen T.N., Konrad C., Waldmann C., Becker M., Fischer G. and Iversen M.H., 2020. “Tracks in the Snow – Advantage of Combining Optical Methods to Characterize Marine Particles and Aggregates”, Frontiers in Marine Science 7:476.

Osborn R., Dillon B., Tran D., Abolfazli E., Dunne K.B.J., Nittrouer J.A. and Strom K., 2021. “FlocARAZI: An In-Situ, Image-Based Profiling Instrument for Sizing Solid and Flocculated Suspended Sediment”, Journal of Geophysical Research: Earth Surface, 126

Shen X. and Maa J. P.-Y., 2016. “A camera and image processing system for floc size distributions of suspended particles”, Marine Geology 376, 132-146.

Russ J.C., 2011. “The image processing handbook”. CRC Press.

Vahedi A., 2010. “Predicting the Settling Velocity of Lime Softening Flocs using Fractal Geometry”, PhD thesis, Department of Civil Engineering, University of Manitoba, Canada.

Ye L., Chen Z., Chen L., Ren J., Wu J., Chen Y., Huang X., Chen H. and Guo Y., 2024. “Volumetric reconstruction of settling mud flocs: A new insight of equilibrium flocculation in saline water”. Water Research 255. https://doi.org/10.1016/j.watres.2024.121512

Zhu Y., Chen Q., Zhang Y., Tang W., Xu C., Li W. and Jia J., 2023. “GraSSAMS: A new instrument designed for the determination of grain size and shape of sand-gravel-sized sediment”, Estuarine, Coastal and Shelf Science 290.

# Concentration and composition of Suspended Particulate Matter along nearshore to offshore transects

Michael Fettweis

Royal Belgian Institute of Natural Sciences, OD Natural Environment, rue Vautier 29, 1000 Brussels, Belgium

Corresponding author: Michael Fettweis, mfettweis@naturalsciences.be

Suspended particulate matter (SPM) is composed of minerals and organic matter (OM). The interaction between them take place in a variety of ways, from the sorption of organic molecules to surfaces, to intercalation into expandable clay minerals, the inclusion of smaller organic particles (bacteria, small phytoplankton, detritus) into small clay mineral aggregates (flocculi), the incorporation of organic particles (phytoplankton, bacteria, detritus) into flocs, and the formation of biofilms. Interactions between minerals and OM are driven by physical, chemical and biological processes that vary along the land-ocean transition, leading to significant spatial and temporal variability in the size, shape, composition, concentration, vertical distribution and transport pathways of the SPM.

SPM concentration and composition is an indicator for the relative importance of physical and biogeochemical processes. A characteristic feature of the SPM is that the composition becomes more organic and the floc size larger with decreasing SPM concentration. The shape of both relationships and their variability are caused by spatio-temporal variations in biogeochemical and physical processes. Flocs largely consist of minerals in estuarine and nearshore turbidity maximum zones, while they contain gradually more organic matter when turbidity decreases. High turbidity zones are characterized by strong tidal currents, intensive resuspension and settling, flocculation in phase with the tides and high primary production. In oligotrophic environments, the SPM consists mostly of large, organic rich and fluffy aggregates. In this regime, physical processes are less important and flocculation occurs on seasonal time scales.

We explain the processes leading to these relationships, and discuss the current understanding of the characteristics, dynamics and interactions of OM and minerals along the continuum from land to ocean. Further we will discuss the role of SPM in biogeochemical cycles as well as the effects of climate change and human activities on SPM characteristics.

# Vertical dynamics of suspended particulate matter and chlorophyll-a in a well-mixed coastal turbid system

Saumya Silori[1], Xavier Desmit[1], Rolf Riethmüller[2], Markus Schartau[3], Nathan Terseleer[1], Michael Fettweis[1]
[1]*OD Natural Environment, Royal Belgian Institute of Natural Sciences, rue Vautier 29, 1000 Brussels, Belgium*
[2]*Institute of Carbon Cycle, Helmholtz Centre Hereon, Max-Planck-Str. 1, 21502 Geesthacht, Germany*
[3]*GEOMAR, Helmholtz Centre for Ocean Research, Wischhofstr. 1-3 24148 Kiel, Germany*

## Introduction

Coastal hydrodynamics are a result of interacting physical forces (tidal currents, waves, density-driven currents, etc.), which significantly influence suspended particulate matter (SPM; Jones et al., 1998) dynamics. SPM composition, more specifically particulate organic matter (POM) content of SPM (POM/SPM; hereafter referred to as POM content), changes characteristically with the SPM concentrations (Liénart et al., 2017; Schartau et al., 2019). SPM typically becomes more organic with decreasing concentrations offshore, due to reduced resuspension and differential settling of mineral versus organic particles (Schartau et al., 2019; Fettweis et al., 2022). Seasonal shifts in SPM composition also occur, especially during phytoplankton blooms, when biologically exuded organic matter enhances aggregation and deposition. While cross-shore and seasonal patterns in SPM composition are relatively well studied, vertical and tidal variations remain poorly resolved. We hypothesize that POM content is higher in surface waters than near the bottom due to the SPM concentration gradient in the water column, analogous to cross-shore patterns. Among the organic fraction, phytoplankton, though minor by mass, play a key role in SPM dynamics (Fetweiss et al., 2022). Our preliminary data from the Belgian coastal zone suggest that the vertical association between Chl*a* and SPM varies seasonally, with strong coupling in winter and decoupling in spring. To investigate this, we analyse vertical profiles of Chl*a* and SPM concentrations to infer the phytoplankton–SPM association. In parallel, we use organic matter quality indicators (POC/PON and POC/Chl*a* ratios) to assess whether the composition of SPM differs between surface and bottom layers. Together, these insights reveal how phytoplankton interact with SPM in well-mixed turbid systems.

## Methods

MOW1 (51.36°N, 3.13°E), located within the Belgian coastal turbidity maximum, was sampled over 29 tidal cycles between 2019 and 2022. Hourly water samples were collected ~2 m below the surface and ~2 m above the seabed using a Sea-Bird SBE09 CTD carousel equipped Niskin bottles. Samples were filtered on board and later analysed for SPM, POC, PON, Chl*a*, and Phaeophytin-*a* (Pheo*a*). In 2019, hourly sensor-based profiles were also recorded during each tidal cycle. An OBS3+ backscatter sensor, mounted on the CTD, provided continuous turbidity measurements. The SPM and Chl*a* vertical profiles were calculated assuming a linear regression between the water depth and the logarithm of the

SPM or Chl*a* concentrations (Dyer, 1986). The depth of the photic layer was estimated using light attenuation coefficients derived from SPM concentrations, following the empirical relationship proposed by Devlin et al. (2008). These fitted profiles were used to quantify the mass of SPM and Chl*a* within the euphotic zone to assess their vertical distribution.

**Results**

SPM, POC, and Chla concentrations showed significant tidal and seasonal variability, with SPM ranging from 8 to 990 mg/l and POC from 0.38 to 34 mg/l across seasons. On average, SPM, POC, and Chl*a* concentrations were higher near the bottom than at the surface, though POC and Chl*a* content were relatively higher in surface waters. Highest Chl*a* concentrations occurred during spring and summer (up to 65 µg/l). Analysis of the expanded dataset (2012–2018), revealed a positive linear relationship between SPM and Chl*a* concentrations in both spring and winter (Fig. 1a). However, the bootstrapped distribution of regression slopes showed greater variability in spring (standard deviation = 0.01) compared to winter (standard deviation = 0.001) (Fig. 1b).

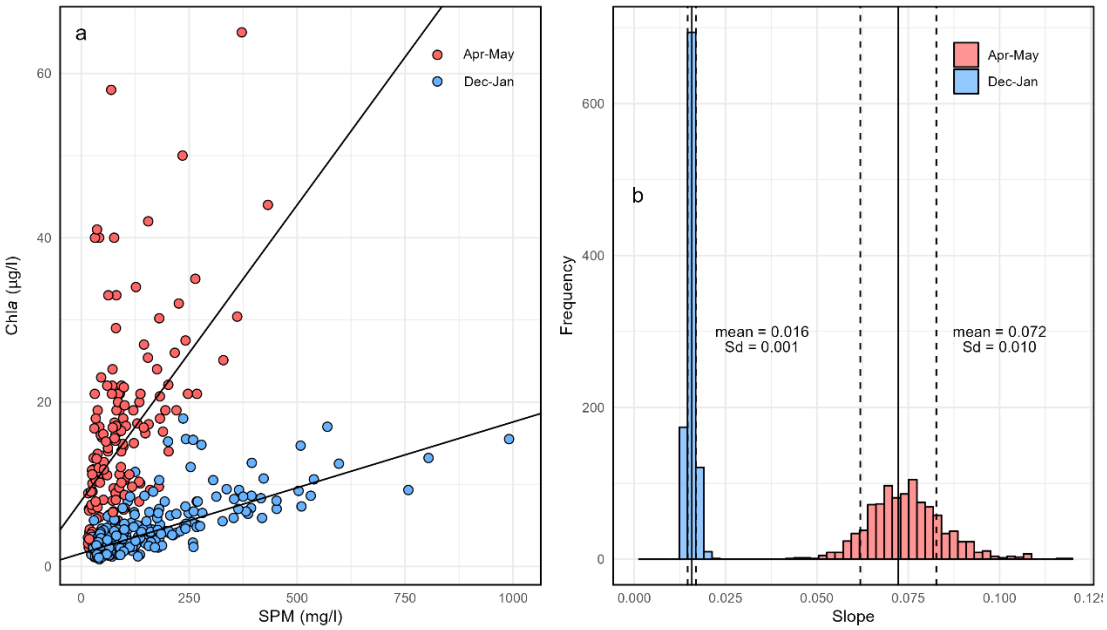


Figure 1: (a) Robust Linear Regression between SPM (mg/l) and Chl*a* (µg/l) in winter (Dec-Jan) and spring (Apr-May).The slope and intercept of the linear fit are mean values of these coefficients derived from bootstrapping. (b) Histograms of bootstrapped sampling distribution of slopes of the robust linear regression between SPM (mg/l) and Chl*a* (µg/l) in winter (Dec-Jan) and spring (Apr-May). The solid black lines represent the mean of the bootstrap slopes, the dashed black lines give the boundaries of one standard deviation (Sd) above and below the mean.

The vertical variation in the Chl*a* content (Chl*a*/SPM) was notably more pronounced than the variation in the POC content. We observed significantly higher Chl*a* content in the upper water column during spring and summer, and occasionally in autumn. Additionally, this evidence for vertical differences in the organic content of the SPM in the water column is supported by significantly lower POC/Chl*a* and POC/PON ratios in surface waters, with

concomitant higher Chl*a*/Pheo*a* ratios. These ratios may serve as potential proxies indicating the quality of organic matter (Savoye et al., 2003; Bouillon et al., 2011), and our results suggest that the surface waters are generally enriched in organic matter of higher trophic quality.

Analysis of hourly profiles of SPM and Chl*a* concentrations during tidal cycles in spring (April 2019) and winter (November 2019) revealed notable disparities between the two seasons (Fig. 2). Throughout both tidal cycles, SPM concentrations exhibited a tendency to increase towards the bed during periods of maximum current velocities, whereas they remained relatively constant on the vertical exhibiting lower values on average during the slack periods . Concurrently, Chl*a* profiles in November (Fig. 2a) closely mirrored the corresponding SPM patterns which was not the case in April. About half of the Chl*a* profiles in April exhibited inversions, where concentrations decreased towards the bed (Fig. 2b). To better quantify the accumulation of Chl*a* in the surface waters, we attempted to determine the average mass of SPM and Chl*a* within the estimated photic layer. The depth-integrated concentration of SPM ([g $m^{-2}$]) within the photic layer during a tidal cycle remains conservative across seasons. However, the mass of Chl*a* within the photic layer during a tidal cycle exhibits seasonal variation, being higher during spring and summer compared to winter and autumn, yet it remains constant within each of these seasons. Further we calculate the percentage of SPM and Chl*a* within the photic layer and the analysis reveals that the percentages of Chl*a* and SPM within the photic layer are identical during a tidal cycle in winter. However, during spring, the Chl*a* percentage in the photic layer approaches 10%, while the SPM percentage is notably lower at 3%. Similarly, in summer, the Chl*a* percentage increases up to 30%, whereas the percentage of SPM in the photic layer rises to 18%.

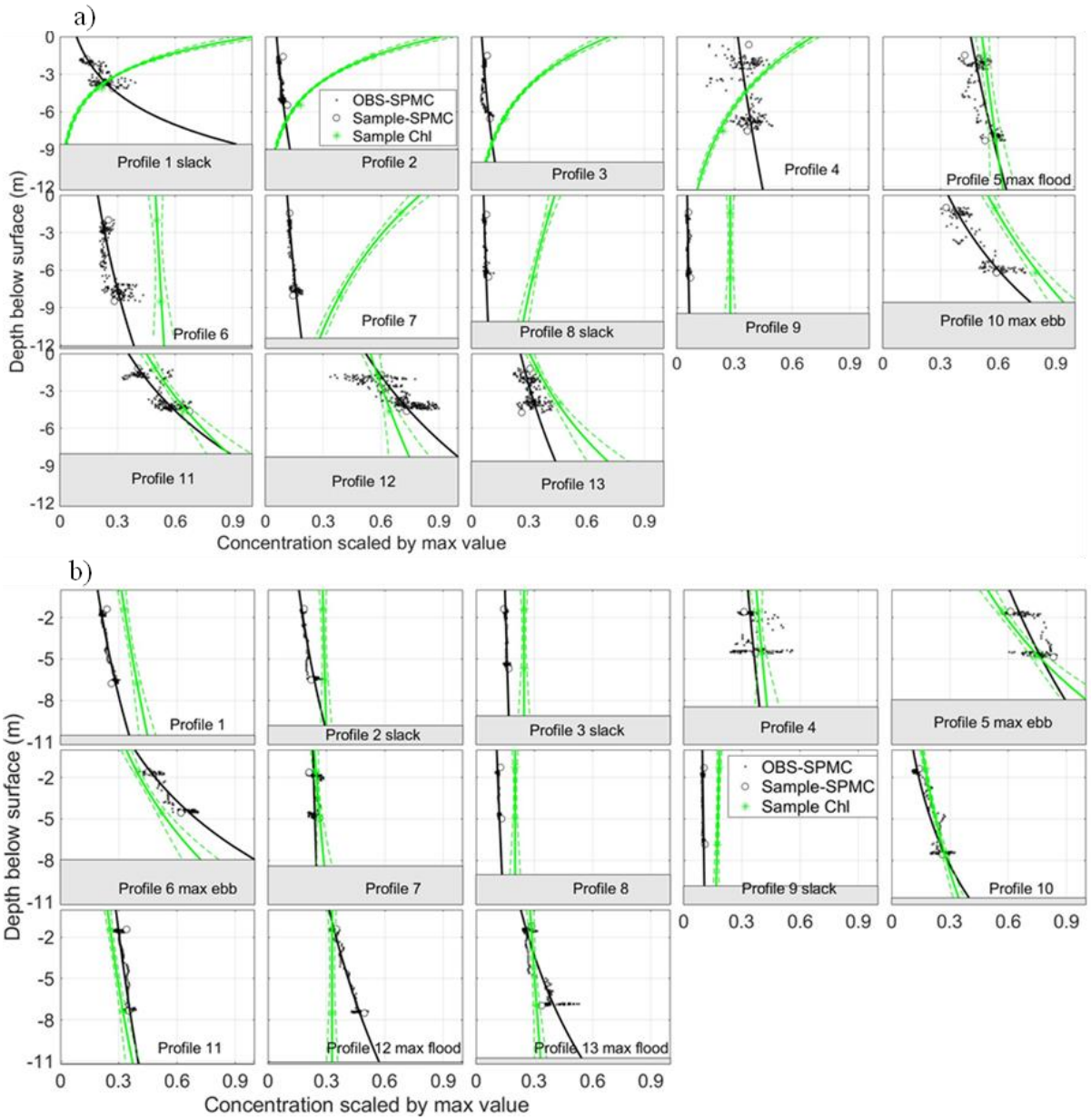


Figure 2: Hourly vertical profiles of SPM (black line) and Chl*a* (green line) concentrations scaled by the maximum value during the tidal cycle in April 2019 (SPM: 366 mg/l, Chl*a*: 33 µg/l) (a) and November 2019 (SPM: 272 mg/l, Chl*a*: 11 µg/l) (b). The Chl*a* profile uncertainty (expressed as a standard deviation is shown as dashed lines. The SPM profile uncertainty, expressed as $R^2$, is between 0.5-0.9, except for profiles 4, 8, 9 and 13 in April and profiles 4, 7 and 9 in November). The light gray box represents the sea bed.

**Discussion**

During the spring bloom, the accumulation of Chl*a* in the surface layer diverges from the more uniform SPM distribution, indicating a seasonal decoupling of phytoplankton and sediment dynamics in an otherwise well-mixed water column. We attribute this divergence to the presence of two functional types of phytoplankton: floc-associated types that follow SPM dynamics and dominate most of the year, and free, buoyant phytoplankton that are decoupled from mineral SPM and dominate during bloom periods. The latter's independent vertical

distribution, likely driven by differences in density and settling behavior, helps explain sustained phytoplankton production in turbid, mixed waters with light limitation. Enhanced turbulence during spring may contribute to fragmentation of larger flocs and promote surface accumulation of buoyant, POC-rich aggregates, especially in species like *Phaeocystis globosa* and lightly silicified diatoms. These findings provide insight into the mechanisms that allow phytoplankton to thrive in dynamic, light-limited environments and highlight the complex interplay between biological and physical processes in coastal ecosystems.
In the turbid Belgian nearshore waters, high surface Chl*a* concentrations during the early spring bloom occur simultaneously with elevated SPM concentrations, highlighting the employment of mechanisms that help retain phytoplankton in the photic zone. Despite smaller variations in SPM concentrations from winter to early spring, Chl*a* concentrations increase in March, suggesting that bloom initiation is triggered by the relaxation of winter light limitation and not by improved water clarity. Free-floating phytoplankton, due to slower settling velocities, may have distinct advantage in early spring, remaining longer in the shallow photic layer. As spring progresses and SPM levels decline, the photic depth increases, reducing this advantage. Vertical profiles show that the probability of Chl*a* being in the photic zone increases from ~2% in January to ~12% in April, peaking in summer when SPM is lowest. Conversely, this probability declines in late summer and autumn as SPM rises. Importantly, Chl*a* consistently shows a higher probability than SPM of being within the photic layer, suggesting that water clarity, modulated by SPM concentration and composition, significantly affects phytoplankton retention and productivity.

**Conclusion**

Our results demonstrate that the enrichment POC content at the surface is driven by similar processes as the horizontal nearshore-offshore gradient, primarily differential settling of mineral versus organic particles. Seasonal differences in POC quality between surface and bottom waters peak in summer, emphasizing the need for sampling both depths even in well-mixed waters. While tidal currents largely shape vertical gradients in SPM and Chl*a* concentrations, higher surface Chl*a* concentrations during the growing season suggests phytoplankton adapt by shifting from floc-attached to free-living forms to remain longer in the photic zone under low light. Understanding phytoplankton strategies affecting buoyancy and particle association is crucial for improving models of organic carbon dynamics in coastal systems.

**References**


1. Jones, S. E., Jago, C. F., Bale, A. J., Chapman, D., Howland, R. J. M., & Jackson, J. (1998). Aggregation and resuspension of suspended particulate matter at a seasonally stratified site in the southern North Sea: physical and biological controls. Continental Shelf Research, 18(11), 1283-1309. https://doi.org/10.1016/S0278-4343(98)00044-2
2. Liénart, C., Savoye, N., Bozec, Y., Breton, E., Conan, P., David, V., ... & Sultan, E. (2017). Dynamics of particulate organic matter composition in coastal systems: A spatio-temporal study at multi-systems scale. Progress in Oceanography, 156, 221-239. https://doi.org/10.1016/j.pocean.2017.03.001

3. Schartau, M., Riethmüller, R., Flöser, G., van Beusekom, J. E. E., Krasemann, H., Hofmeister, R., & Wirtz, K. (2019). On the separation between inorganic and organic fractions of suspended matter in a marine coastal environment. Progress in Oceanography, 171, 231-250. https://doi.org/10.1016/j.pocean.2018.12.011
4. Fettweis, M., Schartau, M., Desmit, X., Lee, B. J., Terseleer, N., Van der Zande, D., ... & Riethmüller, R. (2022). Organic matter composition of biomineral flocs and its influence on suspended particulate matter dynamics along a nearshore to offshore transect. Journal of Geophysical Research: Biogeosciences, 127(1), e2021JG006332. https://doi.org/10.1029/2021JG006332
5. Dyer, K. R. (1986). Coastal and estuarine sediment dynamics. John Wiley & Sons, Chichester, 258p.
6. Devlin, M. J., Barry, J., Mills, D. K., Gowen, R. J., Foden, J., Sivyer, D., & Tett, P. (2008). Relationships between suspended particulate material, light attenuation and Secchi depth in UK marine waters. Estuarine, Coastal and Shelf Science, 79(3), 429-439. https://doi.org/10.1016/j.ecss.2008.04.02
7. Bouillon, S., Connolly, R. M., & Gillikin, D. P. (2011). 7.07 Use of stable isotopes to understand food webs and ecosystem functioning in estuaries. Treatise on estuarine and coastal science, 7. https://doi.org/10.1016/B978-0-12-374711-2.00711-7
8. Savoye, N., Aminot, A., Tréguer, P., Fontugne, M., Naulet, N., & Kérouel, R. (2003). Dynamics of particulate organic matter δ15N and δ13C during spring phytoplankton blooms in a macrotidal ecosystem (Bay of Seine, France). Marine ecology progress series, 255, 27-41. https://www.int-res.com/articles/meps2003/255/m255p027.pdf

# Multi-sensor observations of suspended particulate matter in a tidal coastal environment

Benjamin Van Roozendael[a], Matthias Baeye[a], Duc Tran[a], Romaric Verney[b], Michael Fettweis[a]

[a]Royal Belgian Institute of Natural Sciences, Rue Vautier 31, 1000 Brussels, Belgium
[b]Ifremer, 1625 Route de Sainte-Anne, CS 10070, 29280 Plouzané, France

Corresponding author: Benjamin Van Roozendael; bvanroozendael@naturalsciences.be

## Introduction

Turbidity, or the cloudiness of water, is primarily determined by the amount and type of suspended particulate matter (SPM) in the water column. In coastal environments such as the Belgian part of the North Sea (BPNS), SPM is generated through a combination of biological processes and sedimentary processes. These particles influence light penetration and are therefore a key factor in monitoring water quality (Capuzzo et al., 2015). As such, understanding and measuring SPM is important for both scientific research and effective environmental management.

The BPNS is characterized by a semi-diurnal tidal regime, with average tidal ranges of 4.3 m during spring tides and 2.8 m during neap tides at Zeebrugge. This predictable alternation between high and low tides, together with strong wind-driven flows, creates constantly shifting SPM conditions. Northeasterly winds tend to increase SPM concentrations by resuspending sediments from the seabed, while south-westerly winds often bring in clearer waters from the English Channel, pushing the turbidity maximum towards the Westerschelde estuary. During persistent northeasterly wind events, dense mud suspensions can remain in the water column for several tidal cycles, leading to sustained reductions in water clarity (Baeye et al., 2011). In these waters, SPM concentrations typically range from 20 to 70 mg $l^{-1}$ in the water column near the coast, reaching up to 3,000 mg $l^{-1}$ near the seabed during energetic conditions. Offshore, concentrations are generally lower, usually below 10 mg $l^{-1}$, reflecting the influence of both hydrodynamic and sedimentary processes (Baeye et al., 2011; Fettweis et al., 2022).

Human activities further complicate SPM dynamics in the BPNS. This area is a busy maritime region, with activities such as navigation, commercial and recreational fishing, dredging, and the development and operation of offshore windfarms. Vessel traffic and fishing gear can disturb seabed sediments, while dredging and sand extraction operations directly release sediments into the water column (Fettweis et al., 2011, 2016; Martens et al., 2018; Van Lancker & Baeye, 2015). Offshore windfarms also alter local hydrodynamics and create new habitats for marine life, influencing the production and movement of biological SPM (Baeye & Fettweis, 2015;

Vanhellemont & Ruddick, 2014). These human activities combine with natural processes to produce a highly variable and dynamic suspended particulate environment that can be challenging to measure and monitor accurately.

To address these complexities, this study investigates how SPM concentrations change under these dynamic conditions and how different sensors perform in capturing these variations. Our findings aim to contribute to more accurate SPM monitoring and better environmental management in this active coastal area.

**Methods**

To monitor SPM in both nearshore and offshore areas of the BPNS, we conducted several field campaigns at three stations (Fig. 1). These campaigns covered multiple tidal cycles, different weather conditions, and various seasons. This comprehensive approach ensured that we captured the full range of hydrodynamic and sedimentary environments present in the study area.

Acoustic measurements played a central role in these campaigns. We used an Acoustic Doppler Current Profiler (ADCP) to record both water currents and acoustic backscatter intensity (Kim & Voulgaris, 2014), alongside an EK80 echosounder and a multibeam echosounder (MBES) (Praet et al., 2023), which focused on measuring backscatter intensity in the water column. Operating at different frequencies, these instruments allowed us to assess how various types of particles respond to different acoustic signals and to capture the dynamic distribution of suspended sediments.

To complement the acoustic observations, we also collected optical measurements using a range of instruments. Optical backscatter sensors (OBS) were used to measure turbidity, while the LISST-200 (Laser In Situ Scattering and Transmissometry) instrument provided in situ data on particle size distributions and volume concentrations (Creed et al., 2001; Downing, 2006). Both sensors were installed on a rosette that was lowered frequently to take vertical profiles of the water column. A Hach turbidity sensor offered standard turbidity measurements, adding further detail to the dataset. In addition, imaging systems were deployed to visually characterize the suspended particles, including flocs, organic matter, and sediments. To validate and refine these sensor-based observations, we collected water samples at various depths and locations throughout the study area. In the laboratory, these samples were filtered to determine mass concentrations of SPM and analyzed for other parameters such as salinity, particulate organic carbon (POC), particulate organic nitrogen (PON), chlorophyll, and transparent exopolymer particles (TEP).

The combined dataset from the acoustic and optical sensors, together with the laboratory results, allowed us to evaluate the strengths and limitations of each measurement approach. By integrating these diverse data sources, we gained a comprehensive view of how each sensor performed under the dynamic and often complex conditions typical of the Belgian coastal waters.

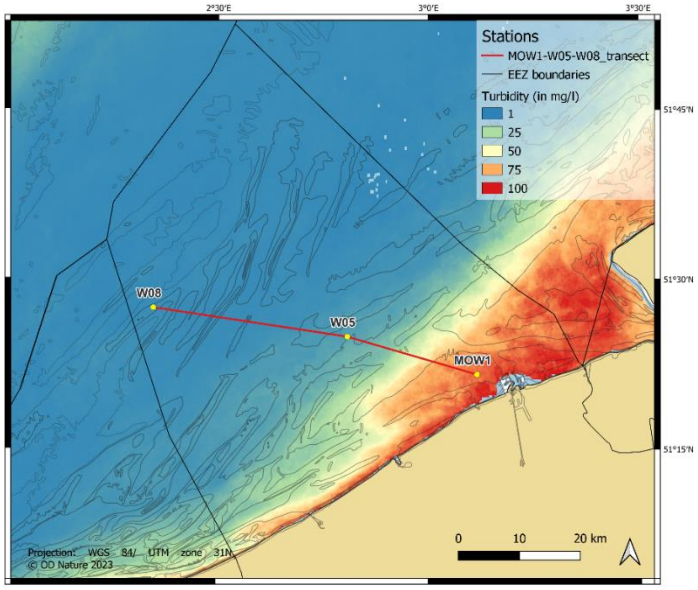


*Figure 1. Map of the BPNS displaying the locations of experiments conducted. The background on the map features the average surface SPMC for the winter period of 2019, derived using the algorithm by (Nechad et al., 2010) to the standard Sentinel-3/OLCI remote sensing reflectance product (RRS) provided by EUMETSAT water processor.*

**Results**

Our observations showed that SPM concentrations and compositions varied strongly with tidal, weather, and seasonal conditions. Near the shore, SPM levels fluctuated significantly in response to changes in tidal currents and wind events. During high-energy tidal phases, larger sand grains and other particles were resuspended, leading to higher acoustic backscatter signals in the bottom water layers. In contrast, periods of calm weather and slack tide were marked by lower SPM concentrations, with fine cohesive particles and flocs dominating the water column.

Acoustic sensors demonstrated a strong response to these dynamic conditions, particularly in detecting periods of intense resuspension when coarser particles were present. However, we noted that these sensors tended to overestimate SPM concentrations when larger particles or flocs dominated the particle assemblage, due to the strong acoustic reflections associated with such materials.

Optical sensors, on the other hand, provided reliable measurements of SPM when fine cohesive particles were the main contributors to turbidity. However, they tended to underestimate concentrations during resuspension events dominated by larger sand grains or aggregates, due to the lower optical scattering efficiency of these coarser particles.

The LISST-200 instrument proved especially useful for monitoring changes in particle size distributions throughout the tidal cycle. It consistently showed that during calmer periods such as slack tide, larger flocs formed as a result of particle aggregation, and these larger particles settled more quickly. In contrast, during peak flood and ebb currents, higher turbulence broke up the flocs, resulting in smaller particle sizes.

Overall, integrating data from multiple sensors revealed the strong variability of SPM in the study area and demonstrated the complementary strengths of different measurement approaches for capturing these dynamics (see Fig.2).

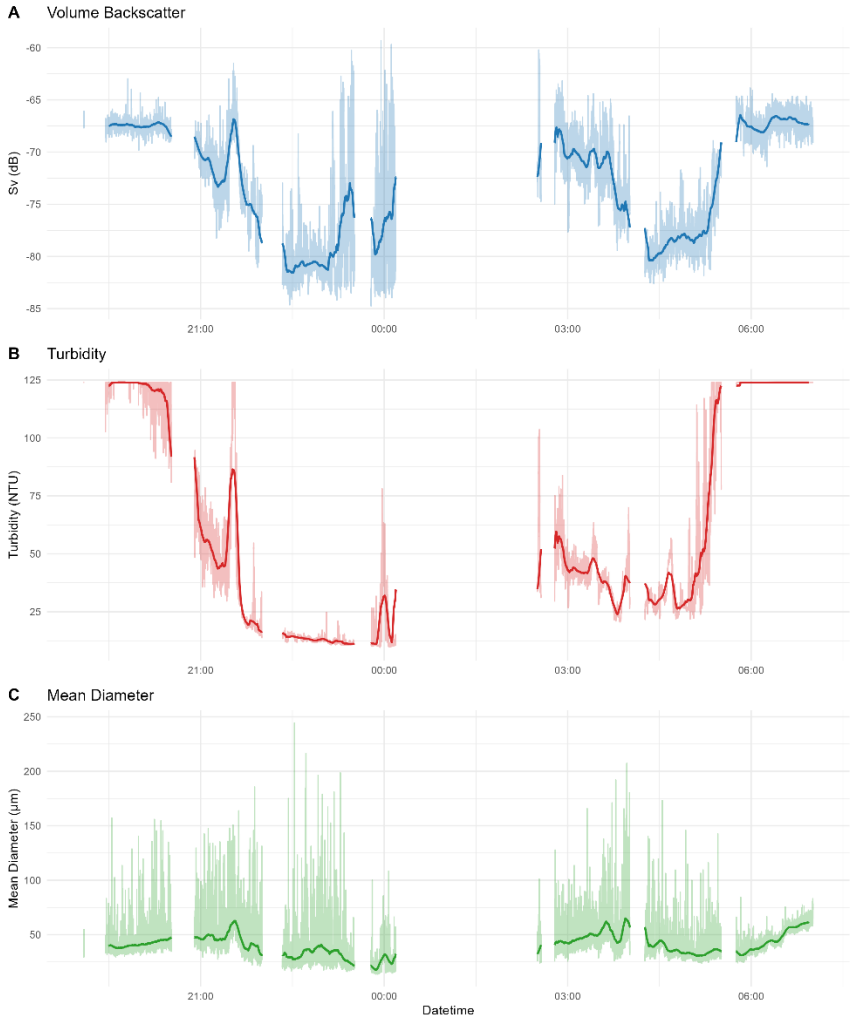


*Figure 2. Example of a time-series of volume backscatter strength (Sv), mean particle diameter (µm), and turbidity (NTU) recorded at station MOW1. Raw data are shown with shaded lines, while smoothed trends highlight the main variations. Data gaps exceeding five minutes are excluded to avoid artificial connections.*

## Discussion

Our study confirms that no single sensor can fully capture the complex variations of SPM in tidal environments. The differences in sensor responses highlight the importance of understanding the physical principles behind each measurement technique. Acoustic backscatter data, depending on their frequency, are influenced by both the size and density of particles, making these sensors particularly sensitive to larger, denser grains. In contrast, optical sensors rely on light scattering, which is more effective for detecting fine, cohesive particles. These differences create challenges when SPM composition shifts rapidly in response to tides and wind-driven resuspension. By integrating data from both sensor types, we obtained a more complete picture of SPM dynamics. Acoustic measurements helped identify energetic resuspension events and the presence of sand in suspension, while optical sensors provided precise measurements of fine sediment concentrations during calmer periods. The LISST-200's particle size data were essential for interpreting these patterns and reconciling differences between sensor readings. The combined dataset also revealed that SPM in the study area is highly variable in time and space, requiring flexible and adaptive monitoring strategies. This variability is driven not only by tidal currents but also by wind-induced flows and episodic events, such as storms and persistent wind conditions, algal blooms, or human activitiets.

## Conclusion

Our observations and analyses show that combining acoustic and optical sensors is essential for accurate and comprehensive monitoring of suspended particulate matter in dynamic tidal environments. Each sensor type provides complementary insights into SPM concentration and composition, and together, they offer a robust approach to characterizing particle dynamics.

This work emphasizes the need for multi-sensor approaches in coastal monitoring programs, especially in regions like the BPNS, where tidal and wind forcing create complex and rapidly changing SPM conditions. These findings have implications for environmental monitoring, ecosystem management, and understanding sediment transport in coastal areas. Future work will focus on refining calibration procedures for different sensors under varying conditions, and developing data fusion methods to produce more reliable and spatially comprehensive SPM maps. Such efforts will contribute to improved water quality assessments and better management of coastal environments.

## References


Baeye, M., & Fettweis, M. (2015). In situ observations of suspended particulate matter plumes at an offshore wind farm, southern North Sea. Geo-Marine Letters 2015 35:4, 35(4), 247–255. https://doi.org/10.1007/S00367-015-0404-8

Baeye, M., Fettweis, M., Voulgaris, G., & Van Lancker, V. (2011). Sediment mobility in response to tidal and wind-driven flows along the Belgian inner shelf, southern North Sea. Ocean Dynamics 2011 61:5, 61(5), 611–622. https://doi.org/10.1007/S10236-010-0370-7

Capuzzo, E., Stephens, D., Silva, T., Barry, J., & Forster, R. M. (2015). Decrease in water clarity of the southern and central North Sea during the 20th century. Global Change Biology, 21(6), 2206–2214. https://doi.org/10.1111/GCB.12854

Creed, E. L., Pence, A. M., & Rankin, K. L. (2001). Inter-comparison of turbidity and sediment concentration measurements from an ADP, an OBS-3, and a LISST. Oceans Conference Record (IEEE), 3, 1750–1754. https://doi.org/10.1109/OCEANS.2001.968098

Downing, J. (2006). Twenty-five years with OBS sensors: The good, the bad, and the ugly. Continental Shelf Research, 26(17–18), 2299–2318. https://doi.org/10.1016/j.csr.2006.07.018

Fettweis, M., Baeye, M., Cardoso, C., Dujardin, A., Lauwaert, B., Van den Eynde, D., Van Hoestenberghe, T., Vanlede, J., Van Poucke, L., Velez, C., & Martens, C. (2016). The impact of disposal of fine-grained sediments from maintenance dredging works on SPM concentration and fluid mud in and outside the harbor of Zeebrugge. Ocean Dynamics, 66(11), 1497–1516. https://doi.org/10.1007/S10236-016-0996-1/METRICS

Fettweis, M., Baeye, M., Francken, F., Lauwaert, B., Van den Eynde, D., Van Lancker, V., Martens, C., & Michielsen, T. (2011). Monitoring the effects of disposal of fine sediments from maintenance dredging on suspended particulate matter concentration in the Belgian nearshore area (southern North Sea). Marine Pollution Bulletin, 62(2), 258–269. https://doi.org/10.1016/J.MARPOLBUL.2010.11.002

Fettweis, M., Schartau, M., Desmit, X., Lee, B. J., Terseleer, N., Van der Zande, D., Parmentier, K., & Riethmüller, R. (2022). Organic Matter Composition of Biomineral Flocs and Its Influence on Suspended Particulate Matter Dynamics Along a Nearshore to Offshore Transect. Journal of Geophysical Research: Biogeosciences, 127(1). https://doi.org/10.1029/2021JG006332

Kim, Y. H., & Voulgaris, G. (2014). Estimation of suspended sediment concentration in estuarine environments using acoustic backscatter from an ADCP. https://www.researchgate.net/publication/228780627

Martens, C., Van den Eynde, D., Lauwaert, B., Van Hoey, G., Devriese, L., Sterckx, T., Malherbe, B., & Vantorre, M. (2018). Dredging and dumping.

Nechad, B., Ruddick, K. G., & Park, Y. (2010). Calibration and validation of a generic multisensor algorithm for mapping of total suspended matter in turbid waters. Remote Sensing of Environment, 114(4), 854–866. https://doi.org/10.1016/j.rse.2009.11.022

Praet, N., Collart, T., Ollevier, A., Roche, M., Degrendele, K., De Rijcke, M., Urban, P., & Vandorpe, T. (2023). The Potential of Multibeam Sonars as 3D Turbidity and SPM Monitoring Tool in the North Sea. Remote Sensing, 15(20), 4918. https://doi.org/10.3390/RS15204918/S1

Van Lancker, V., & Baeye, M. (2015). Wave Glider Monitoring of Sediment Transport and Dredge Plumes in a Shallow Marine Sandbank Environment. PLOS ONE, 10(6), e0128948. https://doi.org/10.1371/JOURNAL.PONE.0128948

Vanhellemont, Q., & Ruddick, K. (2014). Turbid wakes associated with offshore wind turbines observed with Landsat 8. Remote Sensing of Environment, 145, 105–115. https://doi.org/10.1016/J.RSE.2014.01.009

# APPENDIX 2

**Jespers N, Parmentier K, Knockaert M. 2025. Blancoprobleem TEP analyse. Werkdocument Nr.: BMM LAB/WD25-03**

# Blancoprobleem TEP analyse

Toepassing : *SV075 – TEP analyse*

| | Naam | Datum + Handtekening |
|---|---|---|
| Opsteller | N. Jespers | |
| Autorisator<br>Hoofd ECOCHEM | K. Parmentier | |
| Beheerder Document<br>Kwaliteitscoördinator | M. Knockaert | Marc Knockaert (Signature)<br>Digitaal ondertekend door Marc Knockaert (Signature)<br>Datum: 2025.09.09 14:33:47 +02'00' |
| Opmerkingen | | |

# INHOUDSTAFEL

# Zwavelzuurblanco voor TEP analyse

## 1. SAMENVATTING

Na ingebruikname van te platereader voor de TEP analyse werden problemen vastgesteld met de bekomen concentraties. De berekende concentraties waren steeds lager dan verwacht en soms negatief. De volledige methode werd onder de loep genomen en er werd vastgesteld dat bij het analyseren van filterblanco's, stalen en kalibraties nog een zwavelzuurblanco moet worden meegelopen.

## 2. CONCLUSIES EN AANBEVELINGEN

Voorschriften en templates in de betreffende software worden aangepast om de zwavelzuurblanco er in op te nemen.

Oude datasets die werden verkregen met de incorrecte methode worden herrekend, de data wordt opnieuw ingegeven in het SLIMS.

## 3. TESTRESULTATEN

### 3.1 Algemeen

Dezelfde stalen werden 2x na elkaar gemeten, 1 zonder en 1 maal met een blanco-substractie door de software en de resultaten werden vergeleken (tabel 1). Hieruit wordt een correctiefactor bepaald waarmee de reeds bekomen data kan worden herrekend. Bij nieuwe analyses wordt steeds een verse zwavelzuurblanco meegenomen als correctie.

De resultaten van de filterblanco's, de standaarden voor het opstellen van de ijklijn en de stalen zelf worden allen gecorrigeerd een de hand van de bekomen factor.

3.2 Resultaten

Deze resultaten werden bekomen op een alciaan blauw verdunning die werd aangemaakt in 78% H2SO4
Tabel 1: bepalen correctiefactor

| zonder blanco-correctie | | | met blanco-correctie | | | Verschil | |
|---|---|---|---|---|---|---|---|
| **749** | **787** | | **749** | **787** | | **749** | **787** |
| 0.6975 | 0.4862 | | 0.6577 | 0.4431 | | 0.0398 | 0.0431 |
| 0.6899 | 0.4821 | | 0.6480 | 0.4387 | | 0.0419 | 0.0434 |
| 0.6873 | 0.4783 | | 0.6464 | 0.4354 | | 0.0409 | 0.0429 |
| 0.6887 | 0.4802 | | 0.6468 | 0.4367 | | 0.0419 | 0.0435 |
| 0.6835 | 0.4764 | | 0.6438 | 0.4345 | | 0.0397 | 0.0419 |
| 0.6918 | 0.4822 | | 0.6523 | 0.4407 | | 0.0395 | 0.0415 |
| 0.6706 | 0.4703 | | 0.6306 | 0.4274 | | 0.0400 | 0.0429 |
| 0.6823 | 0.4766 | | 0.6414 | 0.4339 | | 0.0409 | 0.0427 |
| 0.6775 | 0.4725 | | 0.6369 | 0.4301 | | 0.0406 | 0.0424 |
| 0.6797 | 0.4729 | | 0.6395 | 0.4313 | | 0.0402 | 0.0416 |
| 0.6777 | 0.4712 | | 0.6372 | 0.4297 | | 0.0405 | 0.0415 |
| 0.6861 | 0.4768 | | 0.6438 | 0.4341 | | 0.0423 | 0.0427 |
| | | | | | Gemiddelde: | **0.0407** | **0.0425** |

3.2.1 Filterblanco's

Tabel 2: waarden filterblanco's zonder zwavelzuurcorrectie

| Nr. | ABS 749nm | ABS 787 nm | ABS 900 nm | ABS 977 nm | Calculated pathlength | Gecorrigeerde A787 | Gecorrigeerde A749 |
|---|---|---|---|---|---|---|---|
| 1 | 0.0677 | 0.0662 | 0.0527 | 0.1035 | 0.99608 | 0.06646063 | 0.067966535 |
| 2 | 0.0699 | 0.0682 | 0.0527 | 0.1028 | 0.98235 | 0.06942515 | 0.071155689 |
| 3 | 0.0734 | 0.0727 | 0.0603 | 0.1116 | 1.00588 | 0.072274854 | 0.07297076 |
| 4 | 0.0751 | 0.0728 | 0.0535 | 0.1032 | 0.97451 | 0.074704225 | 0.077064386 |
| 5 | 0.0761 | 0.0732 | 0.0533 | 0.1037 | 0.98824 | 0.074071429 | 0.077005952 |
| 6 | 0.0665 | 0.0654 | 0.0514 | 0.1016 | 0.98431 | 0.066442231 | 0.067559761 |
| 7 | 0.0720 | 0.0700 | 0.0523 | 0.1024 | 0.98235 | 0.071257485 | 0.073293413 |
| 8 | 0.0713 | 0.0702 | 0.0538 | 0.1024 | 0.95294 | 0.073666667 | 0.074820988 |
| 9 | 0.0685 | 0.0668 | 0.0507 | 0.1009 | 0.98431 | 0.067864542 | 0.069591633 |
| 10 | 0.0765 | 0.0740 | 0.0556 | 0.1058 | 0.98431 | 0.075179283 | 0.077719124 |
| 11 | 0.0778 | 0.0743 | 0.0536 | 0.1029 | 0.96667 | 0.076862069 | 0.080482759 |
| 12 | 0.0823 | 0.0788 | 0.0541 | 0.1052 | 1.00196 | 0.078645793 | 0.082138943 |
| | | | | | Gemiddelde: | **0.072237863** | **0.074314162** |

Tabel 3: waarden filterblanco's met zwavelzuurcorrecties

| Nr. | ABS 749nm | ABS 787 nm | ABS 900 nm | ABS 977 nm | Calculated pathlength | Gecorrigeerde A787 | Gecorrigeerde A749 |
|---|---|---|---|---|---|---|---|
| 1 | 0.02702 | 0.02369 | 0.05270 | 0.10350 | 0.99608 | 0.023784941 | 0.027123031 |
| 2 | 0.02922 | 0.02569 | 0.05410 | 0.10520 | 1.00196 | 0.025641389 | 0.029159491 |
| 3 | 0.03272 | 0.03019 | 0.05270 | 0.10280 | 0.98235 | 0.030734032 | 0.033304391 |
| 4 | 0.03442 | 0.03029 | 0.05360 | 0.10290 | 0.96667 | 0.031336207 | 0.035603448 |
| 5 | 0.03542 | 0.03069 | 0.06030 | 0.11160 | 1.00588 | 0.030512183 | 0.035209552 |
| 6 | 0.02582 | 0.02289 | 0.05560 | 0.10580 | 0.98431 | 0.023256474 | 0.026228088 |
| 7 | 0.03132 | 0.02749 | 0.05350 | 0.10320 | 0.97451 | 0.028210765 | 0.032135815 |
| 8 | 0.03062 | 0.02769 | 0.05070 | 0.10090 | 0.98431 | 0.028132968 | 0.031104582 |
| 9 | 0.02782 | 0.02429 | 0.05330 | 0.10370 | 0.98824 | 0.024580853 | 0.028147817 |
| 10 | 0.03582 | 0.03149 | 0.05380 | 0.10240 | 0.95294 | 0.033046811 | 0.037585391 |
| 11 | 0.03712 | 0.03179 | 0.05140 | 0.10160 | 0.98431 | 0.032298307 | 0.037708167 |
| 12 | 0.04162 | 0.03629 | 0.05230 | 0.10240 | 0.98235 | 0.036943613 | 0.042364271 |
| | | | | | Gemiddelde: | **0.029039879** | **0.032972837** |

3.2.2 Kalibratie

Tabel 4: kalibratie zonder zwavelzuurcorrectie

| Flesnummer | 1 | 2 | 3 | 4 | 5 | 6 |
|---|---|---|---|---|---|---|
| Conc (µg/6 ml) | 5 | 10 | 25 | 50 | 75 | 100 |
| Conc (µg/ ml) | 0.833 | 1.666 | 4.166 | 8.333 | 12.500 | 16.666 |
| Echte conc gem (µg/ ml) | 0.927 | 1.854 | 4.635 | 9.272 | 13.908 | 18.544 |
| Gem. absorbanties A787 | 0.048 | 0.056 | 0.077 | 0.114 | 0.153 | 0.191 |
| Gem. absorbanties A749 | 0.047 | 0.057 | 0.082 | 0.125 | 0.170 | 0.214 |
| Berekende concentratie A787 | 0.965 | 1.980 | 4.603 | 9.262 | 14.096 | 18.816 |
| Berekende concentratie A749 | 0.939 | 1.926 | 4.581 | 9.202 | 13.902 | 18.589 |
| afwijking A787 % | 4.131 | 6.786 | -0.692 | -0.108 | 1.352 | 1.468 |
| afwijking A787 % | 1.346 | 3.905 | -1.168 | -0.752 | -0.044 | 0.243 |
| | **A787** | Rico: | 0.00801055 | y-intercept: | 0.0402763 | |
| | **A749** | Rico: | 0.0094512 | y-intercept: | 0.0383319 | |

Tabel 5: kalibratie met zwavelzuurcorrectie

| Flesnummer | 1 | 2 | 3 | 4 | 5 | 6 |
|---|---|---|---|---|---|---|
| Conc (µg/6 ml) | 5 | 10 | 25 | 50 | 75 | 100 |
| Conc (µg/ ml) | 0.833 | 1.666 | 4.166 | 8.333 | 12.500 | 16.666 |
| Echte conc gem (µg/ ml) | 0.927 | 1.854 | 4.635 | 9.272 | 13.908 | 18.544 |
| Gem. absorbanties A787 | 0.015 | 0.023 | 0.044 | 0.081 | 0.119 | 0.157 |
| Gem. absorbanties A749 | 0.018 | 0.027 | 0.053 | 0.096 | 0.140 | 0.184 |
| Berekende concentratie A787 | 0.961 | 1.936 | 4.574 | 9.143 | 13.924 | 18.602 |
| Berekende concentratie A749 | 0.944 | 1.911 | 4.600 | 9.195 | 13.897 | 18.593 |
| afwijking A787 % | 3.646 | 4.447 | -1.316 | -1.391 | 0.116 | 0.312 |
| afwijking A787 % | 1.889 | 3.073 | -0.756 | -0.834 | -0.083 | 0.268 |

| | | | | |
|---|---|---|---|---|
| **A787** | Rico: | 0.0080236 | y-intercept: | 0.0074108 |
| **A749** | Rico: | 0.0093791 | y-intercept: | 0.0093864 |

4.3.3 Berekening staalresultaten

Met de herrekende filterblanco's en ijklijn worden nu de concentraties van de stalen opnieuw berekend. De rekenbladen hiervan zijn terug te vinden in bijlage.

Tabel 6: vergelijking concentraties met en zonder zwavelzuurcorrectie.
Resultaten 2502 COD center

| zonder zwavelzuurcorrectie | 787 | RSD % |
|---|---|---|
| Center 1 opp | 0.081 | 55.9469 |
| Center 1 opp | 0.288 | |
| | | |
| center 1 bod | -0.1646 | 62.2064 |
| center 1 bod | -0.03835 | |
| | | |
| Center 2 opp | 0.503706 | 5.6328 |
| Center 2 opp | 0.449986 | |
| | | |
| center 2 bod | 0.034513 | 73.8944 |
| center 2 bod | 0.229898 | |
| | | |
| center 3 opp | 0.162942 | 35.5516 |
| center 3 opp | 0.34271 | |

| met zwavelzuurcorrectie | 787 | RSD % |
|---|---|---|
| Center 1 opp | 0.694 | 13.03 |
| Center 1 opp | 0.902 | |
| | | |
| center 1 bod | 0.452 | 11.83 |
| center 1 bod | 0.573 | |
| | | |
| Center 2 opp | 1.094 | 1.64 |
| Center 2 opp | 1.059 | |
| | | |
| center 2 bod | 0.624 | 14.70 |
| center 2 bod | 0.839 | |
| | | |
| center 3 opp | 0.759 | 5.96 |
| center 3 opp | 0.855 | |

| | | |
|---|---|---|
| center 3 bod | 0.475002 | 14.3610 |
| center 3 bod | 0.355704 | |

| | | |
|---|---|---|
| center 3 bod | 1.050 | 4.48 |
| center 3 bod | 0.960 | |

De waarden bekomen met de zwavelzuurcorrectie liggen meer in de lijn van de verwachtingen en voldoen ook aan het criterium voor spreiding tussen de individuele filters (20%)

Bovenstaande tabel toont enkel de waarden voor de absorbanties bepaald op 787 nm. In bijlage bevindt zich het volledige rekenblad waar ook de zwavelzuurcorrectie werd toegepast op absorbanties van 749 nm. Bij 749 nm kunnen dezelfde conclusies getrokken worden als bij 787 nm.

**Opmerking:**
Enkel de absorbanties gemeten op 749 en 787 nm moeten worden gecorrigeerd met de zwavelzuurblanco. De waarden van golflengtes 900 en 977 worden gebruikt voor de pathlength correction en niet voor de berekening van de concentratie. 900nm is het absorbtiemaximum van $H_2SO_4$ en 977 is het achtergrondspectrum van de cuvet/wellplate (polycarbonaat)

## 4. BESLUIT

Wanneer de zwavelzuurcorrectie wordt toegepast op alle absorbanties (absorbantie blanco's, ijklijn en stalen) dan liggen deze dichter bij de verwachte waardes en wordt een betere spreiding bekomen. Het toevoegen van een zwavelzuurblanco is dus noodzakelijk om correcte resultaten te bekomen.

## 5. BIJLAGE

Gebruikte rekenbladen zijn terug te vinden op Data_Chemie\TEPS\2025\testen\zwavelzuurblanco

# APPENDIX 3

**Silori S, Desmit X, Schartau M, Terseleer N, Riethmüller R, Fettweis M. 2025. Vertical dynamics of suspended particulate matter and chlorophyll-a in a well-mixed coastal turbid system. Estuarine, Coastal and Shelf Science 326, 109545**

Estuarine, Coastal and Shelf Science 326 (2025) 109545

Contents lists available at ScienceDirect

Estuarine, Coastal and Shelf Science

journal homepage: www.elsevier.com/locate/ecss

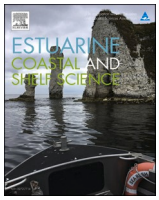

# Vertical dynamics of suspended particulate matter and chlorophyll-a in a well-mixed coastal turbid system

Saumya Silori [a,*], Xavier Desmit [a], Rolf Riethmüller [b], Markus Schartau [c], Nathan Terseleer [a], Michael Fettweis [a]

[a] OD Natural Environment, Royal Belgian Institute of Natural Sciences, rue Vautier 29, 1000, Brussels, Belgium
[b] Institute of Carbon Cycle, Helmholtz Centre Hereon, Max-Planck-Str. 1, 21502, Geesthacht, Germany
[c] GEOMAR, Helmholtz Centre for Ocean Research, Wischhofstr. 1-3, 24148, Kiel, Germany

ARTICLE INFO

*Keywords:*
Suspended particulate matter
Particulate organic matter
Chlorophyll-*a*
Phytoplankton
Turbid waters
Belgian coastal waters

ABSTRACT

The particulate organic carbon (POC) content of suspended particulate matter (SPM) gradually increases along a horizontal gradient from high-turbidity to low-turbidity waters, reflecting a characteristic feature of SPM dynamics. Here, we investigate whether this gradual POC enrichment is also evident in the vertical in a turbid, shallow, well-mixed water column (MOW1), where variation in hydrodynamic forcing and phytoplankton production is likely to differ markedly from the cross-shore transects. Combining SPM, POC, and chlorophyll-*a* (Chl*a*) data collected from surface and bottom layers at MOW1 during multiple tidal cycles between 2019 and 2022, we observe relatively higher POC and Chl*a* content in surface waters, beginning in spring. During this season we observe a larger uncertainty in the Chl*a*-SPM regression analysis, indicating a weaker association between the two, which contrasts winter conditions where the association is better. Monthly vertical profiles of SPM, constructed using optical backscattering sensor data, and Chl*a* profiles from water sample data indicate that a significant fraction of phytoplankton is floc-attached and that free phytoplankton type predominates only during the growing period. Our findings suggest that, similar to the horizontal gradients in POC content of SPM, differential settling amongst various components of SPM seems to contribute to the compositional gradient within the vertical water column. Consequently, free phytoplankton cells may be able to prolong residence in the photic depths, particularly advantageous during the early stages of phytoplankton blooms when SPM concentrations remain high.

## 1. Introduction

Coastal hydrodynamics are a result of interacting physical forces (tidal currents, waves, density-driven currents, etc.), which significantly influence suspended particulate matter (SPM; Jones et al., 1998) dynamics. The SPM composition, more specifically particulate organic matter (POM) content of SPM (POM/SPM; hereafter referred to as POM content), changes characteristically with the SPM concentrations. Studies note a progressive increase in the POM content with decreasing SPM concentrations from nearshore to offshore waters (Schartau et al., 2019; Fettweis et al., 2022). This trend, although not entirely understood, is thought to result either from the decreasing contribution of resuspended bed material, which is likely to be less organic, or from differential settling, where mineral particles sink faster than organic particles, leading to an enrichment of organic particles in the suspended sediment pool. (Bale and Morris, 1998; Schartau et al., 2019). Nonetheless this shift in the SPM composition across the cross-shore gradient, coupled with the influence of the physical forcing, is recognized to significantly impact the SPM behavior (Moulton et al., 2023; Yu et al., 2023). Offshore conditions characterized by lower turbulence and higher POM content promote formation of low-density organic aggregates (Fettweis et al., 2006; Lee et al., 2019). Conversely, in nearshore shallow waters, relatively lower organic content and greater turbulence make large low-density organic aggregates more volatile, as they break up and form during tidal cycles (Fugate and Friedrichs, 2003; Maggi and Tang, 2015; Maerz et al., 2016).

In addition to this spatial variation, SPM composition also undergoes a seasonal variation as its organic content changes during and after phytoplankton blooms. In certain regions, the distinctive seasonality observed in SPM concentrations is an outcome of the seasonal shifts in

* Corresponding author.
*E-mail address:* saumyasilori27@gmail.com (S. Silori).

https://doi.org/10.1016/j.ecss.2025.109545
Received 26 February 2025; Received in revised form 16 September 2025; Accepted 16 September 2025
Available online 17 September 2025

SPM composition (Jago et al., 2007; Van Beusekom et al., 2012). For example, in the coastal turbidity maximum in the Southern Bight of the North Sea, summer SPM concentrations can be lower by about a factor of two than in winter, despite the comparable hydrodynamic conditions. (Fettweis et al., 2016). This decrease is attributed to the interaction between mineral and organic particles (Fettweis et al., 2022). During biologically productive periods, the carbon-enriched exudates from phytoplankton cells and bacteria can form sticky microgels, such as transparent exopolymer particles (TEP), and these appear to promote the formation and subsequent deposition of biomineral aggregates (Fettweis and Baeye, 2015), thereby lowering the SPM concentrations.

While the cross-shore and seasonal patterns in SPM concentrations and composition are increasingly understood, vertical and short-term variations in SPM composition remain poorly resolved. Recent studies demonstrate a relatively simple relationship between the concentration and the composition of the SPM along cross-shore transects where concentration changes by one to two orders of magnitude (Schartau et al., 2019; Fettweis et al., 2022). Due to tidal action, shallow coastal waters can also have a substantial variation in SPM concentrations over short time intervals, in addition to a vertical gradient in SPM concentrations (Winterwerp, 2001; Sommerfield and Wong, 2011). However it remains unclear how SPM composition varies both over tidal cycles and within the vertical water column. Analogous to the cross-shore gradient in SPM composition, we expect a corresponding variation in POM content within the water column (Schartau et al., 2019; Fettweis et al., 2022). Specifically, we anticipate the organic content of SPM to be greater near the surface than in deeper waters where SPM concentrations are higher. Either because of a greater contribution of less organic resuspended bed material to deeper waters or due to differential settling, which retains organic particles in the upper water column. Furthermore, studies in estuarine environments highlight significant differences in POM composition between surface and bottom waters, driven by seasonal and spatial variations in autochthonous (e.g., phytoplankton production) and allochthonous (e.g., terrestrial POM) contributions to the bulk POM pool (Hermes and Sikes, 2016; Deng et al., 2021).

Among the organic components of SPM, phytoplankton, although a minor component by mass, contribute substantially to the organic pool, particularly during productive periods. Their biomass is commonly assessed using chlorophyll-*a* (Chl*a*) concentration as a proxy, though its relationship with phytoplankton carbon is often complex (Boyer et al., 2009; Alvarez-Fernandez and Riegman, 2014). Short-term changes in SPM composition and subsequently in the behavior of SPM flocs that often incorporate phytoplankton cells (Ho et al., 2022) may have important implications for phytoplankton light exposure in dynamic turbid coastal waters, where spring phytoplankton blooms develop over alternating spring-neap cycles (Blauw et al., 2012; Zhao et al., 2019). Hence understanding the vertical distribution of Chl*a* concentrations relative to SPM concentrations may provide insights into how phytoplankton deal with light limitation while being subject to tidal mixing. Our initial observations from the Belgian coastal zone show a significant association between Chl*a* and SPM concentrations during the winter months which weakens during spring (Fig. 1). Hence, we hypothesize a temporally varying association between phytoplankton cells and SPM, subject to phytoplankton's response to environmental drivers. During periods characterized by close coupling, where phytoplankton cells actively participate in the formation and breakup of SPM flocs, we anticipate vertical Chl*a* profiles to closely mirror SPM concentration profiles in the water column. Conversely, during phases of decoupling from mineral SPM particles, phytoplankton cells may exhibit distinct resuspension and settling patterns within the water column influencing their residence times in the photic zone.

To this end, we analyze data collected over several tidal cycles from a well-mixed, shallow station in the Belgian coastal zone. We test the hypotheses that i) a vertical gradient in the particulate organic carbon (POC) content of SPM exists within the water column, analogous to the cross-shore gradient, with higher POC content in surface than in bottom waters, ii) this gradient in POC content is accompanied by differences in POC composition between surface and bottom waters reflecting differences in source contribution, as indicated by compositional indicators such as particulate organic carbon to nitrogen (POC/PON) and POC/Chl*a* ratios, and iii) the Chl*a* and SPM association varies seasonally, with strong coupling in winter and partial decoupling during the productive period in spring, potentially indicating seasonal shifts in dominant phytoplankton functional types. These changes are likely not unique to our study area, as fundamental processes governing suspended particles are expected to be consistent in non-stratified, turbid waters. Accordingly, by examining the vertical dynamics of particles, our results provide valuable insight into how phytoplankton cells modulate their interactions with SPM to enhance residence time in the photic zone and sustain primary production in such turbid systems.

## 2. Methods

### 2.1. Study area

The sampling station MOW1 [51.36 °N, 3.13 °E] lies within the coastal turbidity maximum in the Belgian Coastal Zone, and the typical SPM values vary between 20 and a few hundreds of mg/l at the surface and between 100 and a few thousands mg/l near the bed (Fettweis et al., 2014). This shallow region with 10 m water depth at Mean Lower Low

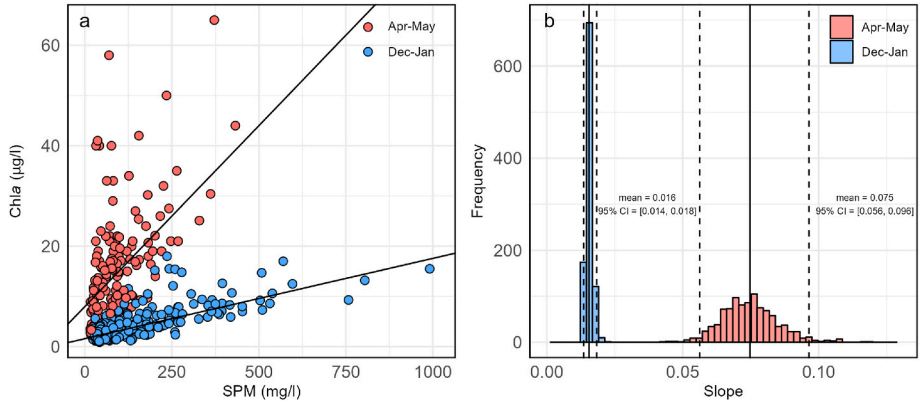


**Fig. 1.** (a) Robust Linear Regression between SPM (mg/l) and Chl*a* (µg/l) concentrations in winter (Dec–Jan) and spring (Apr–May). The slope and intercept of the linear fit are mean values of these coefficients derived from bootstrapping. (b) Histograms of bootstrapped sampling distribution of slopes of the robust linear regression between SPM (mg/l) and Chl*a* (µg/l) concentrations in winter (Dec–Jan) and spring (Apr–May). The solid black lines represent the mean of the bootstrap slopes, the dashed black lines show the 95 % confidence interval based on the distribution.

Water Spring (MLLWS) experiences a semi-diurnal tidal regime, with mean tidal range of 4.3 m (Spring Tide) and 2.8 m (Neap Tide) The tidal current ellipses are elongated at MOW1 and vary between 0.2 and 1.5 m/s during spring tide and 0.2–0.6 m/s during neap tide (Fettweis et al., 2014). Ebb currents are directed towards the southwest and flood currents towards the northeast. The tidal currents are generally flood-dominant, as also the residual water transport. The water column remains well-mixed with negligible gradients in temperature and salinity, owing to strong tidal currents and low freshwater discharge (Lacroix et al., 2004). The spring phytoplankton bloom is the most significant event in the seasonal dynamics. Generally, it starts in March and is particularly notable in April and May coinciding with the highest Chl*a* concentrations (Muylaert et al., 2006). Thereafter, Chl*a* concentrations remain at a moderate level of 3–10 μg/l during summer and autumn months. The phytoplankton succession observed in the Belgian coastal zone follows a distinct pattern (Rousseau et al., 2002). During winter, the dominant group comprises bentho-pelagic diatoms. As spring progresses, these small colonial diatoms are replaced by large-sized diatoms. Later in the spring bloom, *Phaeocystis globosa* colonies become dominant. Subsequently, in summer and autumn, large diatoms regain prominence, only to be succeeded by smaller diatoms thereafter.

### 2.2. In-situ sample collection and analysis

Water samples were collected at MOW1 over monthly tidal cycles (12.5 h) during a period spanning from 2019 to 2022. 29 such tidal cycles were sampled during this period. The water samples have been taken during calm weather (significant wave height was generally below 1 m), thus wave and wind effects are negligible. Every hour, 5 or 10 l Niskin bottles on the Sea-Bird SBE09 CTD carousel were closed at about 2 m above bed and 2 m below the surface, and the carousel was taken on board and the bottles emptied. The water samples were filtered on board and analyzed in the laboratory to obtain the concentration of SPM, POC, PON, Chl*a*, and Phaeophytin-*a* (Pheo*a*). At every sampling occasion, three subsamples for SPM concentration were taken and filtered on board using pre-combusted (405 °C, 24 h), rinsed, dried for 24 h at 105 °C and pre-weighted 47 mm GF/C filters. After sampling the filters were rinsed with ultrapure water (resistivity 18.2 MΩcm normalized at 25 °C) and immediately stored at −20 °C, before being dried during 24 h at 50 °C and weighted to obtain the concentration. The uncertainty (expressed as the RMSE of the triplicates divided by the mean value) decreases with increasing concentration from 8.5 % (SPM concentration <5 mg/l) to 6.7 % (<10 mg/l), 3.5 % (10–50 mg/l), and 2.1 % (>100 mg/l) and represent the random error related to the lack of precision during filtrations. The samples for POC and PON were filtered on board using 25 mm GF/C filters (pretreated as above for SPM), stored immediately at −20 °C, before being analyzed using a Thermo Finnigan Flash EA1112 elemental analyzer (for details see Ehrhardt and Koeve, 1999). The sample for Chl*a* and Pheo*a* concentration was filtered on 47 mm GF/C filters, stored in liquid nitrogen and determined in the lab using ultra high-performance liquid chromatography with fluorometric detection (Van Heukelem and Thomas, 2001). The analytical uncertainty for POC is 12 % and for PON, Chl*a* and Pheo*a* 18 %. We assume that the uncertainty due to filtration errors is the same as for SPM (between 2.1 and 3.5 % for SPM concentration >10 mg/l) which result in a total uncertainty for these parameters that equals nearly the analytical one.

### 2.3. Sensor measurements

Profiles of sensor measurements have been collected during monthly (except in July) tidal cycles (12.5 h) at MOW1 in 2019. In total 143 profiles with sample data and sensor data were collected. An Optical Backscatter Sensor (OBS3+) was connected to the SBE09 CTD. The OBS output was calibrated in the laboratory against a laboratory standard (AMCO clear) in order to convert the sensor output (in Volt) to a backscatter turbidity unit, then the sample SPM concentration was used to convert the turbidity into mass concentration. The linear regression between turbidity and sample SPM concentration had always a $R^2 > 0.9$. The sensor measurements provided data over the whole up and downcast.

### 2.4. Vertical profiles of SPM and Chla concentration

The OBS data cover the water column from about 3 m above the bed towards about 1–2 m below the surface, while the water sampling for SPM and Chl*a* concentration was limited to the near-bed and near-surface. The missing values near the bed, near the surface and in between have been calculated based on a first order power function. The profile was calculated assuming a linear regression between the water depth and the logarithm of the SPM or Chl*a* concentrations. This approach assumes that horizontal advection can be neglected and that the settling velocity ($w_s$) and the vertical turbulent exchange coefficient (A) are constant over the water column, resulting in a zero net horizontal flux of matter (see Dyer, 1986). The resulting exponential profile can be written as:

$$C(z) = C_0 \cdot e^{(\lambda z)} \quad (1)$$

where $C(z)$ is the concentration of SPM or Chl*a* at depth $z$, $C_O$ the concentration at the surface, $z = 0$ at the surface and takes negative values below the surface, and $\lambda$ the fitting parameter that is equal to $-w_s/A$. The approach has been applied and validated for similar stations as ours (Fugate and Friedrichs, 2002; Zhao et al., 2019). Both sample and OBS derived SPM concentration data have been used for constructing the SPM concentration profiles. We assume that Chl*a* increases similarly as SPM concentrations with depth, which is acceptable during most of the year given the reasonably good correlation between both. The Chl*a* concentration profiles have been built only with two sample data using the same method as for SPM, which means that the profile is a perfect fit. The Chl*a* uncertainty (19 %) is taken into account using a bootstrap method, while the uncertainty of the SPM concentration profile is expressed as the coefficient of determination, $R^2$. The bootstrap method is a statistical technique for estimating the mean and standard deviation of a population by averaging estimates from multiple data subsamples randomly selected. We estimated the Chl*a* profile uncertainty by calculating 200 times the profile with surface and the bottom Chl*a* concentrations that were randomly varying between up to ±19 % of the analytical value.

### 2.5. Statistical analysis

We conducted a regression analysis on Chl*a* and SPM data collected during winter (Dec–Jan) and spring (Apr–May) months from 2012 to 2022. Both datasets were combined ensuring consistency in data collection and analysis methods as described in Section 2.1. To mitigate the influence of outliers, we employed robust linear regression using the Robust Linear Model (rlm) function from the MASS package in R, which utilizes robust M-estimation based on Huber's weight function. To quantify the variability associated with the regression coefficients, we employed bootstrapping. Specifically, we randomly resampled 75 % of the data 1,000 times with replacement and calculated the fitting each time. This resampling technique allowed us to derive a normal distribution of the regression coefficients, from which we calculated the mean and standard deviation (Sd).

We conducted a Shapiro-Wilk normality test to assess the normality of the differences between surface and bottom samples. The results indicated that, for most parameters, the differences deviated significantly from a normal distribution ($p < 2.2 \times 10^{-16}$). Consequently, to test for significant differences between the surface and bottom samples, we employed the non-parametric Wilcoxon signed-rank test for paired samples. To test for seasonal differences between in the vertical

gradients (bottom-surface), we used pairwise Wilcoxon rank sum tests. All statistical analyses were performed using R version 4.2.2.

### 2.6. Mass of SPM and Chla in the photic layer

The fitted profiles have been used to calculate the amount of SPM and Chl*a* mass in the photic layer. The depth of the photic layer, $D_{photic}$ (m), is mainly controlled by the SPM concentration and its relationship with the vertical light attenuation coefficient, $k_d$ ($m^{-1}$):

$$D_{photic} = \frac{-ln(a)}{k_d} \quad (2)$$

where a is the fraction of photosynthetically active radiation that remains relative to its surface value (Cloern, 1987). Photic depth is often somewhat arbitrarily defined as the depth where 1 % of the light remains (a = 0.01). As small variations at the pole of the logarithm may induce large variations in $D_{photic}$, we have used light attenuation values of 0.1 %, 1 %, 5 % and 10 % to get an uncertainty estimate of the photic depth and of the mass of particulate matter in the photic layer. The vertical light attenuation coefficient, $k_d$, was derived from the relationship proposed by Devlin et al. (2008) for combined coastal, offshore and transitional UK waters:

$$k_d = 0.086 + 0.067 \times SPM_{surf} \quad (3)$$

where $SPM_{surf}$ is the SPM concentration at the surface. We believe this approach holds relevance for Belgian Coastal waters too. While Chl*a* and colored dissolved organic matter are influential in light attenuation, studies in turbid waters consistently show strong correlations between SPM concentrations and light attenuation coefficients ($k_d$ values). Furthermore this relationship between SPM concentrations and $k_d$ has been previously employed successfully to ascertain photic depths in the North Sea (Capuzzo et al., 2015).

The mass of SPM and Chl*a* in the photic layer was then calculated for every profile by integrating their concentration over $D_{photic}$ (the mass in the photic layer is expressed in units [g $m^{-2}$]). The respective fractions of SPM and Chl*a* in the photic layer were estimated during every tidal cycle by relating the mass in the photic layer in each vertical profile to the total mass available for resuspension during the tidal cycle. The latter was set equal to the maximum mass of SPM and Chl*a* available in a profile during the cycle.

## 3. Results

### 3.1. Probability density distribution of sample SPM, POC and Chla concentrations

The sample data from the tidal cycles has been divided into the following seasonal categories: December, January, and February representing winter; March, April, and May denoting spring; June, July, and August indicating summer; and September, October, and November representing autumn. Sample SPM, POC and Chl*a* concentrations exhibited large variations at tidal and seasonal scales. During spring, SPM concentrations ranged from 14 to 988 mg/l, in summer from 8 to 487 mg/l, in autumn from 11 to 573 mg/l, and in winter from 20 to 990 mg/l. Variations in POC concentration were similar to those of the SPM and the two parameters exhibited a positive correlation at seasonal and tidal scales. During spring, POC concentrations ranged from 0.73 to 34 mg/l, in summer from 0.52 to 16 mg/l, in autumn from 0.38 to 16 mg/l, and in winter from 0.39 to 34 mg/l. On average, the concentrations of SPM, POC, and Chl*a* were higher in bottom waters than at the surface (Table 1). The highest Chl*a* concentrations were recorded during the productive months of spring (2–65 μg/l) and summer (3–40 μg/l), while lower Chl*a* concentrations were seen in autumn (1–24 μg/l) and winter (0.3–18 μg/l). On an average higher POC and Chl*a* concentrations were measured in the surface than bottom waters (Table 1). To establish a robust association between SPM and Chl*a* concentrations, we expanded our dataset for MOW1. In addition to the data gathered during tidal cycles between 2019 and 2022, we incorporated information from earlier periods spanning 2012–2018. Notably, the data collected during these earlier cycles was exclusively obtained near the bed, omitting measurements from the surface. Although we observe a linear positive association between SPM and Chl*a* concentrations during both spring and winter season (Fig. 1 a). The bootstrapped sampling distribution of slopes of the robust linear regression displays a larger variation for the spring months (standard deviation = 0.01) compared to the winter months (standard deviation = 0.001) (Fig. 1b). The higher phytoplankton production in spring, evidenced by higher slope values (Fig. 1b), may have contributed to the large variation in the correlation between SPM and Chl*a* concentrations during these months.

### 3.2. Vertical variations in SPM composition

The collected samples, obtained about 2 m downwards from the surface and 2 m above bed during multiple tidal cycles, allowed investigating the vertical variations in SPM composition (Table 1). At MOW1, the SPM, POC, and Chl*a* concentrations are, except around slack water,

**Table 1**
Geometric means (standard deviation) of parameters measured at the surface (surf) and bottom (bot) depths at MOW1. Data is collected across four seasons (spring, summer, autumn, and winter) spanning from 2019 to 2022, photic depth (1 % light attenuation, see eq. (2)) was calculated for the 11 tidal cycles of 2019. Number of observations = n.

| | Spring | n | Summer | n | Autumn | n | Winter | n |
|---|---|---|---|---|---|---|---|---|
| Photic depth (m) | 1.41 (2.1) | 39 | 3.12 (1.5) | 26 | 1.35 (2.0) | 38 | 0.70 (2.2) | 39 |
| $SPM_{surf}$ (mg/l) | 71.3 (2.1) | 109 | 29.6 (1.8) | 98 | 60.0 (2.1) | 99 | 82.3 (2.1) | 124 |
| $SPM_{bot}$ (mg/l) | 114.6 (2.3) | 129 | 51.1 (2.3) | 98 | 85.3 (2.2) | 96 | 110.2 (2.3) | 162 |
| $POC_{surf}$ (mg/l) | 2.4 (1.9) | 109 | 1.3 (1.4) | 92 | 1.9 (1.9) | 99 | 2.4 (2.0) | 109 |
| $POC_{bot}$ (mg/l) | 3.5 (2.1) | 116 | 2.0 (1.9) | 88 | 2.7 (2.0) | 96 | 3.2 (2.2) | 125 |
| $Chla_{surf}$ (μg/l) | 10.8 (1.9) | 95 | 8.2 (1.6) | 97 | 5.4 (2.0) | 99 | 3.8 (1.9) | 124 |
| $Chla_{bot}$ (μg/l) | 11.8 (2.0) | 103 | 10.3 (1.7) | 96 | 6.5 (1.9) | 95 | 4.2 (1.9) | 135 |
| $Pheoa_{surf}$ (μg/l) | 0.5 (1.9) | 95 | 0.2 (1.7) | 98 | 0.3 (2.0) | 99 | 0.3 (2.6) | 122 |
| $Pheoa_{bot}$ (μg/l) | 0.6 (2.1) | 103 | 0.3 (1.9) | 97 | 0.4 (2.1) | 95 | 0.4 (2.8) | 137 |
| $POC/SPM_{surf}$ (%) | 3.4 (1.3) | 109 | 4.6 (1.4) | 91 | 3.2 (1.3) | 99 | 3.0 (1.3) | 109 |
| $POC/SPM_{bot}$ (%) | 3.3 (1.3) | 116 | 4.1 (1.5) | 88 | 3.2 (1.3) | 96 | 2.9 (1.3) | 125 |
| $Chla/SPM_{surf}$ (%) | 0.014 (2.0) | 95 | 0.028 (1.8) | 96 | 0.009 (2.2) | 99 | 0.004 (1.8) | 124 |
| $Chla/SPM_{bot}$ (%) | 0.011 (2.0) | 103 | 0.020 (2.2) | 96 | 0.008 (2.1) | 95 | 0.004 (1.7) | 134 |
| $POC/PON_{surf}$ (mol/mol) | 8.1 (1.2) | 105 | 7.7 (1.1) | 90 | 8.3 (1.2) | 88 | 8.6 (1.2) | 102 |
| $POC/PON_{bot}$ (mol/mol) | 8.6 (1.2) | 112 | 7.9 (1.1) | 87 | 8.7 (1.2) | 87 | 9.1 (1.2) | 112 |
| $Chla/Pheoa_{surf}$ (μg/μg) | 20.3 (1.6) | 95 | 35.3 (1.6) | 97 | 18.8 (1.9) | 99 | 11.3 (1.7) | 122 |
| $Chla/Pheoa_{bot}$ (μg/μg) | 18.2 (1.5) | 103 | 30.3 (1.6) | 96 | 16.6 (1.8) | 95 | 10.5 (1.7) | 135 |

shaped by the vertical balance of particle fluxes due to gravitational settling, buoyancy, resuspension and turbulent mixing. This influence is evident in the observed concentration patterns where, for the majority of the instances, the concentrations in the deeper samples are higher than in the surface, as indicated by the Wilcoxon signed-rank tests (Fig. 2a–c). In these cases gravitational settling and turbulent mixing control the shape of the vertical concentrations both for SPM and phytoplankton (Chl*a*). The observed vertical gradient in Chl*a* concentrations contrasts with previous findings in the Belgian coastal zone, where surface waters (3 m from the surface) and bottom waters (1 m from the bed) exhibited similar Chl*a* concentrations (Franco et al., 2007), with differences between tidal phases being unresolved. Investigating the SPM composition in the vertical water column, we observed that POC content between bottom and surface waters were significantly different (Fig. 2d), the difference in the POC content between surface and the bottom seems to increase in spring and reach a maximum in summer. The depth-based variation in POC content is likely driven by the gradient in SPM concentrations along the vertical water column, indicating an increase in the POC content of SPM as the SPM concentration decreases towards the surface. Such a relationship between the POC content and the SPM concentration is a well-documented feature (e.g., Manheim et al., 1972; Fettweis et al., 2006; Schartau et al., 2019).

The vertical variation in the Chl*a* content (Chl*a*/SPM; hereafter referred to as Chl*a* content; Fig. 2e) is notably more pronounced than the variation in the POC content. We observed significantly higher Chl*a* content in the upper water column during spring and summer, and occasionally in autumn. The largest vertical difference in Chl*a* content between surface and bottom waters was observed in summer, and it was significantly higher than in other seasons. Additionally, this evidence for vertical differences in the organic content of the SPM in the water column is supported by significantly lower POC/Chl*a* and POC/PON ratios in surface waters, with concomitant higher Chl*a*/Pheo*a* ratios (Fig. 2f–h). Similar to the differences observed for Chl*a* content between surface and bottom waters, the vertical differences in POC/Chl*a* were

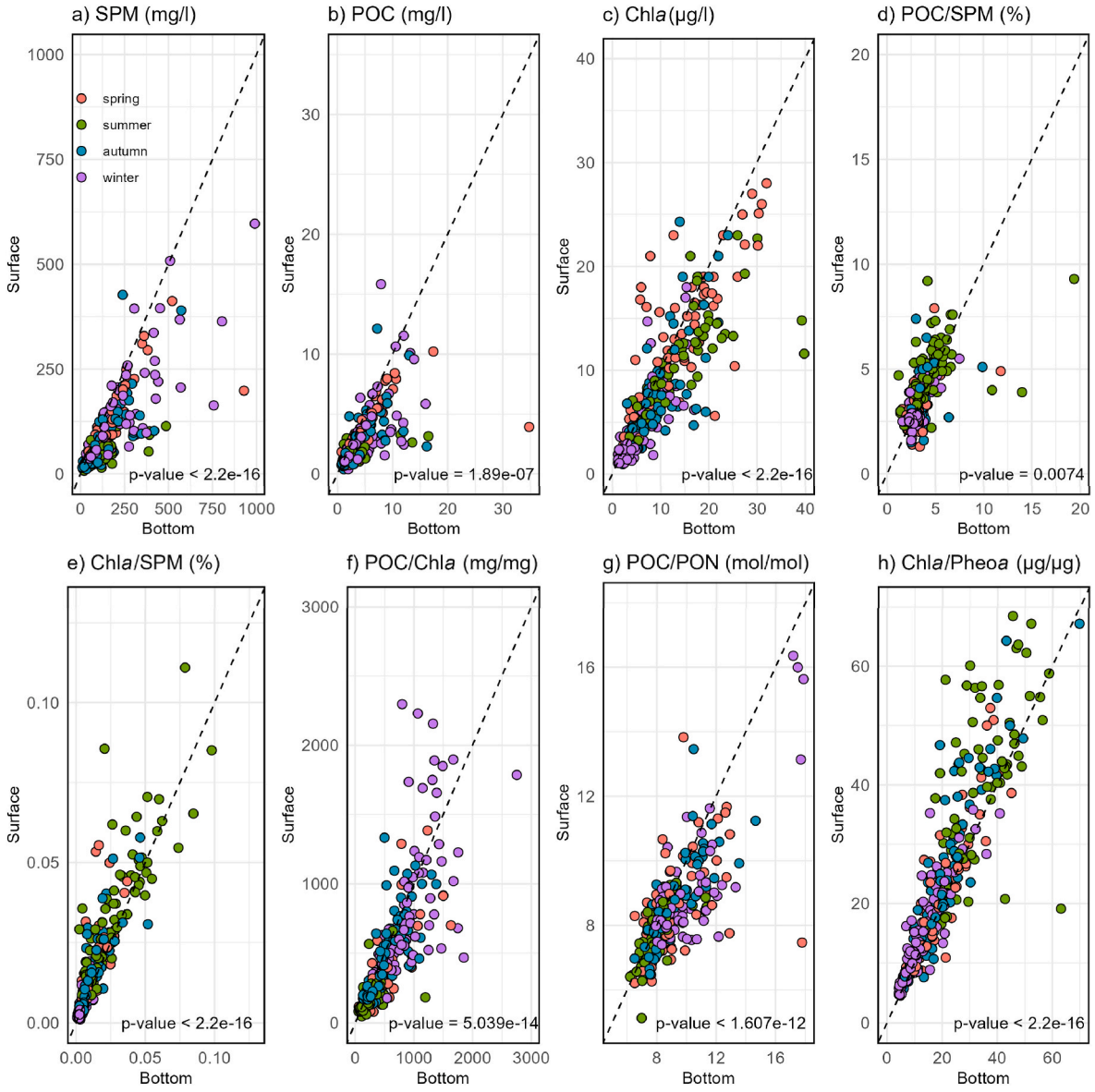


**Fig. 2.** Scatter plots (1:1 line shown) comparing surface and bottom (a) SPM (mg/l) concentrations, (b) POC (mg/l) concentrations, (c) Chl*a* (µg/l) concentrations, (d) POC/SPM (%) ratios (POC content), (e) Chl*a*/SPM (%) ratios (Chl*a* content), (f) POC/Chl*a* (mg/µg) ratios, (g) POC/PON (mol/mol), and (h) Chl*a*/Pheo*a* (µg/µg) ratios. The *p*-values refer to the Wilcoxon signed-rank test for the paired samples. For POC/Chl*a*, lower ratios (40–140 g/g) indicate living phytoplankton cells, intermediate (140–200 g/g) suggest mixed material with the dominance of phytoplankton cells, and higher (>200 g/g) indicate degraded organic matter (Savoye et al., 2003).

lowest in summer, whereas those in Chl*a*/Pheo*a* were highest, and both were significantly different from the other seasons. These ratios may serve as potential proxies indicating the quality of organic matter (Savoye et al., 2003; Bouillon et al., 2011), and our results suggest that the surface waters are generally enriched in organic matter of higher trophic quality.

Analysis of hourly profiles of SPM and Chl*a* concentrations during tidal cycles in spring (April 2019) and winter (November 2019) revealed notable disparities between the two seasons. These patterns cannot be explained by wave and wind effects as these were low during all tidal cycles. Throughout both tidal cycles, SPM concentrations exhibited a tendency to increase towards the bed during periods of maximum current velocities, whereas they remained relatively constant on the vertical exhibiting lower values on average during the slack periods (Fig. 3a and b). Concurrently, Chl*a* concentration profiles in November closely mirrored the corresponding SPM patterns (Fig. 3b). However, in April, distinct differences emerged between the vertical profiles of Chl*a* and SPM concentrations. Most notably, about half of the Chl*a* profiles in April exhibited inversions, where concentrations decreased towards the bed (Fig. 3a, Profiles 1–4, 7–8). Similar patterns as in November have been found during the months May–August and October–November and as in April during the months March and September. Van der Hout et al. (2017) observed consistently high Chl*a* concentrations closer to the bed in the Dutch coastal turbidity maximum. The authors suggest a uniform Chl*a* distribution with an increase only near the bed, contrasting with the exponential increase in SPM concentrations towards the bed. While these findings align with our observation of increasing Chl*a* content on moving up the water column, we also note higher Chl*a* concentrations closer to the surface and relatively lower concentrations closer to the bottom during the spring months. This contrasts with the suggestion of uniform Chl*a* distribution throughout the large part of the water column, which appears unlikely based on our data.

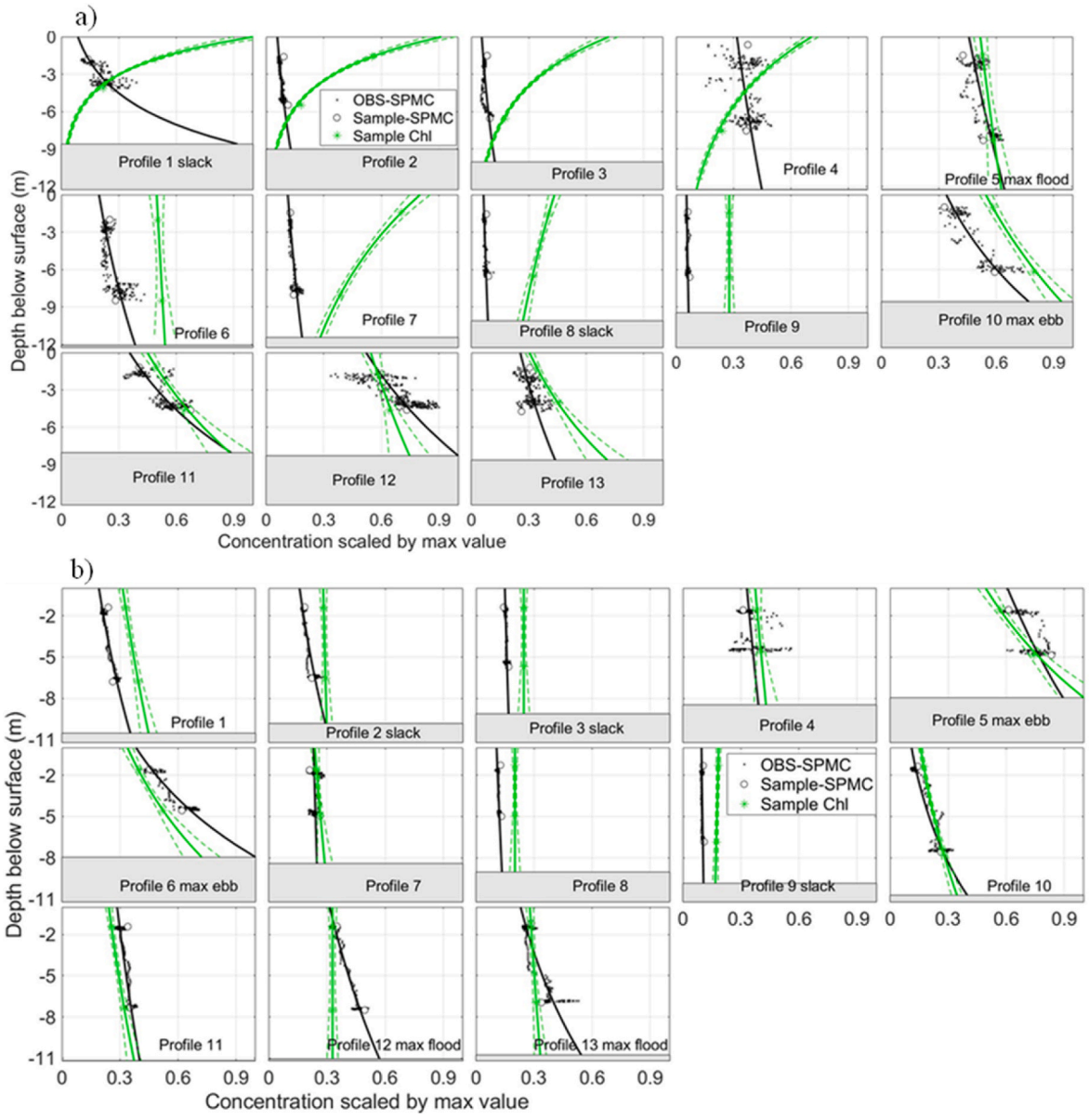


**Fig. 3.** Hourly vertical profiles of SPM (black line) and Chl*a* (green line) concentrations scaled by the maximum value during the tidal cycle in April 2019 (SPM: 366 mg/l, Chl*a*: 33 μg/l) (a) and November 2019 (SPM: 272 mg/l, Chl*a*: 11 μg/l) (b). The Chl*a* profile uncertainty (expressed as a standard deviation is shown as dashed lines. The SPM profile uncertainty, expressed as $R^2$, is between 0.5 and 0.9, except for profiles 4, 8, 9 and 13 in April and profiles 4, 7 and 9 in November). The light gray box represents the sea bed.

### 3.3. Probability of phytoplankton to be in the photic zone

To better quantify the accumulation of Chl*a* in the surface waters, we attempted to determine the average mass of SPM and Chl*a* within the estimated photic layer (generally between 0.5 and 3 m, see Table 1) and extrapolated part of the profile between the sample height (about 1 m below the surface) and the surface during a tidal cycle from the fitted vertical profiles. The depth-integrated concentration of SPM ([g $m^{-2}$]) within the photic layer during a tidal cycle remains conservative across seasons (Fig. 4a). This lack of variability aligns with expectations, considering that the vertical light attenuation coefficient, which determines the photic layer, is mainly controlled by SPM concentrations. However, the mass of Chl*a* within the photic layer during a tidal cycle exhibits seasonal variation, being higher during spring and summer compared to winter and autumn, yet it remains constant within each of these seasons (Fig. 4a). Further we calculate the percentage of SPM and Chl*a* within the photic layer by assuming the highest concentration in the fitted vertical profile as the maximum SPM and Chl*a* concentrations available for resuspension during a tidal cycle (Fig. 4b). The analysis reveals that the percentages of Chl*a* and SPM within the photic layer are identical during a tidal cycle in winter. However, during spring, the Chl*a* percentage in the photic layer approaches 10 %, while the SPM percentage is notably lower at 3 %. Similarly, in summer, the Chl*a* percentage increases up to 30 %, whereas the percentage of SPM in the photic layer rises to 18 %. This observation substantiates the enrichment of Chl*a* compared to SPM in the photic layer and aligns with the established POC/SPM relationship, indicating an inverse correlation between SPM concentration and the POC content (Schartau et al., 2019; Fettweis et al., 2022).

## 4. Discussion

Similar to the increase in POC content across the nearshore-offshore SPM gradient, we observed higher POC content in surface waters compared to bottom waters, in line with the vertical gradient of SPM concentrations. The higher POC content in the surface waters is accompanied by a shift in POC composition, with a greater contribution of phytoplankton derived POC (Section 4.2), also reflected in the higher Chl*a* content at the surface. The difference in POC composition between surface and bottom waters is most pronounced during the phytoplankton growth period. This apparent accumulation of Chl*a* in the surface layer, especially during the spring bloom, indicates a seasonal difference in the vertical distribution of Chl*a* and SPM. In accordance with our initial hypothesis, Chl*a* distribution diverges from the distribution of SPM in a shallow, well-mixed water column (characterized by uniform temperature and salinity), during the phytoplankton bloom period (March–April and September). This is substantiated by the larger variation in slope distribution in spring compared to winter (Fig. 1a). Higher Chl*a* concentrations in the surface samples, result in positive $\lambda_{Chla}$ (eqn. (1)) in the interpolated profile. In contrast SPM profiles have negative $\lambda_{SPM}$ values, reflecting increasing concentrations with depth. The significant increase in the Chl*a* content and concentration of SPM during spring (Figs. 2c and 3a) indicates the role of phytoplankton growth in influencing the trends in Chl*a* concentrations in addition to tidal mixing. The winter, summer and autumn situations (see as example Fig. 4b), in contrast, can be better understood under the assumption that Chl*a* containing phytoplankton cells move generally along similar patterns as the SPM flocs.

Based on these observations, we propose the existence of two distinct phytoplankton functional types, distinguished by their differing associations with the sediment particles (Riebesell, 1993; de Lucas Pardo et al., 2015). The first type is the floc-associated phytoplankton whose dynamics is coupled with SPM dynamics. Its occurrence results in synchronized variations of Chl*a* and SPM concentrations, that is, similar variations in λ. This type of phytoplankton appears to be dominant over most of the year. The second type is the free phytoplankton, that moves independently of the SPM flocs and lacks a direct association with mineral SPM. It exhibits differences in physical properties, such as density and settling velocities. Consequently, this type of phytoplankton is likely to experience decoupled cycles of settling and resuspension compared to SPM flocs, which result in a weaker correlation with SPM. This type appears to be dominant during the growing season. If correct, this hypothesis could contribute to explaining why phytoplankton are able to sustain a net production in turbid, vertically mixed waters having only short duration in the light-flooded uppermost layers. As an extension of this hypothesis we outline the key implications which are further elaborated in the discussion:

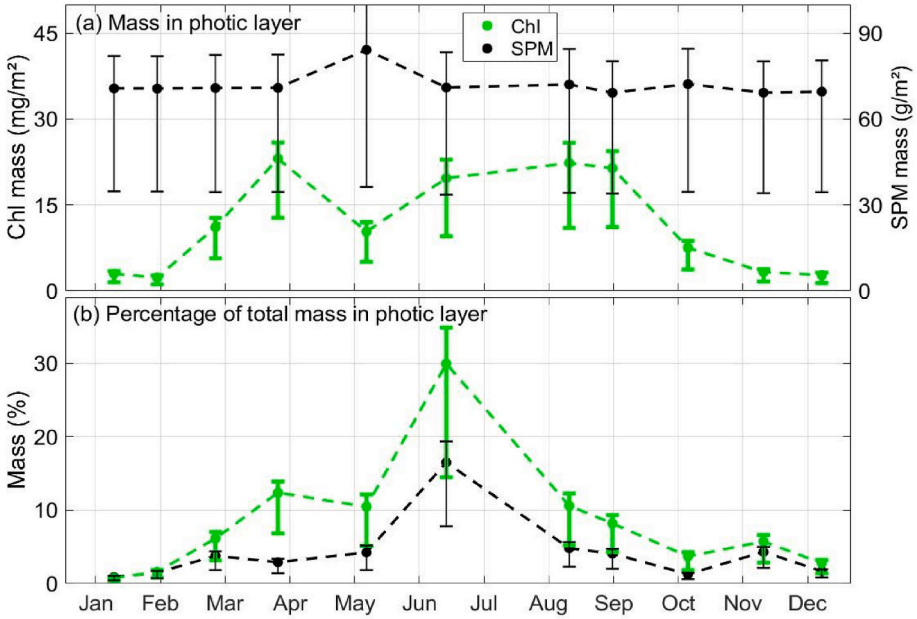


**Fig. 4.** (a) Mass of Chl*a* and SPM integrated over the photic layer per tide and unit area. (b) Percentage of Chl*a* and SPM in the photic layer with respect to their total mass available for resuspension during a tide. The dashed lines consider a photic layer for $a = 4.6$ (1 % light attenuation, see eq. (2)), the error bars do not represent stochastic uncertainties, but encompass photic layers between $a = 6.9$ and $a = 2.3$ (0.1 % and 10 % light attenuation).

- Higher turbulence may result in breaking up of relatively larger SPM flocs into a mixture of smaller flocs with or without phytoplankton cells attached to them.
- Free phytoplankton cells or SPM flocs with higher POC content are likely to have lower settling velocities or negative ones (buoyancy) (Fettweis and Baeye, 2015). This increased POC and Chl*a* content of SPM at the surface can be explained by the different settling of the various SPM components.
- During spring, there are free phytoplankton cells (such as *Phaeocystis globosa*) that are likely to form aggregates and accumulate near the surface because of buoyancy. This results in the inverse Chl*a* profiles observed in March and April.

### 4.1. Photo-acclimation and variability of the Chla concentration profiles

Before we explain our observations of Chl*a* and SPM concentration correlations based on the hypothesis, we elaborate on other explanations. Phytoplankton cells exhibit physiological adaptations that allow them to maintain photosynthetic activity even under light-limiting conditions, as observed in coastal regions where mixing depths can reach up to 20 times the photic depth (Van Spaendonk et al., 1993). These adaptations in response to irradiance, referred to as photo-acclimation, involve functional and structural changes of the photosynthetic apparatus (Jakobsen and Markager, 2016; Striebel et al., 2023). A common manifestation of photo-acclimation is the adjustment of the cellular pigment content, with light-limited cells typically exhibiting elevated Chl*a* concentration per cell in order to maximize growth (Masuda et al., 2021). If photo-acclimation were a significant factor, we would expect to observe higher Chl*a* concentrations at deeper depths due to increased light limitation, and lower concentrations near the surface as a result of photoprotective strategies, however this does not account for the observed inverted Chl*a* profiles. Moreover, under sustained intense mixing in a shallow water column, the regulation of cellular Chl*a* concentrations may be less effective, as physiological adjustments can lag behind rapidly changing light environment (Falkowski et al., 1992; McLaughlin et al., 2020). Finally, the observation of inverted Chl*a* profiles even during night sampling (April 2019), when photo-physiological differences between the surface and bottom are expected to be minimal, further suggests that cellular pigment regulation is not the primary driver of the observed pattern.

Similarly, the expectation of higher Chl*a* concentrations at the surface and lower concentrations at the bottom, typically attributed to higher primary production and phytoplankton mortality, respectively, may not be justified. Variability in the Chl*a* profile over short time scales such as hourly measurements over a tidal cycle are likely governed by physical processes, such as resuspension and turbulent mixing, settling or buoyancy rather than biological processes (Blauw et al., 2012). While tidal advection plays a crucial role in horizontally transporting phytoplankton, its impact on shaping the observed Chl*a* profile appears less significant. It is less likely for adjacent shallow and well-mixed areas to display different vertical Chl*a* distributions. Additionally, the consistent observation of inverted profiles during both ebb and flood periods reduces the likelihood of gradients explaining these patterns. Although we cannot completely rule out the possibility of phytoplankton patchiness contributing to the observed high Chl*a* concentrations near the surface, the occurrences of the inverted profiles during high current velocities suggests a more systematic pattern. This contrasts with a more stochastic pattern that we expect from patchiness and points to a lower significance of this phenomenon.

### 4.2. Vertical variations in SPM composition

In contrast to previous studies that are based mostly on samples taken at the surface of the water column, we use hourly water samples at the surface and the bottom of the water column - and continuous sensors of turbidity - during a full tidal cycle to construct vertical profiles of concentrations for Chl*a* and SPM. To investigate whether vertical differences in SPM composition, particularly with respect to organic matter, exist, we compare compositional proxies (POC/PON, POC/Chl*a*, and Chl*a*/Pheoa) between surface and bottom waters. The rationale lies in our expectation of observing differences in the composition of SPM, that arise from the anticipated differences in the distribution of both SPM and Chl*a* concentrations. Our results reveal a compositional gradient of SPM within the vertical water column similar to the cross-shore gradient (Figs. 2 and 3). Notably, the Chl*a* and POC content begin to diverge between surface and bottom depths in spring, with the disparity reaching its peak during summer. In addition to significantly higher Chl*a* and POC content at the surface, the observations also indicate the disparity in the quality of the organic material between surface and deeper depths. POC/PON, POC/Chl*a*, and Chl*a*/Pheo*a* ratios often used as proxies indicative of biochemical composition of bulk POM suggest prevalence of degraded POM deeper in the water column (Fig. 2d, e, f). The majority of our observed POC/PON ratios align with the commonly assigned range for marine POM (6–12; Martiny et al., 2013) although there is a seasonal variation (Table 1). While the POC/PON ratio is commonly used to infer the sources of organic matter, in systems with limited external inputs, it can also serve as an indicator of degradation status (Xu et al., 2021). Previous estimates of $\delta^{13}C_{POC}$ (−24 to −18 ‰) from the bottom waters in the Belgian coastal zone indicate significant autochthonous production (Franco et al., 2008). Hence elevated POC/-PON ratios in deeper waters likely indicate accumulation of more degraded material, consistent with preferential remineralization of nitrogen (Schneider et al., 2003). Lower values closer to the surface suggest greater contribution of non-degraded phytoplanktonic POM. Moreover, higher POC/Chl*a* ratios further support the dominance of degraded material at deeper depth. Lower ratios (40–140 g/g) typically reflect predominantly living phytoplankton, intermediate values (140–200 g/g) suggest phytoplankton-dominated material including senescent cells and other material, while higher values (>200 g/g) are indicative of predominantly degraded organic matter (Savoye et al., 2003). Notably lower Chl*a*/Pheo*a* ratios in deeper waters similarly indicate the accumulation of Chl*a* degradation products, such as Pheo*a*, through processes such as predation and degradation of phytoplankton cells (Woulds and Cowie, 2009). The concentration of Pheo*a* relative to Chl*a* is a commonly used proxy for the stage of diagenesis, with lower ratios reflecting more advanced degradation of phytoplankton-derived organic matter. Variations in the composition of organic matter based on depth have also been documented within the Delaware Estuary, with the prominence of phytoplankton-derived organic matter in surface waters and more degraded terrestrial organic matter closer to the bed (Hermes and Sikes, 2016). Deng et al. (2021) also reported elevated Chl*a*/SPM ratios closer to the surface than the deeper waters (≈10 m) in the Changjiang Estuary. The depth-based segregation of POM by quality is a further indication that resuspension and settling do not merely result in dilution of the particles that would result in a constant composition independent of concentration. Instead our data shows that particles do not behave homogeneously and that differential settling occurs. This finding calls for a reconsideration of monitoring strategies to include samples from surface and bottom depths during a tidal cycle.

### 4.3. Free and floc-attached phytoplankton

At the tidal scale, the hourly profiles of SPM and Chl*a* during most of the year consistently exhibit a similar distribution. In contrast, during the bloom periods (spring and summer), the observations of higher Chl*a* concentrations near the surface - or a different shape of SPM and Chl*a* concentration in the vertical profiles - suggest instances during the tidal cycle where Chl*a* distribution deviates from its association with SPM. While the specific interactions between phytoplankton cells and SPM remain unclear, high SPM concentrations at MOW1, coupled with tidal turbulence, create favorable conditions for collisions and aggregation

between phytoplankton and mineral particles forming biomineral flocs (Jackson, 2015; Wheatland et al., 2020). In autumn and winter, the phytoplankton community in Belgian waters consists primarily of benthic and tychoplanktonic diatoms, which associate with sediment particles, and smaller, heavily silicified planktonic diatoms, which have higher densities (Nohe, 2019). Both groups are expected to exhibit resuspension and settling dynamics similar to those of SPM, leading to a stronger correlation between Chl*a* and SPM concentrations. The presence of a phytoplankton community closely associated with SPM supports our hypothesis that a floc-associated phytoplankton type dominates during the winter months.

With the relaxation of winter light limitation in spring, the phytoplankton community in Belgian waters becomes dominated by larger, often colonial, and lightly silicified diatom species, along with *Phaeocystis globosa* colonies, with the latter prevailing in the late phase of the spring bloom (Rousseau et al., 1994, 2006; Nohe, 2019). Although the phytoplankton cells are subject to resuspension and settling akin to the mineral particles, unattached free cells are likely to have lower settling velocities due to lower densities compared to mineral-enriched flocs. *P. globosa* colonies with cells embedded in a mucilaginous matrix dominate the late phase of the spring bloom (Apr–May) in the Belgian coastal waters (Rousseau et al., 1994, 2006). Evidence from the German Bight indicates that *Phaeocystis* colonies exhibit a lower aggregation potential, often observed either freely floating or loosely attached to the SPM flocs (Riebesell, 1993). In contrast, the authors found diatom cells to be firmly embedded within the SPM flocs. Furthermore *Phaeocystis*-rich SPM flocs have lower sinking velocities prolonging their residence closer to the surface (Riebesell, 1992). Laboratory and field studies provide substantial evidence that pelagic diatoms can regulate their vacuole sap or produce flocculation inhibitory substances to modify their buoyancy (Kiørboe and Hansen, 1993; Woods and Villareal, 2008; Acuña et al., 2010). This ability is particularly relevant during bloom conditions, where diatoms adjust their buoyancy to remain closer to light and nutrient sources. Kang et al. (2019) showed that phytoplankton can modify their aggregation and buoyancy, allowing some cells to remain relatively free from surrounding particulate matter under turbulence and high SPM concentrations. The prevalence of such mechanisms likely contributes to the independence of phytoplankton cells from SPM, which is reflected in the poor correlation and dissimilarities in the vertical profiles of SPM and Chl*a* concentrations observed during the bloom periods.

The inverted Chl*a* profiles during the bloom period support our assumption of a substantial accumulation of free phytoplankton cells closer to the surface, in addition to floc-attached cells. Profiles with higher Chl*a* concentrations in the upper water column are also observed in shallow waters (10–15 m) during summer in the German Bight (Zhao et al., 2019). Floc break-up occurs during maximum currents throughout the year and suggests that free phytoplankton may also be present in winter. Nevertheless, the increase in Chl*a* content at the surface - or the different shapes of Chl*a* and SPM vertical profiles of concentration - are less pronounced in winter, early summer and late-autumn, which coincides with high SPM and low phytoplankton concentrations (low Chl*a*) with a dominance of small colonial bentho-pelagic diatoms (Rousseau et al., 2002; Muylaert et al., 2006).

### 4.4. How important is water clarity in turbid areas?

A typical occurrence in Belgian nearshore waters is an elevated surface Chl*a* co-occurring with high SPM concentrations varying between 20 and a few hundreds of mg/l during the spring bloom. High Chl*a* concentrations in such turbid waters suggest prominence of mechanisms that aid in increasing the probability of the phytoplankton cells to be retained in the photic zone. The insignificant differences in the SPM concentrations between winter and early spring (March) in the Belgian coastal waters suggests that the photic depth, a measure of water clarity, may not be substantially different during these months, though there will be variations due to spring-neap tides. The observed increase in Chl*a* concentrations during early spring hence indicates a relaxation of winter light limitation and not necessarily an increase in the photic depth. This indicates that once the minimum irradiance threshold for photosynthesis is met, phytoplankton cells can initiate production despite high SPM concentrations. In turbid waters during early spring, free phytoplankton type seem to have a distinct advantage. Due to differential settling, they are likely to spend more time within the shallow photic zone compared to floc-attached phytoplankton cells (independently of buoyancy mechanisms that may even enhance their presence at the surface). The differential settling due to density differences or buoyancy, as evidenced by the inverted Chl*a* profiles, appears to be an important mechanism for further enhancing and sustaining the phytoplankton bloom until late April, when SPM concentrations begin to decrease. Thereafter, as photic depths increase, the advantage of free phytoplankton type diminishes, given the higher likelihood of cells to be within the photic zone (Fig. 4b). Our results show that with decreasing SPM concentration, the probability of phytoplankton to be in the photic layer increases on average over the tidal cycle (for Chl*a* concentration it increases from ~2 % to ~12 % between January and April; Fig. 4b). Vice versa, increasing SPM concentrations, such as at the end of the summer and in the fall, decreases this probability in the same proportion. In the middle of the summer, when SPM concentration is at the lowest, the probability for Chl*a* to be in the photic zone is at the highest. Water clarity is a known controlling factor for phytoplankton production. Our results suggest that water clarity, when it is determined by the SPM concentration subject to tidal and seasonal variability, also influences the probability of a phytoplankton cell to be in the photic layer. This is not only due to the variation in the photic layer depth, but especially to the differential settling. Due to differential settling of organic and mineral particles, the effect of a decrease in water clarity on phytoplankton production is less than it would be if the composition of the SPM would not change as a function of concentration (see Fig. 4b, where Chl*a* has always a similar or higher probability than SPM from March to November).

## 5. Conclusions

Our results show that the vertical enrichment of POM at the surface is governed by the same process as along the horizontal nearshore-offshore gradient, i.e. differential settling of mineral vs organic rich particles, a fundamental property of SPM in turbid areas. Additionally, the seasonal variation in the composition of SPM between surface and bottom waters, peaking in summer, corresponds to notable differences POM quality at these depths. This highlights the importance of sampling both surface and bottom waters, particularly for particulate parameters exhibiting vertical gradients, even in well-mixed waters like MOW1. While tidal currents primarily control the vertical gradients in SPM and Chl*a* concentrations, we observed periods during the phytoplankton growing period when surface Chl*a* concentrations exceed those at the bottom, without a corresponding decrease in SPM concentrations. This suggests that Chl*a* can escape the influence of tidal currents during this period, possibly due to changes in phytoplankton dominance from floc-attached to free forms. Free phytoplankton cells during the growing period appear to spend more time in the photic zone due to differential settling, likely an adaptation to low irradiance conditions. In contrast, floc attachment is not as limiting in summer, where the probability of residing in the photic layer is high due to lower SPM concentrations. Our analysis of the mass of SPM within the photic layer, which remains conservative across months, suggests that the seasonally varying composition of SPM (Chl*a*/SPM) plays a more significant role. This calls for looking in more detail at the strategies deployed by different types of phytoplankton to increase buoyancy or associate with mineral particles. Such associations influence the particle settling properties and understanding them can improve modelling approaches to better estimate the fate of organic carbon in coastal waters.

## CRediT authorship contribution statement

**Saumya Silori:** Writing – original draft, Visualization, Formal analysis, Data curation, Conceptualization. **Xavier Desmit:** Writing – review & editing, Funding acquisition, Conceptualization. **Rolf Riethmüller:** Writing – review & editing, Conceptualization. **Markus Schartau:** Writing – review & editing. **Nathan Terseleer:** Writing – review & editing. **Michael Fettweis:** Writing – original draft, Visualization, Funding acquisition, Formal analysis, Conceptualization.

## Declaration of competing interest

The authors have no conflicts of interest to declare.

## Acknowledgements

The research was supported by the Belgian Science Policy (BELSPO) within the BRAIN-be programme PiNS (contract nr RV/21/PiNS) and BG-PART (contract nr B2/202/P1/BG-PART), the Maritime Access Division of the Flemish Ministry of Mobility and Public Works (MOMO project), and the RBINS BGCMonit program. Scientific input from Markus Schartau and Rolf Riethmüller are integrated in the research topics "Marine and polar life" and "Coastal zones at a time of global change" of the project-oriented funding programme: Changing Earth - Sustaining our Future, funded by the Helmholtz Association of German Research Centers. Ship time with the RV Belgica was provided by BELSPO and RBINS-OD Nature. The SPM and Chl*a* analysis have been done in RBINS's ECOCHEM Laboratory. The authors have no conflicts of interest to declare.

## Data availability

Data will be made available on request.

## References

Acuña, J.L., López-Alvarez, M., Nogueira, E., González-Taboada, F., 2010. Diatom flotation at the onset of the spring phytoplankton bloom: an in situ experiment. Mar. Ecol. Prog. Ser. 400, 115–125. https://www.int-res.com/articles/meps2009/400/m400p115.pdf.

Alvarez-Fernandez, S., Riegman, R., 2014. Chlorophyll in North Sea coastal and offshore waters does not reflect long term trends of phytoplankton biomass. J. Sea Res. 91, 35–44. https://doi.org/10.1016/j.seares.2014.04.005.

Bale, A.J., Morris, A.W., 1998. Organic carbon in suspended particulate material in the North Sea: effect of mixing resuspended and background particles. Cont. Shelf Res. 18 (11), 1333–1345. https://doi.org/10.1016/S0278-4343(98)00046-6.

Blauw, A.N., Beninca, E., Laane, R.W., Greenwood, N., Huisman, J., 2012. Dancing with the tides: fluctuations of coastal phytoplankton orchestrated by different oscillatory modes of the tidal cycle. PLoS One 7 (11), e49319. https://doi.org/10.1371/journal.pone.0049319.

Bouillon, S., Connolly, R.M., Gillikin, D.P., 2011. 7.07 Use of stable isotopes to understand food webs and ecosystem functioning in estuaries. Treatise on Estuarine Coast. Sci. 7. https://doi.org/10.1016/B978-0-12-374711-2.00711-7.

Boyer, J.N., Kelble, C.R., Ortner, P.B., Rudnick, D.T., 2009. Phytoplankton bloom status: chlorophyll a biomass as an indicator of water quality condition in the southern estuaries of Florida, USA. Ecol. Indic. 9 (6), S56–S67. https://doi.org/10.1016/j.ecolind.2008.11.013.

Capuzzo, E., Stephens, D., Silva, T., Barry, J., Forster, R.M., 2015. Decrease in water clarity of the southern and central North Sea during the 20th century. Glob. Change Biol. 21 (6), 2206–2214. https://doi.org/10.1111/gcb.12854.

Cloern, J.E., 1987. Turbidity as a control on phytoplankton biomass and productivity in estuaries. Cont. Shelf Res. 7 (11–12), 1367–1381. https://doi.org/10.1016/0278-4343(87)90042-2.

de Lucas Pardo, M.A., Sarpe, D., Winterwerp, J.C., 2015. Effect of algae on flocculation of suspended bed sediments in a large shallow lake. Consequences for ecology and sediment transport processes. Ocean Dyn. 65, 889–903. https://doi.org/10.1007/s10236-015-0841-y.

Deng, Z., He, Q., Chassagne, C., Wang, Z.B., 2021. Seasonal variation of floc population influenced by the presence of algae in the Changjiang (Yangtze River) Estuary. Mar. Geol. 440, 106600. https://doi.org/10.1016/j.margeo.2021.106600.

Dyer, K.R., 1986. Coastal and Estuarine Sediment Dynamics. John Wiley & Sons, Chichester, p. 258p.

Devlin, M.J., Barry, J., Mills, D.K., Gowen, R.J., Foden, J., Sivyer, D., Tett, P., 2008. Relationships between suspended particulate material, light attenuation and Secchi depth in UK marine waters. Estuar. Coast Shelf Sci. 79 (3), 429–439. https://doi.org/10.1016/j.ecss.2008.04.024.

Ehrhardt, M., Koeve, W., 1999. Determination of particulate organic carbon and nitrogen. Methods Seawater Anal. 437–444. https://onlinelibrary.wiley.com/doi/book/10.1002/9783527613984.

Falkowski, P.G., Greene, R.M., Geider, R.J., 1992. Physiological limitations on phytoplankton productivity in the ocean. Oceanography 5 (2), 84–91. https://doi.org/10.5670/oceanog.1992.14.

Fettweis, M., Baeye, M., 2015. Seasonal variation in concentration, size, and settling velocity of muddy marine flocs in the benthic boundary layer. J. Geophys. Res.: Oceans 120 (8), 5648–5667. https://doi.org/10.1002/2014JC010644.

Fettweis, M., Baeye, M., Cardoso, C., Dujardin, A., Lauwaert, B., Van den Eynde, D., et al., 2016. The impact of disposal of fine-grained sediments from maintenance dredging works on SPM concentration and fluid mud in and outside the harbor of Zeebrugge. Ocean Dyn. 66, 1497–1516. https://doi.org/10.1007/s10236-016-0996-1.

Fettweis, M., Baeye, M., Van der Zande, D., Van den Eynde, D., Joon Lee, B., 2014. Seasonality of floc strength in the southern North Sea. J. Geophys. Res.: Oceans 119 (3), 1911–1926. https://doi.org/10.1002/2013JC009750.

Fettweis, M., Francken, F., Pison, V., Van den Eynde, D., 2006. Suspended particulate matter dynamics and aggregate sizes in a high turbidity area. Mar. Geol. 235 (1–4), 63–74. https://doi.org/10.1016/j.margeo.2006.10.005.

Fettweis, M., Schartau, M., Desmit, X., Lee, B.J., Terseleer, N., Van der Zande, D., et al., 2022. Organic matter composition of biomineral flocs and its influence on suspended particulate matter dynamics along a nearshore to offshore transect. J. Geophys. Res.: Biogeosciences 127 (1), e2021JG006332. https://doi.org/10.1029/2021JG006332.

Franco, M.A., De Mesel, I., Diallo, M.D., Van Der Gucht, K., Van Gansbeke, D., Van Rijswijk, P., et al., 2007. Effect of phytoplankton bloom deposition on benthic bacterial communities in two contrasting sediments in the southern North Sea. Aquat. Microb. Ecol. 48 (3), 241–254. https://doi.org/10.3354/ame048241.

Franco, M.A., Soetaert, K., Van Oevelen, D., Van Gansbeke, D., Costa, M.J., Vincx, M., Vanaverbeke, J., 2008. Density, vertical distribution and trophic responses of metazoan meiobenthos to phytoplankton deposition in contrasting sediment types. Mar. Ecol. Prog. Ser. 358, 51–62. https://doi.org/10.3354/meps07361.

Fugate, D.C., Friedrichs, C.T., 2002. Determining concentration and fall velocity of estuarine particle populations using ADV, OBS and LISST. Cont. Shelf Res. 22 (11–13), 1867–1886. https://doi.org/10.1016/S0278-4343(02)00043-2.

Fugate, D.C., Friedrichs, C.T., 2003. Controls on suspended aggregate size in partially mixed estuaries. Estuar. Coast Shelf Sci. 58 (2), 389–404. https://doi.org/10.1016/S0272-7714(03)00107-0.

Hermes, A.L., Sikes, E.L., 2016. Particulate organic matter higher concentrations, terrestrial sources and losses in bottom waters of the turbidity maximum, Delaware Estuary, USA. Estuar. Coast Shelf Sci. 180, 179–189. https://doi.org/10.1016/j.ecss.2016.07.005.

Ho, Q.N., Fettweis, M., Spencer, K.L., Lee, B.J., 2022. Flocculation with heterogeneous composition in water environments: a review. Water Res. 213, 118147. https://doi.org/10.1016/j.watres.2022.118147.

Jago, C.F., Kennaway, G.M., Novarino, G., Jones, S.E., 2007. Size and settling velocity of suspended flocs during a Phaeocystis bloom in the tidally stirred Irish Sea, NW European shelf. Mar. Ecol. Prog. Ser. 345, 51–62. https://doi.org/10.3354/meps07006.

Jackson, G.A., 2015. Coagulation in a rotating cylinder. Limnol Oceanogr. Methods 13 (4), 194–201.

Jakobsen, H.H., Markager, S., 2016. Carbon-to-chlorophyll ratio for phytoplankton in temperate coastal waters: seasonal patterns and relationship to nutrients. Limnol. Oceanogr. 61 (5), 1853–1868. https://doi.org/10.1002/lno.10338.

Jones, S.E., Jago, C.F., Bale, A.J., Chapman, D., Howland, R.J.M., Jackson, J., 1998. Aggregation and resuspension of suspended particulate matter at a seasonally stratified site in the southern North Sea: physical and biological controls. Cont. Shelf Res. 18 (11), 1283–1309. https://doi.org/10.1016/S0278-4343(98)00044-2.

Kang, L.I., He, Y., Dai, L., He, Q., Ai, H., Yang, G., et al., 2019. Interactions between suspended particulate matter and algal cells contributed to the reconstruction of phytoplankton communities in turbulent waters. Water Res. 149, 251–262. https://doi.org/10.1016/j.watres.2018.11.003.

Kiørboe, T., Hansen, J.L., 1993. Phytoplankton aggregate formation: observations of patterns and mechanisms of cell sticking and the significance of exopolymeric material. J. Plankton Res. 15 (9), 993–1018. https://doi.org/10.1093/plankt/15.9.993.

Lacroix, G., Ruddick, K., Ozer, J., Lancelot, C., 2004. Modelling the impact of the Scheldt and Rhine/Meuse plumes on the salinity distribution in Belgian waters (southern North Sea). J. Sea Res. 52 (3), 149–163. https://doi.org/10.1016/j.seares.2004.01.003.

Lee, B.J., Kim, J., Hur, J., Choi, I.H., Toorman, E.A., Fettweis, M., Choi, J.W., 2019. Seasonal dynamics of organic matter composition and its effects on suspended sediment flocculation in river water. Water Resour. Res. 55 (8), 6968–6985. https://doi.org/10.1029/2018WR024486.

Maggi, F., Tang, F.H., 2015. Analysis of the effect of organic matter content on the architecture and sinking of sediment aggregates. Mar. Geol. 363, 102–111. https://doi.org/10.1016/j.margeo.2015.01.017.

Manheim, F.T., Hathaway, J.C., Uchupi, E., 1972. Suspended matter in surface waters of the Northern Gulf of Mexico. Limnol. Oceanogr. 17 (1), 17–27. https://aslopubs.onlinelibrary.wiley.com/doi/pdf/10.4319/lo.1972.17.1.0017.

Maerz, J., Hofmeister, R., van der Lee, E.M., Gräwe, U., Riethmüller, R., Wirtz, K.W., 2016. Maximum sinking velocities of suspended particulate matter in a coastal transition zone. Biogeosciences 13 (17), 4863–4876. https://doi.org/10.5194/bg-13-4863-2016.

Martiny, A.C., Vrugt, J.A., Primeau, F.W., Lomas, M.W., 2013. Regional variation in the particulate organic carbon to nitrogen ratio in the surface ocean. Glob. Biogeochem. Cycles 27 (3), 723–731. https://doi.org/10.1002/gbc.20061.

Masuda, Y., Yamanaka, Y., Smith, S.L., Hirata, T., Nakano, H., Oka, A., Sumata, H., 2021. Photoacclimation by phytoplankton determines the distribution of global subsurface chlorophyll maxima in the ocean. Commun. Earth Environ. 2 (1), 128. https://doi.org/10.1038/s43247-021-00201-y.

McLaughlin, M.J., Greenwood, J., Branson, P., Lourey, M.J., Hanson, C.E., 2020. Evidence of phytoplankton light acclimation to periodic turbulent mixing along a tidally dominated tropical coastline. J. Geophys. Res.: Oceans 125 (11), e2020JC016615. https://doi.org/10.1029/2020JC016615.

Moulton, M., Suanda, S.H., Garwood, J.C., Kumar, N., Fewings, M.R., Pringle, J.M., 2023. Exchange of plankton, pollutants, and particles across the nearshore region. Ann. Rev. Mar. Sci 15 (1), 167–202. https://doi.org/10.1146/annurev-marine-032122-115057.

Muylaert, K., Gonzales, R., Franck, M., Lionard, M., Van der Zee, C., Cattrijsse, A., et al., 2006. Spatial variation in phytoplankton dynamics in the Belgian coastal zone of the North Sea studied by microscopy, HPLC-CHEMTAX and underway fluorescence recordings. J. Sea Res. 55 (4), 253–265. https://doi.org/10.1016/j.seares.2005.12.002.

Nohe, A., 2019. *Long-term Trends in Phytoplankton Biomass, Composition and Dynamics in the Belgian Part of the North Sea* (Doctoral Dissertation. Ghent University. https://biblio.ugent.be/publication/8601087.

Riebesell, U., 1993. Aggregation of Phaeocystis during phytoplankton spring blooms in the southern North Sea. Mar. Ecol. Prog. Ser. 96, 281–289. https://www.jstor.org/stable/24833556.

Riebesell, U., 1992. The formation of large marine snow and its sustained residence in surface waters. Limnol. Oceanogr. 37 (1), 63–76. https://doi.org/10.4319/lo.1992.37.1.0063.

Rousseau, V., Park, Y., Ruddick, K., Vyverman, W., Parent, J.Y., Lancelot, C., 2006. Phytoplankton Blooms in Response to Nutrient Enrichment. Current Status of Eutrophication in the Belgian Coastal Zone. Brussels. Presses Univ. de Bruxelles, pp. 45–59. https://www.belspo.be/belspo/organisation/publ/pub_ostc/oa/oa14_en.pdf.

Rousseau, V., Leynaert, A., Daoud, N., Lancelot, C., 2002. Diatom succession, silicification and silicic acid availability in Belgian coastal waters (Southern North Sea). Mar. Ecol. Prog. Ser. 236, 61–73. https://doi.org/10.3354/meps236061.

Rousseau, V., Vaulot, D., Casotti, R., Cariou, V., Lenz, J., Gunkel, J., Baumann, M., 1994. The life cycle of Phaeocystis (Prymnesiophycaea): evidence and hypotheses. J. Mar. Syst. 5 (1), 23–39. https://doi.org/10.1016/0924-7963(94)90014-0.

Savoye, N., Aminot, A., Tréguer, P., Fontugne, M., Naulet, N., Kérouel, R., 2003. Dynamics of particulate organic matter δ15N and δ13C during spring phytoplankton blooms in a macrotidal ecosystem (Bay of Seine, France). Mar. Ecol.: Prog. Ser. 255, 27–41. https://www.int-res.com/articles/meps2003/255/m255p027.pdf.

Schartau, M., Riethmüller, R., Flöser, G., van Beusekom, J.E.E., Krasemann, H., Hofmeister, R., Wirtz, K., 2019. On the separation between inorganic and organic fractions of suspended matter in a marine coastal environment. Prog. Oceanogr. 171, 231–250. https://doi.org/10.1016/j.pocean.2018.12.011.

Schneider, B., Schlitzer, R., Fischer, G., Nöthig, E.M., 2003. Depth-dependent elemental compositions of particulate organic matter (POM) in the ocean. Glob. Biogeochem. Cycles 17 (2). https://doi.org/10.1029/2002GB001871.

Sommerfield, C.K., Wong, K.C., 2011. Mechanisms of sediment flux and turbidity maintenance in the Delaware Estuary. J. Geophys. Res.: Oceans 116 (C1). https://doi.org/10.1029/2010JC006462.

Striebel, M., Kallajoki, L., Kunze, C., Wollschläger, J., Deininger, A., Hillebrand, H., 2023. Marine primary producers in a darker future: a meta-analysis of light effects on pelagic and benthic autotrophs. Oikos 2023 (4), e09501. https://doi.org/10.1111/oik.09501.

Van Beusekom, J.E., Buschbaum, C., Reise, K., 2012. Wadden Sea tidal basins and the mediating role of the North Sea in ecological processes: scaling up of management? Ocean Coast Manag. 68, 69–78. https://doi.org/10.1016/j.ocecoaman.2012.05.002.

Van der Hout, C.M., Witbaard, R., Bergman, M.J.N., Duineveld, G.C.A., Rozemeijer, M.J. C., Gerkema, T., 2017. The dynamics of suspended particulate matter (SPM) and chlorophyll-a from intratidal to annual time scales in a coastal turbidity maximum. J. Sea Res. 127, 105–118. https://doi.org/10.1016/j.seares.2017.04.011.

Van Heukelem, L., Thomas, C.S., 2001. Computer-assisted high-performance liquid chromatography method development with applications to the isolation and analysis of phytoplankton pigments. J. Chromatogr. A 910 (1), 31–49. https://doi.org/10.1016/S0378-4347(00)00603-4.

Van Spaendonk, J.C.M., Kromkamp, J.C., De Visscher, P.R.M., 1993. Primary production of phytoplankton in a turbid coastal plain estuary, the Westerschelde (The Netherlands). Neth. J. Sea Res. 31 (3), 267–279. https://doi.org/10.1016/0077-7579(93)90027.

Wheatland, J.A., Spencer, K.L., Droppo, I.G., Carr, S.J., Bushby, A.J., 2020. Development of novel 2D and 3D correlative microscopy to characterise the composition and multiscale structure of suspended sediment aggregates. Cont. Shelf Res. 200, 104112. https://doi.org/10.1016/j.csr.2020.104112.

Winterwerp, J.C., 2001. Stratification effects by cohesive and noncohesive sediment. J. Geophys. Res.: Oceans 106 (C10), 22559–22574. https://doi.org/10.1029/2000JC000435.

Woods, S., Villareal, T.A., 2008. Intracellular Ion Concentrations and Cell Sap Density in Positively Buoyant Oceanic Phytoplankton, 133. Nova Hedwigia Beiheft, pp. 131–145. https://hero.epa.gov/hero/index.cfm/reference/details/reference_id/975724.

Woulds, C., Cowie, G.L., 2009. Sedimentary pigments on the Pakistan margin: controlling factors and organic matter dynamics. Deep Sea Res. Part II Top. Stud. Oceanogr. 56 (6–7), 347–357. https://doi.org/10.1016/j.dsr2.2008.05.033.

Xu, Z., Wang, B., Luo, Y., Li, H., Zhang, J., Jin, H., Chen, J., 2021. Changes of carbon to nitrogen ratio in particulate organic matter in the marine mesopelagic zone: a case from the South China Sea. Mar. Chem. 231, 103930. https://doi.org/10.1016/j.marchem.2021.103930.

Yu, M., Yu, X., Mehta, A.J., Manning, A.J., Khan, F., Balachandar, S., 2023. Persistent reshaping of cohesive sediment towards stable flocs by turbulence. Sci. Rep. 13 (1), 1760. https://doi.org/10.1038/s41598-023-28960-y.

Zhao, C., Maerz, J., Hofmeister, R., Röttgers, R., Wirtz, K., Riethmüller, R., Schrum, C., 2019. Characterizing the vertical distribution of chlorophyll a in the German Bight. Cont. Shelf Res. 175, 127–146. https://doi.org/10.1016/j.csr.2019.01.012.

# APPENDIX 4

**Silori S, Desmit X, Fettweis M. 2025. Spatio-temporal variation in particulate and dissolved organic matter dynamics in the southern North Sea. Biogeochemistry 168**

Biogeochemistry (2025) 168:96
https://doi.org/10.1007/s10533-025-01288-7

# Spatio-temporal variation in particulate and dissolved organic matter dynamics in the southern North Sea

**Saumya Silori · Xavier Desmit · Michael Fettweis**

Received: 3 January 2025 / Accepted: 27 October 2025


**Abstract** Turbid coastal waters are dynamic systems where fine-grained sediments interact with organic matter, significantly influencing the fate of both the components. We investigated the seasonal dynamics of particulate (POC) and dissolved (DOC) organic carbon pools along a suspended particulate matter (SPM) gradient from nearshore to offshore waters in a mid-latitude coastal zone. To assess temporal and spatial variations in POC composition, we quantified the relative contributions of phytoplankton ($POC_{phyto}$), heterotrophs ($POC_{het}$), detritus ($POC_{det}$), and mineral-associated organic matter ($POC_{mineral}$) to the bulk POC pool. In nearshore waters, frequent tidal resuspension and high SPM concentrations led to elevated $POC_{det}$ and $POC_{mineral}$ fractions, masking the increase in $POC_{phyto}$, despite the higher primary productivity during the spring bloom. In contrast, offshore waters exhibited a greater relative contribution of $POC_{phyto}$, with seasonal POC increases corresponding to elevated chlorophyll *a* (Chl*a*) levels in spring and summer, similar to the open-ocean dynamics. These trends were further reflected in particulate organic carbon to nitrogen (POC:PON) ratios and POC:Chl*a* ratios, commonly used to assess sources and quality of organic matter. The cross-shore gradient in organic matter partitioning, with dominance of POC nearshore and DOC offshore, highlights the role of particle resuspension and phytoplankton production in controlling organic carbon distribution between the two pools. Overall, our findings underscore the complex interplay between biological production, nutrient cycling, hydrodynamic forces, and SPM in shaping the composition and fate of organic carbon in turbid coastal systems.

**Keywords** North Sea · Particulate organic matter · Dissolved organic matter · Belgian coastal zone · Turbid waters · Phytoplankton · Suspended particulate matter

## Introduction

Shelf seas are characterized by their dynamic nature, leading to variability in the concentrations and composition of suspended particulate matter (SPM) across temporal and spatial scales. SPM comprises mineral particles and organic matter in particulate form, together forming the suspended material in the water column. Organic matter is commonly classified into particulate (POM) and dissolved (DOM) fractions based on the filtration properties. POM, which includes phytoplankton, large bacterial cells, marine gels, detritus, and fecal pellets is retained on filters with pore sizes ranging from 0.2 to 1 µm (Verdugo

Responsible Editor: Amy M. Marcarelli

S. Silori (✉) · X. Desmit · M. Fettweis
OD Natural Environment, Royal Belgian Institute of Natural Sciences, Rue Vautier 29, 1000 Brussels, Belgium
e-mail: saumyasilori27@gmail.com

Published online: 21 November 2025

2012). In contrast, DOM passes through these filters and is the primary source of energy and nutrients for a diverse group of heterotrophic bacteria (Hansell and Carlson 2014). DOM comprises a wide variety of molecules transformed by biotic and abiotic processes, with lifetimes varying from minutes to millennia. In the euphotic zone, DOM concentrations typically exceed POM by an order of magnitude (Middleburg 2019). As a dissolved component, DOM is transported differently than POM in the aquatic systems, leading to distinct dynamics.

A typical observation in coastal waters is the cross-shore gradient in SPM concentrations, characterized by lower POM content of SPM in nearshore turbid waters compared to higher POM content offshore (e.g. Eisma and Kalf 1979; Jago et al. 1993). Schartau et al. (2019) proposed a semi-empirical model to identify a mineral-associated POM fraction that varies closely with SPM concentrations, and a fresh POM fraction, representing seasonally produced and degraded matter. The mineral-associated POM fraction, as calculated by Schartau et al. (2019), likely comprises a combination of resuspended benthic POM and dissolved organic molecules adsorbed onto clay mineral surfaces (Keil et al. 1994; Keil and Mayer 2014; Fettweis et al. 2025).

Despite differing dynamics, DOM and POM are interconnected through continuous aggregation, disaggregation and degradation processes (Kharbush et al. 2020). One such mechanism is the adsorption and desorption of DOM molecules onto mineral surfaces, which shifts organic matter between the dissolved and particulate phases, maintaining a dynamic equilibrium (Hermann and Heip 1999; Abril et al. 2002). Evidence suggests that organic molecules within mineral matrices are protected them from bacterial exo-enzymes and rapid remineralization, although transformations of the organic molecules still occur at the organic-mineral interface (Hemingway et al. 2019; Kleber et al. 2021). Long-term storage of organic carbon on sediment mineral surfaces can have substantial implications for organic matter lability and preservation in the ocean (Mayer 1994; Hemingway et al. 2019). Therefore, quantifying the mineral-associated organic carbon fraction and comparing its contribution to contributions from other POM fractions is necessary to understand organic matter cycling and carbon burial efficiency in turbid shelf seas.

Common approaches for delineating POM sources and estimating their contributions include analyzing particulate organic carbon (POC) and particulate organic nitrogen (PON) elemental ratios and stable carbon isotopic ratios ($\delta^{13}C_{POC}$). These methods are particularly effective when sources exhibit distinct signatures, such as marine phytoplankton-derived POM (POC:PON $\approx$ 6–10 mol mol$^{-1}$; $\delta^{13}C_{POC} > -24$ ‰) and terrestrial POM (POC:PON > 12 mol mol$^{-1}$; $\delta^{13}C_{POC} < -26$ ‰) in temperate regions (Savoye et al. 2003; Goni et al. 2009). POC to chlorophyll *a* ratios (POC:Chl*a*) supplement this approach to estimate the contribution of phytoplankton biomass (Savoye et al. 2003; Liu et al. 2018). Generally, living phytoplankton exhibit POC:Chl*a* ratios around 40–140 g g$^{-1}$, phytoplankton-dominated POM have ratios below 200 g g$^{-1}$, and non-phytoplankton material have ratios exceeding 200 g g$^{-1}$ (Savoye et al. 2003). Pheophytin-a (Pheo*a*) to Chl*a* ratio further supplement this, Pheo*a* is a degradation product of Chl*a* usually produced due to phytoplankton mortality and hence is an indicator of physiological state of phytoplankton community (Gaffey et al. 2022).

In shelf waters where riverine and macrophyte inputs are minimal, phytoplankton-derived POM can contribute up to 75–97% to the total POM pool (Liénart et al. 2017, 2018). In shallow, well-mixed waters, tidal resuspension makes benthic POM a significant contributor to the overall POM pool (Modéran et al. 2010). Benthic POM is primarily a mixture of benthic primary producers, pelagic detritus, organic molecules adsorbed onto clay mineral surfaces, and where present, macrophytes (Dubois et al. 2012; Keil and Mayer 2014). Terrestrial organic matter may also contribute to shelf water POM, either as free particles or sorbed onto mineral surfaces (Keil et al. 1997; Blattmann et al. 2019). Consequently, POM composition in shelf waters is shaped by both allochthonous and autochthonous sources, including their mineral-associated fractions. In shallow shelf waters, where mineral particles (e.g., quartz, feldspars, carbonates, clay minerals) constitute a substantial portion of suspended matter, ratios such as POC:SPM and Chl*a*:SPM serve as useful indicators of the relative contribution of organic material and, in the case of Chl*a*:SPM, algal versus non-algal particles. These ratios characterize marine particles as "organic-dominated" (POC:SPM > 0.25),

"mineral-dominated" (POC:SPM < 0.06), or of "mixed composition" (POC:SPM = 0.06–0.25) (Wozniak et al. 2010).

The main aim of this study was to characterize and quantify various contributors to POM in turbid shelf seas, where significant interactions between organic matter and fine-grained sediments occur. We used established methods to estimate phytoplankton biomass ($POC_{phyto}$), heterotrophic biomass ($POC_{het}$), and POC adsorbed onto mineral surfaces ($POC_{mineral}$). Estimating the POM components, particularly $POC_{phyto}$ component, is needed to understand the seasonal and spatial variations in POM composition proxies (POC:PON and POC:Chl*a* ratios), especially when phytoplankton dominates POM. This analysis is based on multi-year (2019–2023) SPM, POC, PON, and Chl*a* concentration data collected at three sampling locations across the Belgian coastal-offshore SPM concentration gradient. While the seasonal variability of SPM, POM, and Chl*a* concentrations in Belgian waters has been described (Rousseau et al. 2006; Desmit et al. 2020; Fettweis et al. 2022), the variability of the different fractions composing POM (i.e. the compositional dynamics) remains poorly understood. The Belgian coastal waters, in the southern North Sea, host a spring phytoplankton bloom following the relaxation of winter light limitation. This bloom, peaking in April or May, is dominated by diatoms, with the haptophyte *Phaeocystis globosa* becoming particularly prominent at its peak (Rousseau et al. 2006). The increased phytoplankton production coincides with a reduction in SPM concentrations. Enhanced flocculation, driven by phytoplankton-derived exopolymers, leads to lower tidal-averaged SPM levels during the spring and summer, despite seasonal fluctuations in wind conditions and wave heights (Fettweis and Baeye 2015; Fettweis et al. 2022). In this study, we hypothesized that the different POM fractions ($POC_{phyto}$, $POC_{het}$, $POC_{mineral}$ and the residual fraction, which is detritus) vary in space and time. Some of this variability could be related to the cross-shore SPM gradient that will affect each POM fraction differently. Another part of the variability should be due to the seasonality in phytoplankton production and its impact on SPM concentrations in the water column.

## Materials and methods

### Study area and sampling frequency

Situated in the Southern Bight of the North Sea, the Belgian coastal waters are relatively shallow, with an average depth of ~ 10 m nearshore and a maximum depth of ~ 45 m, offshore. Strong tidal currents (> 1 m $s^{-1}$) and frequent wind forcing result in well-mixed conditions throughout most of the year (Fettweis and Baeye 2015). These waters exhibit a pronounced cross-shore gradient in SPM concentrations, with turbidity decreasing towards the offshore (Fig. 1a). Atlantic inflow via the English Channel accounts for ~ 96% of the Belgian coastal water mass, with the remainder mainly supplied by the Rhine, Scheldt, and Seine rivers, among which the Rhine is the dominant freshwater source (Lacroix et al. 2004; Dulière et al. 2019). River discharge exhibits a seasonal maximum during winter and early spring, with notable interannual variability largely driven by the North Atlantic Oscillation (NAO). A positive NAO phase is associated with stronger south-westerly winds, enhancing the north-eastward dispersion of the Scheldt and Rhine plumes, thus reducing the influence of freshwater in the Belgian coastal zone. Simultaneously, increased precipitation over the Scheldt basin may enhance nutrient delivery to the coastal zone (Breton et al. 2006). Residual flow in the Belgian coastal zone is directed north-eastward; however, oscillating tidal currents induce substantial horizontal dispersion, influencing net transport patterns (Lacroix et al. 2004).

Water samples were collected hourly or every 1.5 h over half or full tidal cycles at three stations from January 2019 to December 2023 (Table 1 and Fig. 1a). Figure 1b shows the months during which these tidal cycles were sampled. During most months, data collection represents one half or full tidal cycle per station, except in April 2023 when two tidal cycles were sampled at all stations. The three stations (MOW1, W05, and W08, shown in Fig. 1a) were positioned along a cross-shore transect, ranging from the nearshore coastal turbidity maximum at MOW1 (~ 10 m water depth) to W05 (~ 20 m water depth), located at the outer margin of the coastal turbidity maximum, and further offshore to W08 (~ 25 m water depth), influenced primarily

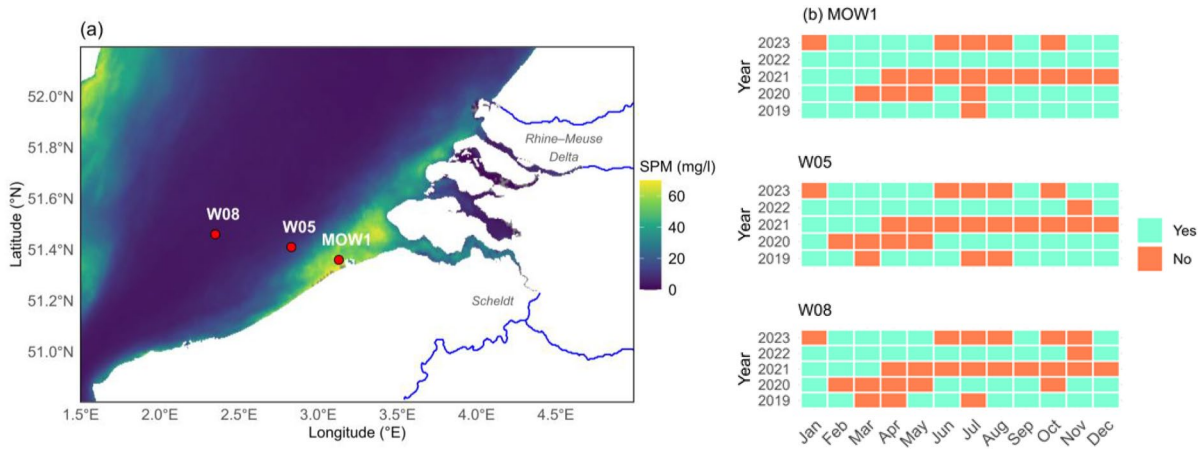


**Fig. 1** **a** Map of the sampling stations MOW1, W05, and W08. The background shows the multiyear (2017–2021) average surface SPM concentrations (mg/l) (satellite-based Earth Observation SPM) for the winter months (monthly averages for December, January, and February). **b** Timeline of monthly sampling between 2019 and 2023 across three stations in the Belgian Coastal Zone. Months marked "Yes" indicate hourly or 1.5 hourly sampling over a full or half tidal cycle, with April 2023 including two distinct tidal cycles sampled at each station

**Table 1** Number of samples for various parameters collected hourly or 1.5 hourly over several half and full tidal cycles at MOW1, W05, and W08 between January 2019 and December 2023

| | No. of samples | | |
|---|---|---|---|
| | MOW1 | W05 | W08 |
| Dissolved inorganic nitrogen (DIN) | 407 | 270 | 74 |
| Dissolved inorganic phosphate (DIP) | 414 | 301 | 145 |
| Dissolved inorganic silicate (DSi) | 404 | 311 | 179 |
| Suspended particulate matter (SPM) | 886 | 649 | 409 |
| Chlorophyll *a* (Chl*a*) | 813 | 602 | 370 |
| Pheophytin *a* (Pheo*a*) | 840 | 606 | 307 |
| Particulate organic carbon (POC) | 825 | 634 | 392 |
| Particulate organic nitrogen (PON) | 782 | 579 | 332 |
| Transparent Exopolymer Particles (TEP) | 685 | 541 | 314 |
| Dissolved organic carbon (DOC) | 392 | 297 | 180 |

by the channel waters (Fig. 1a). During each sampling event, water was collected at 1–2 m below the surface and 2–3 m above the seabed using 5- or 10-L Niskin bottles mounted on a Sea-Bird SBE09 CTD carousel. For dissolved parameters, sampling was performed at a single depth (1–2 m below the surface), assuming uniform mixing, as density stratification is uncommon in these waters (Lacroix et al. 2004).

## In-situ sample collection and analysis

Water samples for dissolved inorganic nitrogen (nitrate + nitrite + ammonia: DIN), phosphate (DIP), silicate (DSi), dissolved organic carbon (DOC) and total dissolved nitrogen (TDN) were filtered onboard using a GF/C filter (1.2 µm pore size) and subsequently frozen for further analysis in the laboratory. Dissolved inorganic nutrient samples were then analyzed using standard colorimetric methods using a Skalar autoanalyzer (see van der Zee and Chou 2005 for details). TDN was measured following oxidation in alkaline persulfate, and total nitrogen (TN) was calculated as the sum of TDN and PON.

Water samples for SPM, POC, PON, Chl*a* and Pheo*a* were filtered on board and subsequently analyzed in the laboratory. During each sampling event, three subsamples for SPM concentration were collected and filtered using pre-weighted and pre-combusted (405 °C for 24 h) 47 mm GF/C filters. After sample filtering, the filters were rinsed with ultrapure water (resistivity 18.2 MΩcm normalized at 25 °C) and immediately stored at − 20 °C. The filters were then dried at 50 °C for 24 h and weighted to obtain the concentrations. The uncertainty (expressed as the RMSE of the triplicates divided by the mean value) decreases with increasing concentration from 8.5% (SPM concentration < 5 mg/l) to 6.7% (< 10 mg/), 3.5% (10–50 mg/l), and 2.1%

(> 100 mg/l) and represents the random error related to the lack of precision during filtrations. Pre-combusted (405 °C for 24 h) 25 mm GF/C filters were used for POC and PON filtration and stored at -20 °C immediately. The filters were fumigated with HCl to remove any traces of particulate inorganic carbon and the samples were subsequently analyzed using a Thermo Finnigan Flash EA1112 elemental analyzer (Ehrhardt and Koeve 1999). GF/C filters (47 mm) were used to collect Chl*a* and Pheo*a*, and were stored in liquid nitrogen. The concentrations were then determined using ultra high-performance liquid chromatography with fluorometric detection. The analytical uncertainty for POC is 12% and for PON, Chl*a* and Pheo*a* is 18%, and was determined from repeated measurements of standards. We assume that the filtration error uncertainty is comparable to that observed for SPM, which ranges between 2.1% and 3.5% for SPM concentrations greater than 10 mg/l. The smaller filtration uncertainty results in the total uncertainty for these parameters approximating the analytical uncertainty.

DOC was determined following acidification of water samples to remove inorganic carbon. Organically bound carbon was oxidized to $CO_2$ by UV irradiation in the presence of persulfate. The resulting $CO_2$ diffused through a gas dialysis membrane, inducing a pH shift in phenolphthalein indicator. The decrease in absorbance was measured spectrophotometrically at 550 nm. Transparent exopolymer particle concentrations were determined colorimetrically following Passow and Alldredge (1995) and Passow (2022). During each sampling event, three subsamples for TEP concentration were filtered through 25 mm polycarbonate filters with a pore size of 0.4 µm under vacuum pressure below 200 hPa. After filtration, the filters were immediately stained with Alcian blue and stored at − 20 °C. In the lab, filters were soaked in sulfuric acid and absorbance at 787 nm was measured spectrophotometrically. The stained particles were quantified as xanthan gum equivalents, reflecting the dye-binding capacity of the acidic polysaccharides that make up TEP. (Passow and Alldredge 1995; Passow 2002). TEP concentrations were reported in units of mg xanthan gum equivalents per liter (mg XG eq./l), with an assumed uncertainty comparable to that of POC measurements.

## Estimation of different POC components

### *Phytoplankton carbon biomass*

To estimate phytoplankton carbon biomass ($POC_{phyto}$), we used the empirical model from Danish waters described by Jakobsen and Markager (2016) to predict C:Chl*a* ratios for temperate coastal phytoplankton. The monthly variation in C:Chl*a* ratios is modelled using a sinusoidal function that accounts for changes in temperature, irradiance, and total nitrogen.

$$C:Chla = win + amp\left(\frac{cos\left(\frac{month-0.5-peaktime}{12}\times 2\pi-\pi\right)+1}{2}\right) \quad (1)$$

The winter minimum (*win*) value for C:Chl*a* ratios is typically set at 15 for temperate waters. For the *peak time*, representing the temporal position of the summer phytoplankton peak relative to 1st July, we used $0.20 \pm 0.11$, derived from estuarine and open waters observations in Danish waters (Jakobsen and Markager 2016). The amplitude (amp) between summer and winter C:Chl*a* was estimated using a non-linear fit between amp and annual mean of total nitrogen [n] ($R^2 = 0.53$).

$$amp = Z + \frac{C}{[n]} \quad (2)$$

where parameters Z and C are $15.07 \pm 5.6$ and $793.1 \pm 159$, respectively.

It is important to note that this approach estimates the POC concentration of living phytoplankton only, phytoplankton detritus is not included in the $POC_{phyto}$ fraction.

### *POC adsorbed onto mineral surfaces ($POC_{mineral}$)*

The $POC_{mineral}$ concentrations in the current study are based on estimates from Fettweis et al. 2025. These estimates were derived from the bulk mineral composition at the three Belgian coastal stations, along with literature data on mineral-specific surface area and organic carbon content per surface area. Non-clay minerals (quartz and feldspar), biogenic minerals (carbonates and opal) and clay minerals (smectite, illite, kaolinite, and chlorite) make up the bulk

mineralogical composition of the SPM in the Belgian waters. The available data covers spring (April) and winter (December) months (Table 2). As the variability in mineral composition between seasons is small, we used an average of both months to calculate the monthly $POC_{mineral}$ concentrations in Belgian coastal waters.

*Heterotrophic carbon biomass*

The estimation of heterotrophic carbon biomass ($POC_{het}$) is based on the relationship between heterotrophic:autotrophic biomass ratios and autotrophic biomass in coastal waters (Gasol et al. 1997; Duarte et al. 2000). Gasol et al. (1997) included heterotrophic bacteria, microzooplankton, and mesozooplankton in the heterotrophic biomass, while autotrophic biomass comprised of phytoplankton. $POC_{phyto}$ concentrations calculated using the C:Chl*a* ratios (Sect. "Phytoplankton carbon biomass"), were taken as the autotrophic biomass concentrations.

$$log\left(\frac{POC_{het}}{POC_{phyto}}\right) = -0.55 log POC_{phyto} + 1.06 \quad (3)$$

Although the dataset that Gasol et al. (1997) used to derive the relationship included data from the southern North Sea and mesocosm studies (incorporating benthic heterotrophs), the majority of it was derived from deeper coastal waters (100–200 m). Consequently, the contribution of benthic heterotrophs may be underestimated, particularly in the study area, which is shallow and well-mixed.

*Detrital carbon biomass*

Detrital carbon biomass ($POC_{det}$) is calculated by subtracting $POC_{phyto}$, $POC_{mineral}$, and $POC_{het}$ from the measured POC in water samples. $POC_{det}$ may include contributions from detritus of pelagic and benthic primary producers (eg., microalgae and macroalgae), heterotrophic organisms (eg., zooplankton and bacteria), and terrestrial POC.

**Table 2** Mean and standard deviation of $POC_{mineral}$ content of SPM for spring (April) and winter (December) months obtained from the mineral specific surface area (Fettweis et al. 2025)

| Stations | April 2023 $POC_{mineral}$ content (%) | December 2023 $POC_{mineral}$ content (%) |
|---|---|---|
| MOW1 | 0.71 ± 0.27 | 0.86 ± 0.33 |
| W05 | 0.46 ± 0.18 | 0.43 ± 0.17 |
| W08 | 0.48 ± 0.18 | 0.39 ± 0.16 |

Redundancy analysis

We conducted redundancy analyses (RDA) with two primary objectives: (1) to identify the environmental variables (salinity, temperature, DIN, DIP, and DSi) driving variation in biological variables (POC, Chl*a*, POC:PON, Chl*a*:SPM, POC:SPM, and POC:Chl*a*) and (2) to assess the influence of measured variables (salinity, temperature, DIN, DIP, DSi, POC, and Chl*a*) on the relative contributions of different POC components along the cross-shore gradient. The RDA was performed using the "vegan" package in R. The data was scaled before the analysis to ensure an even contribution from the variables, preventing variables with larger values or ranges from dominating. RDA can be viewed as a constrained form of principal component analysis (PCA), where the canonical axes, formed as linear combinations of the response variables are restricted to also be linear combinations of the explanatory variables (as determined through multiple linear regression) (Legendre and Legendre 1998).

Organic matter partitioning into dissolved and particulate pool

The partitioning of organic matter in turbid waters is strongly influenced by SPM concentrations. Similar to Freundlich isotherms to model exchange reactions in soil, Herman and Heip (1999) introduced the following equations to describe the balance between the adsorption and desorption of organic matter on mineral particles.

$$\frac{dPOC}{dt} = k_1.SPM.DOC - k_2.POC = 0 \quad (4)$$

where $k_1$ and $k_2$ represent the first-order rate constant for adsorption and desorption, respectively. Equation 4 can be rewritten as:

$$\frac{POC}{TOC} = \frac{SPM}{SPM + K} \quad (5)$$

where $K = k_2/k_1$.

## Results

### Seasonal and spatial variations

#### *Physico-chemical parameters*

The concentrations of the dissolved inorganic nutrients (DIN, DIP, and DSi) displayed a consistent distribution pattern, declining from nearshore (MOW1) to offshore (W08), indicative of dominant riverine nutrient sources. A common trend observed across all three stations was elevated concentrations during winter months (Fig. 2a, b, c), followed by a gradual decrease in spring, reaching the lowest levels in summer, and subsequent regeneration and increased riverine loads of nutrients during autumn months. At W08, DIN concentrations reached their lowest levels in April and remained low throughout summer. However the lowest concentrations were observed much later in July at MOW1 and W05. Notably, DIN:DIP ratios at all three stations exceeded the canonical Redfield ratio of 16 for most of the year, except during July, August, and September when values dipped below or approached 16 (Fig. 2d). Similarly, the lowest DIN:DSi ratios were predominantly observed towards late summer, often close to or less than 1 (Fig. 2e).

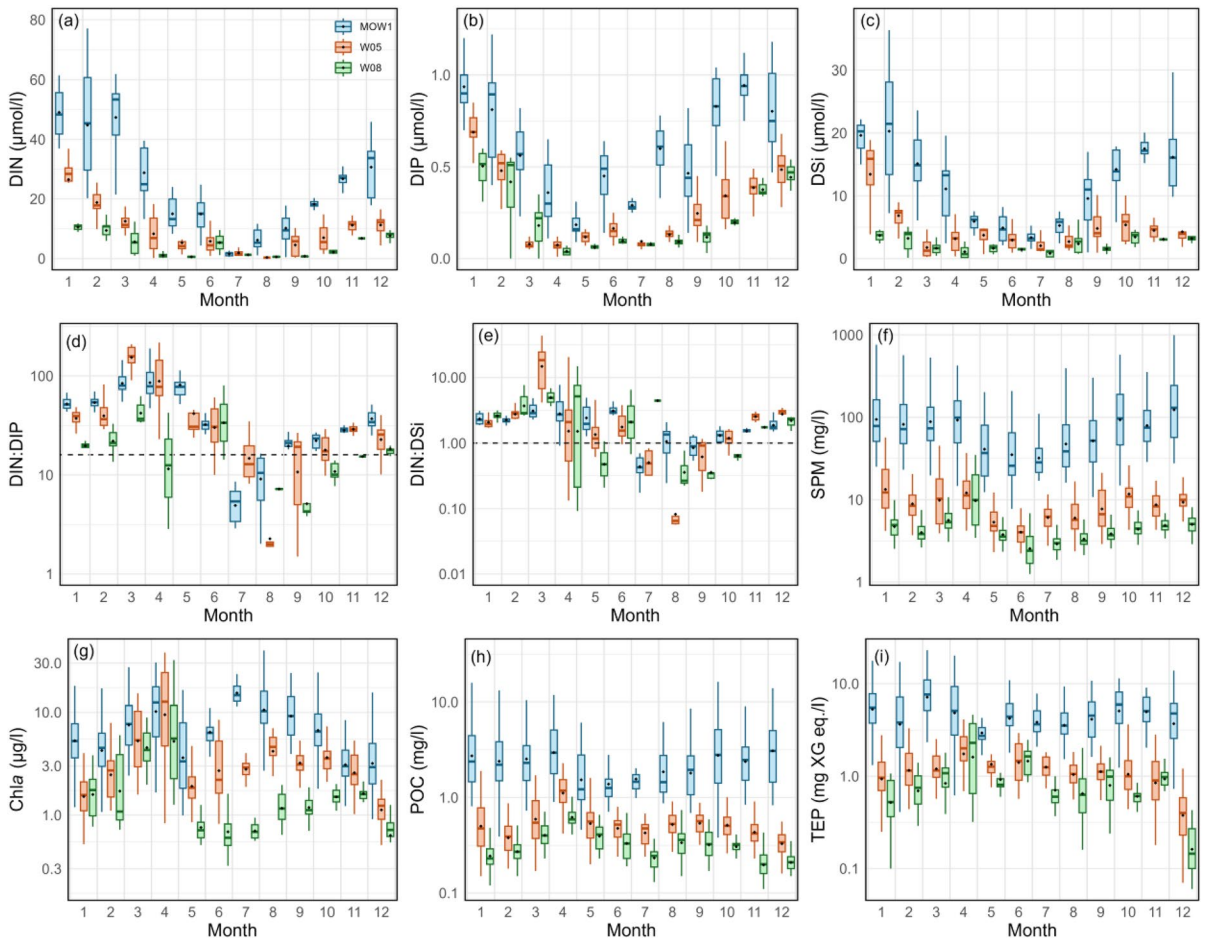


**Fig. 2** Annual variations (mean 2019–2023) in **a** DIN (µmol/l), **b** DIP (µmol/l), **c** DSi (µmol/l), **d** DIN:DIP, **e** DIN:DSi, **f** SPM (mg/l), **g** Chl*a* (µg/l), **h** POC (mg/l), and **i** TEP (mg XG eq./l) at MOW1, W05, and W08. Boxplots show minimum, first quartile, median, third quartile, and maximum, filled black circles display mean values. Values outside the interquartile range have not been displayed. Note the log scale used for panels **d–i**. Dashed line indicates the Redfield-Brzezinski nutrient ratio (DIN:DIP = 16 and DIN:DSi = 1)

*Suspended particulate matter and its constituents*

SPM concentrations exhibit a gradient, progressively decreasing from MOW1 situated within the coastal turbidity maximum, towards W05 and further at W08, reflecting a gradient in bathymetry and SPM transport (Fig. 2f). At MOW1, SPM concentrations can reach several hundreds of mg/l, with values below 10 mg/l being rare. In contrast, concentrations exceeding 10 mg/l are uncommon at W08. Despite the substantial variability observed across the three stations, SPM concentrations exhibit a typical seasonal trend, characterized by a decline in SPM concentrations towards the end of spring, reaching a minimum during summer (June-July), followed by a subsequent increase to reach winter-spring high values by October.

Chl*a* concentrations were generally highest closest to the coast at MOW1. During the peak of the spring bloom in April, however, Chl*a* concentrations at W05 ($14.7 \pm 11.0$ µg/l) and W08 ($7.9 \pm 7.6$ µg/l) were comparable to those at MOW1 ($12.7 \pm 7.4$ µg/l). Despite the difference in Chl*a* concentrations, the seasonal trends were somewhat similar across the three stations, with low concentrations in winter, a sharp increase during the spring bloom, a decrease in May, and a second bloom later in summer (Fig. 2g). The main difference was in the timing and intensity of the second peak, at MOW1, it peaked in July ($15.7 \pm 3.4$ µg/l) and high values persisted until October. At W05 and W08, the later summer-autumn peaks were lower in magnitude (W05: $4.5 \pm 1.6$ µg/l; W08: $1.6 \pm 0.2$ µg/l) and occurred later.

Similar to the SPM and Chl*a* concentrations, POC and PON (not shown) concentrations displayed a cross-shore gradient (Fig. 2h). The distribution patterns of POC and PON were quite similar, hence only POC is elaborated here. POC concentrations greater than 1 mg/l were commonly observed at MOW1, whereas such concentrations were rare at the other sampled stations. The monthly variation in POC concentrations at MOW1 mirrored the SPM pattern, with a distinct reduction towards the end of spring and beginning of summer (June: $1.7 \pm 0.9$ mg/l), followed by a gradual increase, reaching high values (3–4 mg/l) in October, consistent with measurements during other months. Unlike the two distinct peaks in the annual Chl*a* distribution, such discernible increases were not observed in POC concentrations at MOW1. At W05 and W08, the monthly POC pattern differed slightly from the SPM pattern. Similar to the Chl*a* buildup during the spring months and subsequent decline in summer, a gradual buildup and decline in POC concentrations was observed at W05 (Apr: $1.2 \pm 0.4$ mg/l) and W08 (Apr: $0.6 \pm 0.2$ mg/l). The second peak in POC towards the end of the summer, was noted at W05 (September: $0.6 \pm 0.1$ mg/l) and W08 (August: $0.4 \pm 0.1$ mg/l), and the concentrations were higher compared to the winter values.

TEP concentrations displayed a decreasing trend with distance from the coast (Fig. 2i). The highest monthly averages were observed at MOW1 (3.6–8.6 mg XG eq./l), followed by W05 (0.5–2.0 mg XG eq./l), and the lowest at W08 (0.1–2.2 mg XG eq./l). At MOW1, TEP concentrations generally followed the trends in SPM and POC concentrations, with a notable decline in May and during the summer months, while remaining comparable during other months. Conversely, at W05 and W08, the lowest TEP concentrations were recorded during the winter months. These values gradually increased to peak in April, then declined slightly, maintaining moderately high levels until the end of autumn.

*Suspended particulate matter composition*

The Chl*a* content of SPM (Chl*a*:SPM) did not increase consistently with distance from the coast (Fig. 3a). At MOW1, the values ranged from 0.03 to 0.51 ‰, the lowest amongst the stations. In contrast, W05 and W08 showed similar ranges (0.14–1.31 ‰ and 0.14–1.23 ‰, respectively), but values greater than 0.4 ‰ were more frequent at W05. At MOW1, Chl*a*:SPM ratios exhibited a distinct seasonal pattern, differing from the seasonal progression of Chl*a* concentrations. During the spring bloom, values increased slightly to $0.16 \pm 0.13$ ‰ (April) from the winter low of $0.06 \pm 0.03$ ‰ (December). A more significant rise occurred in summer, reaching $0.51 \pm 0.17$ ‰ (July), followed by a gradual decline to the low winter levels. Values at W05 and W08 increased from the winter low to peak in April, unlike the summer peak observed at MOW1.

The POC content of SPM (POC:SPM), generally increased with distance from the coast (Fig. 3b). The lowest values were observed at MOW1 (2.6–5.2%), followed by W05 (3.6–12.4%), and peaking at W08 (4.2–15.6%). The monthly variation in POC:SPM

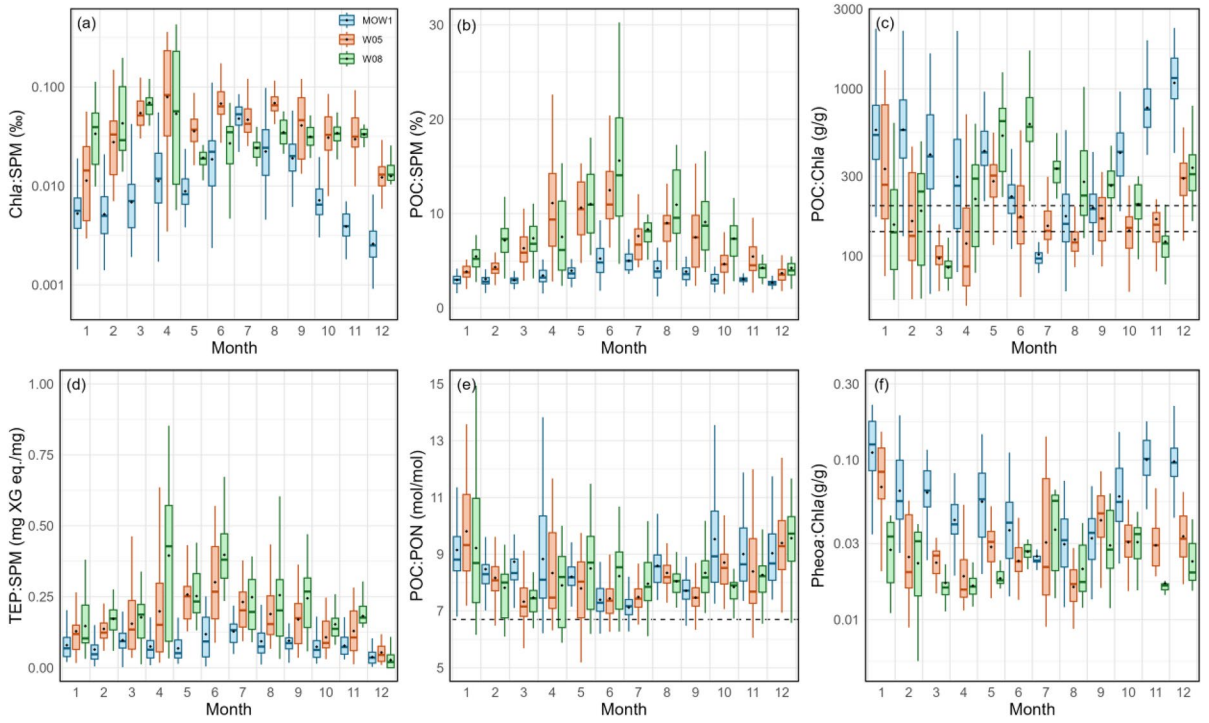


**Fig. 3** Annual variations (mean 2019–2023) in **a** Chl*a*:SPM (‰), **b** POC:SPM (%), **c** POC:Chl*a* (g/g), **d** TEP:SPM (mg XG eq./mg), **e** POC:PON (mol/mol), and **f** Pheo*a*:Chl*a* (g/g) at MOW1, W05, and W08. Boxplots show minimum, first quartile, median, third quartile, and maximum, filled black circles display mean values. Values outside the interquartile range have not been displayed. Data has been collected between 2019 and 2023. Dashed lines in panel c indicate 200 and 140 g/g, the upper bounds of POC:Chl*a* ratios range assigned to living phytoplankton POC (40–140 g/g) and phytoplankton-dominated POC but potentially including contributions from secondary producers, detritus, etc. (140–200 g/g), and the dashed line in panel e indicates the canonical Redfield ratio (POC:PON = 6.7). Note the log scale used for panels a, c, and f

ratios was broadly similar across the three stations, increasing from winter minima to peak in June. At W05 and W08, this was followed by a notable decline in July, a small increase in August and, a subsequent gradual decrease toward winter levels. The spring and summer increase in POC:SPM ratios was more prominent at W05 and W08.

Notably, the peaks in POC:SPM ratios did not coincide with the peaks in POC concentrations at any of the stations. The POC:Chl*a* ratios (g/g) did not display a cross-shore gradient and exhibited different seasonal patterns across the stations (Fig. 3c). At MOW1, values above 200, indicative of detritus dominated or non-phytoplankton material were prevalent from January to June with maximum values in December (1281.1 ± 646.9), except in April when a portion of data fell between 140 and 200, suggesting phytoplankton dominated but detritus influenced POC (Savoye et al. 2003). The ratio dropped below 140, typical of living phytoplankton, in July (105 ± 30), while values between 140 and 200 were observed in August and September, before returning to ratios greater than 200 from October onward. At W05, values above 200 were common in winter (e.g., Jan: 457 ± 355), while values below 140 were common in early spring (e.g., March: 100 ± 26). The ratio increased slightly by May, and throughout summer and autumn, it typically ranged between 140 and 200. In contrast, W08 exhibited the highest values at the end of spring (May: 595 ± 300) and start of summer (June: 682 ± 326), with the lowest values in early spring (March: 85 ± 22 and April: 90 ± 78).

The TEP content of SPM (TEP:SPM) was lowest at MOW1, ranging from 0.04 to 0.13 mg XG eq./mg, compared to W05 (0.05 to 0.30 mg XG eq./mg) and W08 (0.03 to 0.40 mg XG eq./mg) (Fig. 3d). At MOW1, the highest TEP content was measured in summer, with other periods showing comparable

values between 0.06–0.07 mg XG eq./mg. In contrast, W05 and W08 exhibited greater variability, with TEP:SPM increasing from winter lows to high values in spring and summer, then gradually declining back to the winter levels.

A clear spatial trend was not evident in POC:PON ratios (mol/mol) across the three stations, with most values ranging between 6 and 12 (Fig. 3e). However, a seasonal trend, with the highest POC:PON ratios in winter and lower values during spring and summer, was observed at the three stations. At MOW1, the POC:PON ratios showed a gradual decline from January ($9.1 \pm 1.3$) to the lowest values in summer (July: $7.1 \pm 0.6$). In contrast, at W05 and W08, the high values in January ($9.8 \pm 1.7$ and $9.4 \pm 2.5$, respectively) declined rapidly, reaching their lowest in March ($7.3 \pm 0.8$ and $7.5 \pm 0.8$, respectively).

The Pheo*a*:Chl*a* ratios at MOW1 were highest during the winter months, gradually declining through spring and reaching their lowest levels in summer (Fig. 3f). In contrast, at W05 and W08, the high winter values dropped sharply, reaching their minimum during spring. Subsequently, ratios comparable to winter levels reappeared after early summer.

*Particulate organic carbon composition*

$POC_{phyto}$, calculated using an empirical model for C:Chl*a* ratios in Danish coastal waters (see Sect. "Phytoplankton carbon biomass" and Fig. 4a), shows seasonal variation somewhat similar to Chl*a* concentrations across all three stations. At MOW1, $POC_{phyto}$ ranged from 0.08 to 0.67 mg/l, with a first peak in April and a second, higher peak in July (Fig. 4b). In contrast, W05 and W08 displayed lower ranges (0.02–0.43 mg/l at W05 and 0.01–0.31 mg/l at W08), with a comparable first peak in April but a delayed, smaller second peak in August. The estimated $POC_{phyto}$:POC (%) values at MOW1 were generally lower than at the other stations, ranging from 1.2% to 40.1%, with values exceeding 15% only during summer and early

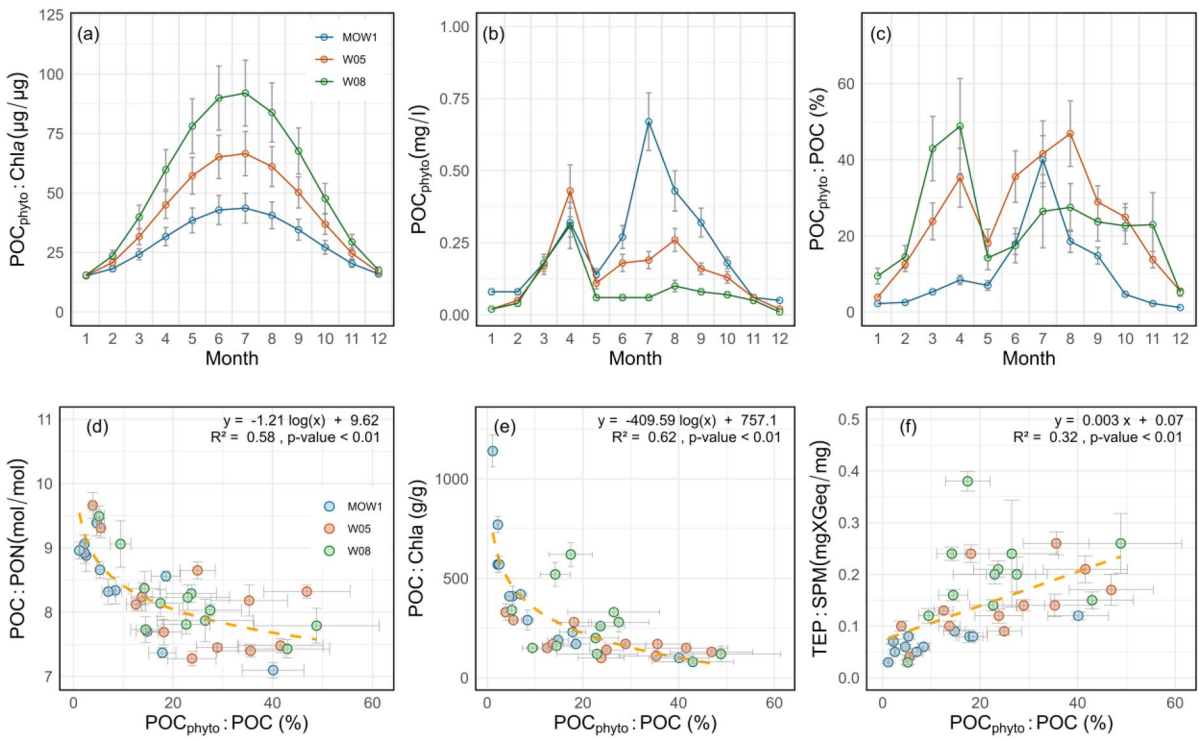


**Fig. 4** Annual cycle ( monthly mean values 2019–2023) of **a** $POC_{phyto}$:Chl*a* (µg/µg), **b** $POC_{phyto}$ (mg/l), and **c** $POC_{phyto}$:POC (%) at the three stations. Error bars represent the standard error from the monthly mean. Regressions of monthly means of **d** POC:PON (mol/mol), **e**) POC:Chl*a* (g/g), and **f**) TEP:SPM (mg XG eq./mg) as a function of $POC_{phyto}$:POC (%) at the three stations. Error bars represent the standard error from the monthly mean

autumn (Fig. 4c). At W05, low winter values (January: ≈ 3.85%) steadily increased, with high value in April (≈35.29%) and remained high through summer (35.39–46.88%), before gradually declining into winter. Similarly, at W08, winter lows steadily rose to a peak in April (≈ 48.83%), but the values then decreased, with only a slight summer increase (17.46–27.45%) (Fig. 4c). The monthly average POC:PON and POC:Chl*a* ratios at all three stations showed significant negative logarithmic regression with the $POC_{phyto}$:POC (%) ($p < 0.01$), suggesting that the higher fractions of $POC_{phyto}$ are associated with lower POC:PON and POC:Chl*a* ratios (Fig. 4d, e). Conversely, TEP:SPM ratio demonstrated a positive linear regression with $POC_{phyto}$:POC ($p < 0.01$) (Fig. 4f).

At MOW1, $POC_{det}$ and $POC_{mineral}$ contribute substantially to the water column POC pool for most of the year, with $POC_{phyto}$ making a notable contribution (17–40%) only during the summer months (Fig. 5). In contrast, at the other two stations, $POC_{mineral}$ remains consistently low (3–12%) year-round, reaching its lowest relative contribution in summer. At W05, $POC_{phyto}$ shows comparable relative abundance (18–47%) in spring and summer, while, $POC_{det}$ dominates in late autumn and winter (46–78%). At W08, $POC_{phyto}$ peaks (42–48%) in March and April, followed by lower values (17–27%) in summer, whereas $POC_{det}$ remains the dominant fraction (35–69%) throughout the year, except during the spring peak.

*Dissolved organic carbon distribution*

Similar to its particulate counterpart, DOC concentrations were highest at MOW1 with monthly averages ranging between 1.13 and 1.89 mg/l, decreasing progressively at W05 (0.72–1.64 mg/l) and W08 (0.72–1.02 mg/l) (Fig. 6a). The seasonal variation of the DOC concentrations seemed to be similar at all three stations: lowest values were observed in winters, followed by an increase in values from April onwards with the highest values generally observed in summer. At W05, however, the peak concentration was observed earlier in May, after which the concentrations gradually declined to lower winter values (Fig. 6a). At W05 and W08, DOC formed the larger part of the total organic carbon (POC + DOC = TOC) pool, with POC:DOC ratios consistently less than 1 (Fig. 6b). It is only during the peak of the spring bloom in April that there is a slight increase in the POC:DOC ratios. In contrast, at MOW1, POC was the larger carbon fraction in the TOC pool, with POC:DOC ratios greater than 1, except at the end of the spring phytoplankton bloom and towards the summer when POC:DOC ratios lower than 1 were observed. The monthly averages of the DOC:TOC ratios were negatively related ($p < 0.01$) to the monthly

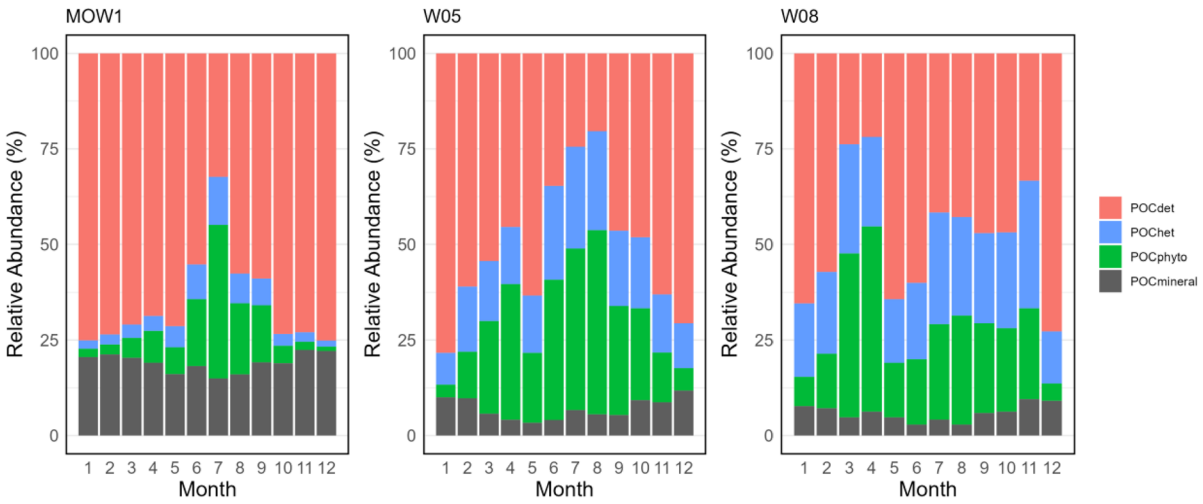


**Fig. 5** Relative abundance of POC components over a year (2019–2023) at MOW1, W05, and W08. $POC_{det}$ stands for detritic organic matter (calculated after subtracting other components from measured POC). $POC_{het}$ stands for heterotrophic biomass, $POC_{phyto}$ stands for phytoplankton biomass, and $POC_{mineral}$ stands for mineral-associated organic matter (based on clay specific surface area available for organic matter adsorption)

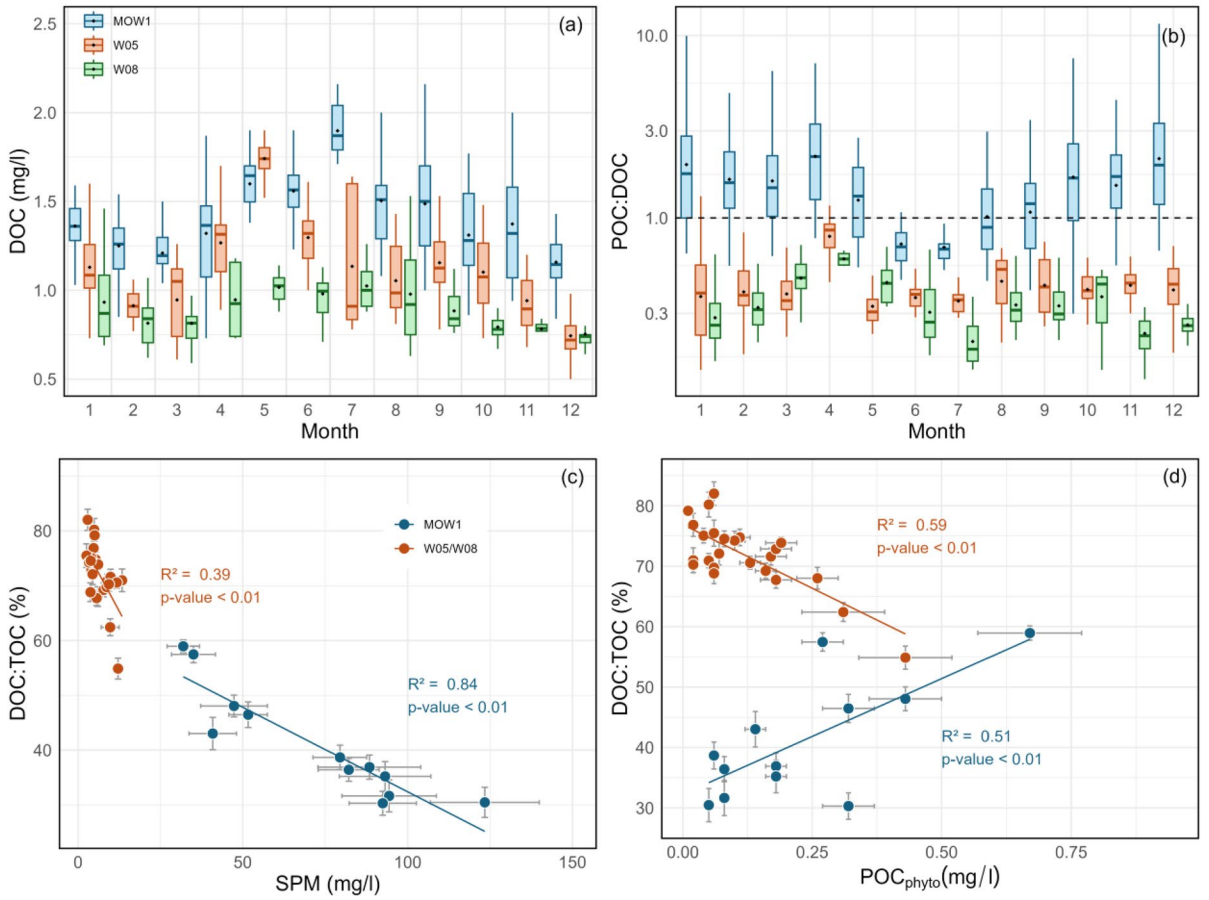


**Fig. 6** Annual cycles (monthly mean values 2019–2023) of **a** DOC (mg/l), and **b** POC:DOC ratios at the three stations. Boxplots show minimum, first quartile, median, third quartile, and maximum, filled black circles display mean values. Dashed line in panel b indicates the 50% mark where DOC concentrations are equal to POC concentrations. Linear regression of monthly means of **c** DOC:TOC (%) and SPM (mg/l), and **d** DOC:TOC (%) and $POC_{phyto}$ (mg/l). Error bars represent the standard error from the monthly mean

SPM averages, with the regression indicating a stronger association at MOW1 than at W05 and W08 (Fig. 6c). At the offshore stations (W05 and W08), significant negative regression was observed between DOC:TOC and $POC_{phyto}$ concentrations, while positive regression was observed at inshore MOW1 station (Fig. 6d).

## Tidal and spatial variations

### *Relationships between suspended particulate matter components*

Hourly or 1.5 h tidal data of SPM concentrations shows peaks close to the highest current velocities and minimum concentrations near the lowest velocities, with the greatest range between maximum and minimum values observed at MOW1. At MOW1, minimum SPM concentrations can be as low as 3–20% of the maximum, increasing offshore to 15–50% at W05 and 30–60% at W08. At MOW1, Chl*a* concentrations generally followed SPM concentrations over the tidal cycles throughout the year. Though the y-intercepts for linear regression were lower in winter than in spring, reflecting higher background Chl*a* concentrations in spring, while the relationship weakened in summer (Fig. 7a, b, c). Similarly, POC and SPM concentrations showed a significant positive regression at MOW1 during most of the year. However, this relationship seemed to weaken in summer, when SPM concentrations are at

the lowest relative to other times of the year (Fig. 8a, b, c). At W05, regression analysis indicated that Chl*a* and SPM concentrations are closely related during some tidal cycles in winter, whereas this relationship is less pronounced at lower SPM concentrations (Fig. 7d). This relationship weakened in spring and summer (Fig. 7e, f). Similarly, POC concentrations were strongly related to SPM concentrations in winter (Fig. 8d) but the relationship deteriorated in spring and was the weakest in summer (Fig. 8e, f). At W08, the regression between Chl*a*, POC, and SPM concentrations indicated moderate to weak correspondence during most tidal cycles (Figs. 7g, h, i and 8g, h, i). POC and PON concentrations were closely related during most tidal cycles throughout the year at all three stations (not shown).

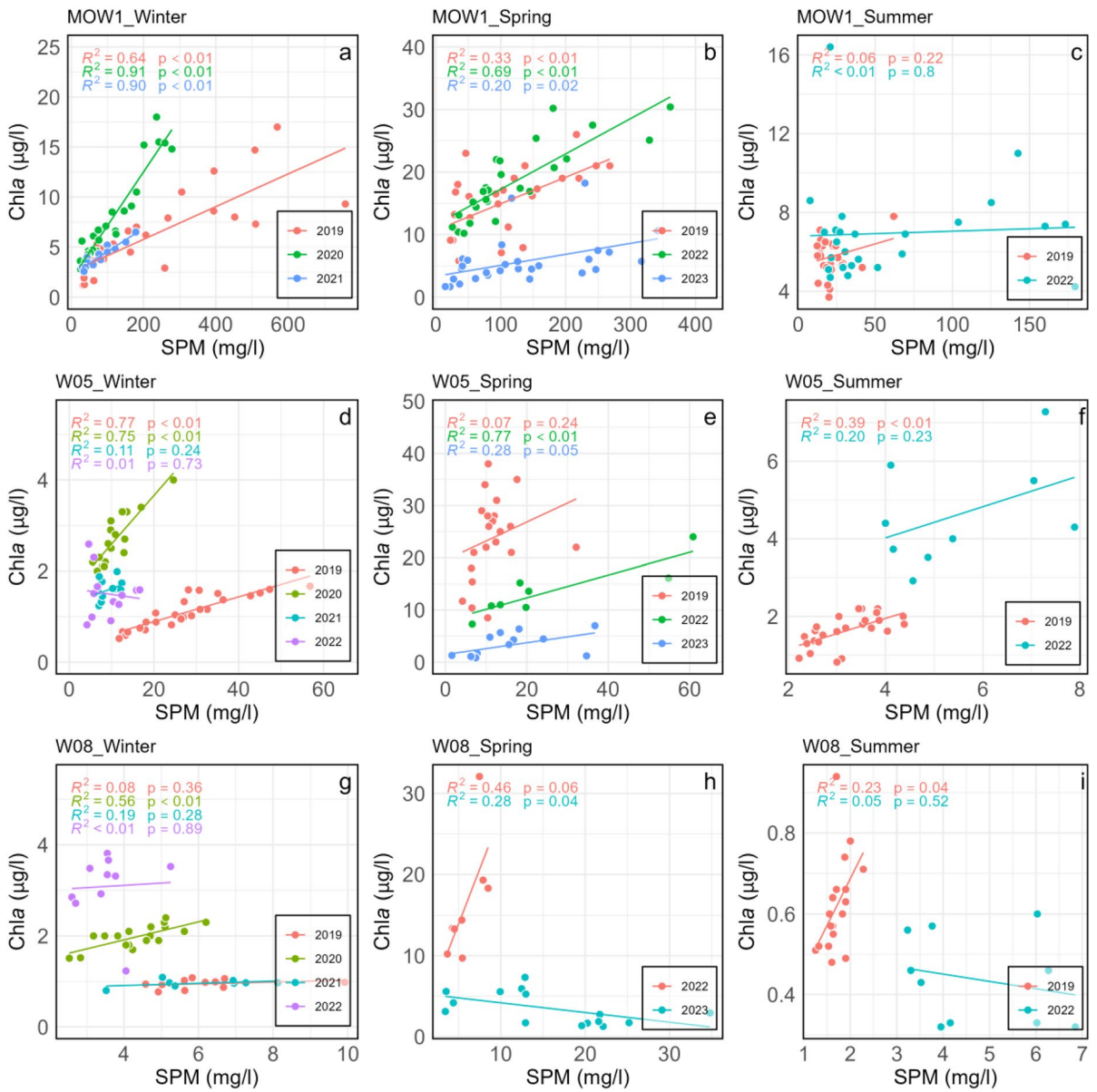


**Fig. 7** Linear regression relationships between Chl*a* and SPM concentrations at MOW1 (**a–c**), W05 (**d–f**), and W08 (**g–i**) during winter, spring and summer. The data for winter, spring, and summer represents tidal cycles sampled during January, April, and June, respectively, over the period from 2019 to 2023 (see legend)

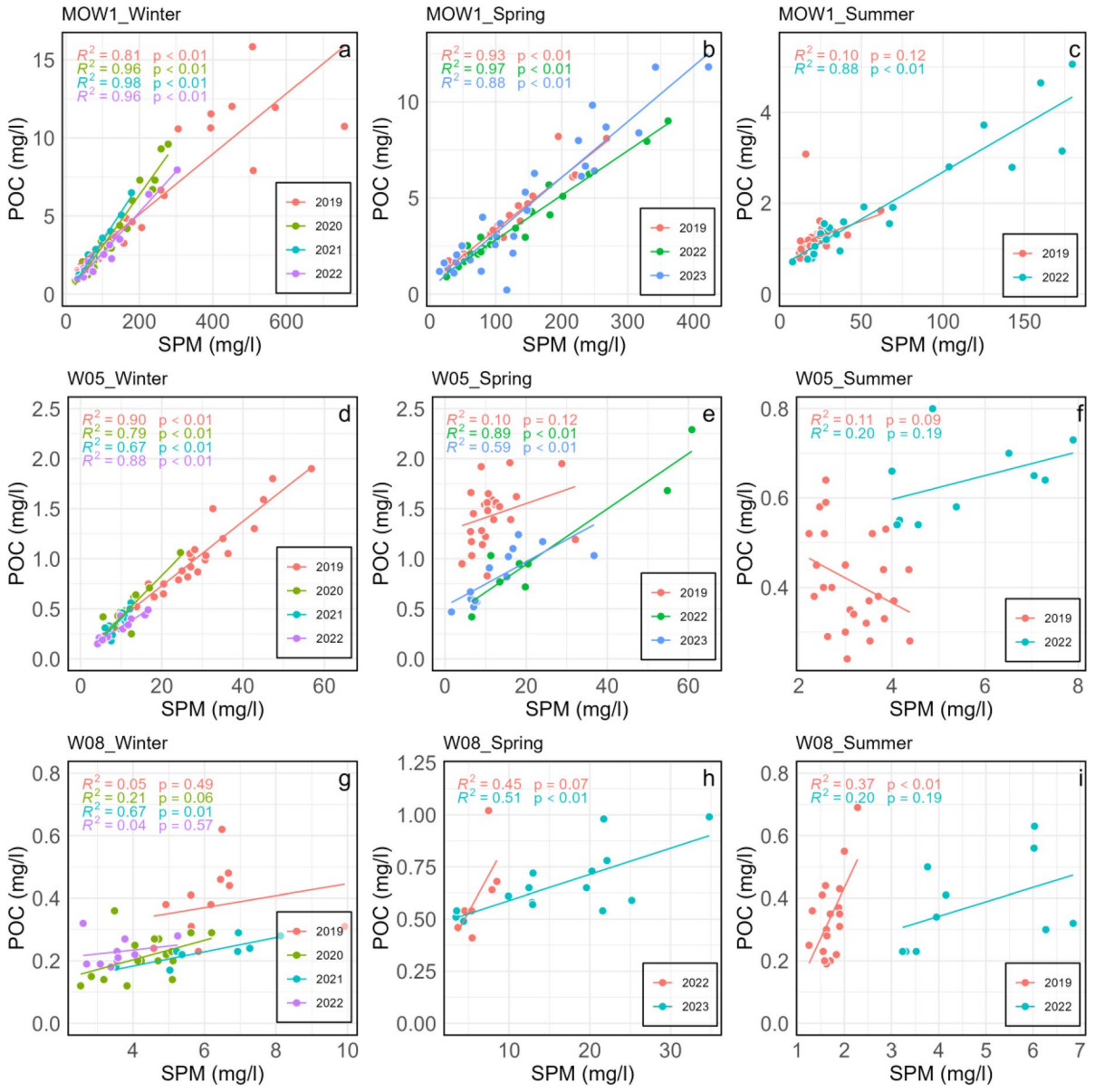


**Fig. 8** Linear regression relationships between POC (mg/l) and SPM (mg/l) concentrations at MOW1 (**a–c**), W05 (**d–f**), and W08 (**g–i**) during winter, spring and summer. The data for winter, spring, and summer represents tidal cycles sampled during January, April, and June, respectively, over the period from 2019 to 2023

## Redundancy analysis

The RDA analysis showed that the first RDA axis was characterized by high biplot scores for SPM (0.95), salinity (-0.52), and dissolved inorganic nutrients (DIN: 0.56, DIP: 0.63, DSi: 0.68). The inclusion of salinity suggested that this axis represents the coastal-offshore gradient (Fig. 9a). The second RDA axis showed high biplot scores for temperature (-0.68) and dissolved inorganic nutrients (DIN: 0.36, DIP: 0.56, DSi: 0.38), likely reflecting seasonal changes. High loading scores for all response variables across both axes indicated the influence of both seasonal and cross-shore gradients. However, Chl*a* concentrations and POC:PON ratios appeared to be more strongly influenced by seasonal patterns, while other response

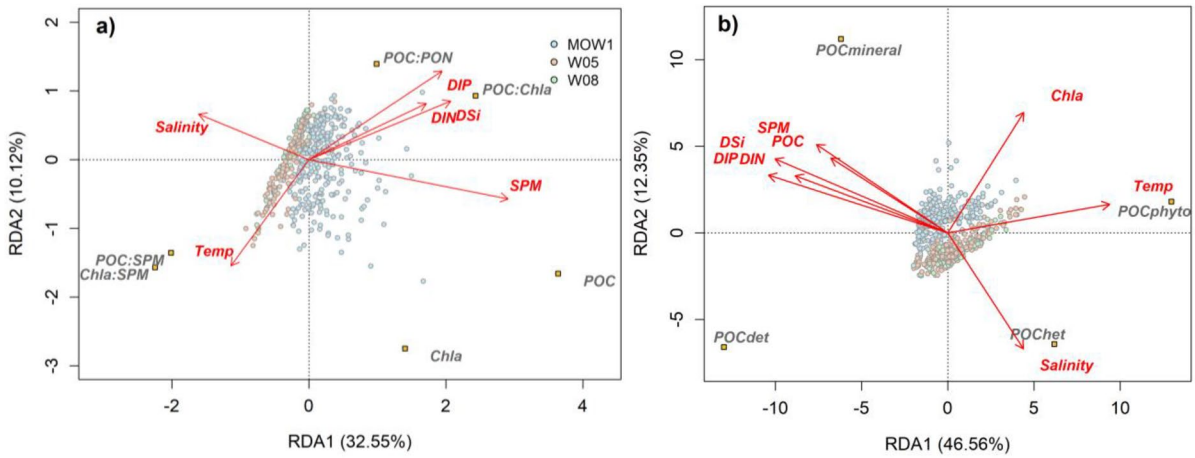


**Fig. 9** Redundancy analyses performed by considering **a** salinity, temperature, DIN, DIP, and DSi as environmental variables and POC, Chl*a*, POC:PON, Chl*a*:SPM, POC:SPM, and POC:Chl*a* as response variables and **b** salinity, temperature, DIN, DIP, DSi, POC, and Chl*a* as explanatory variables and the relative contributions (%) of different POC components ($POC_{phyto}$, $POC_{het}$, $POC_{det}$, and $POC_{mineral}$) as response variables

variables were affected more by the cross-shore gradient.

The RDA analysis of the influence of environmental variables on the relative contribution of different POC components revealed distinct patterns (Fig. 9b). The first RDA axis, with high biplot scores for temperature and dissolved inorganic nutrients, seemed to represent a seasonal gradient. The second RDA axis, characterized by high biplot scores for salinity, SPM, POC, and Chl*a*, likely reflected a cross-shore gradient. The relative contributions of $POC_{det}$ and $POC_{het}$ were influenced by both seasonal and cross-shore gradients, while $POC_{phyto}$ was predominantly shaped by the seasonal gradient, and $POC_{mineral}$ was largely influenced by the cross-shore gradient.

## Discussion

### Estimating particulate organic carbon components in Belgian coastal waters: applicability of $POC_{phyto}$ and $POC_{het}$ biomass models

C:Chl*a* ratios often form the basis of estimating $POC_{phyto}$ from Chl*a* observations, but are tedious to obtain, requiring microscopy and biovolumes estimates. Consequently data capturing the seasonal variability in C:Chl*a* ratios in temperate coastal waters are limited (Calvo-Díaz et al. 2008; Vázquez-Domínguez et al. 2013; Jakobsen and Markager 2016). The available laboratory and field observations across environments from coastal to open-ocean waters show a wide range of C:Chl*a* ratios (6–333) (Cloern et al. 1995; Sathyendranath et al. 2009). These ratios generally decrease under light limitation due to increased Chl*a* production, while higher light availability and nitrogen limitation promotes greater carbon accumulation and limit Chl*a* production. While the effect of temperature is complex and appears to be controlled by nitrogen availability (Geider 1987). The empirical model developed by Jakobsen and Markager (2016) for C:Chl*a* ratios is based on observational data from the Kattegat-Belt Sea, the Wadden Sea, and various Danish estuaries. Although a number of factors would influence the light climate in the water column, the model is relevant to Belgian coastal waters, as the dataset encompasses a range of water column turbidity and seasonal surface irradiance patterns comparable to ours. Furthermore, although the phytoplankton community structure is likely to be different, the seasonal pattern of phytoplankton bloom is similar. Chl*a* concentrations at MOW1 indicate two major blooms (spring and summer), similar to the Wadden Sea and Danish estuaries. In contrast, Kattegat-Belt Sea exhibits seasonal dynamics comparable to W05 and W08, with a pronounced spring bloom but a less distinct late summer or autumn bloom. This spatial gradient in bloom pattern is most likely regulated by

nutrient availability. At MOW1, the annual DIN concentration range (1.5–50 µmol $l^{-1}$) is comparable to the range observed in the Wadden Sea and Danish estuarine waters (3–50 µmol $l^{-1}$). The spring phytoplankton bloom in both regions appears to be phosphate-limited rather than nitrogen-limited. Although the Belgian waters (5–22 °C) have a higher annual temperature range than Danish waters (1–18 °C), the even warmer southern Bay of Biscay (Spain) exhibits a sinusoidal C:Chl*a* pattern (12–120 g $g^{-1}$; coastal station 20 m depth; Vázquez-Domínguez et al. 2013) similar to the Danish waters. Moreover, the empirical model closely reproduces these seasonal dynamics in the Bay of Biscay, supporting its applicability in temperate waters where nutrient and light availability are the primary drivers of C:Chl*a* variability (Jakobsen and Markager 2016). The winter minimum C:Chl*a* (15) used here is based on the estimates suggested for temperate waters, consistent with observations from the Bay of Biscay (~12) and laboratory studies under low light, high nutrient conditions typical of temperate coastal waters in winters (Geider 1987; Calvo-Díaz et al. 2008; Jakobsen and Markager 2016).

Based on a meta-analysis of data from open-ocean (e.g., Mediterranean, North Atlantic, tropical Pacific) and coastal regions (e.g., North Sea, Skagerrak, Peru upwelling) $POC_{het}$ to $POC_{phyto}$ ratios vary systematically with $POC_{phyto}$, as nutrient availability governs $POC_{phyto}$ and subsequently regulates $POC_{het}$ (Gasol et al. 1997). Consequently, eutrophic systems typically exhibit biomass pyramids dominated by primary producers that substantially exceed heterotrophs (Duarte et al. 2000; Yuan and Pollard 2018). In contrast, oligotrophic waters frequently exhibit inverted biomass pyramids, where $POC_{het}$ is comparable to or exceeds $POC_{phyto}$, reflecting a tight coupling between primary and secondary producers (Gasol et al. 1997; Leblanc et al. 2012). Despite its broad scope, this between relationship $POC_{phyto}$ and $POC_{phyto}$ holds at more localized scales too. In the Baltic Sea, observed heterotrophic biomass was of the same order of magnitude as that predicted by Gasol et al. (1997) (Scheffold and Hense 2020). Similarly, mesocosm experiments using Mediterranean coastal plankton community showed that heterotrophic biomass scaled with autotrophic biomass to the 1/5th power, consistent with the empirical relationship (Duarte et al. 2000). Thus, while the relationship proposed by Gasol et al. (1997) may not reflect all local processes, it offers a useful first-order approximation of $POC_{het}$ based on broadly accepted ecological principles, particularly in the absence of detailed seasonal data.

## Origin of coastal organic matter

POC:PON ratios, along with other proxies, are commonly used to determine the organic matter sources in coastal systems. Ratios > 12 indicate terrestrial origins, while ratios between 6 and 10 suggest marine phytoplankton (Savoye et al. 2003). POC:PON ratios in this study rarely exceed 12.5 even at MOW1, and $\delta^{13}C_{POC}$ values of -22 to -18 ‰ observed at a nearby coastal station 115bis (51° 09.2'N, 02° 37.2'E, located next to MOW1), both indicate limited terrestrial contribution (Vanaverbeke et al. 2008). Although the POC compositional proxies such POC:PON, POC:Chl*a*, POC:SPM, and Chl*a*:SPM display seasonal and spatial variation, they can be explained partly by the contribution of different POC fractions. The increase in $POC_{phyto}$ relative abundance in spring and summer (Fig. 9b), likely drove these seasonal compositional shifts. At all stations, the highest POC:PON and Pheo*a*:Chl*a* ratios occurred in winter, likely due to a larger resuspended detrital fraction. Detritus typically shows higher POC:PON ratios compared to phytoplankton biomass, due to preferential remineralization of nitrogen over carbon (Savoye et al. 2003; Harmelin-Vivien et al. 2008). However, the lowest POC:PON ratios were observed during the spring bloom at the offshore stations but later in summer at MOW1, consistent with the $POC_{phyto}$ dynamics. Negative regression between the $POC_{phyto}$ fraction and POC:PON ratio indicated fresh phytoplankton biomass addition to a relatively more refractory resuspended winter POC pool. At MOW1, the large $POC_{mineral}$ pool may have further influenced the POC:PON ratios. Composed of DOC molecules adsorbed onto clay mineral particles (Herman and Heip 1999; Fettweis et al. 2025), the $POC_{mineral}$ pool may exhibit higher C:N ratios due to the carbon-rich dissolved pool (~6–21; Biddanda and Benner 1997). However, POC:PON ratios at MOW1 were not significantly higher than other stations. This could be due to (i) greater seasonal variations in POC:PON ratios masked spatial differences (Fig. 9a), and/or (ii) relatively low C:N ratios (< 15) of the dissolved pool in Belgian coastal waters, particularly in summer

(Painter et al. 2018), which would make it difficult to distinguish from marine POC pool.

## Spatial variation in particulate organic matter composition

Dominance of phytoplankton-derived POC in marine-influenced coastal systems is widely observed (Cresson et al. 2012; Berto et al. 2013; Lowe et al. 2014; Liénart et al. 2017). In Belgian waters, however, the higher phytoplankton production at the coast, although important, is not the only factor contributing to variations of the POC composition. RDA analysis (Fig. 9a) showed that MOW1, the nearshore station, exhibited notably different POC composition compared to offshore W05 and W08 stations. The first RDA axis, reflecting a spatial gradient, separated MOW1 (characterized by higher SPM concentrations, lower salinity and higher POC:Chl*a* ratios), from W05 and W08 (associated with higher salinity and higher POC:SPM and Chl*a*:SPM ratios). Among POC components, the relative abundance of $POC_{mineral}$ and $POC_{het}$ seemed to be influenced by this spatial gradient, decreasing and increasing with salinity, respectively (Fig. 9b). At MOW1, the station closest to shore, $POC_{mineral}$ can contribute up to a quarter of the POC pool. This contribution, however, decreased significantly at the offshore stations (Fig. 5) and was driven by the higher availability of SPM and clay minerals nearshore (Table 2). At MOW1, $POC_{mineral}$ and $POC_{det}$ constituted the majority of the POC pool, with $POC_{det}$ originating from autotrophs and heterotrophs. Since $POC_{mineral}$ was defined as organic matter adsorbed onto mineral surfaces (primarily clay minerals), a relationship between $POC_{mineral}$ and SPM is expected. However, the observed association between SPM and POC concentrations during the tidal cycles suggested that $POC_{det}$, like $POC_{mineral}$, follows the same settling-resuspension dynamics as SPM at MOW1. $POC_{det}$ dominated the bulk POC pool, particularly at MOW1. At the two offshore stations, $POC_{det}$ also contributed substantially to the POC pool, except during spring and summer when $POC_{phyto}$ and $POC_{het}$ increased. Detrital dominance of the POC pool is common in pelagic waters, though contributions vary spatially and temporally, with greater variability in eutrophic systems (Volkman and Tanoue 2002). In the Baltic Sea, detrital POC ranged from 63 to 94% seasonally (Andersson and Rudehäll 1993), while non-living particles comprised 58–74% of total particulate carbon in North Pacific Subtropical Gyre surface waters (Henderikx-Freitas et al. 2021).

The transition zone between coastal and offshore waters in the southern North Sea, generally located around the 20 m water depth, represents a distinct regime in terms of particle dynamics (Maerz et al. 2016; Desmit et al. 2024). As bathymetry controls the propagation of the turbulent kinetic energy in the water column, the transition zone exhibits a decrease in turbulence that promotes particle settling. Depending on the cross-shore system, particles may be transported back to the coast during the tidal cycle, thus enhancing their coastal-offshore gradient. In turn, this drives a separation between turbid coastal and clear offshore waters (Desmit et al. 2024). In the Belgian waters, the transition zone encompasses station W05. While coastal particles are likely to be retained at the coast by alongshore tidal currents and because their transport to the offshore is limited by the transition zone, dissolved substances, such as inorganic nutrients and DOC, are not subject to such limitations and can be transported to the offshore waters. With mineral particles mostly confined at the coast, the relative contribution of $POC_{phyto}$ and $POC_{het}$ was comparatively higher at W05 and W08. Dissolved inorganic nutrients exhibit concentration gradients due to dilution. As a result, the Chl*a* content of SPM did not exhibit the same offshore increase observed for the POC content of SPM. While SPM concentrations declined substantially between stations MOW1 and W05, Chl*a* concentrations decreased primarily between W05 and W08 as nutrient availability decreased offshore. The relatively high Chl*a* content of SPM at W05 is reflected in the highest relative contribution of $POC_{phyto}$, particularly during the summer months (Fig. 4c). POC:Chl*a* ratios at W05 also provide insight into the dominance of living phytoplankton in the POC pool. For most of the year, POC:Chl*a* ratios at W05 remained below 200 g/g, indicative of a phytoplankton-dominated POC pool (Savoye et al. 2003). This contrasts with the offshore station W08, where POC:Chl*a* ratios exceeded 200 g/g, suggesting a detritus-dominated POC pool most likely a result of inorganic nutrient limitation.

### Seasonal variation in particulate organic matter composition

The spring bloom develops earlier at W05 and W08, with significant nutrient depletion in March, while at MOW1 nutrients are lowest in the period between April-June. The earlier phytoplankton development offshore is likely driven by the earlier relaxation of the winter light limitation in less turbid waters. Muylaert et al. (2006) also noted a similar temporal shift along the coast, with earlier development in the southwest attributed to lower turbidity compared to the more turbid northeast waters closer to the Scheldt estuary. Nutrient ratios further indicated phosphorus limitation as a potential driver of spring bloom termination, consistent with previous studies (van der Zee and Chou 2005; Billen et al. 2011; Desmit et al. 2018). The second Chl*a* peak varied in timing and intensity across the cross-shore transect, driven by nutrient availability. It occurred earlier (July–August) at the nearshore MOW1 station and later (October–November) with lower intensity at the offshore W08 station. At MOW1, riverine inputs sustained moderate DIN levels after spring bloom, while offshore DIN concentrations remained low until summer remineralization. Similarly, DIP concentrations reached their lowest in May but increased earlier at MOW1, remaining low offshore until after summer.

The seasonal variability of POC concentrations differed from those in Chl*a* concentrations, particularly at MOW1. During winter, physical forcings play a dominant role in shaping the distribution of both POC and Chl*a* in the coastal zone (MOW1). Here, the strong associations between POC, Chl*a*, and SPM concentrations during winter suggest that, in the absence of production, resuspended sediments drive the relatively high concentrations of POC and Chl*a* in the water column. With a relatively low $POC_{phyto}$, the winter POC pool is likely to be more refractory. In spring, the dynamics begins to shift with Chl*a* concentrations gradually increasing. Yet, this rise is not accompanied by a substantial increase in POC concentrations ($POC_{phyto}$ fraction in April at MOW1 = 8% of the POC pool). The decoupling between Chl*a* and POC was also evident from their regression with SPM, at MOW1. Chl*a* concentrations showed little association with SPM, whereas POC concentrations exhibited a stronger relationship. At MOW1, the bulk POC pool is largely controlled by resuspended sediments, and the $POC_{phyto}$ fraction remained relatively small despite the substantial spring phytoplankton bloom. At W05, regression analysis showed that POC and SPM or Chl*a* and SPM concentrations, are closely related during winter, when the $POC_{phyto}$ fraction was still low, indicating that SPM dynamics, mainly tidal resuspension, controlled their concentrations. However, as the contribution of the $POC_{phyto}$ fraction increased in spring and summer, these relationships become less pronounced. At W08, regressions showed little correspondence between POC, Chl*a* and SPM concentrations throughout the year, even during winter. This highlights the relatively low impact of tidal resuspension on POC and Chl*a* distribution in the deeper offshore waters, where diel Chl*a* production and horizontal transport of phytoplankton communities dominate (Blauw et al. 2018). Thus, the contribution of the $POC_{phyto}$ fraction influenced the composition of SPM and the quality of the bulk POC pool, with different outcomes along the cross-shore SPM gradient. During the growing season, the POC fraction of SPM increased substantially offshore, while the coastal waters exhibited a relatively reduced impact despite higher phytoplankton production.

### Dissolved and particulate forms of organic matter

The southern North Sea, particularly the Belgian coast, has some of the highest DOC concentrations in the North Sea, and a substantial fraction of this organic pool has marine origins (Van Engeland et al. 2010; Painter et al. 2018). While the Scheldt river is a concentrated DOC source with geographically limited impact, the Rhine and Meuse rivers, the second major freshwater inputs to the Belgian coast, serve as a more dilute DOC source (Lacroix et al. 2004; Dai et al. 2012). Autochthonous production, driven by the cross-shore nutrient gradient, also influences the DOC distribution. The highest DOC concentrations, observed after the spring bloom in summer (Fig. 6a) have been previously attributed partly to extracellular phytoplankton release (Suratman et al. 2009; Sintes et al. 2010). This release typically occurs late in the bloom when nutrient depletion causes excess dissolved inorganic carbon fixed by phytoplankton to be released as DOC (Toggweiler 1993). The delayed DOC rise has also been linked to the of phytoplankton biomass degradation (Wetz et al. 2008). In Belgian waters, the spring–summer DOC increase in above

winter background levels is greater at the productive coastal station than at offshore W08. This is reflected in contrasting relationships between DOC:TOC ratio and $POC_{phyto}$ concentrations across stations (Fig. 6d). At offshore stations, $POC_{phyto}$ production increased both POC and DOC, but a greater increase in POC concentrations relative to winter levels resulted in negative regression between the two. In contrast, at MOW1, where background POC concentrations from mineral and detrital sources remained high, the relative increase in $POC_{phyto}$ during the bloom was low, whereas DOC concentrations rose significantly, leading to a positive relationship between DOC:TOC and $POC_{phyto}$ concentrations. Furthermore, organic matter partitioning into particulate and dissolved pools differed significantly between coastal and offshore waters (Fig. 6b). In offshore waters, POC:DOC ratios remained below 1, consistent with the typical DOC dominance in marine systems, where it constitutes ~ 90% of the organic carbon pool (Hansell et al. 2009). POC becomes a substantial fraction only during high phytoplankton productivity periods (Wetz and Wheeler 2003; Engel et al. 2012). Conversely, at the turbid coastal station MOW1, POC:DOC ratios exceeded 1, a pattern also observed in turbid waters elsewhere (Abril et al. 2002; Zhao and Gao 2019). To summarize, the cross-shore gradient of the POC:DOC ratio (Fig. 6b) was partly driven by higher phytoplankton production and significant presence of $POC_{mineral}$ near the coast compared to offshore areas. Particles are retained in the coastal zone whereas dissolved substances are transported and diluted across the cross-shore axis (Desmit et al. 2024). Such a difference in transport dynamics supports the less pronounced cross-shore gradient in DOC concentrations compared to POC, and accounted for the observed POC:DOC ratio gradient (Fig. 6b).

## Dynamic exchange between DOC and $POC_{mineral}$

POC fraction of TOC and the SPM concentrations demonstrate a positive non-linear relationship in turbid estuarine waters (Herman and Heip 1999; Abril et al. 2002; Middleburg and Herman 2007). This relationship has been described with the Freundlich isotherm model (Eq. 4), which has been widely used to describe the sorption of organic matter onto mineral surfaces, reinforcing the role of SPM in governing organic matter partitioning in aquatic systems. Despite the substantial variation in POC:SPM ratios across these estuaries (Middleburg and Herman 2007), ranging from lower values in the Gironde estuary (< 5%) to higher ratios in the Scheldt estuary (~ 5–15%), the overall data aligns well with Eq. 4. The K values (the ratio of desorption to adsorption rate constants) remain comparable among the different estuaries (Fig. 10). Even though data from MOW1 aligns with Eq. 4, the value of K (~ 40) differs from that observed in the tidal estuaries (Fig. 10). While Eq. 4 assumes that changes in POC mass are primarily driven by DOC adsorption–desorption onto mineral particles, this may not always hold. Accordingly we also assessed the relationship between the $POC_{mineral}$:DOC ratio and SPM at MOW1, where the mass of $POC_{mineral}$ fraction, being associated with adsorption–desorption is expected to be more stable. This yields a higher *K* value (~ 166), as shown in Fig. 10.

A smaller K value (40) in Belgian coastal waters when considering bulk POC:TOC ratio suggests that POC remains dominant over DOC at lower SPM concentrations compared to estuarine turbid waters; hence, the switch to DOC dominance (POC/TOC ratios < 0.5 in Fig. 10) occurs at SPM concentrations

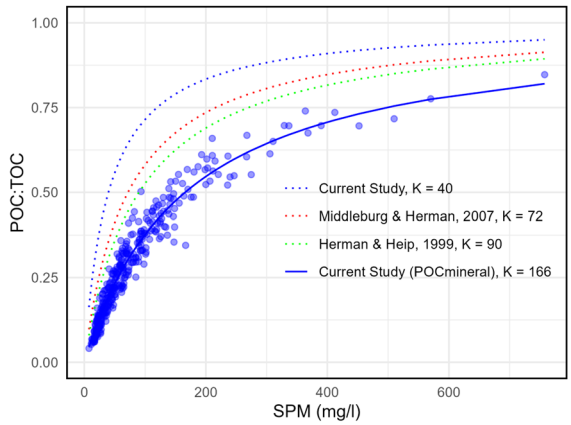


**Fig. 10** POC:TOC ratio as a function of SPM concentrations. All dotted lines represent non-linear regression fit to Eq. (4). The blue dotted line in the figure corresponds to this study, based on bulk POC data from MOW1 only ($R^2 = 0.81$). Herman and Heip (1999) presented data from high turbidity zones in the Elbe, Scheldt, and Gironde Estuaries. Middleburg and Herman (2007) expanded their dataset to include additional estuaries such as the Ems, Thames, Rhine, Loire, Douro, and Sado. The solid blue line represents a fit considering only $POC_{mineral}$ in the POC:TOC ratio rather than bulk POC

smaller than ~ 40 mg/l compared to ~ 90 mg/l in the estuarine waters. This implied a higher organic matter content of the mineral particles or a higher fraction of non-mineral POC in Belgian coastal waters compared to the estuaries. However, the differences in mineralogy between the Belgian coastal waters and Scheldt estuary are very small, which weakens this argument (Adriaens et al. 2018). This points to considering other factors that differ between coastal and estuarine waters, such as the origin and quality of organic matter (marine vs. terrestrial), the phytoplankton production, which is higher in the estuaries, and physicochemical conditions like ionic strength (salinity), and pH, which are known to influence the adsorption and desorption of organic matter (Henrichs 1995; Keil et al. 1997; Blattman et al. 2019).

## Conclusion

POC composition varied with SPM concentrations, showing clear differences between nearshore turbid and offshore clearer waters. Nearshore waters exhibited higher POC concentrations and elevated SPM concentrations and frequent tidal resuspension resulted in higher relative contributions of $POC_{mineral}$ and $POC_{det}$. These components, often more refractory, masked seasonal variations in the bulk POC pool. $POC_{mineral}$ represents organic matter adsorbed onto mineral surfaces, limiting enzymatic degradation, while $POC_{det}$ consists of a mixture of organic compounds at various degradation stages. In contrast, offshore waters showed reduced contributions of $POC_{mineral}$ and a higher relative abundance of fresher, more labile $POC_{phyto}$. Tidal resuspension had a limited influence here, as indicated by weaker associations between POC, Chl*a*, and SPM concentrations at tidal scales. Instead, processes like horizontal advection of phytoplankton biomass and diurnal Chl*a* variability played more dominant roles in controlling POC dynamics offshore. Hence, the $POC_{phyto}$ fraction altered the composition and quality of the bulk POC pool differently along the cross-shore SPM gradient, with a marked increase in the organic fraction offshore during the growing season and a comparatively limited effect in coastal waters despite higher phytoplankton production. Furthermore, the partitioning between dissolved and particulate organic fractions also varied along the SPM concentration gradient, with POC dominating the TOC pool in nearshore turbid waters, whereas DOC prevailed offshore. The POC:TOC ratio followed a similar nonlinear trend with SPM concentration in coastal and estuarine systems. Yet, the POC content of SPM was higher in Belgian coastal waters than in estuaries. This discrepancy may result from differences in clay particle composition, organic matter characteristics, and physicochemical properties of the water column.

**Acknowledgements** The research was supported by the Belgian Science Policy (BELSPO) within the RVBelgica research programme PiNS (contract nr RV/21/PiNS) and the BRAIN-be programme BG-PART (contract nr B2/202/P1/BG-PART), the Maritime Access Division of the Flemish Ministry of Mobility and Public Works (MOMO project), and the RBINS BGC-Monit program. Ship time with the RV Belgica was provided by BELSPO and RBINS-OD Nature. The SPM, POC, PON, TEP, and Chl*a* analyses have been done at the Royal Belgian Institute of Natural Sciences ECOCHEM Laboratory.

**Author contributions** SS: Visualization; Data Analysis; writing–original draft preparation (lead), conceptualization; formal analysis. XD: writing–review and editing, conceptualization, funding acquisition. MF: writing–review and editing, conceptualization, funding acquisition, project management.

**Funding** The research was supported by the Belgian Science Policy (BELSPO) within the BRAIN-be programme (BG-PART, contract nr B2/202/P1/BG-PART, and PiNS, contract nr RV/21/PiNS), the Maritime Access Division of the Flemish Ministry of Mobility and Public Works (MOMO project), and the Royal Belgian Institute of Natural Sciences BGCMonit program.

**Data availability** Data of in situ SPM, Chl*a,* POC, PON, and TEP concentrations are freely available on request at https://www.bmdc.be/NODC/search_dat a.xhtml.

**Declarations**

**Conflict of interest** The authors have no relevant financial or non-financial interests to disclose.

## References


Abril G, Nogueira M, Etcheber H, Cabeçadas G, Lemaire E, Brogueira MJ (2002) Behaviour of organic carbon in nine contrasting European estuaries. Estuar Coast Shelf Sci 54(2):241–262. https://doi.org/10.1006/ecss.2001.0844

Adriaens R, Zeelmaekers E, Fettweis M, Vanlierde E, Vanlede J, Stassen P, Elsen J, Środoń J, Vandenberghe N (2018) Quantitative clay mineralogy as provenance indicator for recent muds in the southern North Sea. Mar Geol 398:48–58. https://doi.org/10.1016/j.margeo.2017.12.011

Andersson A, Rudehäll Å (1993) Proportion of plankton biomass in particulate organic carbon in the northern Baltic Sea. Mar Ecol Prog Ser 95:133–139. https://doi.org/10.3354/meps095133

Berto D, Rampazzo F, Noventa S, Cacciatore F, Gabellini M, Aubry FB, Brusà RB (2013) Stable carbon and nitrogen isotope ratios as tools to evaluate the nature of particulate organic matter in the Venice lagoon. Estuar Coast Shelf Sci 135:66–76. https://doi.org/10.1016/j.ecss.2013.06.021

Biddanda B, Benner R (1997) Carbon, nitrogen, and carbohydrate fluxes during the production of particulate and dissolved organic matter by marine phytoplankton. Limnol Oceanogr 42(3):506–518. https://doi.org/10.4319/lo.1997.42.3.0506

Billen G, Silvestre M, Grizzetti B, Leip A, Garnier J, Voss M, Howarth R, Bouraoui F, Lepistö L, Kortelainen P, Johnes P, Curtis C, Humborg C, Smedberg E, Kaste Ø, Ganeshram R, Beusen A, Lancelot C. (2011) Nitrogen Flows from European Regional Watersheds to Coastal Marine Waters. In: Sutton M., Britton C., Erisman J.W., Billen G., Bleeker A., Greenfelt P., van Grinsven H., Grizzetti B., (editors). The European Nitrogen Assessment: Sources, Effects and Policy Perspectives. Cambridge University Press

Blattmann TM, Liu Z, Zhang Y, Zhao Y, Haghipour N, Montluçon DB, EglinFfton TI (2019) Mineralogical control on the fate of continentally derived organic matter in the ocean. Science 366(6466):742–745. https://doi.org/10.1126/science.aax5345

Blauw AN, Benincà E, Laane RW, Greenwood N, Huisman J (2018) Predictability and environmental drivers of chlorophyll fluctuations vary across different time scales and regions of the North Sea. Prog Oceanogr 161:1–18. https://doi.org/10.1016/j.pocean.2018.01.005

Calvo-Díaz A, Morán XAG, Suárez LÁ (2008) Seasonality of picophytoplankton chlorophyll a and biomass in the central Cantabrian Sea, southern Bay of Biscay. J Mar Syst 72(1–4):271–281. https://doi.org/10.1016/j.jmarsys.2007.03.008

Cloern JE, Grenz C, Vidergar-Lucas L (1995) An empirical model of the phytoplankton chlorophyll: carbon ratio-the conversion factor between productivity and growth rate. Limnol Oceanogr 40(7):1313–1321. https://doi.org/10.4319/lo.1995.40.7.1313

Cresson P, Ruitton S, Fontaine MF, Harmelin-Vivien M (2012) Spatio-temporal variation of suspended and sedimentary organic matter quality in the Bay of Marseilles (NW Mediterranean) assessed by biochemical and isotopic analyses. Mar Pollut Bull 64(6):1112–1121. https://doi.org/10.1016/j.marpolbul.2012.04.003

Dai M, Yin Z, Meng F, Liu Q, Cai WJ (2012) Spatial distribution of riverine DOC inputs to the ocean: an updated global synthesis. Curr Opin Environ Sustain 4(2):170–178. https://doi.org/10.1016/j.cosust.2012.03.003

Desmit X, Thieu V, Billen G, Campuzano F, Dulière V, Garnier J, Lassaletta L, Ménesguen A, Neves R, Pinto L, Silvestre M, Sobrinho JL, Lacroix G (2018) Reducing marine eutrophication may require a paradigmatic change. Sci Total Environ 635:1444–1466. https://doi.org/10.1016/j.scitotenv.2018.04.181

Desmit X, Nohe A, Borges AV, Prins T, De Cauwer K, Lagring R, der Van Zande D, Sabbe K (2020) Changes in chlorophyll concentration and phenology in the North Sea in relation to de-eutrophication and sea surface warming. Limnol Oceanogr 65(4):828–847. https://doi.org/10.1002/lno.11351

Desmit X, Schartau M, Riethmüller R, Terseleer N, Van der Zande D, Fettweis M (2024) The transition between coastal and offshore areas in the North Sea unraveled by suspended particle composition. Sci Total Environ 915:169966. https://doi.org/10.1016/j.scitotenv.2024.169966

Duarte CM, Agustí S, Gasol JM, Vaqué D, Vazquez-Dominguez E (2000) Effect of nutrient supply on the biomass structure of planktonic communities: an experimental test on a Mediterranean coastal community. Mar Ecol Prog Ser 206:87–95. https://doi.org/10.3354/meps206087

Dubois S, Savoye N, Grémare A, Plus M, Charlier K, Beltoise A, Blanchet H (2012) Origin and composition of sediment organic matter in a coastal semi-enclosed ecosystem: an elemental and isotopic study at the ecosystem space scale. J Mar Syst 94:64–73. https://doi.org/10.1016/j.jmarsys.2011.10.009

Dulière V, Gypens N, Lancelot C, Luyten P, Lacroix G (2019) Origin of nitrogen in the English Channel and Southern Bight of the North Sea ecosystems. Hydrobiologia 845:13. https://doi.org/10.1007/s10750-017-3419-5

Ehrhardt M, Koeve W (1999) Determination of particulate organic carbon and nitrogen. Methods Seawater Anal. https://doi.org/10.1002/9783527613984

Eisma D, Kalf J (1979) Distribution and particle size of suspended matter in the Southern Bight of the North Sea and the Eastern Channel. Neth J Sea Res 13(2):298–324. https://doi.org/10.1016/0077-7579(79)90008-5

Engel A, Harlay J, Piontek J, Chou L (2012) Contribution of combined carbohydrates to dissolved and particulate organic carbon after the spring bloom in the northern Bay of Biscay (North-Eastern Atlantic Ocean). Cont Shelf Res 45:42–53. https://doi.org/10.1016/0077-7579(79)90008-5

Fettweis M, Baeye M (2015) Seasonal variation in concentration, size, and settling velocity of muddy marine flocs in the benthic boundary layer. J Geophys Res Oceans 120(8):5648–5667. https://doi.org/10.1002/2014JC010644

Fettweis M, Schartau M, Desmit X, Lee BJ, Terseleer N, Van der Zande D, Riethmüller R (2022) Organic matter

composition of biomineral flocs and its influence on suspended particulate matter dynamics along a nearshore to offshore transect. J Geophys Res Biogeosciences 127(1):e2021JG006332. https://doi.org/10.1029/2021JG006332

Fettweis M, Silori S, Adriaens R, Desmit X (2025) Clay minerals and the stability of organic carbon in suspension along coastal to offshore transects. Geochim Cosmochim Acta 395:229–237. https://doi.org/10.1016/j.gca.2025.03.003

Gaffey CB, Frey KE, Cooper LW, Grebmeier JM (2022) Phytoplankton bloom stages estimated from chlorophyll pigment proportions suggest delayed summer production in low sea ice years in the northern Bering Sea. PLoS ONE 17(7):e0267586. https://doi.org/10.1371/journal.pone.0267586

Gasol JM, Del Giorgio PA, Duarte CM (1997) Biomass distribution in marine planktonic communities. Limnol Oceanogr 42(6):1353–1363. https://doi.org/10.4319/lo.1997.42.6.1353

Geider RJ (1987) Light and temperature dependence of the carbon to chlorophyll a ratio in microalgae and cyanobacteria: implications for physiology and growth of phytoplankton. New Phytol. https://doi.org/10.1111/j.1469-8137.1987.tb04788.x

Goni MA, Aceves H, Benitez-Nelson B, Tappa E, Thunell R, Black DE, Varela R (2009) Oceanographic and climatologic controls on the compositions and fluxes of biogenic materials in the water column and sediments of the Cariaco Basin over the late Holocene. Deep-Sea Res I Oceanogr Res Pap 56(4):614–640. https://doi.org/10.1016/j.dsr.2008.11.010

Hansell DA, Carlson CA, Repeta DJ, Schlitzer R (2009) Dissolved organic matter in the ocean: a controversy stimulates new insights. Oceanography 22(4):202–211

Hansell, DA, Carlson, CA. (Eds.). (2014). Biogeochemistry of marine dissolved organic matter. Academic press https://doi.org/10.5670/oceanog.2015.76

Harmelin-Vivien M, Loizeau V, Mellon C, Beker B, Arlhac D, Bodiguel X, Salen-Picard C (2008) Comparison of C and N stable isotope ratios between surface particulate organic matter and microphytoplankton in the Gulf of Lions (NW Mediterranean). Cont Shelf Res 28(15):1911–1919. https://doi.org/10.1002/lno.10338

Hemingway JD, Rothman DH, Grant KE, Rosengard SZ, Eglinton TI, Derry LA, Galy VV (2019) Mineral protection regulates long-term global preservation of natural organic carbon. Nature 570(7760):228–231

Henderikx-Freitas F, Karl DM, Björkman KM, White AE (2021) Constraining growth rates and the ratio of living to nonliving particulate carbon using beam attenuation and adenosine-5′-triphosphate at station ALOHA. Limnol Oceanogr Lett 6(5):243–252. https://doi.org/10.1002/lol2.10199

Herman PM, Heip CH (1999) Biogeochemistry of the MAximum TURbidity zone of estuaries (MATURE): some conclusions. J Mar Syst 22(2–3):89–104. https://doi.org/10.1016/S0924-7963(99)00034-2

Jago CF, Bale AJ, Green MO, Howarth MJ, Jones SE, McCave IN, Williams JJ (1993) Resuspension processes and seston dynamics, southern North Sea. Phil Trans Royal Soc Lon Series a: Phys Eng Sci 343(1669):475–491. https://doi.org/10.1098/rsta.1993.0060

Jakobsen HH, Markager S (2016) Carbon-to-chlorophyll ratio for phytoplankton in temperate coastal waters: seasonal patterns and relationship to nutrients. Limnol Oceanogr 61(5):1853–1868. https://doi.org/10.1002/lno.10338

Keil RG, Mayer LM (2014) 12.12 – Mineral Matrices and Organic Matter. In: Turekian HDHK (ed) Treatise on Geochemistry, 2nd edn. Elsevier, Oxford, pp 337–359

Keil RG, Montluçon DB, Prahl FG, Hedges JI (1994) Sorptive preservation of labile organic matter in marine sediments. Nature 370(6490):549–552

Keil RG, Mayer LM, Quay PD, Richey JE, Hedges JI (1997) Loss of organic matter from riverine particles in deltas. Geochim Cosmochim Acta 61(7):1507–1511. https://doi.org/10.1016/S0016-7037(97)00044-6

Kharbush JJ, Close HG, Van Mooy BA, Arnosti C, Smittenberg RH, Le Moigne FA, Mohr W (2020) Particulate organic carbon deconstructed: molecular and chemical composition of particulate organic carbon in the ocean. Front Mar Sci 7:518. https://doi.org/10.3389/fmars.2020.00518

Kleber M, Bourg IC, Coward EK, Hansel CM, Myneni SC, Nunan N (2021) Dynamic interactions at the mineral–organic matter interface. Nat Rev Earth Environ 2(6):402–421. https://doi.org/10.1038/s43017-021-00162-y

Lacroix G, Ruddick K, Ozer J, Lancelot C (2004) Modelling the impact of the Scheldt and Rhine/Meuse plumes on the salinity distribution in Belgian waters (southern North Sea). J Sea Res 52(3):149–163. https://doi.org/10.1016/j.seares.2004.01.003

Leblanc K, Arístegui J, Armand L, Assmy P, Beker B, Bode A, Breton E, Cornet V, Gibson J, Gosselin M-P, Kopczynska E, Marshall H, Peloquin J, Piontkovski S, Poulton AJ, Quéguiner B, Schiebel R, Shipe R, Stefels J, van Leeuwe MA, Varela M, Widdicombe C, Yallop M (2012) A global diatom database–abundance, biovolume and biomass in the world ocean. Earth Syst Sci Data 4(1):149–165. https://doi.org/10.5194/essd-4-149-2012

Legendre P, Legendre L (1998) Numerical Ecology, 3rd edn. Elsevier, Amsterdan, p 853

Liénart C, Savoye N, Bozec Y, Breton E, Conan P, David V, Sultan E (2017) Dynamics of particulate organic matter composition in coastal systems: a spatio-temporal study at multi-systems scale. Prog Oceanogr 156:221–239. https://doi.org/10.1016/j.pocean.2017.03.001

Liénart C, Savoye N, David V, Ramond P, Tress PR, Hanquiez V, Susperregui N (2018) Dynamics of particulate organic matter composition in coastal systems: forcing of spatio-temporal variability at multi-systems scale. Prog Oceanogr 162:271–289. https://doi.org/10.1016/j.pocean.2018.02.026

Liu Q, Kandasamy S, Lin B, Wang H, Chen CTA (2018) Biogeochemical characteristics of suspended particulate matter in deep chlorophyll maximum layers in the southern East China Sea. Biogeosciences 15(7):2091–2109. https://doi.org/10.5194/bg-15-2091-2018

Lowe AT, Galloway AW, Yeung JS, Dethier MN, Duggins DO (2014) Broad sampling and diverse biomarkers allow characterization of nearshore particulate organic matter. Oikos 123(11):1341–1354. https://doi.org/10.1111/oik.01392

Maerz J, Hofmeister R, van der Lee EM, Gräwe U, Riethmüller R, Wirtz KW (2016) Maximum sinking velocities of suspended particulate matter in a coastal transition zone. Biogeosciences 13(17):4863–4876. https://doi.org/10.5194/bg-13-4863-2016

Mayer LM (1994) Surface area control of organic carbon accumulation in continental shelf sediments. Geochim Cosmochim Acta 58(4):1271–1284. https://doi.org/10.1016/0016-7037(94)90381-6

Middelburg JJ, Herman PM (2007) Organic matter processing in tidal estuaries. Mar Chem 106(1–2):127–147. https://doi.org/10.1016/j.marchem.2006.02.007

Middelburg, J. J. (2019). Marine carbon biogeochemistry: A primer for earth system scientists. Springer Nature.

Modéran J, Bouvais P, David V, Le Noc S, Simon-Bouhet B, Niquil N, Fichet D (2010) Zooplankton community structure in a highly turbid environment (Charente estuary, France): spatio-temporal patterns and environmental control. Estuar Coast Shelf Sci 88(2):219–232. https://doi.org/10.1016/j.ecss.2010.04.002

Muylaert K, Gonzales R, Franck M, Lionard M, Van der Zee C, Cattrijsse A, Vyverman W (2006) Spatial variation in phytoplankton dynamics in the Belgian coastal zone of the North Sea studied by microscopy, HPLC-CHEMTAX and underway fluorescence recordings. J Sea Res 55(4):253–265. https://doi.org/10.1016/j.seares.2005.12.002

Painter SC, Lapworth DJ, Woodward EMS, Kroeger S, Evans CD, Mayor DJ, Sanders RJ (2018) Terrestrial dissolved organic matter distribution in the North Sea. Sci Total Environ 630:630–647. https://doi.org/10.1016/j.scitotenv.2018.02.237

Passow U (2002) Transparent exopolymer particles (TEP) in aquatic environments. Prog Oceanogr 55(3–4):287–333. https://doi.org/10.1016/S0079-6611(02)00138-6

Passow U, Alldredge AL (1995) A dye-binding assay for the spectrophotometric measurement of transparent exopolymer particles (TEP). Limnol Oceanogr 40(7):1326–1335. https://doi.org/10.4319/lo.1995.40.7.1326

Rousseau, V., Park, Y., Ruddick, K., Vyverman, W., Parent, JY., & Lancelot, C. (2006). Phytoplankton blooms in response to nutrient enrichment. Current status of eutrophication in the Belgian coastal zone. Brussels: Presses Univ. de Bruxelles, 45–59.

Sathyendranath S, Stuart V, Nair A, Oka K, Nakane T, Bouman H, Platt T (2009) Carbon-to-chlorophyll ratio and growth rate of phytoplankton in the sea. Mar Ecol Prog Ser 383:73–84. https://doi.org/10.3354/meps07998

Savoye N, Aminot A, Tréguer P, Fontugne M, Naulet N, Kérouel R (2003) Dynamics of particulate organic matter δ15N and δ13C during spring phytoplankton blooms in a macrotidal ecosystem (Bay of Seine, France). Mar Ecol Prog Ser 255:27–41. https://doi.org/10.3354/meps255027

Schartau M, Riethmüller R, Flöser G, van Beusekom JEE, Krasemann H, Hofmeister R, Wirtz K (2019) On the separation between inorganic and organic fractions of suspended matter in a marine coastal environment. Prog Oceanogr 171:231–250. https://doi.org/10.1016/j.pocean.2018.12.011

Scheffold MIE, Hense I (2020) Quantifying contemporary organic carbon stocks of the Baltic Sea ecosystem. Front Mar Sci 7:571956. https://doi.org/10.3389/fmars.2020.571956

Sintes E, Stoderegger K, Parada V, Herndl GJ (2010) Seasonal dynamics of dissolved organic matter and microbial activity in the coastal North Sea. Aquat Microb Ecol 60(1):85–95. https://doi.org/10.3354/ame01404

Suratman S, Weston K, Jickells T, Fernand L (2009) Spatial and seasonal changes of dissolved and particulate organic C in the North Sea. Hydrobiologia 628:13–25. https://doi.org/10.1007/s10750-009-9730-z

Toggweiler JR (1993) Carbon overconsumption. Nature. https://doi.org/10.1038/363210a0

Van Der Zee C, Chou L (2005) Seasonal cycling of phosphorus in the Southern Bight of the North Sea. Biogeosciences 2(1):27–42. https://doi.org/10.5194/bg-2-27-2005

Van Engeland T, Soetaert K, Knuijt A, Laane RWPM, Middelburg JJ (2010) Dissolved organic nitrogen dynamics in the North Sea: a time series analysis (1995–2005). Estuar Coast Shelf Sci 89(1):31–42. https://doi.org/10.1016/j.ecss.2010.05.009

Vanaverbeke, J., Franco, M., Van Oevelen, D., Leon, M., Provoost, P., Steyaert, M., Vincx, M. (2008). Benthic responses to sedimentation of phytoplankton on the Belgian Continental Shelf. In Current status of eutrophication in the Belgian coastal zone (pp. 73–90). Presses Universitaires de Bruxelles. http://hdl.handle.net/1854/LU-527846

Vázquez-Domínguez E, Morán XAG, López-Urrutia A (2013) Photoacclimation of picophytoplankton in the central Cantabrian Sea. Mar Ecol Prog Ser 493:43–56. https://doi.org/10.3354/meps10549

Verdugo P (2012) Marine microgels. Annu Rev Mar Sci 4(1):375–400. https://doi.org/10.1146/annurev-marine-120709-142759

Volkman JK, Tanoue E (2002) Chemical and biological studies of particulate organic matter in the ocean. J Oceanogr 58(2):265–279. https://doi.org/10.1023/A:1015809708632

Wetz MS, Wheeler PA (2003) Production and partitioning of organic matter during simulated phytoplankton blooms. Limnol Oceanogr 48(5):1808–1817. https://doi.org/10.4319/lo.2003.48.5.1808

Wetz MS, Hales B, Wheeler PA (2008) Degradation of phytoplankton-derived organic matter: implications for carbon and nitrogen biogeochemistry in coastal ecosystems. Estuar Coast Shelf Sci 77(3):422–432. https://doi.org/10.1016/j.ecss.2007.10.002

Woźniak SB, Stramski D, Stramska M, Reynolds RA, Wright VM, Miksic EY, Cieplak AM (2010) Optical variability of seawater in relation to particle concentration, composition, and size distribution in the nearshore marine environment at Imperial Beach, California. J Geophys Res Oceans. https://doi.org/10.1029/2009JC005554

Yuan LL, Pollard AI (2018) Changes in the relationship between zooplankton and phytoplankton biomasses across a eutrophication gradient. Limnol Oceanogr 63(6):2493–2507. https://doi.org/10.1002/lno.10955

Zhao L, Gao L (2019) Dynamics of dissolved and particulate organic matter in the Changjiang (Yangtze River) estuary and the adjacent East China Sea shelf. J Mar Syst 198:103188. https://doi.org/10.1016/j.jmarsys.2019.103188